Understanding the impacts of climate variability and change on rainfed crop production in Ethiopia

Mosisa Tujuba Wakjira

Diss. ETH No. 30002
ETH Zurich

Diss. ETH No. 30002

Understanding the impacts of climate variability and change on rainfed crop production in Ethiopia

A thesis submitted to attain the degree of

Doctor of Sciences
(Dr. sc. ETH Zurich)

presented by

Mosisa Tujuba Wakjira

MSc in Water Resource Engineering and Management, Hawassa University, Ethiopia

Born on 09.01.1989

Accepted on the recommendation of
Prof. Dr. Peter Molnar, examiner
Prof. Dr. Johan Six, co-examiner
Prof. Dr. Nadav Peleg, co-examiner
Prof. Dr. Paolo Burlando, co-examiner
Prof. Dr. Declan Conway, co-examiner
Prof. Dr. Christoph Studer, co-examiner

2024

DOI: https://doi.org/10.3929/ethz-b-000672129

To my late father, Obbo Tujuba Wakjira, whose legacy as a role model smallholder farmer continues to inspire my agricultural engineering research career. Recognized multiple times by the North Shoa Zone Bureau of Agriculture, he was a beacon of dedication and hard work in his community. His remarkable achievement of winning the gold medal for successfully implementing the rural development package in 2010 from Oromia Regional State is a testament to his dedication and hard work.

In loving memory of my sister, Kibe Tujuba, who was so excited about my PhD journey but never saw its end.

Abstract

About three quarters of global cropland is under rainfed agriculture, producing an estimated 60% of the global food demand. In sub-Saharan Africa, and particularly in Ethiopia, rainfed agriculture (RFA) constitutes nearly 95% of croplands, serving as a crucial source of food and household income for the rural population, and contributing significantly to the national economy. The RFA system is characterized by smallholder and subsistence farming practices, high vulnerability to weather and climate shocks, low productivity, and high poverty rate in the sector. For this reason, agricultural transformation in Ethiopia and the sub-continent is the top sustainable development priority for poverty eradication (SDG 1) and ensuring food security (SGD 2). However, challenges, such as climate change, population growth, armed conflict, etc., complicate the current state and hinder the achievement of these development goals. Success requires a deeper data-driven understanding of the agro-environmental conditions within the context of global changes, in order to inform national and sub-national agricultural development plans, policies and decisions aimed at increasing productivity and ensuring a resilient RFA system. The objective of this thesis is to provide such an understanding by investigating the climate-crop and climate-agroecological interactions that are relevant for climate risk and water management planning, decisions and policy making in the face of a changing climate in Ethiopia.

As a first step, I addressed climate data limitations by developing a robust framework for downscaling and de-biasing globally available gridded temperature data. This involved leveraging low-quality station observations through a hybrid spatial interpolation method coupled with a quantile mapping bias-adjustment technique. The framework was applied to ERA5-Land 2-m air temperature, resulting in a bias-corrected ERA5-Land (BCE5) daily maximum and minimum temperature dataset covering the period 1981-2010 over the Ethiopian domain. The accuracy of BCE5 was found to be 68% higher for maximum temperature and 25% higher for minimum temperature compared to the original ERA5-Land. The increase in performance highlights that even low-quality station temperature observations can reduce the statistical biases in gridded global datasets and produce locally accurate spatial data in data-scarce regions for a range of agroecological applications.

Second, the effects of variabilities in rainfall timing and seasonality on seasonal crop production were explored by statistical analyses of the relationships between cereal production and four

temporal rainfall attributes: seasonality, dates of onset and cessation, and duration of the rainy season, derived from the CHIRPS quasi-global rainfall dataset. The results highlight the importance of rainfall regimes. In regions characterized by unimodal rainfall regimes, cereal crop production is primarily influenced by the onset of the rainy season. A late onset of the rainy season results in crop production losses (on average by 1.5% for every 5-day delay) underscoring the significance of onset-informed planting. In regions with a bimodal rainfall regime, rainfall seasonality (monthly distribution) was found to be the main determinant of crop production. Implementing soil moisture conservation measures in these regions may prove more effective.

Third, water-limited attainable yield potential (AY) was evaluated. For this, an agrohydrological modelling framework integrating climatic-hydrological-crop interactions was developed and applied to both the present and future climate scenarios. With regional variations based on climatic regimes, the average AY for the main growing season (Meher) and the short growing season (Belg) was determined to be 79% (of unstressed yield potential) and 37%, respectively. Projected climate-driven changes in water-limited AY in Meher fall in the range of -5% to 5% with major decreases observed primarily in semi-arid regions, particularly under the high emission scenario by the end of the century. Conversely, Belg-producing regions are expected to experience major increases in AY by up to 20% by the end of the century. On the other hand, a substantial yield gap is identified between actual and water-limited yield, emphasizing the need for integrating green water management strategies with improved agronomic practices to close these yield gaps.

Finally, the current potential and future changes in the crop agroecological suitability across the RFA region of Ethiopia were investigated using a numerical model of cropland suitability derived from relationships between observed crop yield and a range of climatic and soil factors. Sorghum was identified as the most versatile crop with nearly two-third of the cultivable RFA area being suitable, followed by teff and maize with over half of the RFA area being suitable for both crops. Wheat is the least versatile crop with less than one-third of the RFA area being suitable. Climate change is expected to significantly impact future cropland suitability. The projected effects involve shifts from lowland to highland areas for maize and sorghum and losses in suitable areas for teff and wheat. These impacts pose serious consequences for the future availability of cropland in Ethiopia, emphasizing the urgent need for sustainable adaptation plans and policies.

Zusammenfassung

Etwa drei Viertel der globalen Ackerfläche werden sind zur Gänze abhängig von natürlichen Niederschlägen (Regenfeldbau). Diese Ackerflächen decken etwa 60% der weltweiten Nahrungsnachfrage. Im subsaharischen Afrika, insbesondere in Äthiopien, umfasst der Regenfeldbau (RFA) fast 95% aller Ackerflächen und ist dadurch bedeutende Grundlage für die Lebensmittelversorgung und Haushaltseinkommen vor allem in ländlichen Gebieten und trägt erheblich zur nationalen Wirtschaft bei. Regenfeldbau (RFA) ist gekennzeichnet durch Kleinbauern- und Subsistenzpraktiken, hoher Anfälligkeit für Wetter- und Klimaänderungen, geringe Produktivität und hohe Armutsrate. Daher ist eine nachhaltige landwirtschaftliche Transformation in Äthiopien und auf dem gesamten Subkontinent oberste Priorität zur Armutsbekämpfung (SDG 1) und zur Gewährleistung der Ernährungssicherheit (SDG 2). Herausforderungen wie u.a., Klimawandel, Bevölkerungswachstum, und bewaffnete Konflikte erschweren jedoch den derzeitigen Zustand und behindern das Erreichen dieser Entwicklungsziele. Die erfolgreiche Umsetzung der Entwicklungsziele erfordert daher ein tiefgehendes, datenbasiertes Verständnis der agroökologischen Bedingungen im Kontext globaler Veränderungen. Dies ist wesentlich um die nationalen und subnationalen landwirtschaftlichen Entwicklungspläne und politischen Entscheidungen wissensbasiert zu implementieren, die Produktivität zu steigern und ein widerstandsfähiges RFA-System zu gewährleisten. Ziel dieser Dissertation ist es die Zusammenhänge zwischen klimatischen Bedingungen, Nutzpflanzen und der Agrarökologie zu untersuchen, die für die Planung und Entscheidungsfindung politischer Maßnahmen im Bereich Klimarisiken und Wasserbewirtschaftung unter Berücksichtigung des Klimawandels in Äthiopien relevant sind.

Im ersten Schritt habe ich mich mit den Limitierungen der verfügbaren Klimadaten befasst, indem ein robuster Arbeitsablauf zur Skalierung und Entzerrung global verfügbarer temperaturbezogener Rasterdaten entwickelt wurde. Dies umfasste die Nutzung von oft nur in geringer Qualität vorhandenen Messstationsdaten durch eine hybride räumliche Interpolationsmethode in Verbindung mit einer Optimierungstechnik mittels Quantilsregression. Die Methode wurde auf ERA5-Land Daten für Lufttemperatur in 2m Auflösung angewendet und führte zu einem korrigierten ERA5-Land Datensatz für tägliche Maximal- und Minimaltemperaturen (BCE5) für den Zeitraum 1981-2010 für Äthiopien. Die

Genauigkeit von BCE5 konnte im Vergleich zum Original-ERA5-Land Datensatz für Maximaltemperaturen um 68% und für Minimaltemperaturen um 25% gesteigert werden. Diese Qualitätserhöhung zeigt, dass selbst mit nur in geringer Qualität vorhandenen Messstationsdaten die statistischen Verzerrungen, die in weltweiten Gitterdatensätzen existieren, reduziert werden können und genauere kleinräumige Datenreihen für datenarme Regionen erstellt werden können, die die Grundlage für eine Vielzahl agroökologischer Anwendungen bilden.

Im zweiten Teil habe ich mittels statistischer Analysen die Auswirkungen von Schwankungen im zeitlichen Auftreten und Saisonalität von Niederschlägen auf die saisonale Getreideproduktion untersucht. Dabei wurden, basierend auf dem globalen Niederschlagsdatensatz CHIRPS, vier wesentliche zeitliche Regenattribute abgeleitet und untersucht: der Saisonalität, Startzeitpunkt, Dauer sowie Ende der Regenzeit. Die Ergebnisse unterstreichen die wesentliche Bedeutung der Regenregime für die Getreideproduktion. In Regionen mit unimodalen Regenregimen wird die Getreideproduktion hauptsächlich vom Startzeitpunkt der Regenzeit beeinflusst. Ein späterer Startzeitpunkt der Regenzeit führt zu Ernteverlusten (im Durchschnitt etwa 1.5% je 5 Tage Verzögerung), was die Bedeutung einer auf den Startzeitpunkt der Regenzeit ausgerichteten Aussaat unterstreicht. In Regionen mit bimodalen Regenregimen wurde die Saisonalität des Niederschlags (also die monatliche Verteilung der Niederschläge) als Haupteinflussfaktor der Getreideproduktion identifiziert. In diesen Regionen könnten Massnahmen zur längerfristigen Erhaltung der Bodenfeuchte eine ertragreichere Getreideproduktion sichern.

Im dritten Teil habe ich das wasserbegrenzte, erreichbare Ertragspotenzial (AY) für landwirtschaftliche Flächen in Äthiopien bewertet. Dazu wurde ein agrohydrologisches Modell entwickelt, das klimatische, hydrologische und agrarische Interaktionen kombiniert und auf gegenwärtige und zukünftige Klimaszenarien angewendet. Mithilfe regionaler Variationen basierend auf den regionalen klimatischen Regimen, wurde der durchschnittliche AY für die Hauptanbausaison (Meher) und die kurze Anbausaison (Belg) mit 79% bzw. 37% (des nicht wasserbegrenzten Ertragspotenzials) bestimmt. Die prognostizierten klimabedingten Veränderungen des AY in Meher-produzierenden Regionen reichen von -5% bis 5%, wobei in semiariden Regionen erhebliche Abnahmen hauptsächlich unter dem Szenario hoher Emissionen bis zum Ende des Jahrhunderts beobachtet werden. Im Gegensatz dazu werden in Belg-produzierenden Regionen bis zum Ende des Jahrhunderts erhebliche Zunahmen des AY

um bis zu 20% erwartet. Ausserdem wurde eine erhebliche Ertragslücke zwischen tatsächlichem und wasserbegrenztem Ertrag identifiziert, was die Notwendigkeit betont, grüne Wasserbewirtschaftungsstrategien mit verbesserten agronomischen Praktiken umzusetzen, um diese zu erwartende Ertragslücken zu schließen.

Letztendlich wurden das aktuelle Potenzial und die Auswirkungen zukünftiger Veränderungen der agroökologischen Eignung von Kulturpflanzen in der RFA-Region Äthiopiens mithilfe eines numerischen Modells zur Beurteilung der Eignung von Anbauflächen untersucht. Dieses Modell basiert auf Beziehungen zwischen beobachtetem Getreideertrag und verschiedenen Klima- und Bodenfaktoren. Sorghum wurde als die vielseitigste Kulturpflanze identifiziert, wobei fast zwei Drittel der bewirtschaftbaren RFA-Flächen geeignet sind, gefolgt von Teff und Mais, für die jeweils mehr als die Hälfte der bewirtschaftbaren RFA-Flächen geeignet ist. Weizen ist die am wenigsten vielseitige Kulturpflanze mit weniger als einem Drittel der bewirtschaftbaren RFA-Flächen, die dafür geeignet ist. Es ist zu erwarten, dass der Klimawandel die zukünftige Eignung von Anbauland erheblich beeinflussen wird. Die prognostizierten Auswirkungen umfassen Verschiebungen von Tiefland- zu Hochlandgebieten für Mais und Hirse sowie Verluste an geeigneten Flächen für Teff und Weizen. Diese Auswirkungen haben grundlegende Konsequenzen für die zukünftige Verfügbarkeit von Anbauflächen in Äthiopien und unterstreichen die dringende Notwendigkeit nachhaltiger Anpassungspläne und Agrarpolitik.

Acknowledgements

This thesis research project was funded by ETH for Development (ETH4D), ETH Zurich, through the E4D Doctoral Scholarship Program, generously supported by the Sawiris Foundation for Social Development and the Swiss Agency for Development and Cooperation. I am deeply grateful to ETH4D for the opportunity that enabled me to delve into this important topic.

The Hydrology and Water Resources Management (Hydrol) Group at the Institute of Environmental Engineering has been my academic home at ETH Zurich for the last 4.5 years, providing me with the facilities, scientific support, and funding for the final year of my thesis. I sincerely thank Prof. Dr. Paolo Burlando and Prof. Dr. Peter Molnar for welcoming me into the group and for their incredible support towards the successful completion of my PhD thesis. I would also like to express my gratitude to Ms. Manuela Haas for her assistance with all administrative matters.

My thesis research received incredible scientific support from many scientists who rallied around me. In this regard, my special thanks go to my supervisor, Prof. Peter Molnar, for his amazing guidance. Peter's support was unwavering from the conception of this research topic in 2018 to the successful completion of the project. It has been a tradition for me to walk into his office with unclear thoughts or rough drafts in PowerPoint and return to my desk with a clear idea after fruitful and often lengthy discussions. My heartfelt gratitude also goes to my second advisor, Prof. Dr. Nadav Peleg, whose active involvement and invaluable contributions remarkably improved the quality of my thesis work throughout. Nadav's prompt and insightful engagements have always motivated me to move forward. The agroecological aspect of my thesis was backed by my co-supervisor, Prof. Dr. Johan Six, and his Sustainable Agroecosystems (SAE) Group at ETH Zurich. Thank you very much, Jo, for your important contributions and for welcoming me into SAE. I have also greatly benefited from the annual thesis committee meetings within the Science and Policy PhD program, in which I have participated. Once again, I express my gratitude to Prof. Molnar, Prof. Burlando, Prof. Six, and Prof. Peleg for serving on my thesis committee. I thank all my co-authors for their enriching contributions to the articles we published. It has been an honor working with all of you.

Work-family-social balance has been an important issue for me during this journey. I am extremely grateful to Dr. Darcy Molnar and her family for their kindest and extraordinary care and support. The story of my PhD journey began in 2018 during a field excursion to Maggia Valley in southern Switzerland, part of the MAS program coordinated by Darcy. It was during this time that Darcy first planted the seed of pursuing a PhD at ETH Zurich, offering encouragement and valuable insights into funding opportunities. From that initial spark to the completion of my doctoral studies, Darcy's support has been invaluable, spanning both academic and social spheres. I extend my gratitude to Ms. Patricia Heuberger for her incredible assistance in facilitating my family's relocation to Switzerland. As the former Head of Funding Programmes at ETH4D, Patricia's feedback on my annual progress reports have been inspirational for my journey. My appreciation to Dr. Anna Costa and her family for the enriching family experiences and thoughtful support. My sincere thanks also go to Zusanna and Silvan Ragettli for their amazing neighborhood and, most importantly, for graciously sharing their garden with my family. Being in such a welcoming social environment made us feel truly fortunate and at home.

My profound thanks to my current and former colleagues and friends at Hydrol: Jovan Blagojevic, Jessica Droujko, Stefano Martinetti, Sophia Demmel, Ludovico Agostini, Tamirat Haile, Yue Zhu, Marius Floriancic, Scott Sinclair, Sasha Löffler, Dennis Eberli, Sebastian Moraga, Chunming Sui, Jacob Hirschberg, Giulia Battista, Martina Botter, Elena Leonarduzzi, and Gianluca Bergami. Your scientific feedback and input have been instrumental. The moments we shared during lunches and coffee breaks, our group retreats, and your support for me and my family were stunning. My appreciation also goes to all the members of the SAE Group for the scientific experiences we shared.

The love and support of my family have been a source of strength for me. I express my deepest thanks to my mom, Asoo, for her empowering and encouraging words. A special thanks to my sweet-hearted sister, Gete, who gave me 'her own chance' to go to school (a long story in short), and to my brothers, Ejara, Mamo, Asmera, Hora, and Tashe, who have always motivated me to work hard and move forward. Finally, I would like to thank my wife, Berile, for standing by my side, supporting me, and taking care of our children.

List of Abbreviations and Acronyms

AED	Atmospheric Evaporative Demand
AgSS	Agricultural Sample Survey
AMC	Antecedent Moisture Condition
AUC	Area Under the Curve
AY	Attainable Yield
C3S	Copernicus Climate Change Service
CDS	Climate Data Store
CHIRPS	Climate Hazards Infrared Precipitation with Station
CHIRTS	Climate Hazards Infrared Temperature with Station
CLS	Cropland Suitability
CN	Curve Number
CSA	Statistical Service Agency of Ethiopia
Dp	Deep Percolation
DSI	Dimensionless Seasonality Index
ECMWF	European Center for Medium-Range Weather Forecast
ENSO	El Niño Southern Oscillation
ESI	Evaporative Stress Index
ETa	Actual Evapotranspiration
ETo	Reference Evapotranspiration
FAO	Food and Agriculture Organization
FC	Field Capacity
GCM	Global Circulation (Climate) Model
GCM	Global Circulation Model
GHCN	Global Historical Climatology Network
GHG	Greenhouse Gas
GWA	Green Water Availability
IDW	Inverse Distance Weighted Interpolation
IGDW	Inverse Generalized Distance Weighted Interpolation
ITCZ	Intertropical Convergence Zone
LOOCV	Leave-Out-One Cross Validation
LR	Linear Regression
MAE	Mean Absolute Error
NDC	Nationally Determined Contribution
NMSA	National Meteorological Service Agency of Ethiopia
PYR	Partial Yield Response

QM	Quantile Mapping
RAW	Readily Available Water
RE	Relative Entrophy
RF	Rainfall
RFA	Rainfed Agriculture
RMSE	Root Mean Squared Error
ROC	Receiver Operating Characteristics
Rs	Short wave radiation
S2C	Sand-to-Clay ration
SDG	Sustainable Development Goals
SI	Suitability Index
SM	Soil Moisture
SMD	Soil Moisture Deficit
SOC	Soil Organic Carbon
SSA	Sub-Saharan Africa
SSP	Shared Socioeconomic Pathways
SST	Sea Surface Temperature
STRM	Shuttle Radar Topography Mission
TCP	Total Cereal Production
UN	The United Nations
UNDP	United Nations Development Program
WMO	World Meteorological Organization
WP	Wilting Point
Ya	Actual Yield
Yp	Potential Yield
Yw	Water-limited Yield

Table of Contents

List of Figures

List of Tables

Chapter 1

Introduction

1.1. Background

1.1.1. Agriculture and sustainable development

Agriculture is at the center of global development topics, and one of the top prioritized sectors for the achievement of the United Nations (UN) Sustainable Development Goal (SDG) of the Agenda 2030 (Rockström et al., 2010). On one hand, it is an indispensable sector that is key for global food security, as emphasized by SDG 2 (UN, 2015), which envisages the eradication of hunger, ensuring food security, improving nutrition, and promoting sustainable agriculture (Fig. 1.1). In the long-term, global food production should sustainably intensify in order to the feed the growing global population, projected to reach 9.8 billion by 2050 (FAO, 2023). On the other hand, the development of the agriculture sector is crucial for economic growth of nations and livelihoods of the majority of the rural population (World Bank, 2003).

A recent report by the United Nations Development Program (UNDP) and Oxford Poverty and Human Development Initiatives (OPHI) shows that an estimated 84% of the all poor people across the globe live in rural areas (UNDP and OPHI, 2023), with the highest number residing in Sub-Saharan Africa (~445 million) followed by Southeast Asia (~340 million). In Ethiopia, the nation with an estimated population of over 107 million (CSA, 2023), a World Bank survey in 2016 showed that the poverty rate (the percentage of population living on less than US$1.9 per person per day) in the rural area was 26%, which is over 21 million people (World Bank, 2020). Because of the strong reliance of the rural population on agriculture, poverty rate is highest in the agricultural sector (Castañeda et al., 2016; World Bank, 2022). Development of the agriculture sector is thus considered as a fundamental step towards the eradication of poverty (SDG 1), especially in rural areas (FAO, 2015a).

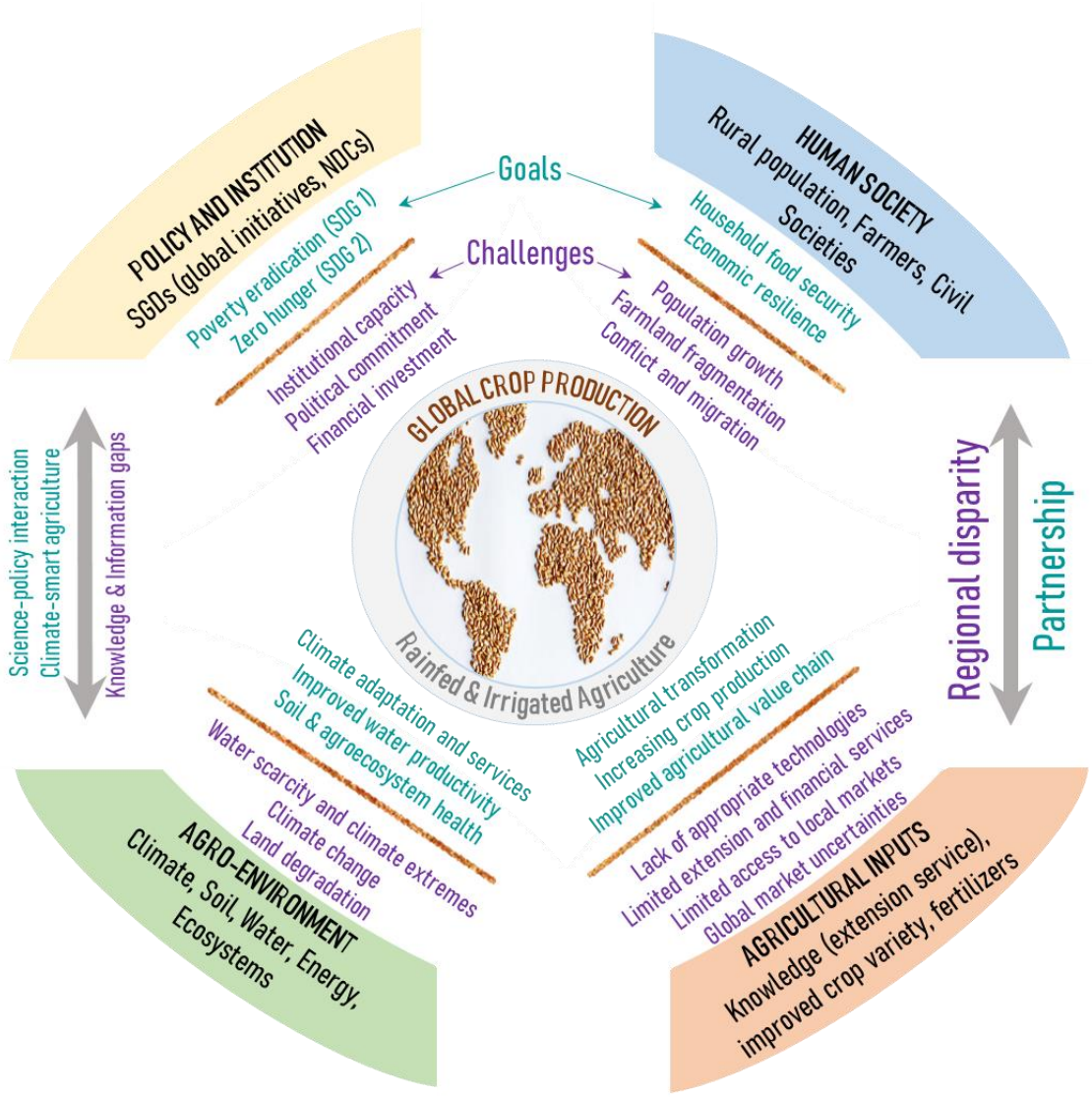

Fig. 1.1: Summary sketch illustrating the various dimensions of agriculture-centered development goals and highlighting the multiple challenges impeding their achievement, as conceptualized based on the literature used in this chapter). NDCs: Nationally Determined Contributions, SGDs: Sustainable Development Goals

1.1.2. Trends in global cereal production and regional disparities

Global food production has undergone significant increases over the past decades. For example, over the last 30 years (1992-2021), per capita cereal production (global average is 704 kg per person per year) has been rising by 7 kg every year, while cereal crop yields (global average is 3.2 ton/ha) have been increasing at a rate of 0.06 ton/ha per year (Ritchie et al., 2023) due to improvements in agricultural inputs and technologies as well as expansion of croplands.

However, these developments are marked by noticeable regional disparities. While agro-environmental resource (climate, soil, water, light and plant genetics) limitations fundamentally determine agricultural productivity of regions, the institutional dimension is also a decisive factor of the development of these agro-environmental resources and the improvement of productivity (Glover et al., 2019; Ofori et al., 2021; von Braun and Birner, 2017). Agricultural technology utilization, policies and regulations (including subsidies and market pricing), financial investment, and political commitment (governance), among others, are the key aspects of institutional dimensions that influence agricultural productivity (Godfray et al., 2010).

In the context of Africa, institutional capacity and governance is major limitation to agricultural productivity (Benin et al., 2016; Byerlee et al., 2007; Conway and Schipper, 2011; Vogel et al., 2019). Referring back to the global agricultural production data from Our World in Data (Ritchie et al., 2023), we find that the average per capita cereal production in Africa, considering the last three decades (1993-2021), is 152 kg (only 20% of the global average), the lowest in the world. Similarly, the average cereal crop yield of 1.5 ton/ha, which is also the lowest and 44% of the global average, is recorded in Africa. In countries where policies and institutional initiatives facilitating better agricultural inputs, extension services and the expansion of croplands were in place, promising performances have been witnessed (OECD and FAO, 2016). In Ethiopia, for example, per capita cereal production has been increasing at 6 kg per year, close to the global average rate, while cereal crop yield has been increasing at 0.07 ton/ha per year (more than the global growth rate). Nevertheless, both the average per capita production and yield (182 kg/person and 1.7 ton/ha) are still much lower than the global average (Ritchie et al., 2023), highlighting the urgent need to address institutional, technical and technological constraints to increase productivity (Hillocks, 2014).

1.1.3. Crop production under global change

The efforts to ensure future food security and alleviate poverty also face significant challenges from ongoing and emerging global changes, particularly climate change, land degradation, and conflicts (Hirons et al., 2020; Manaye et al., 2023; Prăvălie et al., 2021; Rosenzweig et al., 2014; Tenzing and Conway, 2023; Webb et al., 2017). East Africa in general and Ethiopia in particular is exceptionally prone to drought (Masih et al., 2014), with a longstanding history of drought-conflict co-occurrences (Anderson et al., 2021; Raleigh and Kniveton, 2012). The

frequency of these events has demostrateably increased over the recent decades (Kimutai et al., 2022; Palmer et al., 2023) and is projected to rise further under future climate conditions (Ahmadalipour et al., 2019; Haile et al., 2020), amplifying both their occurrence and overall risk.

Climate impacts and risks in agriculture are primarily associated with increases in temperature and rainfall uncertainty (FAO, 2008). The effects of temperature are two-fold: firstly, it defines the agroecological limits of crops through thermal stress effects (Burke et al., 2009; Eyshi Rezaei et al., 2015), and secondly, it determines crop water demand through evapotranspiration (Allen et al., 1998). Additionally, changes in temperature have been observed to impose external challenges, including pest and disease pressure (L. Schneider et al., 2022; Singh et al., 2023), and result in major postharvest losses (Tefera, 2012). On the other hand, rainfall determines crop water supply, either directly in the form of green water (soil moisture recharged from infiltrated rainfall) in rainfed systems, or indirectly in the form of blue water from surface and groundwater resources in irrigated systems (Chiarelli et al., 2020; FAO, 2018; Rosa et al., 2018). It is notable that at least three-quarters of the global cropland is under rainfed agriculture (RFA), which relies on green water flow, producing nearly 60% of the global food crops (Molden, 2007; Rockström et al., 2009). In Sub-Saharan Africa (SSA) in general, and in Ethiopia in particular, smallholder farms (landholding of 2 hectares or less) dominate food production, with about 95% of the cropland under RFA practices (FAO, 2015b; Mutimura et al., 2018).

1.1.4. Rainfed agriculture and future food and livelihood security in Africa

There is a widespread argument that RFA has the potential to generate sufficient food for the global population if the current green water productivity is enhanced (e.g., Falkenmark, 2013; Mekonnen and Hoekstra, 2011; Molden, 2007b; Rockström et al., 2009; Sposito, 2013). Improved green water management also includes the co-management of green and blue water resources, for example through supplementary irrigation and water harvesting, in order to increase and stabilize yields (Rockström et al., 2009; Studer, 2021). However, investments in agricultural water management in SSA, from both private and public sectors, have disproportionately favored irrigated agriculture, undermining the development of the RFA sector (Abrams, 2018; Leal Filho et al., 2022).

This bias arises from the perception that irrigated agriculture carries lower risk and higher productivity compared to rainfed systems, where water availability is largely uncertain during the growing season, leading to higher yield fluctuation and risk of under-productivity (Falkenmark, 2013). In fact, Africa has still immense irrigation potential that could be developed to complement the rainfed systems in order to boost agricultural production on the continent (Altchenko and Villholth, 2015; You et al., 2011). Nevertheless, there are physical, socioeconomic and environmental sustainability considerations that necessitate RFA receive equal if not more attention (Abrams, 2018; Molden, 2007a).

One crucial consideration that should be made in agricultural water management policies and regulations is to acknowledge the fact that not every plot can be irrigated due to physical blue water scarcity and topographic constraints (Falkenmark, 2013). Conversely, improved green water management is needed at every plot, even in conditions of excess rainfall, to maintain optimal green water availability and to maximize crop productivity (Borgomeo et al., 2020). Public sector investments in agricultural water management in regions like SSA, where economic water scarcity is widespread (Liu et al., 2017; Rosa et al., 2020), need to be efficient and fair to achieve the food security and poverty reduction targets (Cooper et al., 2008). In this regard, investment in RFA systems development is believed to be more effective both in terms of cost and anticipated benefits leading to yield enhancement (Abrams, 2018). Unlike irrigated agriculture, which is associated with various environmental impacts such as blue water withdrawal with no or less return flow and soil salinization (Poore and Nemecek, 2018), green water management largely brings environmental benefits, especially in terms of soil conservation and soil regeneration (Descheemaeker, 2020; Hurni, 2016; Studer, 2021).

In summary, green water management is crucial for enhancing crop yields, thereby improving food security and incomes for smallholder farmers. In the long term, this contributes to building household resilience and collectively supports the achievement of sustainable development goals at both national and global scales. Despite this potential, addressing the impacts of climate change requires additional considerations (Fig. 1.1). It is widely agreed that tackling this issue necessitates coordinated, committed, and continuous efforts from multiple actors in science, practice, and governance, with farmers at the center (e.g., Anderson et al., 2020; Howden et al., 2007; Studer, 2021). These efforts are crucial for creating a better understanding of problems and pursuing of solutions through participatory research, future scenario analysis, co-creation of knowledge, development and adoption of technologies, and the establishment of

institutional, policy, and regulatory frameworks that facilitate sustainable practices (OECD, 2023). Our knowledge and information on weather and climate dynamics, and their influences on crops at various spatial and temporal scales, form one of the key parts of the holistic efforts toward building climate-resilient RFA systems.

The purpose of this thesis is to provide in-depth analyses of the climate-crop and climate-agroecological relationships (the agro-environmental dimension in Fig. 1.1) to inform climate risk and water management planning, decisions and policy making in the context of Ethiopia. Due focus is given to research gaps that are crucial for nationally determined contributions to SDGs and long-term agricultural transformation, as well as national climate adaptation plans in Ethiopia.

1.2. State of research and gaps

1.2.1. Global datasets for agro-environmental applications

High quality climate data is a prerequisite for agro-environmental research and operational activities. Over the last three decades, mainly following the advent of satellite remote sensing technologies, several global, quasi-global, and regional gridded datasets have been developed, offering spatio-temporally continuous fields of climate variables (e.g., Beck et al., 2019; Funk et al., 2015; Harris et al., 2020; Hersbach et al., 2020; Karger et al., 2020; Muñoz-Sabater et al., 2021; Saha et al., 2010; Sheffield et al., 2006; Tang et al., 2022; Verdin et al., 2020). These datasets, mainly precipitation, can be categorized based on underlying data sources and techniques used to generate them as: satellite estimates, gauge-interpolated, combined gauge and satellite estimates, reanalysis, and merged multi-source products (Degefu et al., 2022). The availability of gridded datasets has significantly overcome data limitations in data-scarce regions (Dembele et al., 2020; Sheffield et al., 2018). Additionally, the spatial and temporal continuity of these datasets has enabled a wide range of research and operational activities across various sectors, including agriculture, at local to global scales (Joseph et al., 2020; Pradhan et al., 2022).

One of the most relevant applications of gridded datasets is the analysis of rainfall variability and its teleconnections with sea surface temperature (SST) anomalies and oceanic phenomena. This is particularly evident in the context of Ethiopia and East Africa where distinct behaviors of the rainy seasons are significantly influenced by these teleconnections (Alhamshry et al.,

2020; Broman et al., 2020; Degefu et al., 2017; Dubache et al., 2019; Gleixner et al., 2017; Taye et al., 2021; Viste and Sorteberg, 2013; Zaitchik, 2017). These studies suggest that wetter than normal rainfall conditions during June to September (kiremt) across the main producing regions (central, western, and northwestern parts) of Ethiopia are largely associated with negative Equatorial Pacific and Tropical Atlantic SST anomalies, and vice versa. Conversely, the rainfall climate over the southern and southeastern parts of the country during February to May (Belg) is positively correlated with Equatorial Pacific SST and Indian Ocean Dipole. This understanding has improved the predictions of rainfall by enhancing the forecast skills of seasonal forecast models (Ehsan et al., 2021; Taye et al., 2021).

Gridded climate datasets have played a crucial role in characterizing past and recent drought episodes in a spatially explicit way (Agutu et al., 2020; Alasow et al., 2023; Degefu and Bewket, 2023; Gebrechorkos et al., 2020; Gebremeskel Haile et al., 2020; Philip et al., 2018; Tierney et al., 2015; Viste et al., 2013). Past studies found increased drought frequency, duration and impacts since 1980s, particularly in the recent years (Kimutai et al., 2022), with a projected intensification in the future (Haile et al., 2020) over the East African region. Such gridded climate datasets provide great potential for the analysis of climate-induced uncertainties and risks in crop production (Kamali et al., 2022, 2018a), for assessing the vulnerability of the agricultural sector (Kamali et al., 2018b; Shukla et al., 2021), identifying hotspot areas for prioritized risk management and response actions. Local response actions in agriculture require information at high spatial details, derived from high-resolution, accurate climate datasets.

Gap 1: We need to enhance the accuracy and spatial resolution of gridded climate datasets for local applications in agrometeorological research and practice.

Despite the indispensable value of gridded climate datasets in data-scarce countries like Ethiopia, there are limitations in accuracy and spatial resolution. These features are particularly crucial in agrometeorological operational and research exercises, where accurate climate information is needed for local-level decision-making (Dinku et al., 2014; RICCAR, 2022). Specifically, good quality data of precipitation and temperature, which primarily determine atmospheric moisture supply and demand, are needed to extract useful information from them (Dembele et al., 2020; Lobell and Burke, 2008).

The accuracy of gridded datasets is influenced by the quality and availability of the station observations used in the station-interpolated gridded dataset and the uncertainty in the satellite observations assimilated into the satellite-based and reanalysis products (Joseph et al., 2020). To make these datasets suitable for local applications, it is essential to balance the tradeoffs between spatial continuity and data accuracy. This can be achieved by incorporating local climate statistics (Chaney et al., 2014; Collins, 2011; Dinku et al., 2018b). Such an approach is particularly crucial for addressing data quality issues, especially for variables like air temperature, which is currently limited in terms of availability and spatial resolution compared to precipitation datasets (Dembele et al., 2020).

1.2.2. Climate risk reduction in crop production through informed actions

As the triple challenges of food security, poverty, and climate vulnerability, strongly linked to smallholder RFA systems in SSA, become increasingly urgent in the face of climate change, the importance of climate information for strategic planning and decision-making becomes paramount (Simpson et al., 2021; Trisos et al., 2022). The types of information needed differ across scales. At the national level, climate information is essential for designing agricultural policy frameworks that encompass broader responses, such as finance, infrastructure, institutional setup, and agricultural services, including climate services, that facilitate decisions and actions toward building climate-resilient agricultural systems (Howden et al., 2007).

The climate information needed for informed actions at national scale is primarily aimed for a broader understanding of the system across the geographic domain and long-term changes in time, through impact, adaptation, and risk management researches based on state-of-the-art climate data analyses, crop-climate modelling, and field investigations (Cooper et al., 2008). Alongside long-term impact information, local decisions, on the other hand, mostly rely on daily to monthly forecast information. This type of information is crucial for farmers to schedule their agricultural operations (Antwi-Agyei et al., 2021; Chiputwa et al., 2022).

Nevertheless, the use of climate information faces challenges due to systemic barriers in its production and utilization. Traditionally, information producers determine the purpose and access of climate information, while users (such as farmers, planners, and policymakers) decide whether to use it based on their awareness, experience, usefulness of the information, and trust. This dynamic undermines the anticipated impacts on the ground (Tall et al., 2018; Vogel et al.,

2019). In recent climate service practices, the principles of co-production, representing non-linear processes where stakeholders actively participate in the production of climate information, have been proposed and implemented to demonstrate promising impacts (Conway and Vincent, 2021; Dinku et al., 2022). Co-production of climate information not only enhances transparency and trust in the climate information production, thereby creating demand and promoting its uptake, but also improves the climate information production process itself through stakeholder engagement (Grossi and Dinku, 2022a, 2022b).

Among the most crucial climate information for rainfed farmers are the timing and temporal distribution of growing season rainfall, as these directly influence moisture availability during the growing period to cover crop water requirements (Guan et al., 2015; Torres et al., 2019). The occurrence of pre-onset rain events serves as a crucial signal for smallholder farmers in Ethiopia, indicating when it is time to commence tillage operations for subsequent planting (Temesgen et al., 2008). The subsequent onset of the rainy season marks the typical planting time for major cereals such as maize, sorghum, barley, and wheat (Ademe et al., 2020; Lala et al., 2021). Delays in the rainy season serve as an early indication of subsequent dry spell periods and potential drought conditions (Kimutai et al., 2022; Raes et al., 2004). The temporal distribution (seasonality) of rainfall over the year determines crop water stress conditions at various growth stages, and in turn, it influences the final crop yield (Barron et al., 2003; Prasad et al., 2018).

The onset of the rainy season in Ethiopia is closely correlated with the low-frequency climate signals in oceanic and atmospheric variables. In their prediction of the June to September rainfall (kiremt) over Ethiopia, Lala et al. (2020) identified geopotential height and sea level pressure over the eastern Mediterranean and the Red Sea as important predictors of the rainy season onset. Interestingly, they also reported that the association between SST and kiremt rainfall onset is insignificant. This is in contrast to the significant correlation observed between anomalies of kiremt rainfall magnitude and SST anomalies over various regions of the Pacific, Atlantic (including the Gulf of Guinea), and Indian Oceans (Alhamshry et al., 2019; Diro et al., 2011a; Korecha and Barnston, 2007; Segele and Lamb, 2005; Seleshi and Camberlin, 2006). This difference in the teleconnections of rainfall timing and amount with oceanic and atmospheric variables offers the possibility of separate forecasts for the rainy season onset and the expected amount, both of which are highly relevant climate information in order to support farmers' informed actions.

Gap 2: The impacts of rainfall seasonality and timing on crop production across the RFA region of Ethiopia has not been adequately quantified.

The focus of previous studies (e.g., Kebede et al., 2017; Omay et al., 2023; Segele and Lamb, 2005) has predominantly been on characterizing the onset of growing season rainfall. However, the impacts on crop yield and associated risks stemming from variabilities in the temporal characteristics of growing season rainfall such as the onset, cessation, and seasonality, can vary across regions. Similarly, the agronomic and water management measures required to offset the impacts of delays in the rainy season, as well as the erratic distribution of rainfall during the growing period are likely to vary. To be able to propose effective measures, we need to understand the impact that variability in temporal characteristics of rainfall may have on crops.

One such measure involves selecting the planting date based on the rainy season onset to align the growing period with optimal conditions, ensuring that the crop receives sufficient moisture throughout its growth cycle (Lala et al., 2021; Minoli et al., 2022). This aspect of rainfall-crop relationship should be thoroughly investigated at local scales and the resulting information should be integrated into climate services or provided through extension services.

1.2.3. Enhancing water-limited yields in smallholder rainfed farming systems

Crop yield is the function of three levels of factors (Lobell et al., 2009; van Ittersum et al., 2013): The first level consists of the primary defining factors, namely, temperature, radiation, light, atmospheric CO_2 and cultivar characteristics. These dictate the theoretical (potential) yield when crops are grown under optimally provided water and nutrients, and fully controlled biotic stresses like weeds, pests and diseases. The second level factors, water and nutrients, are considered as yield limiting factors. In rainfed and deficit-irrigated systems with optimal nutrient supply and biotic stresses fully controlled, the maximum yield that can be attained under these conditions is considered as the water-limited yield potential. The third level encompasses biotic factors, also known as yield reducing factors. These controllable factors determine the actual yield depending on how farmers manage their crops.

The limitations of rainfall in rainfed systems are related mainly to characteristics such as rainfall depth, intensity, and duration at the event scale, as well as timing, cumulative amount, and temporal distribution at the seasonal scale (Porporato et al., 2004). Biophysical factors such as soil properties, terrain slope, and surface characteristics, influence the partitioning of

incoming rainfall between surface runoff and infiltration—the component constituting green water that crops access, and deep percolation that recharges groundwater (Falkenmark and Rockström, 2004; Rockström and Falkenmark, 2000). The extent to which available green water satisfies crop water needs and atmospheric evaporative demand determines crop water stress and, subsequently, water-limited yields (Barron et al., 2003; Hatfield and Dold, 2019).

To reduce crop water stress, management interventions that are currently in practice focus on modifying biophysical factors. Water harvesting (retaining) techniques allow, among other benefits, for the diversion of more rainwater to infiltration, thereby increasing green water storage (Hurni, 2016; Makurira et al., 2009; Marval et al., 2022; Studer, 2021). Enhancing green water use efficiency is in principle achievable through the shift of non-productive evaporative loss to productive plant transpiration. This needs to be combined with improved soil nutrient management and good crop protection, and improved crop variety that provides high harvest index, i.e., yield to biomass ratio (Falkenmark, 2013; Rockström, 2003; Rockström et al., 2009; Studer, 2021). Furthermore, agronomic measures such as rainfall onset-informed planting, as discussed earlier, can significantly boost seasonal green water use and reduce water-limited yield gaps (Fatima et al., 2020; Lala et al., 2021).

Gap 3: The current potential and climate-driven changes in water-limited yields for sustainable intensification of RFA in Ethiopia has not been analyzed in depth.

Yield gaps in rainfed systems, which is the difference between the water-limited yield and actual yield, can be very large in countries like Ethiopia (Van Ittersum et al., 2016). This underscores significant untapped potential crucial for achieving a country's development goals (FAO, 2015b; Godfray et al., 2010). Van Dijk et al. (2020) identify four components contributing to yield gaps that hinder reaching the water-limited yield. These components include technical efficiency yield gaps arising from agro-environmental resource management inefficiencies, allocative yield gaps caused by limited resource allocation, economic yield gaps related to issues in the production-marketing chain, and technological yield gaps resulting from a lack of appropriate technology. In addition to these gaps, climate change is anticipated to exacerbate rainfall variability and uncertainty, and intensify atmospheric evaporative demand, further reducing the attainable water-limited yield (Burke et al., 2009; Getnet et al., 2022; Rosenzweig et al., 2014; Van Ittersum et al., 2016). Therefore, understanding the current water-limited yield potential and its changes under future climates is of paramount importance for

sustainable RFA intensification and the planning of adaptation actions. In this regard, the Global Agro-Ecological Zones (GAEZ) database (Fischer et al., 2021), developed jointly by the International Institute for Applied Systems Analysis (IIASA) and the Food and Agriculture Organization (FAO), offers extensive agroecological spatial datasets worldwide, encompassing agro-environmental resource distribution, crop production suitability, and potential yield at a grid scale. However, in-depth analyses incorporating state-of-the-art input data and modeling techniques are needed to deepen our understanding of specific contexts, such as Ethiopia.

1.2.4. Adaptation to agroecological shifts under changing climate

Crop production challenges are often viewed from the yield gap perspective, which is influenced by water and nutrient availability as well as crop management to control various yield-reducing elements (Ittersum et al., 2013; Rong et al., 2021; Zhao et al., 2017). However, agroecological condition is also a key perspective determining cropland availability. The yield-defining factors, particularly temperature, constrain crop yield through their influence on crop physiology (Minoli et al., 2022; Ramankutty et al., 2002). As a result, crops can only survive within a specific temperature range, limiting also the topographic extent of a crop (Hatfield and Prueger, 2015; Zabel et al., 2014). In dry areas where irrigation systems cannot be established due to physical and economic water scarcity, rainfall climate also becomes a defining factor for crop niches (Kazemi and Akinci, 2018; Mesgaran et al., 2017).

Climatic factors combined with soil and topographic characteristics describe the suitability of agroecological zones for a specific crop. Steep topographic slopes are less suitable for crop cultivation due to the shallow root zone depth that the soil can provide, severe soil erosion risk, and inconvenience for agricultural operation (Ebabu et al., 2023; Eweg et al., 1998; Hurni et al., 2010). Croplands that are topographically suitable, exhibit various soil physical, chemical and biological properties that further influence their suitability. For example, soil texture, structure, and organic matter content govern water flow, storage in the soil, and consequently, water availability (Bonetti et al., 2021; Fatichi et al., 2016b; Pan et al., 2021). Soil salinity (commonly found in irrigated areas), acidity, and alkalinity represent major soil-related agroecological limitations that undermine cropland productivity, posing a significant challenge in Ethiopia as well (Desta et al., 2021; Ivushkin et al., 2019; Qureshi et al., 2019).

It is widely reported that climate change impacts on agroecological conditions is a major threat to the future global food production (Burke et al., 2009; Kummu et al., 2021; Lesk et al., 2022; J. M. Schneider et al., 2022b; Zabel et al., 2014). This involves a notable redistribution of global cropland, with a high risk of suitability losses in the tropics and an advantage of suitability gains in temperate regions, primarily following temperature warming (Kummu et al., 2021; Mbow et al., 2019; Ofori et al., 2021; Trisos et al., 2022). Additionally, cropland productivity faces increasing risks due to the combined pressures of a growing population and extreme climatic events that lead to land degradation (Muir and Smith, 2023; Webb et al., 2017). In summary, even though currently cultivated cropland of Ethiopia is known (Hurni, 1998), the potentially suitable crop agroecologies and how they will change in the future is largely unknown. This limits effective adaptation and local mitigation actions to minimize risks and increase resilience.

Gap 4: An in-depth understanding of the potential suitability of cropland and the foreseeable impacts of climate change for adaptation planning in Ethiopia is missing

To achieve the adaptation and resilience-building goals in rainfed systems in Ethiopia, future management interventions need to be comprehensive (Mbow et al., 2019), considering both agronomic and agroecological challenges. In this regard, understanding the untapped potential and challenges posed by climate change is crucial for informed adaptation planning and decision-making. Previous studies in this direction in Ethiopia were often limited by data availability and quality (Evangelista et al., 2013), with some focusing on local-scale assessments (e.g., Abebe et al., 2023; Gebresamuel et al., 2022). I believe the use of state-of-the-art climate and soil datasets offers a unique opportunity to analyze the limitations of key climatic and soil factors for present and future cropland suitability for multiple crops.

1.3. Research questions

In light of the research gaps identified in section 1.2, this thesis aims to address the following four general research questions (RQ).

RQ 1: How can we utilize low-quality station temperature observations for adjusting statistical biases and enhancing spatial details in gridded climate datasets for local applications?

To address this question, a statistical bias adjustment and downscaling framework that assimilates quality-controlled statistical information from ground station observations into gridded temperature datasets was developed. The framework involves the following main steps: i) extraction of quality-controlled local temperature statistics (mean and standard deviation) at monthly (climatology) and interannual timescales from networks of ground stations; ii) spatial interpolation of the temperature statistics using a hybrid approach that combines linear regression and inverse non-Euclidean distance weighting interpolation techniques; iii) bias adjustment of the gridded global temperature using a two-step quantile mapping bias-correction method; and iv) evaluation of the bias-adjusted dataset. This framework was implemented to produce Bias-Corrected and Downscaled ERA5-Land (BCE5) daily 2-m air temperature datasets at a 0.05° x 0.05° grid resolution with improved quality over Ethiopia. BCE5 that covers the period 1981-2010 is compatible with widely used high-resolution precipitation datasets like CHIRPS, making it suitable for a broad range of environmental applications, such as hydrology, agriculture, and ecology.

RQ 2: What are the influences of rainfall timing and seasonality on seasonal crop production and what implications do they have for agronomic and water management decisions across the RFA region of Ethiopia?

This research question was addressed by: i) defining the rainfall timing attributes -- onset, cessation and duration -- of the rainy season using cumulative rainfall anomaly curves, and analyzing their temporal variabilities and changes; ii) determining the rainfall seasonality based on an entropy-based dimensionless seasonality index representing the monthly distribution of the annual rainfall; iii) performing correlation and regression analyses to assess the relationship between crop production, and rainfall timing and seasonality. With these analyses the spatial variabilities of the responses of the major cereal crops cultivated in Ethiopia -- teff, maize, sorghum and wheat to these key temporal features of rainfall and based on the findings, implications for agronomic and water management have been indicated.

RQ 3: What is the current climatology of water-limited attainable yield potential under RFA practices, and how is it expected to change under future climate conditions in Ethiopia?

To address this question, an agrohydrological modelling framework was developed to simulate climatic-hydrological-crop interactions. This framework was applied to both present and future climates, derived from multiple Global Circulation Model (GCM) projections, to evaluate current green water availability and water-limited yield potential for major crops and to assess climate-driven changes during the growing seasons (June to September and February to May). The relative influences of rainfall and atmospheric evaporative demand on the future changes in water-limited yield potential was analyzed. The results are presented with a view towards the potential for sustainable intensification and climate resilience building through sustainable green water and soil management interventions.

RQ 4: What is the potential cropland suitability across the RFA region of Ethiopia and how will it change under the projected future climate?

To address this question, cropland suitability indices were constructed using numerical modelling approaches that integrate crop yield data with climatic and soil factors (texture, pH, and soil organic carbon) for four major cereal crops cultivated in Ethiopia. The suitability models were applied to soil factors and present and future climate data across the rainfed agricultural region of Ethiopia to map potential suitability and analyze projected changes. The produced potential suitability maps provide valuable insights that can guide the sustainable intensification of major cereal crops in Ethiopia. The presented predictions of changes in cropland suitability are crucial for adaptive land use and farm management planning, considering the climate and location contexts.

1.4. Thesis structure

This thesis addresses the formulated research questions in the following chapters 2 – 5 (see Fig. 1.2) by four research articles, followed by a conclusion in chapter 6.

In C**hapter 2,** the framework for bias correction and downscaling of temperature datasets in data-scarce regions (RQ 1), along with the resulting BCE5 dataset: “Gridded daily 2-m air temperature dataset for Ethiopia derived by debiasing and downscaling ERA5-Land for the

period 1981–2010", which was published by Wakjira et al. in Data in Brief is presented. The performance of the dataset and the utility of poor-quality station-observed temperature data is discussed. The open-access BCE5 data served as the reference temperature climate in the works presented in Chapters 4 and 5.

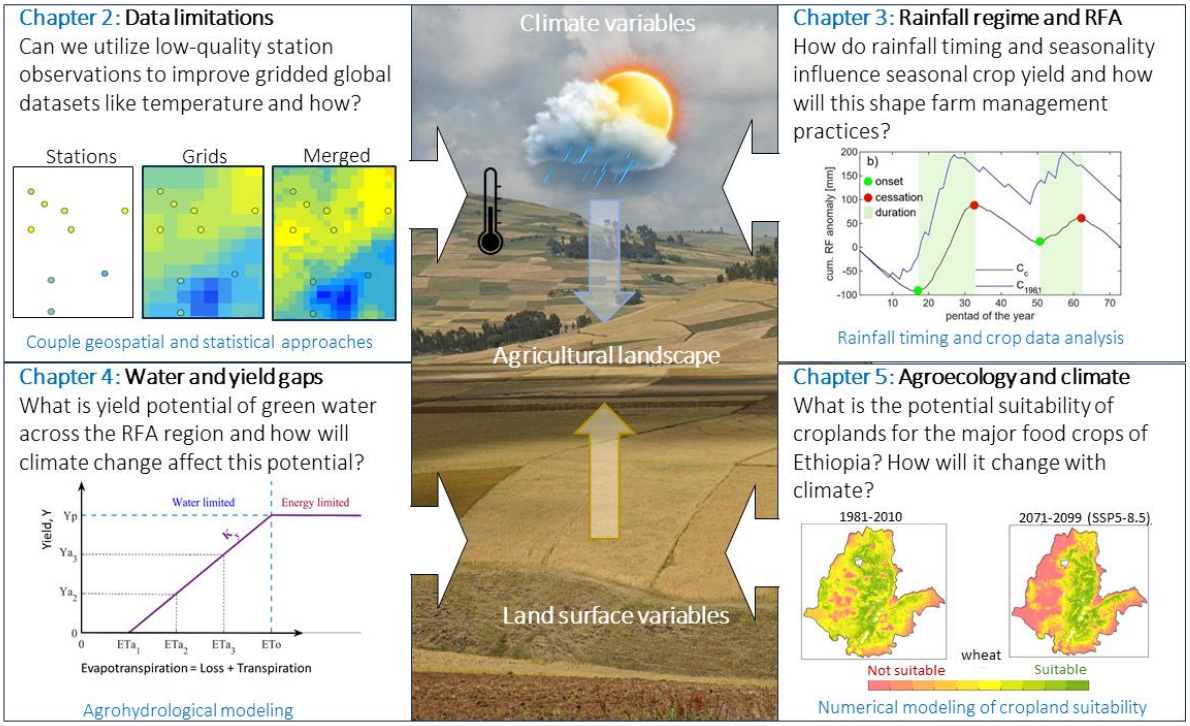

Fig. 1.2: Sketch of the thesis structure summarizing the research questions and the scope of the research. The background photo is from Wheat fields in the Arsi highlands, Ethiopia, 2015. (Photo: CIMMYT/ Peter Lowe). Link

In C**hapter 3,** the assessments of rainy season onset, cessation, duration and seasonality, and their effects on cereal crops produced in Ethiopia (RQ 2) are covered. The agronomic and water management implications of the influences in different rainfall regime across the RFA region of Ethiopia are highlighted. The research article was published as "Rainfall seasonality and timing: implications for cereal crop production in Ethiopia", by Wakjira et al. in Agricultural and Forest Meteorology.

In **Chapter 4,** RQ 3 is addressed by assessing the present climatology and future changes in green water availability and water-limited attainable yield. The relative influences of rainfall supply and evaporative demand on water-limited attainable yield are examined and it is discussed how these factors influence the adoption of adaptive water practices are examined.

The manuscript for this chapter is currently under preparation by Wakjira et al. for submission to Hydrology and Earth Systems Science.

In **Chapter 5,** the climate- and soil-defined potential cropland suitability under the present climate, and climate-driven future changes (RQ 4) is evaluated. The modes of changes in cropland suitability (altitudinal shifts and areal changes) are assessed. Rainfall and temperature sensitivity of the changes are also analyzed. The research article has been submitted as "Climate-driven changes in cropland suitability for cereal production across the rainfed agricultural landscapes of Ethiopia" by Wakjira et al. to Agricultural and Forest Meteorology.

In **Chapter 6**, the summary of the works covered in this thesis is presented, followed by a discussion on the scientific and practical relevance of this research. Finally, the limitations of the research and an outlook in the topic are presented

Chapter 2

Gridded daily 2-m air temperature dataset for Ethiopia derived by debiasing and downscaling ERA5-Land for the period 1981-2010

Author
Mosisa Tujuba Wakjira

Co-authors
Nadav Peleg, Paolo Burlando and Peter Molnar

Published in Data in Brief
Published online on 20 December 2022

Key finding

- Low-quality station observation data were systematically integrated with the ERA5-Land dataset.
- A temperature dataset with higher accuracy and spatial resolution was produced for Ethiopia.
- The new dataset has 68% more accuracy than the original ERA5-Land for maximum temperature.
- The uncertainty associated with data gaps in station observations was less than 0.25°C.

Author's contributions

Conceptualization, data collection and preprocessing, methodology, discussion, original draft, preparation, revision.

Co-authors' contributions

N. Peleg: methodology, discussion, reviewing and editing. ***P. Burlando***: discussion, review and editing. ***P. Molnar***: methodology, discussion, reviewing and editing, supervision.

Specifications table

Subject	Earth and planetary science
Specific subject area	Climate science, meteorology, hydrology, agriculture, forestry, and human and environmental-related subjects
Type of data	Raw Analyzed Derived
How the data were acquired	(1) Spatial downscaling of the raw ERA5-Land (ERA5L) maximum (Tx) and minimum (Tn) temperature from 0.1° x 0.1° to 0.05° x 0.05° using bilinear interpolation; (2) Spatial interpolation of the observed Tx and Tn statistics (mean and standard deviation) at 154 stations using an inverse generalized distance weighting technique; (3) Quantile mapping to adjust the statistical biases in the downscaled ERA5L Tx and Tn using the transfer function constructed from the observed temperature field; and (4) Evaluation of the dataset using the Leave-One-Out Cross-Validation method.
Data format	Figure Table Image NetCDF
Description of data collection	The daily temperature records for Ethiopia used as a reference for bias correction and spatial downscaling were obtained from 154 In-situ OBServed (IOBS) climate stations with record lengths ranging from 5 to 30 years between the period 1981-2010. The raw daily ERA5L Tx and Tn were retrieved from the hourly ERA5L 2-m air temperature.

Data source location	Raw ERA5L Tx and Tn dataset source: • Institution: European Center for Medium-Range Weather Forecast (ECMWF) • Data center: Copernicus Climate Change Service (C3S) Climate Data Store (CDS) • Website: https://cds.climate.copernicus.eu/cdsapp#!/dataset/reanalysis-era5-land?tab=form Observed Tx and Tn data source for stations in Ethiopia: • Institution: National Meteorological Service Agency of Ethiopia • City: Addis Ababa • Country: Ethiopia Observed Tx and Tn data source for stations in the neighboring countries: • Institution: National Oceanic and Atmospheric Administration (NOAA) • Dataset: Global Historical Climatology Network (GHCN) daily • Website: https://www.ncei.noaa.gov/products/land-based-station/global-historical-climatology-network-daily
Data accessibility	Dataset file name: BCE5.zip Repository name: ETH Zurich Research Collection Data identification number: 10.3929/ethz-b-000546574 Direct permanent URL to data: https://doi.org/10.3929/ethz-b-000546574

Value of the data

- The Bias-Corrected ERA5-Land (hereafter BCE5) temperature data is downscaled to a spatial resolution that matches common gridded precipitation products (such as the CHIRPS rainfall). Thus, it is highly convenient for use in combination with these datasets in a wide range of applications at national, regional, catchment and local scales.
- Compared to the raw ERA5L, BCE5 has an improved accuracy that is assimilated from the local temperature gradient at 154 ground observation stations, because the temperature statistics from the stations provide an unprecedented local temperature space-time variation for Ethiopia not incorporated in other gridded temperature datasets.

- The mean absolute errors in the BCE5 daily climatology are about 0.7°C for Tx and 1.1°C for Tn, reducing the statistical biases in the ERA5L Tx and Tn by 68% and 25% respectively. For monthly climatology, 40 - 64% of the biases were removed for Tx and while for Tn the reductions range from 19 - 32%.
- The BCE5 dataset is useful for researchers, practitioners, planners and decision-makers in various disciplines, for instance, agriculture, hydrology, and ecology, where weather and climate data are crucial.
- In particular, it can be used in climate impact assessment, heatwave and drought assessment, catchment hydrological modelling, crop growth modelling and monitoring, agricultural water management, water resources planning, ecological system monitoring, and understanding the complex water-energy-food-environment nexus in Ethiopia.

2.1. Data description

2.1.1. The bias-corrected dataset

The bias-corrected temperature dataset presented in this paper has a spatial resolution of 0.05° x 0.05°. It is available at daily time steps for the period 1981 – 2010 covering Ethiopia and areas within 20 – 30 km (i.e., 4 – 6 grids) outside the boundary of Ethiopia. The data raster has a geographic coordinate system (WGS 84). The data files are stored in NetCDF format -- a self-describing file format with an extension .nc that can be read and written using programming languages (Python, MATLAB, R, Ruby, IDL and Perl), programming interfaces (C, C++, Java, and Fortran), and graphical user interfaces like GIS. The dataset file is named "BCE5.nc" (stands for 'Bias-Corrected ERA5-Land') and has two climatic variables, the maximum and minimum daily temperature in °C. The variables of the BCE5.nc file are as follows:

- "Lat" is latitude in decimal degrees with a dimension of 260 x1
- "Lon" is longitude in decimal degrees with a dimension of 340 x 1
- "Time" is a time variable in days from 1981-2010 with a dimension of 10957 x 1
- "Tmax" is the maximum daily temperature in °C with a dimension of 260 x 340 x 10957
- "Tmin" is the minimum daily temperature in °C with a dimension of 260 x 340 x 10957

2.1.2. Input datasets

The input data used in the derivation of BCE5 are: the raw daily ERA5L Tx and Tn, the IOBS Tx and Tn statistics, and the Shuttle Radar Topography Mission (SRTM) digital elevation data. ERA5L (Muñoz-Sabater et al., 2021) is a high-resolution reanalysis global dataset of several land variables governing the water and energy cycles. It is produced by re-running the land component of the European Center for Medium-Range Weather Forecast (ECMWF) ERA5 climate model on an enhanced grid resolution (0.1° x 0.1°) at hourly time steps using the atmospheric forcing from ERA5 (Hersbach et al., 2020) as inputs, covering the period from 1950 to 2-3 months before the present time. The period 1981-2010 was considered for the derivation of the BCE5 dataset. The IOBS data at 146 stations were obtained from the National Meteorological Service Agency (NMSA) of Ethiopia, while the data for additional 8 stations in Eritrea, Kenya, South Sudan, and Sudan were collected from the Global Historical Climatology Network (GHCN) daily dataset (Menne et al., 2012).

Fig. 2.1 shows the digital terrain model of Ethiopia and the neighboring countries, and the spatial distribution of the IOBS stations. The IOBS datasets have enormous data gaps, which undermine the temporal continuity and overlapping of the time series. For this reason, the derivation of the BCE5 dataset was based on the first and second-order temperature statistics, rather than the complete IOBS temperature time series. The temperature data at the stations where the record is available for 5-30 years in the period 1981-2010 were used for the computation of the temperature statistics. The record length at the stations is indicated by the colors of the circles in Fig. 2.1. The IOBS temperature datasets follow closely a Gaussian distribution. This is illustrated in Fig. 2.2a and b, which indicate the probability density of the daily maximum and minimum temperatures respectively, at each station in Ethiopia. Fig. 2.2c reveals the estimates of uncertainties in the mean annual Tx and Tn temperature that is associated with the differences in record length.

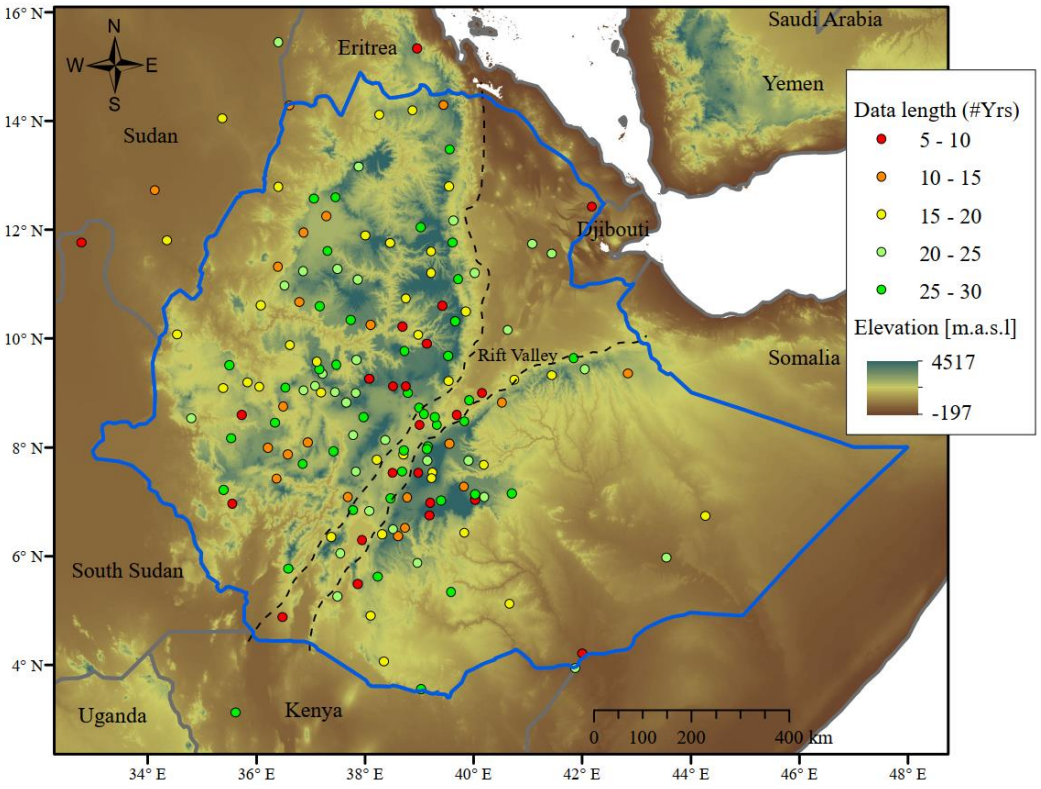

Fig. 2.1 The observed temperature station network used in this study and data record lengths in years (shown by the colors of the circles) from 1981 to 2010. The background feature is the SRTM digital elevation model (https://cgiarcsi.community/ last accessed in July 2021). The dashed lines show the approximate position of the Great East African Rift Valley in Ethiopia.

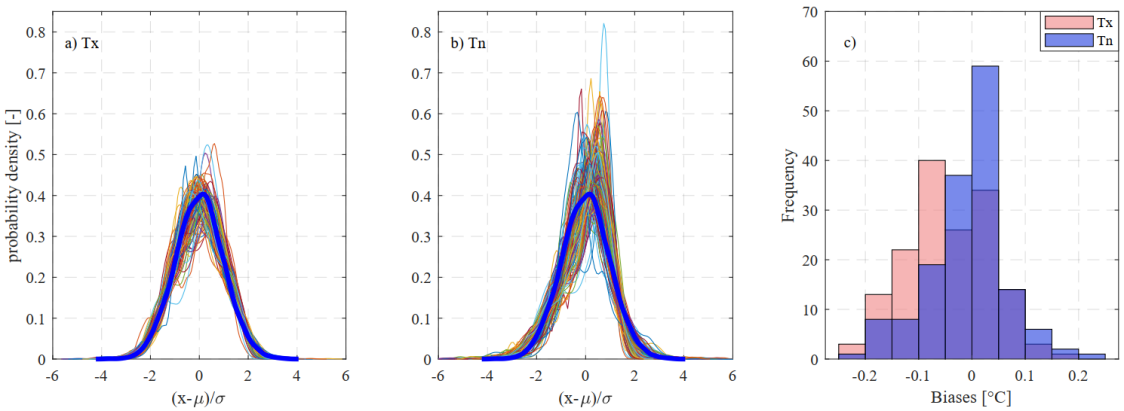

Fig. 2.2 Kernel densities of standardized a) maximum daily temperature (Tx) and b) minimum daily temperature (Tn) at 146 IOBS stations over the period 1981 – 2010. The thick blue kernels correspond to a standardized normally distributed set of random numbers with a sample size equal to the record length of a 30-year daily temperature dataset (n = 10957). c) The estimated errors (sampling uncertainties) arising from the differences in record length based on the annual mean Tx and Tn.

2.1.3. Performance of the dataset

The performances of the bias correction are indicated using error statistics – the mean absolute error (MAE) and root mean squared error (RMSE), temperature extreme indices and Pearson correlation coefficient. Table 2.1 presents the comparison of the error statistics for the daily climatologies of the derived BCE5 Tx and Tn datasets, the validation dataset that is based on the Leave-One-Out Cross Validation (LOOCV), the raw ERA5L, and the Climate Hazards group Infrared Temperature with Station (CHIRTS) – an independent gridded temperature dataset of similar temporal and spatial resolution (Verdin et al., 2020). The error statistics (MAE) for the monthly climatologies of BCE5, LOOCV, ERA5L and CHIRTS datasets are displayed in Fig. 2.3 whereas the MAE for the annual Tx and Tn over the period 1981-2010 is depicted in Fig. 2.4 Furthermore, the comparison of the extreme temperature indices, namely the probabilities of warm days (Prob(Tx > 90^{th} percentile of Tx)), warm nights (Prob(Tn > 90^{th} percentile of Tn)), cold days (Prob(Tx < 10^{th} percentile of Tx)), and cold nights (Prob(Tx < 10^{th} percentile of Tx)) (Donat et al., 2013; YIN and SUN, 2018) among BCE5, LOOCV, ERA5L, and CHIRTS datasets are presented in Fig. 2.5. The maps in Fig. 2.6 shows the differences between the new BCE5 and the original ERA5L datasets on the climatological time scale. In Fig. 2.7, the correlation between the IOBS and BCE5 temperatures at various aggregation timescales has been illustrated using the Pearson correlation coefficient at Addis Ababa and Dire Dawa stations.

Table 2.1: MAE and RMSE of the bias-corrected ERA5L (BCE5), cross-validation (LOOCV), raw ERA5L, and CHIRTS compared for daily climatology of mean and standard deviation from all IOBS locations

	Tx				Tn			
	Mean		Std		Mean		Std	
Dataset	MAE (°C)	RMSE (°C)	MAE (°C)	RMSE (°C)	MAE (°C)	RMSE (°C)	MAE (°C)	RMSE (°C)
BCE5	0.05	0.07	0.07	0.11	0.01	0.02	0.08	0.10
LOOCV	0.68	0.91	0.27	0.37	1.07	1.27	0.48	0.63
ERA5L	2.14	2.55	0.26	0.33	1.43	1.77	0.64	0.86
CHIRTS	1.30	1.64	0.40	0.50	2.53	2.94	0.56	0.73

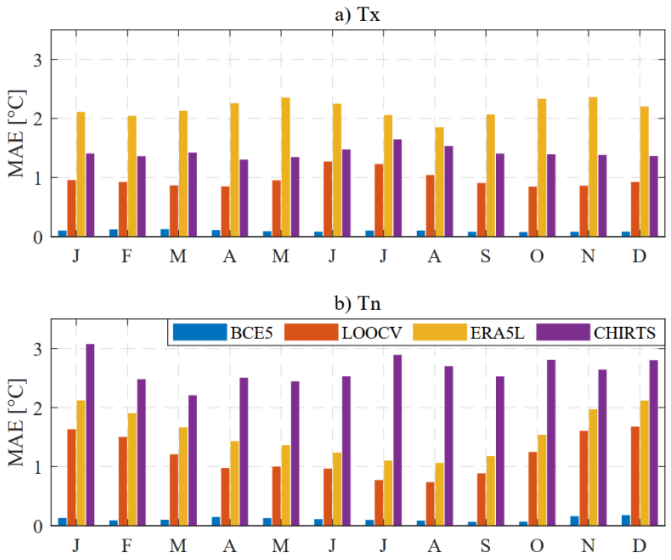

Fig. 2.3 Comparison of the mean absolute errors (°C) in the monthly climatology of the BCE5 and LOOCV with ERA5L and CHIRTS for Tx (panel a) and Tn (panel b) for the period 1981-2010.

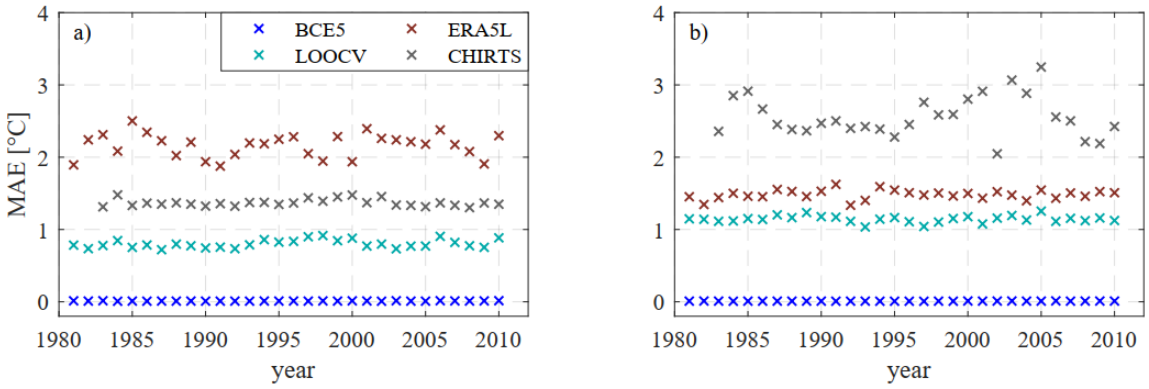

Fig. 2.4 Comparison of the mean absolute errors in the annual mean BCE5 and LOOCV with ERA5L and CHIRTS for Tx (panel a) and Tn (panel b) at 146 ground stations in Ethiopia.

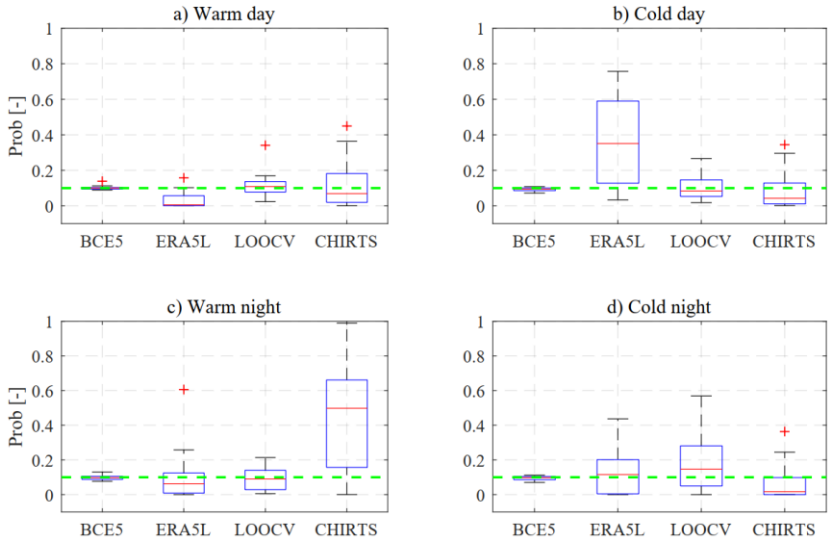

Fig. 2.5 Comparison of temperature extreme probabilities in the corrected BCE5, cross-validation LOOCV, ERA5L, and CHIRTS datasets. a) warm day probability defined as Prob(Tx > 90th percentile(Tx)), b) cold day probability -- Prob(Tx < 10th percentile(Tx)), c) probability of warm night -- Prob(Tn > 90th percentile(Tn)), d) probability of cold night -- Prob(Tx < 10th percentile(Tn)), all computed for 24 stations with continuous records of at least 25 years during 1983 – 2010 (chosen to match the start of CHIRTS dataset). The green dashed line shows the threshold probability of 0.1 corresponding to the frequencies computed from the IOBS data.

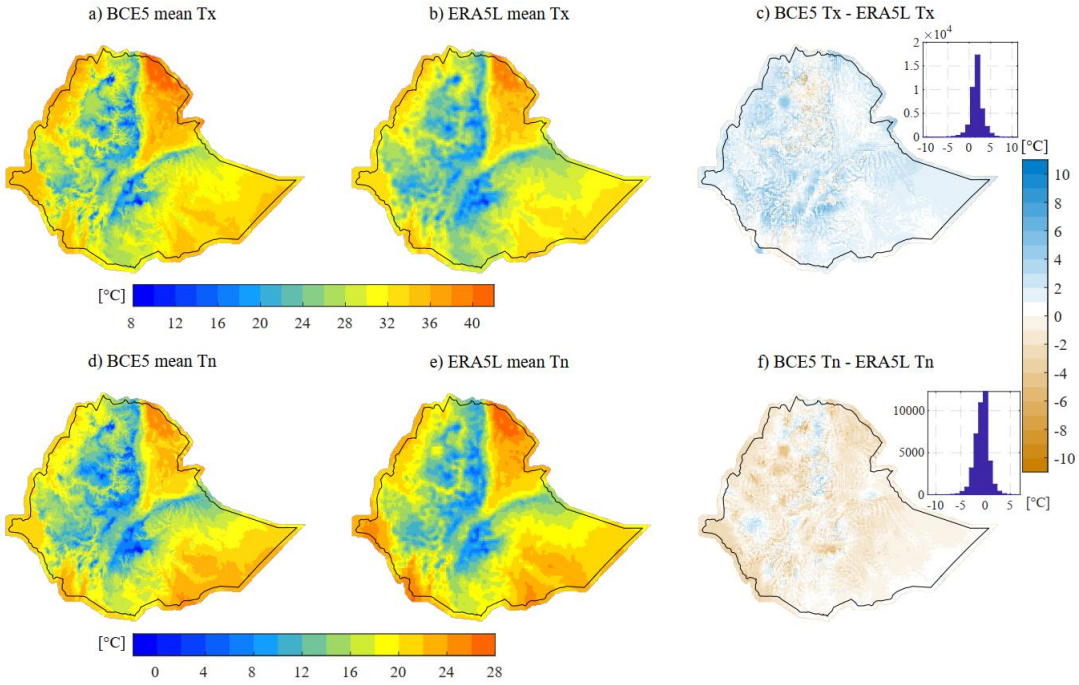

Fig. 2.6 Comparison of climatological means of the bias-corrected ERA5L (BCE5) and the original ERA5L Tx (a and b) and Tn (d and e), and their differences (c and f). The insets in c and f are the histograms of the differences between BCE5 and ERA5L Tx (c) and Tn (f). The circles show the climatological means of IOBS at each of the 146 stations considered in this study.

2.2. Experimental Design, Materials and Methods

The BCE5 dataset was derived by downscaling the ERA5L to a higher spatial resolution of 0.05°, i.e. ~5 km, and adjusting its statistical biases using observed temperature at ground stations as a reference. The bias adjustment was made using quantile mapping (QM) where the transfer function was parameterized by the first and second-order temperature statistics summarized at the IOBS stations in Ethiopia and a few stations along the borders of the neighboring countries as discussed in section 2.1.

2.2.1. Data quality control

Prior to the computation of the statistics from the IOBS, quality control measures were taken to fix the data quality issues such as outliers and homogeneity. The outliers in the datasets were checked and removed using a z-score based approach, where z-scores were computed based on the mean and standard deviation of every 30-day window, and a data point with six times or greater standard deviation from the mean over the window was considered as an outlier (Durre et al., 2010).

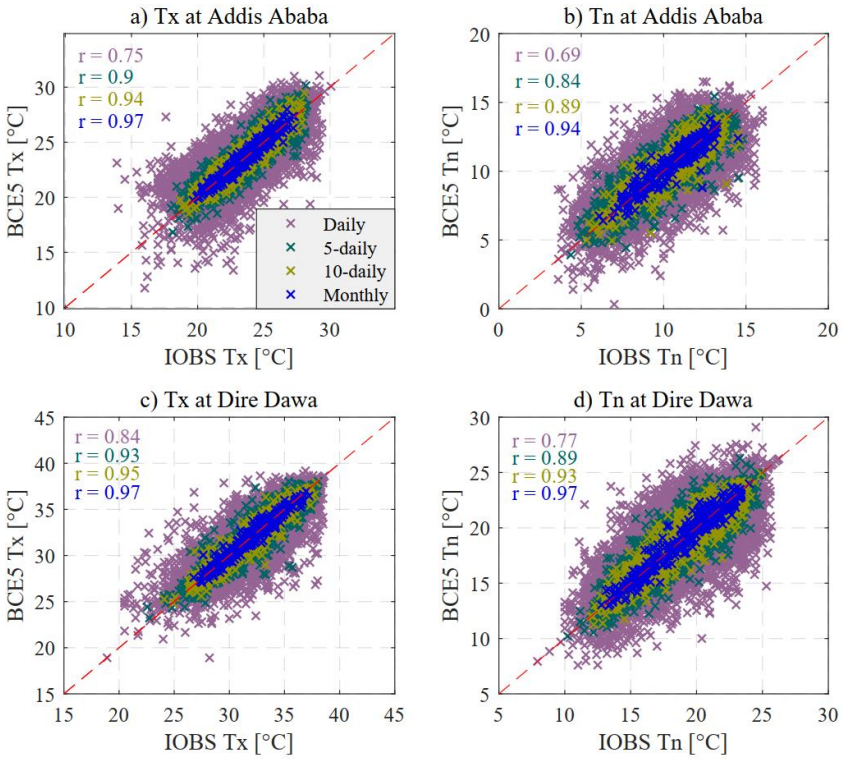

Fig. 2.7 Illustrations of correlation coefficients (r) between the observed and corrected Tx and Tn datasets at different aggregation times at Addis Ababa (a and b) and Dire Dawa (c and d) stations.

Inhomogeneity detections and treatments were based on manual methods (WMO, 2020), as automated tests were barely suitable for the detection of inhomogeneities due to the presence of significantly large and irregular data gaps in the IOBS time series. Through visual inspection of the temperature time series, three types of possible inhomogeneities were identified in Tx and Tn at some of the IOBS stations, namely: abrupt jumps in the mean, abrupt changes in the spread, and simultaneous jumps in the mean and the spread of the data. Inhomogeneities due to the abrupt jumps in the mean were corrected by shifting the arithmetic mean of the offset segment towards the mean of the time series before and after the offset segment. In the cases where the inhomogeneity involved a change in the spread of the data, the segments with the offset standard deviation were removed from the time series because the cause of these random fluctuations is difficult to determine with confidence. The removal of the segments will certainly increase the data gaps in the time series, but the effect on the statistics that are computed from the time series is minimal, as illustrated in Fig. 2.2c.

2.2.2. Computation of the IOBS temperature statistics

The temperature statistics (mean and standard deviation) were computed from the quality-controlled IOBS data. For the computation of the statistics and thus, the derivation of the BCE5 dataset, only the period 1981-2010, for which relatively sufficient IOBS data is available for this particular work was considered. Moreover, this period is also a standard climate period for various climate analyses, as recommended by the World Meteorological Organization (WMO) (WMO, 2017).Keeping in mind the possible biases (sampling uncertainties) that could result from the differences in the record length, the climatological monthly statistics were computed from the Tx and Tn of all days of the month over the entire record length during the period 1981-2010. Similarly, the annual statistics were calculated from all days of the year in which records are available for at least 50% of the days of the year. This minimum record threshold for the annual statistics was imposed to reduce biases in the annual statistics that could arise from the temperature seasonality. This implies that for the years with no or insufficient records, the computation leaves gaps in the annual statistics. The missing values in the annual statistics were filled using a linear regression (LR) model combined with inverse generalized distance weighting interpolation (Frei, 2014) of four closest stations (details in section 2.2.3). Note that the differences between the mean of the statistics before and after the filling result in systematic errors associated with the short records, which are also manifested in the monthly statistics.

Therefore, the computed errors were added to the monthly statistics to account for some of the uncertainties that could arise from shorter record lengths.

2.2.3. Spatial interpolation of the IOBS temperature statistics

The stationary monthly and non-stationary annual temperature statistics at IOBS stations were interpolated in space onto 0.05° x 0.05° grid cells using the hybrid interpolation approach proposed by Frei (Frei, 2014) that combines regression and deterministic interpolation techniques in two separate steps. In the first step, the background fields of the temperature statistics were determined at every grid based on a multivariate LR model of the monthly and annual temperature statistics with elevation (z), and longitudinal (x) and latitudinal (y) locations as predictor variables. Accordingly, the background temperature mean μ_b at a target grid cell (x,y) was modelled as a function z and y using $\mu_b(x,y) = \beta_0 + \beta_1 z(x,y) + \beta_2 y(x,y)$ while background standard deviation σ_b was determined as a function of z, y, and x using $\mu_b(x,y) = \beta_0 + \beta_1 z(x,y) + \beta_2 y(x,y) + \beta_3 x(x,y)$, where β_0 is the intercept, $\beta_1, \beta_2, \beta_3$ are the multivariate LR model slopes, in particular β_1 defines the lapse rate (°C/m) whereas β_2 and β_3 are longitudinal and latitudinal location coefficients and the models were applied to determine the background Tx and Tn monthly and annual statistics. In Ethiopia, the temperature is strongly correlated with elevation and thus the predictive power of the temperature-elevation LR model is solid, making the hybrid interpolation a better approach. The coefficient of determination (R^2) of the multivariate LR model for every month is given in Table 2.2.

In the second step, the residuals of the modelled temperature statistics were computed at every station and interpolated in space using the Inverse Generalized Distance Weighting (IGDW) approach to determine the residual fields. The residual mean (μ_r) and standard deviation (σ_r) at a station s are the deviations of the observed mean (μ_o) and standard deviation (σ_o) from the modelled background temperature statistics and these are given as $\mu_r(s) = \mu_b(s) - \mu_o(s)$ for residual mean and $\sigma_r(s) = \sigma_b(s) - \sigma_o(s)$ for residual standard deviation.

Table 2.2: R^2 of the linear regression model of the mean (μ) and standard deviation (σ) of Tx and Tn versus elevation (z), longitude (x), and latitude (y) based on the 154 IOBS stations.

Month	Maximum temperature		Minimum temperature	
	$\mu_{T_x} = f(y,z)$	$\sigma_{T_x} = f(x,y,z)$	$\mu_{T_n} = f(y,z)$	$\sigma_{T_x} = f(x,y,z)$
Jan	0.87	0.17	0.78	0.13
Feb	0.89	0.17	0.81	0.12
Mar	0.91	0.10	0.88	0.17
Apr	0.93	0.21	0.92	0.31
May	0.93	0.32	0.93	0.24
Jun	0.86	0.15	0.94	0.21
Jul	0.87	0.13	0.95	0.17
Aug	0.90	0.14	0.95	0.09
Sep	0.93	0.20	0.94	0.12
Oct	0.94	0.24	0.90	0.18
Nov	0.92	0.10	0.81	0.08
Dec	0.89	0.14	0.77	0.10

The IGDW interpolation approach follows the same principles of the classical Inverse Distance Weighting (IDW) interpolation but considers a non-Euclidean distance to assign weights to the stations. This is an important consideration, particularly in the context of Ethiopia to account for the effects of topographic barriers on horizontal air mass transfer between two locations in the mountainous regions. IDGW accounts for this effect to determine terrain-adjusted distance weights by penalizing the Euclidean distance between two locations L_1 and L_2 depending on their elevation difference. The penalized Euclidean distance is termed as a generalized distance and is computed as (Frei, 2014): $D_{\lambda,(L_1 \to L_2)} = \sqrt{(x_1 - x_2)^2 + (y_1 - y_2)^2 + (\lambda.(z_1 - z_2))^2}$, where D_λ is the generalized distance between two points, x_1 - x_2 are the longitudinal distances, y_1 - y_2 are the latitudinal distances, z_1 - z_2 are the elevation differences between the two locations, and λ[m/m] is a layering coefficient, i.e. a predefined free parameter that imposes an additional distance penalty per unit increase in elevation difference between the locations.

The layering coefficient λ was determined based on leave-one-out cross-validation (Frei, 2014; Hiebl and Frei, 2016). A set of predefined values of $\lambda \in$ [0, 10, 20, 30, 40, 50, 60, 70, 80, 90, 100, 200] were evaluated for the monthly and annual mean, and an optimal λ was chosen based on minimal root mean squared error (RMSE) as shown in Fig. 2.8.

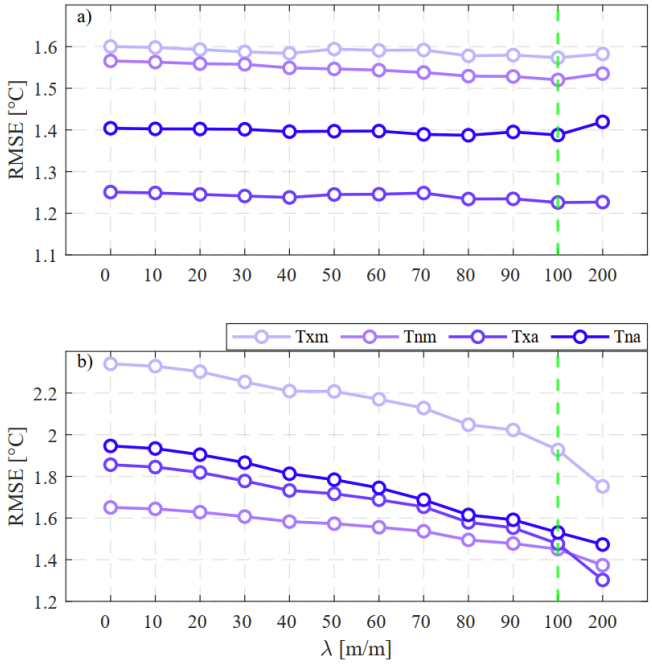

Fig. 2.8 Selection of the layering coefficient λ. a) Mean cross-validation RMSE of monthly Tx and Tn (Txm and Tnm) and annual Tx and Tn (Txa and Tna) for a set of $\boldsymbol{\lambda}$ considering all stations. b) Mean cross-validation RMSE at highly sensitive stations, i.e., stations at which RMSE is reduced by 0.5 °C or more at λ = 100 compared to the RMSE at $\boldsymbol{\lambda}$ = 0. The optimum value (indicated by the green dashed line) used for the interpolation of the residual fields was chosen to be $\boldsymbol{\lambda}$ = 100.

Once the optimal layering coefficient was identified, the IGDW interpolation scheme was implemented to determine the residual fields at every grid: $\mu_r(x,y) = \frac{\sum_{i=1}^{n}(D_{\lambda,i}^{-q}\mu_{r,i})}{\sum_{i=1}^{n} D_{\lambda,i}^{-q}}$ where i is a station and n is the total number of stations accounted for in the estimation of the residuals at grid (x,y). Four nearby stations (n=4) were considered optimal given the rather low station network density in the study area. An exponent of distance weight q = 2 was used. Note that the above equation is an IGDW scheme for the residuals of temperature mean (μ_r). The same equation, but with λ = 0 (the classical IDW interpolation) was applied to the residuals of temperature standard deviation (σ_r) considering the weak correlation between elevation and the temperature variance. Finally, the gridded monthly and annual IOBS statistics that are needed to define the transfer function for the QM were obtained by adding the background and residual fields of the temperature statistics.

2.2.4. Quantile mapping

The fundamental principle of QM is to transform the distribution of a modelled variable (in our case ERA5L temperature, T_m) to the distribution of the corresponding observed variable T_o, and the concept can be formulated as $T_o = F_o^{-1}(F_m(T_m))$ where F_o is the cumulative distribution function (CDF) of T_o , which serves as a transfer function, and F_m is the CDF of T_m to be transformed. In our application, the CDF of T_o is described by the interpolated statistics derived from IOBS stations as discussed in section 2.2.3, and the QM bias correction is applied to T_m, which is derived from ERA5L Tx and Tn at every grid. Before the implementation of QM, the ERA5L Tx and Tn were downscaled from their original spatial resolution of 0.1° x 0.1° to the target resolution of 0.05° x 0.05° using a bilinear interpolation.

The corrections of the ERA5L Tx and Tn were performed in two steps to quantify separately the effect of de-biasing on a seasonal basis and account for nonstationarity in time. First, the temperature datasets were corrected at every grid for monthly climatology assuming stationarity, by sampling the ERA5L temperature of all days in month m over the entire period (1981-2010), determining the Gaussian CDF of the sub-sample (containing 847, 900, or 930 data values depending on the month), and mapping it to the CDF of the observed temperature, which is defined by the monthly statistics of the IOBS. Second, the temperature time series that was corrected for monthly climatology was additionally corrected for every year using annual sub-samples of the time series from the first step (the number of data values is 365 or 366), and the annual IOBS statistics. This step is targeted to reproduce the IOBS-based interannual variability in the bias-corrected ERA5L 2-m air temperature (hereafter BCE5).

The QM-based corrections applied to the annual sub-samples combined with the corrections for monthly climatology (QMASS) in the derivation of this data yield similar results to the QM that is applied to seasonal sub-samples (QMSSS) by others, e.g., (Maraun, 2013; Pierce et al., 2015; Rajczak et al., 2016; Ruffault et al., 2013) as demonstrated in Fig. 2.9. The advantage of the procedure presented here is that it allows the use of quality-controlled first and second-order statistics instead of a complete time series for the observed variables in the cases where data availability is limited. This is particularly vital for enhancing the quality of the gridded climate datasets for local applications in data-scarce regions.

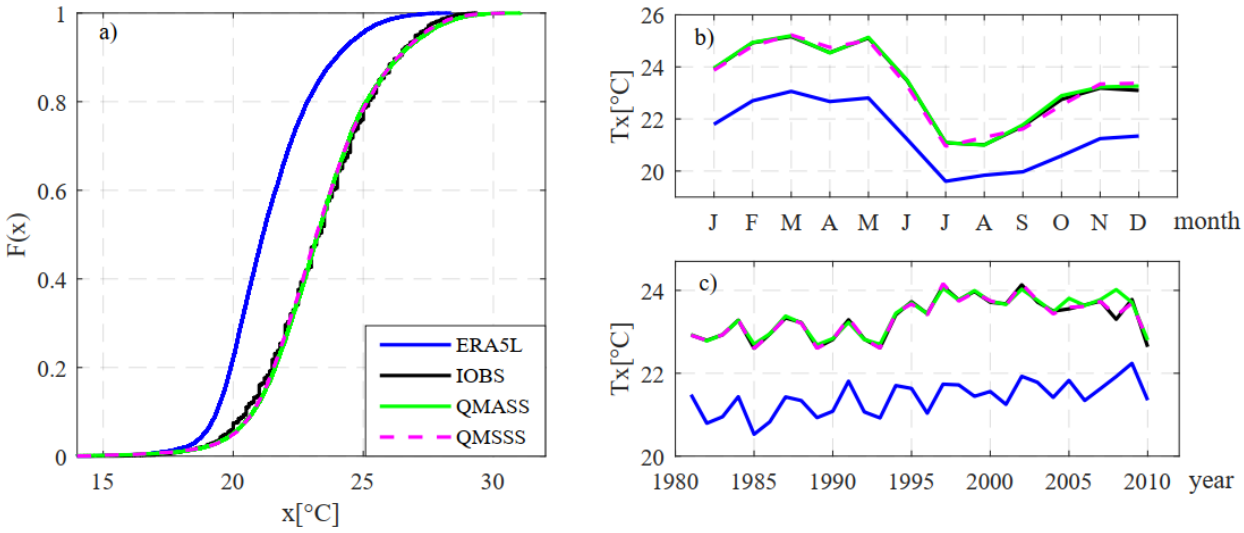

Fig. 2.9 Performance comparison of sub-sampling-based QM – annual sub-samples combined with monthly climatology (QMASS, this study) and seasonal sub-samples (QMSSS, others) to IOBS and ERA5L. a) Empirical cumulative distributions, b) monthly climatology, c) interannual variability of ERA5L, IOBS, and corrected Tx, an example at Addis Ababa station for the period 1981-2010.

2.2.5. Evaluation of the dataset

The final corrected dataset BCE5 variables Tx and Tn were evaluated using the leave-one-out cross-validation (LOOCV) approach. The evaluation was undertaken at all IOBS stations in Ethiopia which were considered in this application, using root mean squared error (RMSE) and mean absolute error (MAE) as evaluation statistics. The performance of BCE5 corresponding to the LOOCV was compared to the raw ERA5L and CHIRTS datasets for daily, monthly, annual statistics, and four extreme temperature indices – warm day, warm night, cold day and cold night probabilities, as described in section 2.1.3.

In principle, QM corrects the biases in the distribution parameters, i.e. mean and standard deviation, but not the biases in the temporal sequence of the individual daily values (Rajczak et al., 2016). Consequently, uncertainties are expected in the daily data. These uncertainties however sharply decrease at coarser aggregation times, for instance at pentadal (5-day) scale and coarser as illustrated in Fig. 2.7. Therefore, users can choose the aggregation time at which the bias-corrected dataset can be reliably used for desired applications.

2.3. Data availability

The BCE5 daily maximum and minimum temperature dataset at 0.05° x 0.05° grid resolution for the period 1981 – 2010, covering Ethiopia and areas within 20 – 30 km (i.e., 4 – 6 grids) outside the boundary of Ethiopia, is freely available for scientific, commercial and non-commercial use. The dataset (Wakjira et al., 2022) is stored in a single NetCDF file in an open-access format and can be accessed at the ETH Zurich research collection through a permanent link (https://doi.org/10.3929/ethz-b-000546574)

Chapter 3

Rainfall seasonality and timing: implications for cereal crop production in Ethiopia

Author
Mosisa Tujuba Wakjira

Co-authors
Nadav Peleg, Daniela Anghileri, Darcy Molnar, Tena Alamirew, Johan Six and Peter Molnar

Published in Agricultural and Forest Meteorology
Published online on 8 September 2021

Key finding

- Seasonality and timing are key rainfall attributes that dictate cereal production.
- Rainfall onset determines the rainy season duration and seasonal rainfall amount.
- Late-onset of rainy seasons reduces cereal production in unimodal rainfall regimes.
- High rainfall seasonality favors cereal production in semi-arid bimodal regimes.

Author's contributions

Conceptualization, data collection and preprocessing, methodology, discussion, original draft preparation, revision.

Co-authors' contributions

N. Peleg: methodology, discussion, reviewing and editing. ***Daniela Anghileri***: discussion, review and editing. ***Darcy Molnar***: discussion, review and editing. ***Tena Alamirew***: discussion, review and editing. ***Johan Six***: discussion, review and editing. ***P. Molnar***: methodology, discussion, reviewing and editing, supervision.

3.1. Introduction

Rainfed agriculture (RFA) is based solely on green water (Falkenmark, 2006; Wani et al., 2009). The productivity of the rainfed farming system is determined by the temporal distribution of rainfall with respect to the cropping period in a given hydrological year (Guhathakurta and Saji, 2013; Hao et al., 2013) because this controls the amount of water stored in the soil that is available for biomass production. In RFA systems, farmers rely on their local knowledge of seasonal rainfall timing to match the cropping season with the time window over which rainfall provides adequate water to meet the water demand by the crop (Radeny et al., 2019). However, this is successful only when rainfall has a predictable temporal pattern, i.e. when the interannual variability at the start and end of the rainy season is low. The unpredictability of the timing of seasonal rainfall undermines productivity in smallholder RFA systems, particularly in sub-Saharan Africa, leading to food and livelihood crises (Guan et al., 2015; Torres et al., 2019). Thus, understanding the characteristics of seasonal rainfall concerning the growing season is of vital importance for planning and decision-making in rainfed farming systems (Guido et al., 2020; Victor et al., 1996).

In Ethiopia, about 95% of crop production is under smallholder rainfed practice (FAOSTAT, 2018) and largely takes place during the long rainy season called ‘Meher’ (April - September). Specifically, the June - September rainy months (locally known as ‘Kiremt’) account for 65 – 95% of the annual rainfall total over large parts of the country (Segele and Lamb, 2005). The arrival of Kiremt is preceded by the migration of the Intertropical Convergence Zone (ITCZ) (Hills, 1979) that brings the short rainy season (March - May), locally called ‘Belg’ (Korecha and Barnston, 2007). The Kiremt rainfall variability arises from its connection to the atmospheric circulation patterns at seasonal and interannual scales (Segele et al., 2009a) with local effects connected to topography (Dinku et al., 2008).

In light of its importance for agriculture, rainfall in Ethiopia has been extensively studied in relation to the mechanisms of atmospheric moisture transport to the region (Berhane and Zaitchik, 2014; Segele et al., 2009b; Viste and Sorteberg, 2013; Williams et al., 2012), teleconnections to large-scale oceanic and atmospheric phenomena (Camberlin, 1997; Degefu et al., 2017; Diro et al., 2011a, 2011b; Gleixner et al., 2017; Shanko and Camberlin, 1998), and the role of these teleconnections for rainfall prediction and forecasting (Gissila et al., 2004; Korecha and Barnston, 2007; MacLeod, 2018; Taye et al., 2021), as well as for seasonal and

interannual variability and trends (Alhamshry et al., 2020; Cheung et al., 2008; Segele et al., 2015; Seleshi and Zanke, 2004). In addition, extreme climatic conditions that can have catastrophic effects on RFA systems, such as droughts, were also extensively studied (e.g., Funk et al., 2005; Philip et al., 2018; Temam et al., 2019; Viste et al., 2013).

The temporal rainfall attributes, such as the strength of seasonality in rainfall, the onset, cessation, and duration of the rainy season, are extremely relevant for decision-making in the RFA system. Rainfall seasonality is a measure of the spread in time of rainfall during the year (Walsh and Lawler, 1981). It has been studied in various parts of the globe to assess the responses of vegetation to the seasonal cycle of rainfall (e.g., Borchert, 1998; Dubois et al., 2014; Potter et al., 2005; Rohr et al., 2013; Souza et al., 2016; Suepa et al., 2016), and the impacts of seasonal rainfall variability on agriculture (e.g.,Ayanlade et al., 2018; Guhathakurta and Saji, 2013; Sadiq, 2020). The onset and cessation of the rainy season have been studied in different parts of the world, such as in west Africa (e.g., Dodd and Jolliffe, 2001; Marteau et al., 2009; Omotosho et al., 2000), South America (González et al., 2007; Liebmann and Marengo, 2001; Marengo et al., 2001), and south and east Africa (Mugalavai et al., 2008; Raes et al., 2004). In Ethiopia, Segele and Lamb (2005) defined the Kiremt onset and cessation, and assessed its spatial variability across the country. Others explored the temporal properties of rainfall in Ethiopia and assessed the changes in dry spells, droughts and irrigation demand (e.g., Araya and Stroosnijder, 2011; Kebede et al., 2017; Seleshi and Camberlin, 2006). These studies are based on sparse station rainfall observation and thus, the findings are limited to specific sites, or spatially interpolated. Alternatively, high-quality gridded rainfall datasets (e.g., remote sensing and reanalysis products) can provide consistent results in regional studies.

One critical aspect that has not yet been studied in depth is the sensitivity of RFA to the temporal distribution of rainfall in Ethiopia. Thus, in this work, we quantify the temporal rainfall attributes using the Climate Hazards Group Infrared Precipitation with Station (CHIRPS) rainfall (Funk et al., 2015) and explore how they affect cereal crop production in the RFA areas of Ethiopia using national crop production data. We aim to answer three specific research questions: (a) how does the seasonality of rainfall vary in space across rainfed agricultural areas in Ethiopia? (b) do the temporal rainfall attributes describing seasonal rainfall exhibit trends in time, and (c) is crop production significantly related to these attributes and their changes?

3.2. Study area and data

The study area covers the entire arable RFA area (Fig. 3.1a) of Ethiopia (cropland covers 33% of the RFA area, elevation ranges between 340 and 4500 m.a.s.l) that was delineated by Kassawmar et al. (2019) by reclassifying the biophysical factors (rainfall, temperature, altitude and slope) and combining them with crop production data. The size of the study area is about 667,000 km2, which is 59% of the total landmass of Ethiopia and is inhabited by more than 90% of the total population (CSA, 2007). The climate varies from arid on the eastside peripheral areas, where the mean annual rainfall is as low as 270 mm, to humid in the western and southwestern areas with mean annual rainfall up to 2100 mm (Fig. 3.1b). Mean annual temperature (Fig. 3.1c) generally increases from the central and northern highlands towards the western and northwestern lowlands and from eastern highlands to the southeastern lowlands, separated by the southwest-northeast oriented warm Rift Valley corridor.

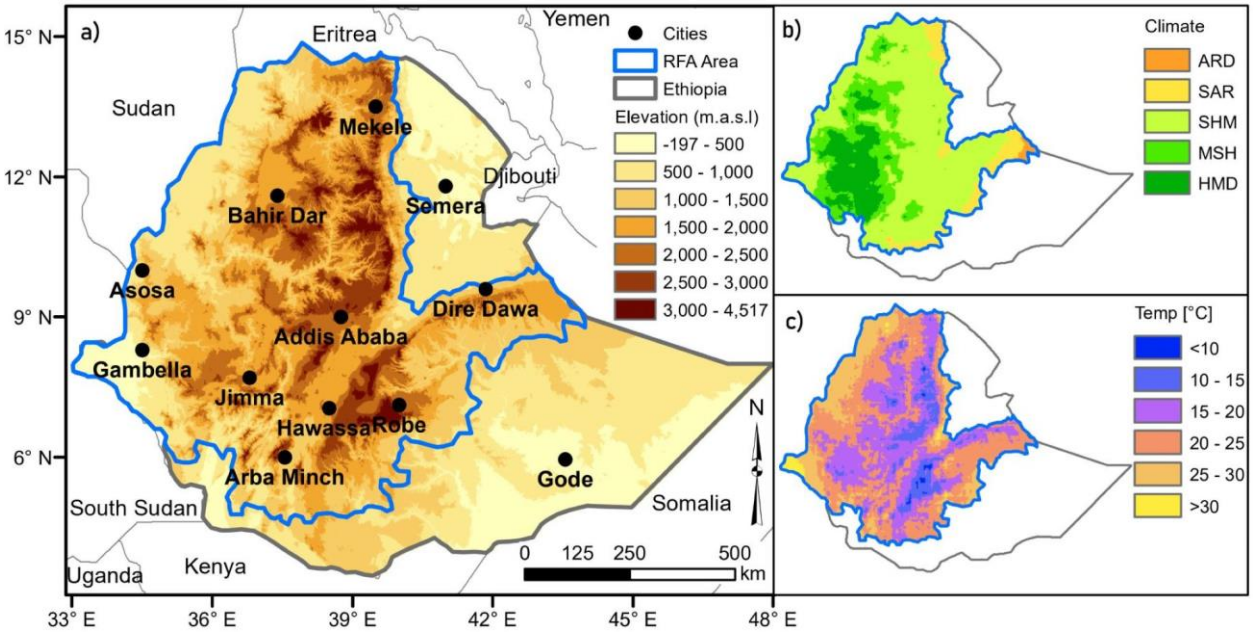

Fig. 3.1: (a) Map of Ethiopia and the RFA area (blue outline (Kassawmar et al., 2019)). (b) Climatic zones based on the FAO classification (FAO, 1986) of mean annual CHIRPS rainfall (1981-2010). ARD = arid, SAR = semi-arid, SHM = sub-humid, MSH = moist sub-humid, HMD = humid. (c) Mean annual temperature (1981-2010) based on the CFSR data (Saha et al., 2010).

Daily rainfall data at a spatial resolution of 0.05° x 0.05° for the region were obtained from the CHIRPS dataset (Funk et al., 2015) for the period 1981-2010. CHIRPS rainfall was evaluated in past studies across East Africa (Dinku et al., 2018a; Gebrechorkos et al., 2018) and for

specific watersheds in Ethiopia (Bayissa et al., 2017; Gebremicael et al., 2019; Musie et al., 2019), where it outperformed other gridded global rainfall datasets. CHIRPS data were also compared with the rainfall at 65 ground stations in the study area and it was demonstrated that they sufficiently match at pentadal (5-day accumulation) scale as shown in Fig. 3.2. The comparison of CHIRPS and stations shows little bias and a high correlation (ρ=0.86), with expected spread due to point versus grid rainfall and estimation errors, and larger discrepancies at stations southeast of the rift valley. This is also observed in other gridded rainfall datasets (Dinku et al., 2018a).

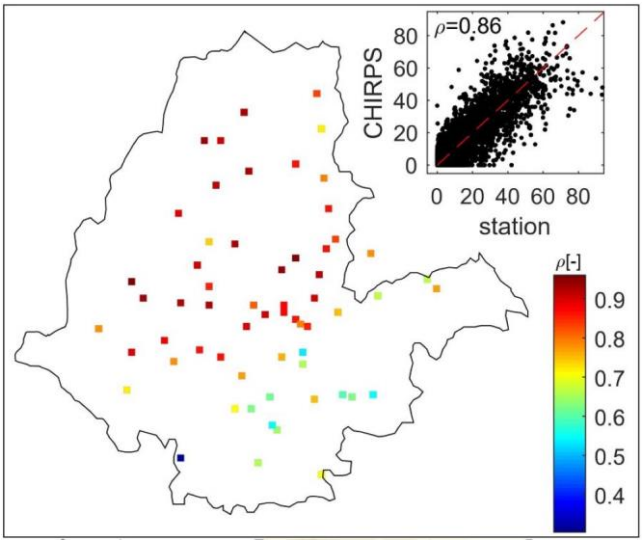

Fig. 3.2. Correlation coefficient (ρ) of CHIRPS grids versus ground station pentadal (5-day accumulation) rainfall averaged for all 73 pentads of every calendar year over the period 1998-2007 at 65 sites across the study area. The inset shows the scatterplot of the gridded and station pentad rainfall with 65x73 data points. Pentads with zero mean rainfall are included in the analysis.

The CHIRPS gridded data allows the classification of the RFA area into several rainfall regimes (Fig. 3.3) based on the seasonal rainfall pattern (unimodal or bimodal) and the FAO classification of climatic zones (FAO, 1986). Regimes 1-3 (R1-R3) are characterized by a unimodal rainfall pattern while regimes 5-6 (R5-R6) have a bimodal pattern, and regime 4 (R4) is considered as transitional (unimodal to bimodal).

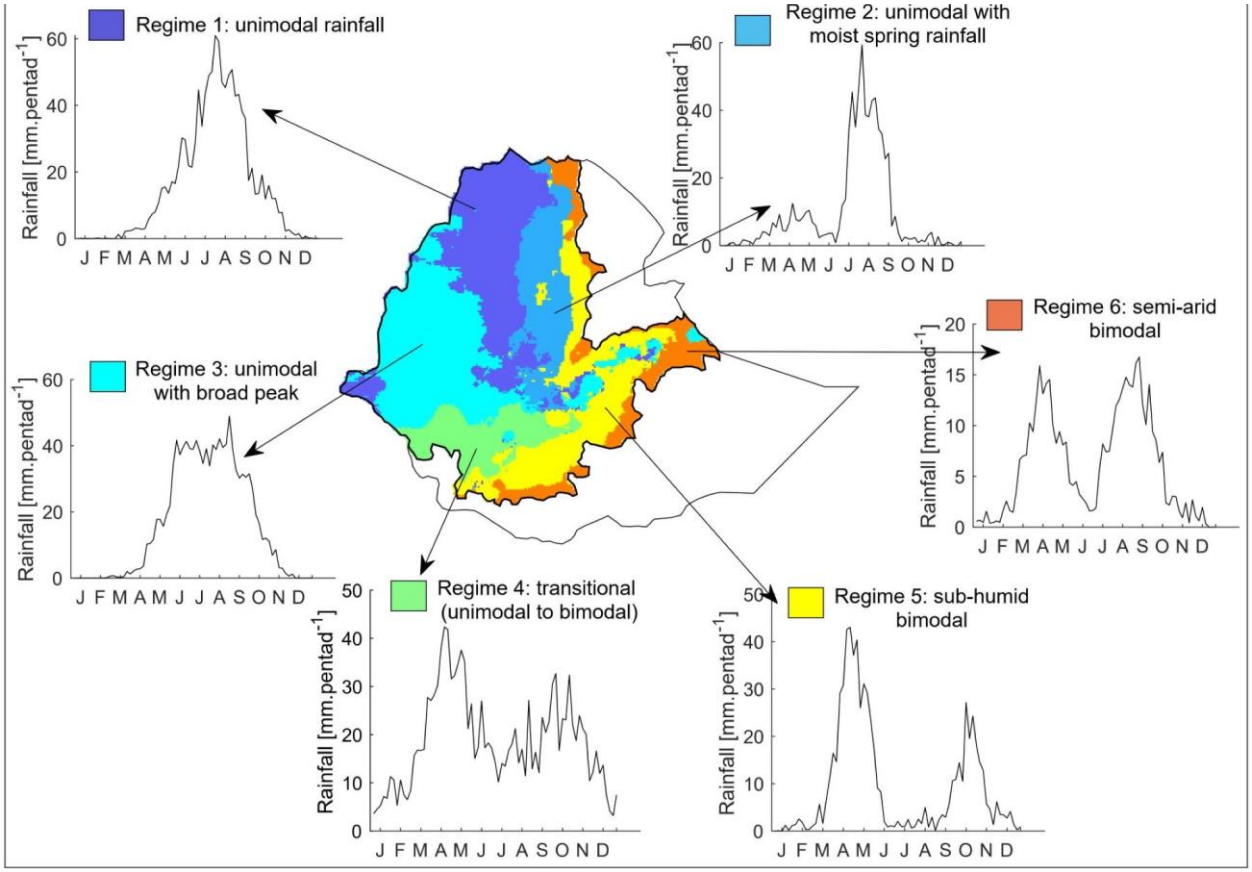

Fig. 3.3. Rainfall regimes of the RFA area of Ethiopia as classified based on CHIRPS rainfall climatology of the period 1981-2010. Insets show examples of pentad (5-day) mean rainfall at arbitrary locations for each regime.

We obtained the annual Meher crop production data from the annual statistical bulletin (available at https://www.statsethiopia.gov.et/our-survey-reports/) of the Central Statistical Agency (CSA) of Ethiopia. The CSA conducts an annual post-harvest agricultural survey that involves more than 32,000 agricultural households across the country to collect crop production data of all crop types that are produced in the country, and summarizes the crop statistics at regional and zonal (sub-regional administrative unit) scales (CSA, 2010). Cereals (maize, teff, sorghum, wheat, barley, millet, oats and rice) are staple crops and account for about 87% of the total grain production in the country.

3.3. Methods

In the analyses of temporal rainfall patterns and their effects on crop production, we first quantified the strength of rainfall seasonality using the method introduced by Feng et al. (2013). The approach is based on the concept of entropy (Cover and Thomas, 2005) and defines a

seasonality index based on two rainfall properties: annual rainfall and a measure of monthly rainfall variability labeled as relative entropy. This approach enables a spatial mapping of rainfall seasonality with respect to a predefined reference location (e.g., location with maximum rainfall). Next, we defined the rainfall timing attributes, i.e. the onset and cessation of the rainy season, from cumulative rainfall anomaly curves (Dunning et al., 2016; Liebmann et al., 2012; Liebmann and Marengo, 2001). This well-established objective approach is particularly suitable for analysis of rainfall timing at regional scales (González et al., 2007; Hampf et al., 2020; Jiang et al., 2019; MacLeod, 2018; Zhang et al., 2018). We then analyzed the variability and trends in all the temporal rainfall attributes. Lastly, we examined the statistical relationships between these attributes and total cereal production using parametric Pearson correlation and linear regression. Details of the methods are presented in the following sections.

3.3.1. Determination of rainfall seasonality

We examined the rainfall seasonality over the RFA area at grid-scale for the period 1981-2010 based on the method proposed by Feng et al. (2013). They defined two rainfall seasonality metrics: the Relative Entropy (RE) and the Dimensionless Seasonality Index (DSI). The relative entropy for a given calendar year k, RE_k, where in our analysis $k \in [1,30]$, is a measure of how different the actual rainfall distribution is from the uniform distribution. It is computed for each grid point as $RE_k = \sum_{m=1}^{12} p_{k,m}\, log_2(p_{k,m}/q_m)$, where $p_{k,m} = r_{k,m}/R_k$ is the actual monthly rainfall probability ($r_{k,m}$ is the rainfall in the month m of year *k*, and R_k is annual total rainfall of year *k*), and $q_m = 1/12$ is the theoretical monthly rainfall probability of a non-seasonal (uniform) rainfall regime. Theoretically, RE_k is zero when Rk is equally distributed over all months of the year (i.e., when $p_{k,m} = q_m = 1/12$ for $m \in [1,12]$) and attains a maximum value when R_k is concentrated in a single month. The dimensionless seasonality index for a given calendar year *k* is then computed as $DSI_k = (R_k/R_{max})RE_k$, where the scaling factor R_{max} is the maximum annual rainfall in the dataset, which in our study area is 2678 mm. A maximum value of DSI_k corresponds to a rainfall regime with R_k concentrated within a single month (maximum RE_k), whereas a zero value of DSI_k is due to either a completely dry year (R_k=0) or a uniformly distributed R_k (RE_k=0).

3.3.2. Defining the onset and cessation of the rainy season

We defined the timing of the rainy season at grid-scale by the dates of the onset and cessation of rainfall based on pentad (5-day) rainfall totals. In the first step, we computed for each grid cell the climatological mean rainfall P_c of each pentad i of the calendar year as: $P_{c,i} = (\sum_{k=1}^{30} P_{i,k})/30$, ($i \in [1,73]$, i.e., 73 pentads in a calendar year), as well as the long-term pentadal mean $\overline{P} = (\sum_{i=1}^{73} P_{c,i})/73$ from the 30-year rainfall record. In the second step, we calculated the climatological cumulative rainfall anomaly, $C_c(p) = \sum_{i=1}^{p}(P_{c,i} - \overline{P})$ with $p \in [1,73]$.

We used the same expression to compute the cumulative rainfall anomaly for every calendar year k as a cumulative sum of the difference between the pentadal rainfall of that year and $\overline{P}$. In Fig. 3.4 we show an example of cumulative anomaly curves constructed from a bimodal rainfall regime (climatological and an example of a single year). The long-term pentadal mean $\overline{P}$ at any grid cell is the threshold that determines the onset and cessation pentad of the year, i.e., when $P_{c,i}$ is less than $\overline{P}$, the cumulative anomaly curve has a negative slope and vice versa. The onset pentad is defined as the pentad after which the slope of the curve changes from a persistent negative to a persistent positive (the green dots in Fig. 3.4b). Likewise, the cessation pentad is the pentad after which the slope changes from positive to negative (the red dots in Fig. 3.4b). The duration of the rainy season is defined as the difference between the date of the cessation and onset pentad.

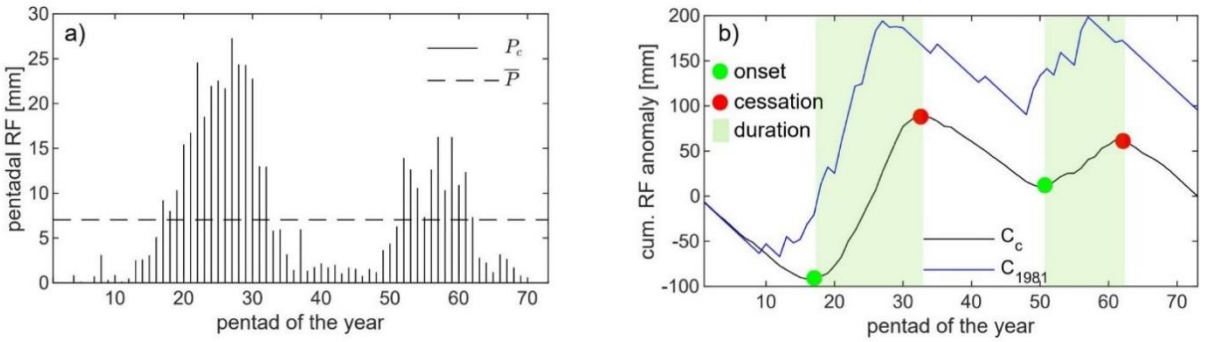

Fig. 3.4. Example of cumulative anomaly curves for the bimodal rainfall regime: (a) Climatological pentadal rainfall at grid cell 8.07°N and 41.82°E and mean P. (b) The corresponding climatological cumulative anomaly curve (black) and cumulative anomaly curve for the year 1981 (blue). The onset (green dots) and cessation (red dots) pentads define the climatology of the two rainy seasons (light green areas) and their durations.

We located the onset and cessation pentads by identifying the minimum and maximum of the anomaly curve for both unimodal (one onset and cessation) and bimodal (two onsets and cessations) regimes. To mask out local minima and maxima along the curve (e.g. blue curve in Fig. 3.4b), we smoothed the curve (not shown in Fig. 3.4b) using the non-parametric LOESS smoother (Cleveland, 1979). Locating the onset and cessation pentads in all rainfall regimes except Regime 4 is straightforward. Regime 4 is a transitional regime (see Fig. 3.3) where the rainfall pattern lacks interannual consistency and the rainfall cumulative anomaly curve has multiple peaks even after smoothing, which complicates the location of the cessation pentad. In this case, we assumed the last peak of the curve as the cessation pentad. Finally, we examined the long-term trends of the temporal rainfall attributes (seasonality, onset, cessation and duration) from the annual estimates. For this purpose, we applied the non-parametric Mann-Kendall test (Kendall, 1975; Mann, 1945) to detect trends and estimate their statistical significance, and the Sen slope estimator (Sen, 1968) to estimate the magnitude of the trends.

3.3.3. Correlation between temporal rainfall attributes and crop production

The temporal rainfall attributes obtained above were related to the annual Total Cereal Production (TCP) during the Meher (April to September) season in 45 zones (Fig. 3.5a) across the RFA area. To match the spatial resolution of the TCP dataset with that of the CHIRPS rainfall dataset, we disaggregated the zonal TCP in space down to the CHIRPS grid (5 km x 5 km) using the Cropland Cover Fraction (CCF) map obtained from the Copernicus Global Land Services (Buchhorn et al., 2020). The annual CCF maps are available at 100 m x 100 m resolution for the period 2015-2019. We averaged the CCF during the period 2017-2019 (2015-2016 were excluded as these were drought years) and aggregated the data to a 5 km x 5 km grid (Fig. 3.5b), from which we computed the cropland area in km2 in every grid cell (i, j) as: $A_{(i,j)} = 25(CCF_{(i,j)}/100)$. The TCP of a grid cell (Fig. 3.5b**)** that is located in zone $n \in [1,45]$ in the calendar year $k \in [1,16]$ was then calculated as: ${}^{n,k}TCP_{i,j} = {}^{n,k}TCP({}^{n}A_{i,j}/\sum({}^{n}A_{i,j}))$, where the sum goes over all cells in zone n. The temporal ranges of CCF (2017-2019) and TCP (1995-2010) do not overlap and this could introduce uncertainties in the disaggregation if cropland cover changes significantly over time. However, these changes can be considered slow as they involve both degradation (abandoned cropland) and expansion (Kassawmar et al., 2018) and thus, the effects of these changes compensate when

the CCF data is aggregated from the fine to coarse resolution. The disaggregation process is illustrated in Fig. 3.5.

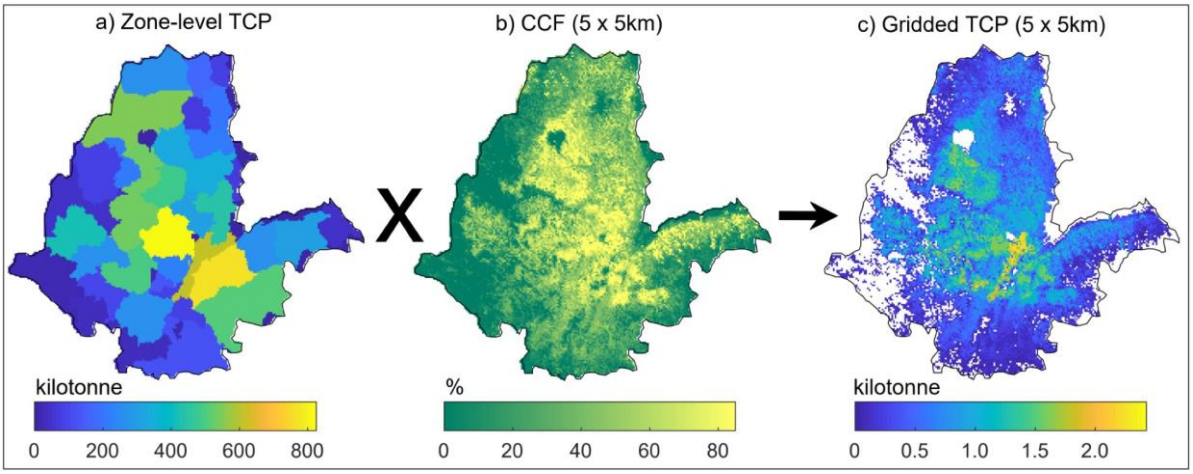

Fig. 3.5. Spatial disaggregation of crop data: (a) zonal Meher total cereal production (averaged over 1995-2010), (b) cropland cover fraction (CCF) aggregated from 100 m x 100 m to 5 km x 5 km resolution, and (c) disaggregated gridded TCP.

We observed a significant upward trend (on average at 6% yr^{-1}) in the TCP dataset over the entire RFA area, which is primarily attributed to non-climatic factors, including improvements in agricultural inputs like access to fertilizer, seed, cultivation and harvesting technologies (Gebeyehu, 2016; Shikur, 2020), and some expansion of the cultivated areas (Taffesse et al., 2012). We de-trended the TCP data to remove these effects, so that interannual variability in TCP can be more clearly related to the temporal rainfall attributes only (Kukal and Irmak, 2018). We then computed the Pearson correlation between the anomalies in the temporal rainfall attributes and the de-trended TCP, after inspecting the linearity of the predictor-response relationship, normality of the residuals, and independence of the data. To understand the relationship between specific cereal crop production and changes in the temporal rainfall attributes, we separately analyzed the correlation at 25 grid cells across the RFA area where each of the four major cereal crops (maize, teff, sorghum and wheat) dominates the total cereal production as mapped in the Atlas of the Ethiopian Rural Socioeconomy (IFPRI and CSA, 2006). Lastly, we estimated the magnitude of the effects of changes in the temporal rainfall attributes on crop production by fitting a univariate linear regression model with anomalies in the attributes as a predictor and the de-trended TCP as a response variable.

3.4. Results and Discussion

3.4.1. Rainfall seasonality and its dynamics

High rainfall seasonality is observed in the northern RFA area, particularly in regimes R1, R2 and parts of R3, where RF and RE are simultaneously intermediate to high (Fig. 3.6). However, the pattern of DSI largely follows the pattern of RF indicating that the strength of rainfall seasonality in these regions is mainly controlled by the annual rainfall amount. In contrast, the southern part of the RFA area (R4-R6) is characterized by low rainfall seasonality. The pattern of DSI predominantly follows the pattern of RE and thus, the strength of rainfall seasonality in these areas is mainly controlled by the monthly distribution of rainfall. For example, the southwestern area (R4 and lower part of R3) where DSI is extremely low is characterized by short dry months (low RE) and medium to high RF (sub-humid to humid climate), although the effect of RF on seasonality is not visible in this region (Fig. 3.6).

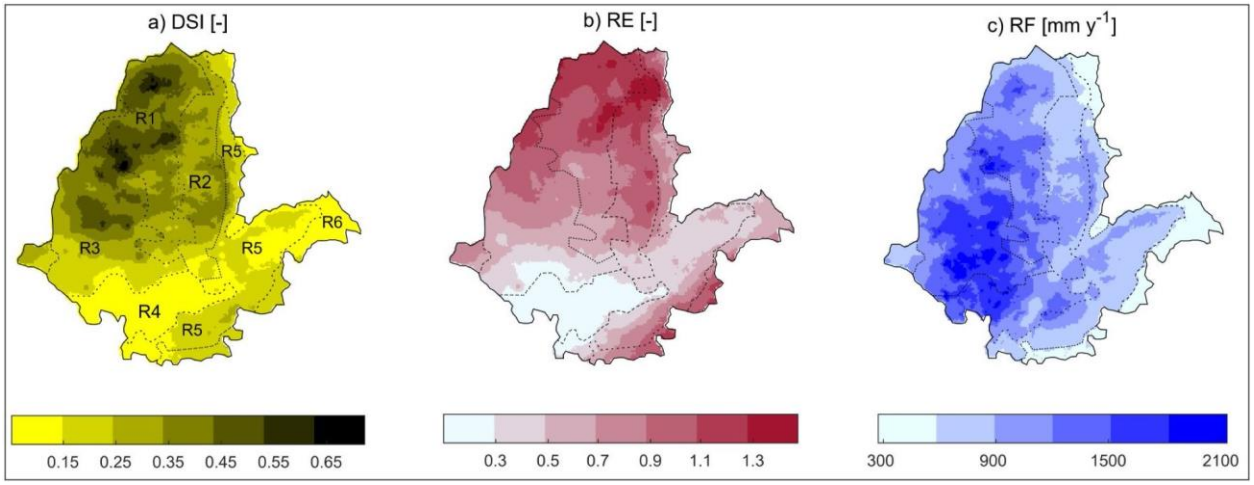

Fig. 3.6. Maps of the rainfall seasonality metrics in the RFA area of Ethiopia: (a) mean dimensionless seasonality index (DSI), (b) mean relative entropy (RE), and (c) mean annual rainfall (RF), computed for the period 1981-2010. The layer with dotted boundaries shows the rainfall regimes R1-R6 (see Fig. 3.3 for their detailed representation).

The relevance of rainfall for rainfed crop production is determined by its temporal distribution in reference to the cropping season (Mutsaers, 1979; Yengoh et al., 2010). In this regard, the observed low seasonality in R4 and parts of R3 in the southwest of the RFA area is desirable because it allows effective exploitation of the high annual rainfall for double-cropping, while the temporal distribution of rainfall in the wet regions such as the middle and upper parts of R3

(Fig. 3.6a, c) tends to limit double-cropping due to high seasonality, despite high annual rainfall. Conversely, low seasonality is problematic in arid and semi-arid climates such as R5 and R6 because low rainfall over an extended period can constrain the relevance of the rainy season for crop production. For example, the bimodal regime (low seasonality) in the eastern semi-arid parts of the RFA area where the annual rainfall is less than 600 mm is less efficient for crop production because the annual rainfall is partitioned into two distinct seasons but with lower rainfall amounts.

Considerable interannual variability in rainfall seasonality is observed over large parts of the RFA area. The northeastern semi-arid and sub-humid areas that include parts of R2 and R5 (Fig. 3.7a), show an average coefficient of variation (CV) of 0.34, which is due to variability in RE (Fig. 3.7b) intensified by the small variability in the RF (Fig. 3.7c). Similarly, the natural variability in the seasonality of rainfall is high in R4 with a regional average CV of 0.38, and this variability is purely attributed to the variability in RE. The western and northwestern side (parts of R1 and R3) of the RFA area is characterized by stable seasonality patterns, whereas R5, R6 and parts of R2 and R3 have moderate variability in rainfall seasonality.

Parts of the RFA area experienced a significant increase in seasonality (DSI, Fig. 3.7d) in the period 1981-2010. Specifically, R2 and R5 (area marked by the red rectangle) are found to have an increase in the seasonality of 2% yr^{-1} on average, as a result of the expanding number of dry months (increase in RE, Fig. 3.7e) and an increase in annual rainfall (Fig. 3.7f). Similar trends are also observed in parts of R4 and R5 in the southern sub-humid area (the green rectangle). Furthermore, the increasing tendency of seasonality over the northwestern lowlands (R1) is exclusively attributed to the positive trend in annual rainfall. On the contrary, seasonality tends to significantly decrease across the belt of the RFA area (Fig. 3.7d, blue dashed arrow) following the decreasing tendency of RE. A significant decrease in DSI is observed over the dry southeastern part (blue rectangle) of the RFA area because of the decreasing trend in annual rainfall (Fig. 3.7f).

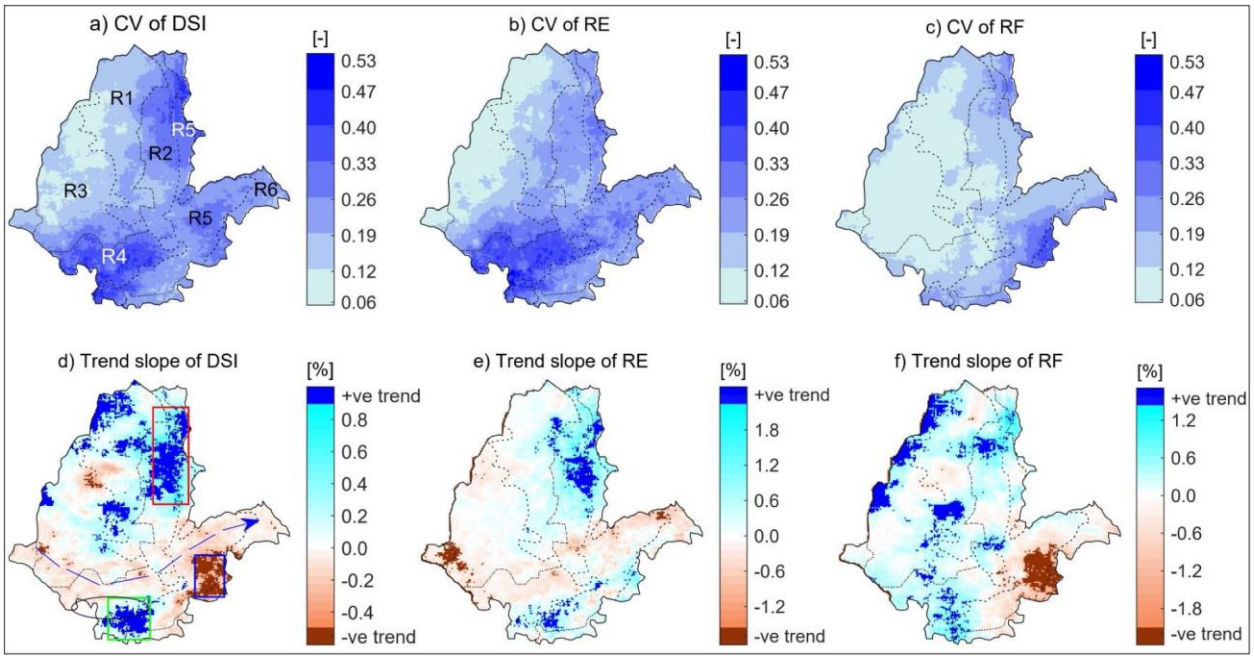

Fig. 3.7. Interannual variability and trends in rainfall seasonality metrics: (a-c) Coefficient of variation of the dimensionless seasonality index DSI, relative entropy RE, and annual rainfall RF. (d-f) Trend slope in %/yr (shown by the light blue and light brown color schemes) and statistically significant trends ($\boldsymbol{\alpha}$ = 0.05) in the metrics in the period 1981-2010; dark blue color - positive trend, and dark brown - negative trend. The dotted lines represent the rainfall regimes (R1-R6).

The observed changes of rainfall seasonality in time are related to drought occurrences over the RFA area. Viste et al. (2013) investigated droughts in Ethiopia over 40 years, including the period considered in this analysis. They found a frequent Belg (March to May) drought with a 36% probability of occurrence over the northeastern semi-arid and sub-humid areas (parts of R2 and R5), and a frequent Kiremt drought with a 42% probability of occurrence over the southern humid and sub-humid areas (parts of R4 and R5). Given that the increase in seasonality in these regions is attributed to the combined effects of the simultaneous increase in the annual rainfall and the number of dry months, it can be concluded that an increase in seasonality expected when the increase in rainfall occurs during the long rainy season (Kiremt in the northeast and Belg in the south), and a decrease in rainfall occurs during the short rainy season (Belg in the northeast and end of Kiremt in the south). Therefore, the observed increase in the rainfall seasonality is strongly related to rainfall deficit during Belg in the northeast, and during Kiremt over the southern parts of the RFA areas. On the contrary, a decrease in seasonality can occur due to a rainfall deficit mainly during the Kiremt season. The Kiremt

rainfall deficit over Ethiopia is largely related to El Niño conditions (e.g., Diro et al., 2011b; Gleixner et al., 2017; Korecha and Barnston, 2007; Segele and Lamb, 2005) and thus, one can expect a systematic relation between El Niño conditions and rainfall seasonality. From a simple comparison of the temporal patterns of the mean annual NINO3.4 SST index and the median annual DSI anomalies over the entire RFA grids, we found that rainfall seasonality over the RFA areas is negatively correlated (ρ=-0.66) with the Equatorial Pacific sea surface temperature. This implies that a decrease in rainfall seasonality is expected under El Niño conditions.

3.4.2. Rainfall onset, cessation and their dynamics

The climatological onset of the rainy season ranges from early March to early September (Fig. 3.8a). The earlier onset is in R4 in the south and southwest (dark blue areas) and rapidly propagates to later dates in R3. The subsequent propagation of the onset follows northwestward from R3 and advances slowly in the northeast direction across R1 and R2 until it arrives at R5 in the northeastern and eastern peripheral areas (yellow areas) in late June/early July. The later onset in the southern and southeastern areas (light brown areas in R5 and R6) is related to the onset of the short rainy season in autumn that ends in late November.

The climatological cessation of rainfall (Fig. 3.8b) generally follows the reverse direction of the onset with early cessation during late September in the northeastern semi-arid areas (dark green color). It first progresses southward along R2 and R5 to the central part over about two weeks and then propagates slowly southwestward until the end of October, followed by the later episode of cessation of the short autumn rainfall at the end of November. As a result, the duration of the main rainy season (Fig. 3.8c) over the RFA area generally decreases from R4 in the southwest (250 days) across R3 towards east and northeast where the duration is as short as 80 days. The total rainfall enclosed by the defined onset and cessation dates accounts on average for about 79% of the annual rainfall across the RFA area (Fig. 3.8d).

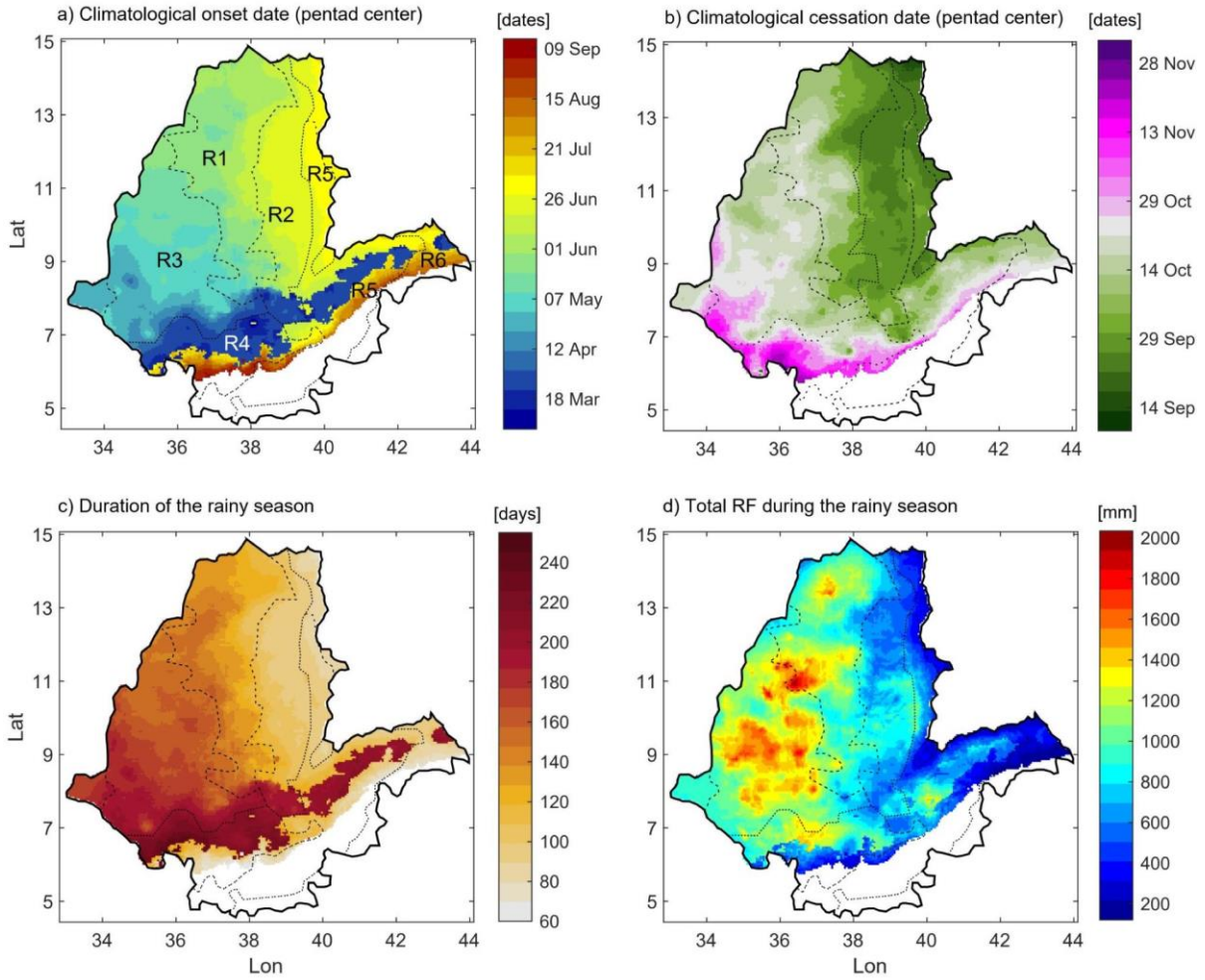

Fig. 3.8. Climatology of the average onset (a) and cessation (b) of the rainy season given by the mean date, length of the rainy season (c), and total rainfall during the main rainy season (d) for the period 1981-2010. The blank part of the maps represents areas where the Kiremt rainfall is <25% of the annual rainfall and the duration of the rainy season is <60 days. The dotted lines represent the rainfall regimes (R1-R6).

Comparable findings were documented by Segele and Lamb (2005) who followed a threshold-based approach using rainfall data from 121 ground weather stations to define the onset and cessation of Kiremt over a similar study area. A significant discrepancy with this study lies in the long rainy season in R5 along the eastern highlands (the dark blue strip in Fig. 3.8a). In fact, the rainfall pattern over this region has a bimodal tendency, but without distinct dry periods between the peaks. With the approach we used for the definition of the onset and cessation, the rainfall peaks are not detectable on the cumulative anomaly curve unless the subsequent pentads are persistently drier than the long-term pentadal mean, which is not the case in this region.

The progression of rainfall timing in space is associated with the atmospheric flow pattern over the East African region. The earlier onset in March across the southwest–east strip (see Fig. 3.8a) is triggered by the northward migration of the ITCZ following the warming of the northern hemisphere (Segele and Lamb, 2005). This is followed by a continuous influx of moist air masses mainly from the Gulf of Guinea (Diro et al., 2011b; Segele et al., 2009b; Viste and Sorteberg, 2013) that flow northeastward, i.e. the same orientation of the onset progression, supplying moisture to the region during the entire Kiremt. The moisture flux into the region is controlled by the equatorial Pacific sea surface temperature anomalies (Diro et al., 2011a; Gleixner et al., 2017; Segele and Lamb, 2005), with a retarding effect during El Niño conditions. As a result, about 54% of the late-onset during the period 1981-2010 occurred under El Niño conditions. The southwestward retreat of Kiremt is triggered by the weakening of the westerly winds and the southward movement of the ITCZ (Dunning et al., 2016; Segele and Lamb, 2005). The latest cessation of the rainy season during late November over the southwestern region (pink areas in Fig. 3.8b) is related to the persistence of the ITCZ in the south.

Analyzing annual data, we observed high interannual variability in the onset (median standard deviation of 4.13 pentads, Fig. 3.9a) and in the duration (median standard deviation of 3.67 pentads, Fig. 3.9c) of the rainy season, which are also well correlated (Pearson's ρ=0.96). The patterns of variability in onset and duration change in the opposite direction with the pattern of rainfall seasonality (Section 3.4.1) with ρ=-0.6. In other words, the onset date and duration of the rainy season is highly variable in bimodal rainfall regimes (R5 and R6, parts of R2 and R4). Furthermore, we found that the variability of rainy season duration explains a substantial portion (ρ=0.66) of the variability in DSI.

The cessation of the rainy season is more stable (median standard deviation of 1.91 pentads, Fig. 3.9b) compared to the onset. This difference can be partially attributed to the topography of the RFA area that influences the air mass flow (Dinku et al., 2008; Gissila et al., 2004) during the onset of the rainy season. The extreme variability along the southern and southeastern periphery (dark grey areas in Fig. 3.9a-c) is related to instability of the onset in the strongly erratic and unpredictable rainfall areas.

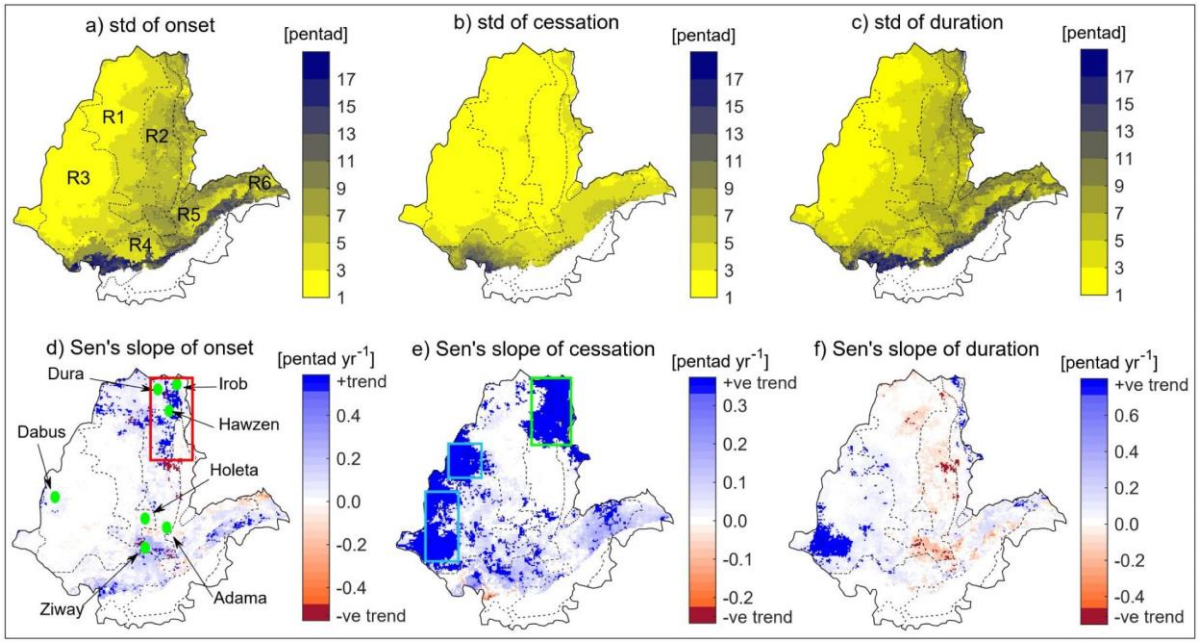

Fig. 3.9. Interannual variability and trends in rainfall timing: standard deviation of onset (a), cessation (b) and the duration of the rainy season (c) in pentads for the period 1981-2010; Sen's slope and trends in the onset (d), cessation (e) and length of the rainy season (f). The dark blue and brown colors in panels d-f represent statistically significant positive and negative trends respectively. The green dots in (d) are the site locations of recent studies (Asrat and Simane, 2018; Habtemariam et al., 2016; Hundera et al., 2019; Kahsay et al., 2019; Tesfahunegn et al., 2016) where farmers' perception of local climate changes were documented. The dotted lines represent the rainfall regimes (R1-R6).

Our findings on spatial variability are not in full agreement with the findings of Segele and Lamb (2005) in terms of the pattern and magnitude of the variability in the onset of the rainy season. They found a decrease in the standard deviation of the onset from northeast to southwest regions with a lower average magnitude of approximately 3 pentads. However, the findings on variability in the cessation date agree to a larger degree, both in terms of pattern and magnitude. The discrepancy may be due to the methods used in defining the rainfall onset, as well as the differences in interpolated ground station used by Segele and Lamb (2005) versus the CHIRPS rainfall data that we used.

Regarding the long-term changes in the rainfall timing attributes over the period 1981-2010, we found a significant trend of late-cessation of the rainy season over large parts of the northeastern semi-arid areas (green rectangle, Fig. 3.9e), western sub-humid lowlands in R3 (blue rectangles), and certain parts in the central and eastern parts of the RFA area. The trend towards late-cessation in the northeast (R2 and R5) coincides with parts of the areas where a

significant increase in seasonality was detected (see Section 3.4.1). Additionally, few areas in this particular region (red rectangle, Fig. 3.9d) have undergone significant changes toward late-onset and shortening of the duration (Fig. 3.9f). These three signals of change (late-onset, late-cessation and shortened duration) complement our earlier finding that the increase in seasonality in this region is associated with the recurrent failure of the Belg rainfall (Viste et al., 2013) and increased and (slightly shifted and shortened) Kiremt rainfall.

The changes observed in the onset and duration of the rainy seasons are in agreement with the farmers' perception, particularly in the hotspot regions, such as the northeastern semi-arid areas in R2. In recent assessments of farmers' perception of local climate change at various sites (the green dots in Fig. 3.9d), e.g., at Dura (Tesfahunegn et al., 2016), Irob and Hawzen (Kahsay et al., 2019), and at Ziway (Habtemariam et al., 2016), over 81% of the respondents reported a perceived late-onset of the rainy season. Asrat and Simane (2018) show farmers' perception in the Dabus area of shortening duration of the rainy season (in agreement with our findings) and late-onset (contradicting our findings). At Holeta (Habtemariam et al., 2016) and Adama (Hundera et al., 2019), farmers perceive late-onset, while we found a tendency of early-onset in these areas. Although the periods considered in these studies do not perfectly match with the period covered in our analysis, the data indicate that the impacts of the changes detected in climatic indicators are perceived at the farm level.

The trends in the temporal rainfall attributes, i.e., seasonality (section 3.4.1), onset, cessation and duration of the rainy season during the recent climate normal (1981-2010) is an indication of the impact of climate change on the temporal distribution of rainfall in the study region. Given the importance of the temporal attributes of rainfall for rainfed farming systems, these changes can have major impacts on crop production as discussed in section 3.4.3. It is important also to note that changes in the temporal rainfall attributes can intensify under future climate (Dunning et al., 2018; Gaetani et al., 2020; Pascale et al., 2016), which may have additional implications on the RFA systems.

3.4.3. Implications of rainfall seasonality and timing for crop production

Among the four temporal rainfall attributes (seasonality, onset, cessation, and duration), the onset of the rainy season strongly determines the Meher TCP (Fig. 3.10a). Late-onset (positive onset anomaly) is accompanied by a decrease in TCP and vice versa. The effect of cessation

on TCP (Fig. 3.10b) is spatially inconsistent, although positive or negative correlations are detected in specific areas. TCP is positively correlated with the duration of the rainy season in many areas (Fig. 3.10c). We also observed a weak positive correlation between TCP and seasonality (median ρ=0.03 considering all regions, Fig. 3.10d).

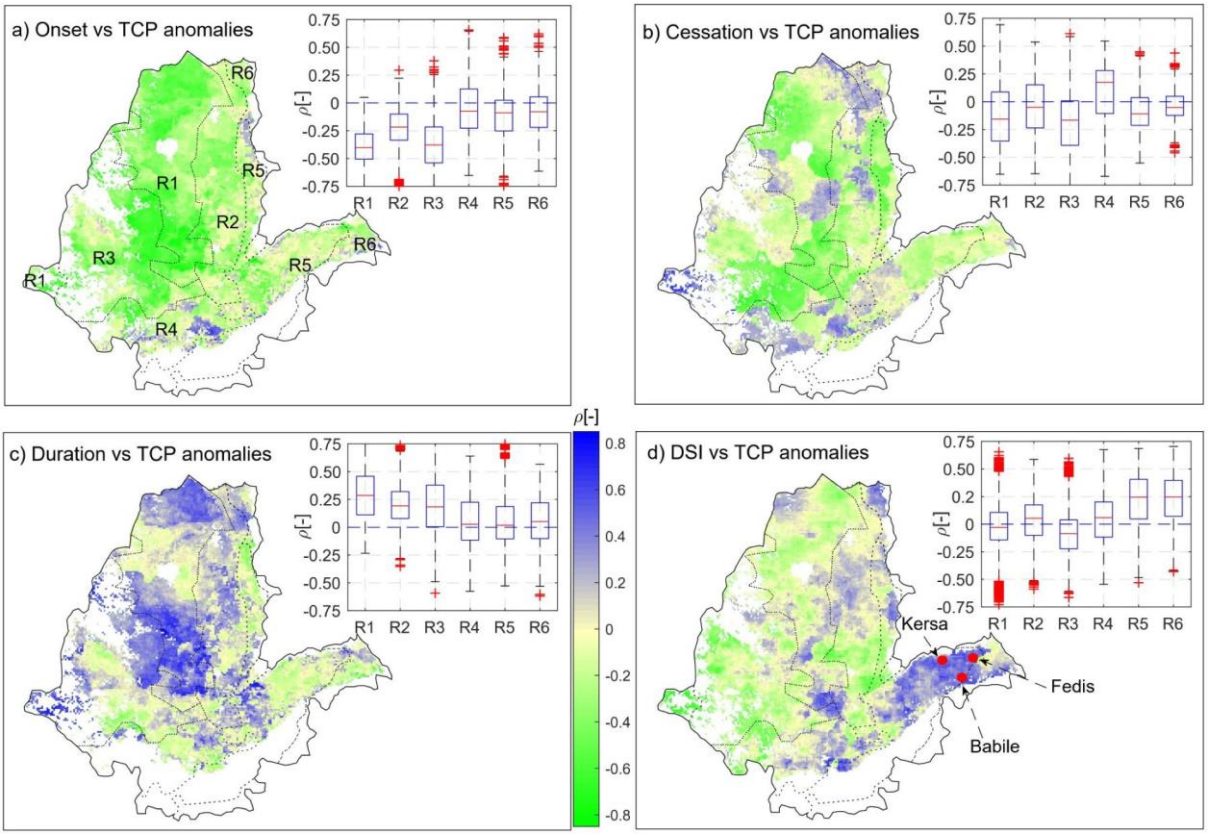

Fig. 3.10. Pearson correlation coefficient ρ for the relationship between the de-trended total cereal production (TCP) and (a) onset date anomaly (-ve/+ve anomaly corresponds to early/late), (b) cessation date anomaly, (c) rainy season duration anomaly, and (d) DSI anomaly. The red dots in (d) are site locations of a recent study (Tesfaye and Seifu, 2016) where farmers' perception of local climate changes were documented. The boxplots summarize the variability of the correlation in the six rainfall regimes -- regime 1 (R1) to regime 6 (R6) (see Fig. 3.3 for a detailed map). Correlations are computed for the period 1995-2010.

The influence of the rainfall onset on TCP is more pronounced in unimodal regimes, R1 and R3 (ρ=-0.40 and -0.38, respectively). The negative correlation in R1 is associated with high rainfall seasonality where the rainy season is confined between June and September. TCP in both R1 and R3 are positively correlated with the duration of the rainy season (ρ = 0.28 and 0.19, respectively). However, the effect of seasonality in these regimes is small and tends to be negative. Compared to R1 and R3, the correlation between TCP and onset is lower in R2 (ρ =

-0.22), where Kiremt is preceded by the short Belg rainfall. This may be related to the soil moisture memory from the Belg season that can reduce crop failure during germination before the Kiremt onset. The positive correlation (ρ=0.19) with the duration is not manifested in DSI in R2.

TCP is weakly correlated with the rainfall onset and duration of the rainy season in R4, R5 and R6 where rainfall is less seasonal. For example, in R4, where there are only a few dry months, the most important rainfall timing attribute is the rainfall cessation (ρ=0.17). This is because Meher is the second production season after the main Belg production (CSA, 2016), and thus late cessation is an advantage. In the bimodal regimes R5 and R6, we found that seasonality is the most determinant factor for TCP because it is positively correlated with DSI (ρ=0.2, for both regimes), while the correlation with the other attributes is relatively weak. As discussed in section 3.4.1, overextended rainfall (less seasonal) in regions with low rainfall such as R5 and R6 is not reliable for crop production during the growing season. In line with the present findings, Tesfaye and Seifu (2016) reported that the failure of rainfall to support crop production is one of the effects of climate variability and change perceived by farmers over the previous 10-15 years at Babile, Fedis and Kersa sites in the eastern part of the RFA area (see the red dots in Fig. 3.10d).

Next, we explored if the relationships between TCP and the temporal rainfall attributes discussed above when considering the total cereal production is different for specific crops. We found that the general pattern of the correlation for specific crops follows the same direction as that of the total cereal production, but the strength of the correlation changes between crops (Fig. 3.11). Rainfall onset has a greater impact on maize and teff (ρ=-0.37 and -0.32, respectively) compared to sorghum and wheat (ρ=-0.19 for both). The influence of the duration of the rainy season (Fig. 3.11c) is highest for teff (ρ=0.34) compared to the other crops. A weak correlation is observed for DSI (Fig. 3.11d), with a negative tendency for teff and maize versus a positive tendency for sorghum and no correlation for wheat.

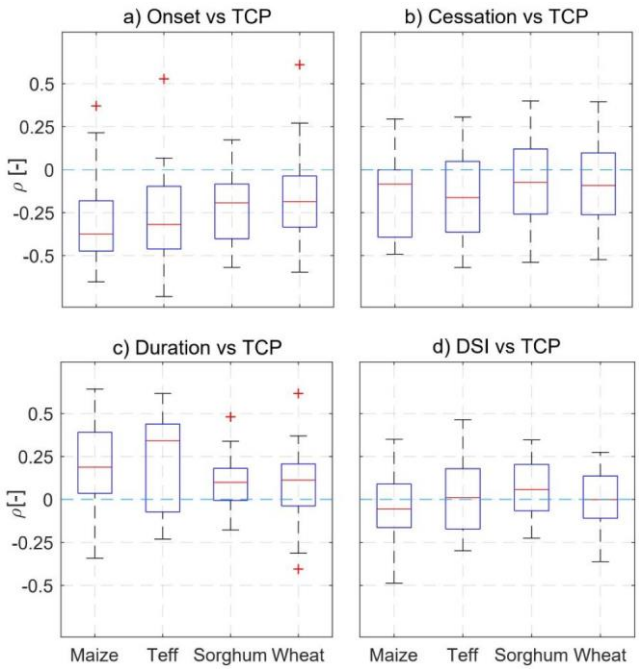

Fig. 3.11. Pearson correlation (ρ) between the anomaly in production dominated by specific crops and (a) onset anomaly, (b) cessation anomaly, (c) duration anomaly, and (d) DSI anomaly. Boxplots represent the variability between 25 sampled sites in the domain. Correlations are computed for the period 1995-2010.

The strong sensitivity of teff to the onset of the rainy season is linked to its high crop water requirement at the initial stage of growth (shortly after sowing in July/August), with the FAO crop coefficient ($K_{c,\,ini}$) of 0.8 – 1, nearly 3 times that of sorghum and wheat (Araya et al., 2011; Paff and Asseng, 2018). Teff productivity is also affected by water deficit during the grain-filling stage (Mengistu and Mekonnen, 2012), which is 65-72 days after sowing (Araya et al., 2011). The high correlation of maize production with the onset can be explained by the fact that the length of the growing period of maize is about 180 days (Allen et al., 1998) and its sowing in RFA systems starts in April before the onset of rainfall (see Fig. 3.8a). Hence, the arrival of rainfall in April is critical for the growth of maize during the early stage. Funk et al. (2003) also documented that the April-May rainfall over large parts of Ethiopia determines the subsequent Meher production, thus this can be the case in maize-dominated regions.

The importance of the rainfall onset is not limited to the crop growth period; pre-planting operations like tillage require optimal soil moisture for the soil workability. In the context of the smallholder RFA systems in Ethiopia, where tillage is an intense operation that is carried out using draft animals, the timing of the operation follows the onset or pre-onset of rain showers (Temesgen et al., 2008) when the soil is moist and workable. Therefore, the late-onset

of the rainy season delays the tillage operation, which in turn delays the planting activities. The foreseeable way to offset this impact is to improve the tillage power availability, e.g., switching from animal draft power to mechanical (tractor) power when possible.

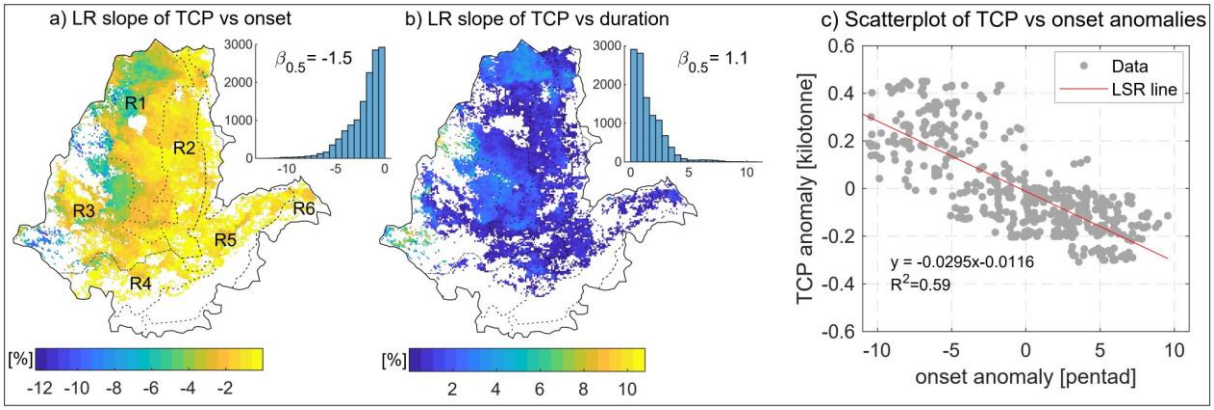

Fig. 3.12. Changes in the total cereal production in % per pentad of (a) onset anomaly and (b) duration anomaly, computed for the period 1995-2010. The histograms present the distribution of the changes. $\beta_{0.5}$ is the median of the % change in TCP per pentad. (c) Example of linear regression (LR) model performance for TCP vs onset of all grid cell in which TCP is strongly correlated to the rainfall onset (ρ>0.75); the least-squares regression (LSR) line represents an average LR model for these grid cells.

The impact of the rainy season onset on TCP is highly pronounced in the western and northwestern parts of the RFA area (Fig. 3.12a) where the rainfall is highly seasonal with a duration ranging from 100 days in the north to 150 days in the lower northwest. The pattern of the impact is similar for the duration but with a lower magnitude (Fig. 3.12b). The eastward decrease in the magnitude of the changes arises from the fact that crops take advantage of the soil moisture memory from the Belg season in the areas where the rainfall has a bimodal tendency. On average 1.5% reduction in TCP per unit pentad late-onset and a 1.1% reduction in TCP per unit pentad shorter duration of the rainy season is expected across the RFA area during the Meher production, but locally reductions of more than 10% TCP per unit pentad are possible.

The effects of early and late-onset of rainfall tend to differ in terms of variability in the TCP anomaly (see Fig. 3.12c), which can affect the performance of the linear regression model. This can be linked to the asymmetry of farmers' response to the early and late-onset events. For our purpose, we consider the model performance to be sufficient because it is intended to determine the average rates of changes and spatial patterns of the sensitivity of rainfed crop production to

variability and changes in the temporal rainfall attributes in the RFA area. However, we recommend variable transformation in cases of strong nonlinearity, if the use of linear regression models is intended for the prediction of seasonal crop production.

Farmers often respond to a late-onset of the rainy season by adjusting their planting/sowing schedule and thus, planting often takes place after the arrival of the first rainy days (Marteau et al., 2011). The observed reduction in TCP per pentad of late-onset is largely due to the inherent decrease in the total rainfall during the season as a result of the late-onset because the onset of the rainy season and the total rainfall in season are negatively correlated (median ρ = -0.88). This implies that farmers need to implement additional coping strategies, e.g., cultivation of crop varieties that require less water, reducing non-productive rainwater losses (Porkka et al., 2021; Rockström, 2003), such as evaporation (mulching) and runoff outflow (runoff water harvesting), to offset the effect of late-onset of the rainy season on rainfed crop production.

3.5. Conclusions

The temporal characteristics of rainfall dictate not only the seasonal rainfall amount that is reliably available for crop production but also the timing of the farming activities, including tillage and planting operations, which in turn affect crop production in the RFA system in Ethiopia. In this study, we evaluated the variability and changes in the temporal rainfall attributes -- the rainfall seasonality, onset and cessation dates, and duration of the rainy season -- and assessed how these may potentially affect cereal crop production.

We found that the northern RFA areas are characterized by high rainfall seasonality, while in the southern RFA areas the rainfall seasonality is less pronounced. The onset of the main rainy season starts in the southern part in early March and advances in the northeast direction until late June or early July, while the cessation dates follow the exact opposite direction starting in late September and ending in the southwest during late October. The northeastern semi-arid region is climatologically unstable, as it undergoes substantial changes and interannual variability in rainfall seasonality, timing and duration of the rainy season, and this is predominantly related to the frequent failure of Belg (February - May) rainfall**.**

Cereal production during the Meher season is highly correlated to the onset and length of the rainy season in regions where the rainfall seasonality is high. The highest (and negative)

correlation between onset and total cereal production is observed in maize (ρ=-0.37) and teff (ρ=-0.32) dominated areas. The effects of late-onset and shorter duration of the rainy season on crop production are more pronounced in the western part of the RFA areas where the rainfall has a unimodal pattern and the effects are less evident in the eastern parts where the rainfall pattern is bimodal. On average, a late-onset of the rainy season leads to 1.5% of rainfed cereal crop production loss per pentad, while a shorter rainy season leads to 1.1% of production loss per pentad. The cessation of the rainy season has less effect on crop production. In regions with a bimodal rainfall regime, the Meher cereal production is positively correlated to rainfall seasonality. This is particularly the case in the eastern highland regions where the limited annual rainfall is distributed over two shorter and agriculturally less relevant seasons.

With this analysis, we demonstrate that temporal rainfall attributes in relation to rainfed agriculture can provide useful information for the prediction of seasonal crop production. We expect that such information can be useful for developing early warning systems, RFA system vulnerability assessment, and for climate adaptation planning for sustainable food production in Ethiopia. The methods used in this study can be extended to other regions including other East African countries to understand the response of crop production to the temporal properties of rainfall. However, we advise against direct extrapolation and scaling of the findings of this study for a different region because crop productivity differs between regions depending on the existing agrometeorological services, farming technologies and other factors that can support farmers' decision and actions to respond to weather and climate variabilities.

Chapter 4

Green water availability and water-limited crop yields under a changing climate in Ethiopia

Author
Mosisa Tujuba Wakjira

Co-authors
Nadav Peleg, Johan Six and Peter Molnar

To be submitted to Hydrology and Earth System Sciences
Submitted on 30 January 2024

Key finding

- The average water-limited attainable yield (AY) of the main growing season (Meher) is 79% of energy-limited yield.
- AY will change in order of ±5% in Meher depending on climate and location in the future.
- The shorter growing season (Belg) will experience significant increases in AY
- AY is mainly ETo-sensitive in moisture-limited Meher and rainfall-sensitive in Belg

Author's contributions

Conceptualization, data collection and preprocessing, methodology, discussion, original draft preparation, revision.

Co-authors' contributions

N. Peleg: methodology, discussion, reviewing and editing. ***Johan Six***: discussion, review and editing. ***P. Molnar***: methodology, discussion, reviewing and editing, supervision.

4.1. Introduction

Green water, the infiltrated part of rainfall that is stored in the soil root zone and returns to the atmosphere in the form of evapotranspiration (Falkenmark, 2006), is the sole source of moisture in rainfed agriculture (RFA) systems (Rockström, 1999). Green water accounts for an estimated 80 % of the global agricultural evapotranspiration fluxes, and RFA systems produce ~60 % of the global food (Mekonnen and Hoekstra, 2011; Molden et al., 2011; Rockström et al., 2010; Sposito, 2013). The reliance on green water varies across regions, with sub-Saharan Africa (SSA) being particularly dependent on this water resource, where close to 95 % of croplands are under rainfed agriculture practices (Abrams, 2018; Laderach et al., 2021). Due to the highly dynamic nature of green water availability (GWA), influenced by climatic and biophysical factors that vary in space and time, RFA systems are strongly climate-sensitive under moisture-limited conditions (Kang et al., 2009; Meng et al., 2023; Park et al., 2022). Climate change presents an additional major challenge to the system, undermining crop production with potential consequences of food insecurity, livelihood losses, and economic crises (FAO, 2022).

Previous global-scale assessments have highlighted the challenges posed by climate change on agriculture, both in the past and in the future, leading to regionally varying intensification of agricultural water scarcity and decreases in crop yields (e.g., Borgomeo et al., 2020; Jägermeyr et al., 2021; Lobell et al., 2011; Rosenzweig et al., 2014). This is particularly evident across the tropics including the highly climate-vulnerable SSA countries (Burke et al., 2009; Kummu et al., 2021; Müller et al., 2011; Rezaei et al., 2023; Rosenzweig et al., 2014; Schlenker and Lobell, 2010). Adaptation actions tailored to specific contexts are now a top priority for mitigating the impacts of climate change-induced water scarcity in rainfed agriculture (RFA) systems, primarily at the national scale through the implementation of National Adaptation Plans (NAP) under the auspices of the United Nations Framework Convention on Climate Change (UNFCCC, 2021) and other programs.

Ethiopia is one of the countries committed to formulating and implementing the NAP, including in agriculture, the sector which the country and its population heavily rely on (FDRE, 2019). In fact, climate adaptation is a much-needed action in Ethiopian smallholder agriculture, of which ~95 % is dependent on GWA, and at the same time it is an indispensable activity supporting the food and income of nearly 80 % of the population. The NAP and its

implementations are, in principle, based on analyses of climate change impacts and vulnerability, along with relevant adaptation actions (UNFCCC, 2021; Warren et al., 2018). The Global Agroecological Zones (GAEZ) database (Fischer et al., 2021), developed by the Food and Agriculture Organization of the United Nations (FAO) in collaboration with the International Institute for Applied Systems Analysis (IIASA), provides water-limited yields and various other agroecological information at a global grid scale. However, for effective national and sub-national level planning and decision-making, it is essential to have country-specific details and critical analyses of this information. Previous studies on the impact of climate change on crop yields in Ethiopia have primarily focused on local case studies (e.g., Abera et al., 2018; Araya et al., 2015; Degife et al., 2021; Hadgu et al., 2015; Kassie et al., 2014; Markos et al., 2023; Moges and Gangadhara, 2021), making them patchy and insufficient as a comprehensive guide for the NAP. Here we propose a framework, which allows for a regional comprehensive analysis of agrohydrological responses to climate change across the RFA regions of Ethiopia.

This framework builds on the key factors that influence GWA and their cascading effects on crop yield, to guide appropriate agricultural water management planning, decisions and actions. Several factors influence GWA. While rainfall amount and distribution fundamentally determine the green water supply, rainfall event characteristics such as intensity, frequency, and duration, combined with surface biophysical conditions (mainly soil, land cover, terrain slope, and roughness), govern the partitioning of rainfall into overland flow and infiltration (Rockström and Gordon, 2001; Schuol et al., 2008). Soil properties (e.g., textural composition, organic matter content, thickness, and salinity) in particular determine the rainfall partitioning to infiltration and runoff, the subsurface flow, green water storage capacity, and plant accessibility, while potential evapotranspiration driven by air temperature, radiation, wind, relative humidity, and vegetation controls the return flow of green water to the atmosphere (Ringersma et al., 2003).

In moisture-limited regions, crop yield is proportional to the magnitude of the evapotranspiration flux, which is constrained by moisture availability (Hatfield and Dold, 2019; Steduto et al., 2012). The maximum yield that can be achieved with the available green water under the best nutrient input and crop management conditions in RFA systems is considered to be the *water-limited attainable yield* (Lobell et al., 2009; van Ittersum et al., 2013). In conditions where water is not a limiting factor, like in RFA systems in humid

agroecologies and fully irrigated systems in dry agroecologies, maximum achievable crop yield is limited by energy, and thus is called *energy-limited yield potential*.

Quantification of the complex interactions between climate, soil, cultivar and crop management is commonly done with mechanistic crop models, for example, APSIM (Holzworth et al., 2014), AquaCrop (Raes et al., 2009; Steduto et al., 2009), CROPSYST (Stöckle et al., 2003), DSSAT (Jones et al., 2003), EPIC (Williams, 1990), and WOFOST (van Diepen et al., 1989), which are used to simulate crop growth and yields at field scale. These models combine hydrological models that simulate hydroclimatic processes to estimate water availability in space and time, and crop growth models that simulate the crop physiological responses to the agro-environmental and management conditions (Siad et al., 2019). Model complexity, and associated issues such as data requirement and computational demand, are major constraints of mechanistic crop models especially when applied in a distributed setting to a large geographic domain, which necessitates a compromise between the level of complexity and the purpose of the modelling (Adam et al., 2011; Ramirez-Villegas et al., 2017).

Here, we employ a simplified agrohydrological modelling framework to assess the impacts of climate change on GWA and the subsequent effects on major cereal crops (teff, maize, sorghum, and wheat) produced in the entire RFA region of Ethiopia. We address three research questions that are relevant for future agricultural water management planning and decision-making in Ethiopia: (i) what is the current green water availability and how will it change under the future climate across the RFA region?; (ii) how will these changes affect water-limited attainable crop yields (AY)?; and (iii) which hydroclimatic factor (rainfall or evapotranspiration) dominantly drives these changes and where? We base our assessment on crop response conditions where all crop growth factors except water are unlimited so that we can capture the effects of climate-driven changes in crop yields in a relative manner. Furthermore, we critically discuss the implications of the changes for water management in the NAP and similar agricultural development initiatives. We also present the workflow of our modeling framework to ensure its robust application in addressing similar or related agrohydrological research questions.

4.2. Methods

4.2.1. Study area

The study area covers the entire rainfed arable parts of Ethiopia (hereafter RFA region), as mapped in previous land use analysis (Kassawmar et al., 2018), encompassing an area of about 667,000 km^2 (59% of the landmass of Ethiopia, see the blue outline in Fig. 4.1a). The climate of the RFA region ranges from humid to semi-arid (Fig. 4.1c) with mean annual potential evapotranspiration ranging from 700 mm in the highland regions to 1800 mm in the western lowland part of the RFA region. The mean annual rainfall of the RFA region ranges from 270 mm in the eastern part to 2100 mm in the western and southwestern parts (Fig. 4.1b). The rainfall has unimodal patterns in the central, western, northern, and northeastern parts with highest rainfall in July/August depending on the location (Segele and Lamb, 2005; Wakjira et al., 2021). This rainy season typically spans from May to September, coinciding with the main growing season, locally known as 'Meher', during which approximately 88% of the total annual crop harvest occurs (CSA, 2007). The southern and eastern parts of the RFA region on the other hand, largely experience a bimodal pattern with spring and autumn being the two rainy seasons. The spring (February-May) rainy period is considered the second and shorter growing season, locally known as ‘Belg’, in the southern and southeastern part of the RFA region. Cereals account for about 80 % of the crops produced, with teff, maize, sorghum, wheat, and barley being the top species, also serving as the main staple food crops in the country (CSA, 2010, 2007)**.**

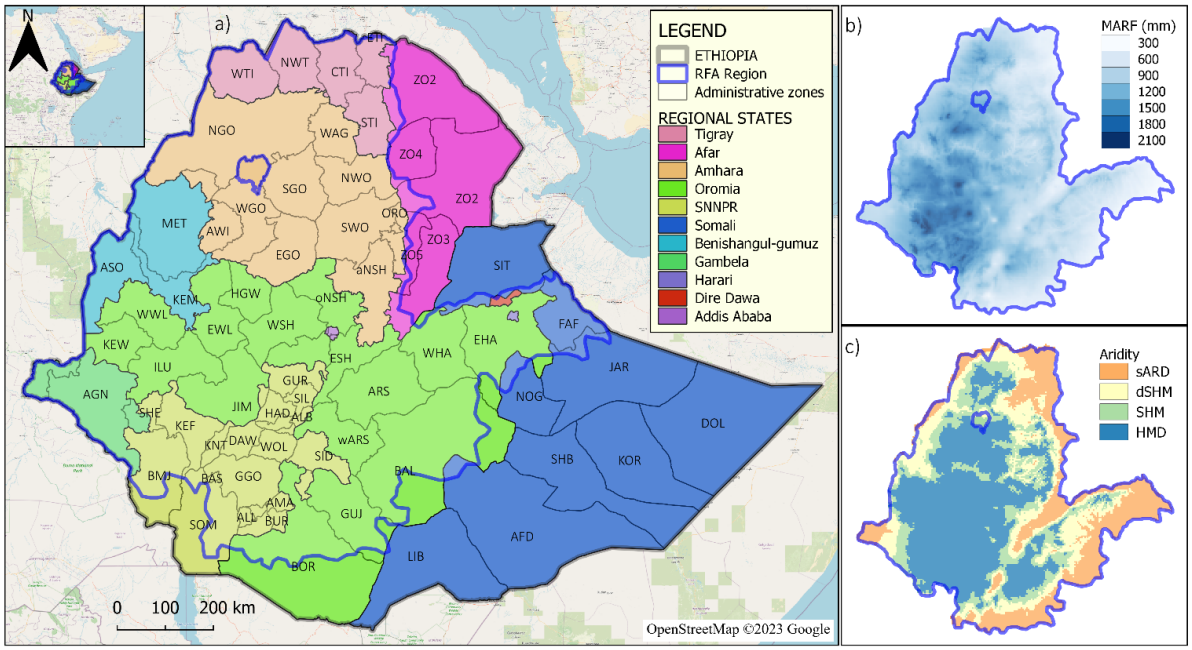

Fig. 4.1: (a) Map of Ethiopia, the spatial extent of the rainfed agricultural region (blue outline, Kassawmar et al., 2018), administrative zones (designated by short names) in the nine regional states. The complete list of the zones with full names is given in Table S4.1 (Appendix A) of the supplementary material. (b) Mean annual rainfall (MARF) of the RFA area for the period 1981-2010, based on CHIRPS. (c) Climatic regimes (aridity) of the RFA area (classification based on Spinoni et al., (2015)). sARD: semi-arid, dSHM: dry sub-humid, SHM: sub-humid, HMD: humid

4.2.2. Data

Daily rainfall data for the reference period (1981-2010) was obtained from the Climate Hazards Infrared Precipitation with Station (CHIRPS) dataset (Funk et al., 2015), which is available at 0.05° x 0.05° spatial resolution. Maximum and minimum daily 2-m air temperature data consists of the bias-corrected and downscaled ERA5-Land (BCE5) dataset (Wakjira et al., 2023, 2022), which is also available at 0.05° x 0.05° spatial resolution. Other climate variables (solar radiation, wind speed, and dew point temperature) were retrieved from ERA5-Land (Muñoz-Sabater et al., 2021) and disaggregated to a resolution of 0.05° x 0.05° using a bilinear interpolation method.

Future climate data were derived by downscaling multiple Global Circulation Model (GCM) projections, i.e., 26 for precipitation and solar radiation and 21 for maximum and minimum daily temperatures (listed in Table S4.2), from their native coarse resolution to 0.05° x 0.05° grid resolution using the change factor (delta) approach (e.g., Anandhi et al., 2011; Teutschbein and Seibert, 2012). The future climate scenarios include three Shared Socioeconomic Pathways

SSPs (Meinshausen et al., 2020; O'Neill et al., 2016), namely the SSP1-2.6 (low greenhouse gas emission), SSP2-4.5 (intermediate emission) and SSP5-8.5 (high emission).

Gridded soil texture and organic carbon content data were retrieved from SoilGrids (Poggio et al., 2021). Although the SoilGrids soil data is available at 250 m grid resolution, we upscaled the data to 0.05° (~5 km) to harmonize the spatial resolution with that of the climate datasets. Curve number (CN) values for agricultural land use were obtained from the USDA (1985) lookup table according to the hydrologic soil group dataset developed by Ross et al. (2018).

Independent actual evapotranspiration (ETa), surface runoff, and crop production datasets were utilized to evaluate the agrohydrological model simulations. ETa datasets were retrieved from five products – SSEBop (Senay et al., 2020), PML-v2 (Zhang et al., 2019), MOD16A2 (Mu et al., 2019), GLDAS 2.1 (Rui and Beaudoing, 2020), and TerraClimate (Abatzoglou et al., 2017), covering the period 2003-2010. Surface runoff data were collected from published runoff plot measurements at 17 locations (Table S4.3) across the RFA region of Ethiopia. Regarding the crop data, total cereal production (TCP), consisting of the sum of all cereals (maize, teff, sorghum, wheat, barley, millet, oat, and rice) produced in Ethiopia, was derived from the annual Agricultural Sample Survey (AgSS) reports (e.g., CSA, 2010) gridded by Wakjira et al. (2021) for the period 1995-2010.

4.2.3. Agrohydrological modelling

The agrohydrological modelling framework (Fig. 4.2) that interlinks climate-hydrological-crop (CHC) interactions was developed to simulate the effects of climate change on green water fluxes, and its cascading influences on crop yield. The CHC model consists of three modules for climate, hydrology and crops.

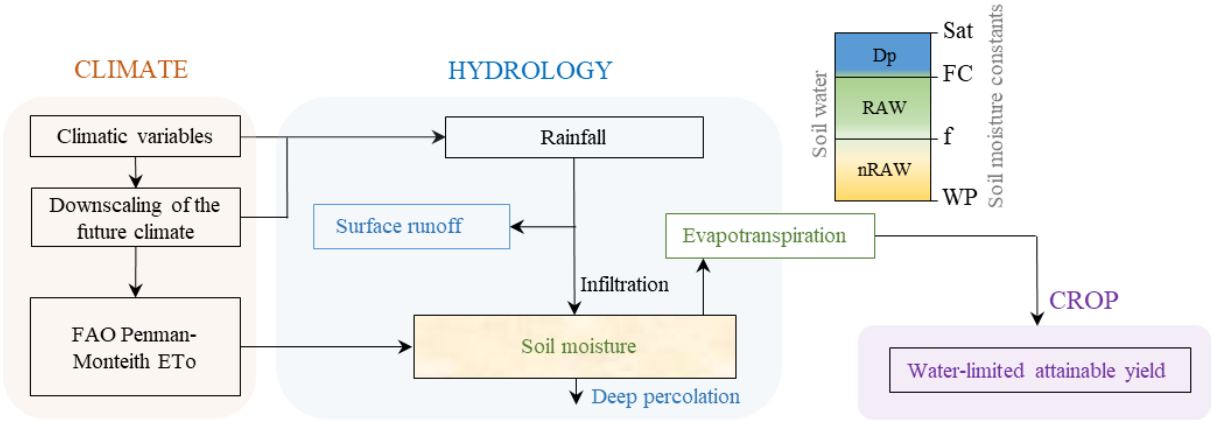

Fig. 4.2: The CHC model used for the assessment of climate-driven changes in green water availability and water-limited attainable yields. Dp = deep percolation, RAW = readily available water, nRAW = non-readily available water, FC = field capacity, WP = wilting point, f = critical moisture depletion factor.

Climate module

The climate module uses climatic variables to compute the daily reference evapotranspiration ETo [mm d^{-1}] using the FAO Penman-Monteith equation considering a hypothetical reference grass (Allen et al., 1998):

$$\mathrm{ETo} = \frac{0.408\Delta(\mathrm{R_n} - \mathrm{G}) + \gamma \frac{900}{\mathrm{T}+273}\mathrm{u_2}(\mathrm{e_s} - \mathrm{e_a})}{\Delta + \gamma(1 + 0.34\mathrm{u_2})} \quad (4.1)$$

where R_n [MJ m^{-2}] is net radiation at the crop surface, G [MJ m^{-2}] is soil heat flux, T [°C] is 2-m mean daily air temperature, u_2 [m s^{-1}] is 2-m daily wind speed, $e_s - e_a$ [kPa] is saturation vapor pressure deficit, Δ [kPa °C^{-1}] is the slope of the vapor pressure curve, and γ [kPa °C^{-1}] is the psychometric constant.

Hydrology module

The hydrology module simulates the dynamic soil water balance without lateral surface and subsurface routing. A conceptual (bucket) water balance model is applied to the soil hydrological fluxes – surface runoff Q [mm], actual evapotranspiration ETa [mm], deep percolation Dp [mm], and changes in soil moisture ΔSM [mm] from rainfall input P [mm] at daily time step t:

$$\Delta SM_t = P_t - Q_t - ETa_t - Dp_t \tag{4.2}$$

Surface runoff is simulated according to the US Soil Conservation Service (SCS) curve number method (USDA, 1985):

$$Q_t = \begin{cases} \frac{(P_t - I_{a,t})^2}{(P_t - I_{a,t}) + S_{20,t}}, & \text{if } P_t > I_a \\ 0 & \text{otherwise} \end{cases} \tag{4.3}$$

In the original SCS curve number model, the initial abstraction I_a [mm] was assumed to be 20% of S (indicated by the subscript in Eq. (4.3)). However, recent insights led to an update in this value to 5%, which yielded higher runoff prediction performance of the SCS model. A proposed conversion function from S_{20} to S_{05} is expressed by Hawkins et al. (2020):

$$S_{05} = 1.42 S_{20} \tag{4.4}$$

S is determined by the land surface conditions including soil characteristics as represented by the hydrologic soil group, land use land cover, terrain slope and antecedent soil moisture, all of which are parameterized as a dimensionless CN value. We estimated *S* using Eq. (4.5).

$$S_{20} = 254\left(\frac{100}{CN} - 1\right) \tag{4.5}$$

CN is updated daily for antecedent moisture conditions (AMC), which are often categorized as *dry*, *normal*, and *wet*. The *CN* values obtained from the USDA lookup table correspond to the *normal* AMC condition. Accordingly, we estimated the CN values for the *dry* and *wet* AMC following Raes et al. (2022) and Smedema and Rycroft (1983):

$$\begin{aligned} CN_{dry} &= 16.91 + 1.348CN - 0.01379(CN)^2 + 0.0001172(CN)^3 \\ CN_{wet} &= 2.5838 + 1.944CN - 0.014216(CN)^2 + 0.000045829(CN)^3 \end{aligned} \tag{4.6}$$

We then adjusted *CN* at every time step by linearly interpolating between CN and CN_{dry} or CN_{wet} depending on the soil moisture condition, assuming the soil moisture content

corresponds to θ_{WP} for CN_{dry}, $\theta_{0.5(\theta_{FC}+\theta_{WP})}$ for CN, and θ_{FC} for CN_{wet}. Note that θ_{FC} [m^3 m^{-3}] and θ_{WP} [m^3 m^{-3}] are volumetric moisture contents at field capacity and wilting point and they were estimated using the widely used pedotransfer function developed by Saxton and Rawls (2006).

Applying the conversion from Eq. (4.4) for S_{05} and then expressing I_a in terms of S_{20} in Eq. (4.3), the expression for Q can be rewritten as:

$$\mathrm{Q_t} = \frac{\left(\mathrm{P_t} - 0.071\mathrm{S_{20,t}}\right)^2}{\left(\mathrm{P_t} + 1.349\mathrm{S_{20,t}}\right)} \quad \text{if } \mathrm{P_t} > 0.071\mathrm{S_{20}}, \text{else } \mathrm{Q_t} = 0 \tag{4.7}$$

The rainfall that is in excess of Q (Eq. (4.7)) infiltrates into the soil and refills the available soil storage $V_t[\mathrm{mm}] = 1000Z(\theta_{sat} - \theta_{t-1})$, where θ_{sat} [m^3 m^{-3}] and θ_{t-1} [m^3 m^{-3}] are volumetric soil moisture content at saturation and on the previous day (respectively), and Z [m] is the soil depth. We considered that the top 60 cm homogeneous soil layer contains the majority of the root biomass (e.g., Fan et al., 2016; Mthandi et al., 2013), and hence this is the agrohydrological active soil depth Z for the major crops. ETa is determined by moisture availability (green water) relative to the readily available water, RAW [mm] $= 1000Zf(\theta_{FC} - \theta_{WP})$, where f [-] is a critical depletion fraction that represents the soil moisture level below which plants experience moisture stress. For all four cereal crops studied, the value of f was set to 0.55 following Allen et al. (1998). ETa was computed as $ETa_t = K_{s,t}ET_{o,t}$, where *Ks* [-] is the soil moisture stress coefficient (Allen et al., 1998):

$$\mathrm{K_{s,t}} = \begin{cases} \dfrac{\mathrm{SM_t}}{\mathrm{RAW}} & \text{if } \mathrm{SM_t} < \mathrm{RAW} \\ 1 & \text{if } \mathrm{SM_t} > \mathrm{RAW} \end{cases} \tag{4.8}$$

If the soil is saturated, the infiltrated water which is in excess of the soil field capacity percolates into deeper soil layers at the rate $Dp_t = 1000Z(\theta_t - \theta_{FC})$.

Crop module

The crop module simulates water-limited attainable yield (AY) based on the FAO water production function (Doorenbos and Kassam, 1979), which establishes a linear relationship

between relative crop yield losses and seasonal crop water use under water-limited climatic conditions:

$$1 - \frac{\mathrm{Y_w}}{\mathrm{Y_p}} = \mathrm{K_y}\left(1 - \frac{\mathrm{ETa}}{\mathrm{ETo}}\right) \quad (4.9)$$

where Y_w [ton ha^{-1}] and Y_p [ton ha^{-1}] are water-limited and energy-limited potential yields (respectively), and K_y [-] is the yield response factor that accounts for the complex crop characteristics that determine the crop water use. We redefined for AY, the ratio of water-limited yield Y_w, and potential yield Y_p as a function of evaporative stress index $ESI = 1 - \frac{ETa}{ETo}$:

$$\mathrm{AY} = 100(1 - \mathrm{K_y ESI}) \quad (4.10)$$

The recommended K_y values were set to 1.25 for maize, 0.9 for sorghum, and 1.15 for wheat, obtained from the FAO irrigation and drainage paper 66 (Steduto et al., 2012), and to 1.04 for teff (Araya et al., 2011).

Model evaluation

The CHC modelling framework was not explicitely calibrated, all parameters were taken from literature and global dataset, however the results were validated with independent datasets. Due to the limited availability of observed data we could not conduct a formal validation, however we compared the simulated values against the two most important observed agrohydrological variables *Q* and ETa at annual scale. The simulated mean annual *Q* was compared to published mean annual runoff observations from 17 sites within the RFA region (Table S4.3). We used the Nash-Sutcliffe Efficiency (NSE, Nash and Sutcliffe, 1970) and coefficient of determination R^2 to quantify the prediction skill. Similarly, we compared the simulated annual cycle and seasonality of ETa with five independent satellite- and model-based ETa products for the period 2003-2010. Finally, we examined how temporal variations in AY explain variabilities in seasonal crop production. For this, we correlated AY and total cereal production (TCP) at each computation grid during the period 1995-2010.

4.2.4. Assessment of Green water availability and its yield potentials

We evaluated the climatology of GWA and AY during the two growing seasons, Meher (May to September) and Belg (February to May) from the simulations for the reference period 1981-2010. We used soil moisture deficit (SMD) as a metric to evaluate GWA:

$$\mathrm{SMD} = 100\left(1 - \frac{\theta_{\mathrm{clim}}}{\theta_{\mathrm{FC}}}\right) \tag{4.11}$$

where θ_{clim} [m^3 m^{-3}] is the climatological mean seasonal soil moisture. *SMD* [%] is a dimensionless metric ranging from 0 (no moisture deficit) to 100% (maximum moisture deficit). The yield metric, *AY* [%], which was determined using Eq. (4.10) is also a relative quantity that explains the percentage of the energy-limited potential yield that can be viably attained under the actual water-limited conditions when all other agro-environmental factors such as nutrients are not limiting the yield, thus its values range from 0 (no yield) to 100% (non-water-limited potential yield). AY is nonlinearly related to SMD, decreasing with an increasing moisture deficit (Fig. 4.3). This nonlinearity results from the combined effects of climatic and soil characteristics. Fig. 4.3 also shows that attainable yield diminishes as the soil moisture deficit reaches its maximum, which is about 70% of the soil moisture at field capacity.

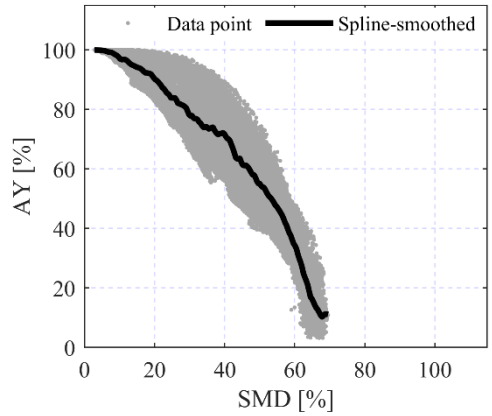

Fig. 4.3: The relationship between AY and SMD in the RFA region of Ethiopia. Each data point represents a single grid cell in the RFA domain considering both Meher and Belg growing seasons.

4.2.5. Future changes and climate sensitivity analysis

The modelling framework was applied to the future climate to assess changes in GWA and its implications for AY. We investigated the changes during three future periods: 2020-2049

(2030s), 2045-2074 (2060s), and 2070-2099 (2080s), under SSP1-2.6 (low greenhouse gas emission), SSP2-4.5 (intermediate emission), and SSP5-8.5 (high emission). The impact assessments presented here are based on the median of downscaled multiple GCM projections of future changes in rainfall, air temperature, and solar radiation. Other climatic variables were assumed to remain unchanged (Peleg et al., 2019). The impact analyses compare SMD and AY during the three future periods with the reference period for the two growing seasons, Meher and Belg, and four major crops grown in Ethiopia (teff, maize, sorghum and wheat).

We also examined the sensitivity of AY to changes in rainfall (green water supply) and atmospheric evaporative demand (AED) as represented by ETo. We determined the rainfall- and AED-sensitivity metrics, β_{RF} and β_{ED}, as the ratio of percent change in AY and percent change in rainfall or ETo on the basis of one-at-a-time analysis approach (Hamby, 1994), where the CHC modelling framework was forced by the future RF and ETo for all the three emission scenarios and three future periods:

$$\beta_{RF} = \frac{\%\Delta AY_{(RF)}}{\%\Delta RF} \qquad \beta_{ED} = \frac{\%\Delta AY_{(ED)}}{\%\Delta ETo} \tag{4.12}$$

We computed the comparative influences of the future changes in rainfall and AED on AY using the sensitivity ratio computed as $\beta_{ratio} = \beta_{RF} / \beta_{ED}$. The values of β_{ratio} range from zero to infinity with values less one indicating temperature sensitivity, and β_{ratio} values greater than one indicating AED sensitivity. This approach is based on the assumption that the changes in rainfall and ETo are independent, which was confirmed by the low squared correlation (R^2 = 0.098) between rainfall and ETo computed for the period 2020-2099 for the three SSPs at every grid point.

4.3. Results

4.3.1. Evaluation of the CHC model

We first evaluate the simulated runoff (*Q*), actual evapotranspiration (ETa), and water-limited attainable yield (AY) against other independent data. The comparison of simulated and observed mean annual *Q* (Fig. 4.4a) at the 17 field locations demonstrates a good performance (R^2 = 0.80 and NSE = 0.53) of the hydrological module. It is important to note that this comparison involves a point-to-grid value, and a perfect match cannot be expected due to this scale difference. The model underestimates the simulated *Q* at the two most humid locations. The comparison for ETa was made for six arbitrarily defined sub-regions of the RFA region as shown in the inset in Fig. 4.4b. The simulated mean annual ETa aligns well with the average estimates (hereafter, observed) from five independent ETa datasets (R^2 = 0.82), particularly in the north, northeast, and west sub-regions. Poorest fit is observed in the central sub-region where the model predicts higher ETa than observed, followed by the east sub-region where the simulated ETa is lower than observed. However, the simulated ETa estimates well the monthly cycles (Fig. S4.1) and annual ETa (Fig. S4.2).

We evaluated the simulations of *AY* [%] in terms of their correlation to variations in *TCP* [ton y^{-1}]. The rationale here is that in some regions TCP will follow the climate-driven attainable yield (high correlation), while in others the non-climatic factors, including nutrient input, improved cultivars, and pest and weed management, will play a role (low or negative correlation). Because TCP in the RFA region of Ethiopia exhibited an average increase of 0.36 ton ha^{-1} y^{-1} during the studied period (1995-2010), despite an almost constant AY, we conducted the correlation analysis on detrended TCP, thereby removing some of the effects of the non-climatic component of the variabilities in TCP (Kukal and Irmak, 2018; Mohammadi et al., 2023; Wakjira et al., 2021). The correlation analysis between detrended TCP and AY anomaly reveals mostly positive correlations (median Pearson's correlation coefficient, $\rho = 0.37$), particularly in the primary Meher-producing northern half of the RFA region (Fig. 4.4c).

Some areas, primarily in the humid and sub-humid regions of the southern and southwestern parts, and to a lesser extent in the western and southeastern parts of the RFA region, exhibited negative correlations between TCP and AY. This can be attributed to climatic regimes, land use, and socioeconomic practices. Two main factors may govern the AY-TCP correlation with

climate. In less water-limited humid areas like the southwestern part, the linear relationship assumed in the crop yield response to water availability (Eq.(4.9)) does not hold, as AY is weakly dependent on rainfall. Additionally, in these humid climates and areas with poor soil drainage (e.g., areas marked as E1 in Fig. 4.4c), crop yield can be adversely affected by saturated soil conditions, leading to waterlogging problems. Concerning land use and socioeconomic practices, the majority of areas with evident negative correlation are forest and/or agroforestry ecoregions (see E2 and E3 in Fig. 4.4c) (Kassawmar et al., 2018), while other areas are agropastoral (E4) where seasonal crop production is an optional practice. Thus, interannual variabilities in TCP depend largely on how much farmers opt for cereal production in a given production year.

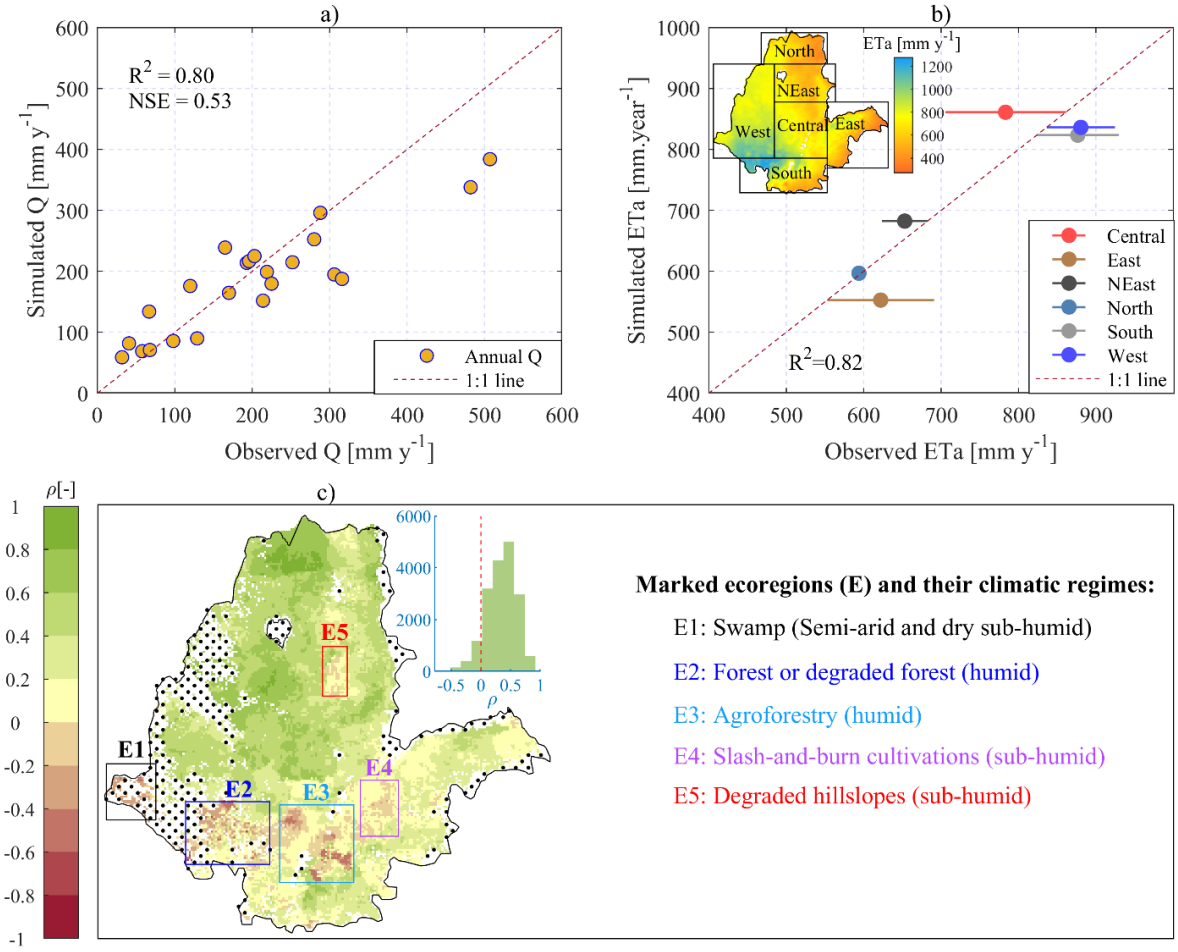

Fig. 4.4: Comparison of: a) Simulated and observed mean annual runoff (Q), measured over varying years at 17 locations, collected from published studies across the RFA region (Table S4.3). This is a grid-to-point comparison. b) Simulated and satellite- and model-based mean annual ETa (2003-2010) from five data products (see section 4.2.2) spatially averaged over six arbitrarily defined sub-regions shown on the inset map. The error bars represent the variability (deviation from the median value) of ETa among the five products. c) Map of Pearson correlation

coefficient (ρ) of detrended total cereal production (TCP) and AY for the period 1995-2010. TCP represents the sum of all cereals produced during the Meher growing season. The dots show uncultivated areas based on cropland cover fraction data from Copernicus Land Services (Buchhorn et al., 2020). The inset histogram shows the distribution of ρ. The rectangular marks (E1-E5) show ecoregions where the correlations are weak or negative.

4.3.2. Green water availability and attainable yield potentials

The reference climatology of growing season GWA and water-limited yield across the RFA region based on the computed SMD and AY values, is presented in Fig. 4.5, considering alfalfa as a reference crop (Ky = 1.1). During the Meher growing season, the southern and southwestern humid regions of the RFA exhibit low soil moisture deficit, with values less than 10 % of θ_{FC} (see Fig. 4.5a). Moving from the southwestern areas, the Meher SMD gradually increases in the northern and northeastern directions. In the peripheral semi-arid regions in the northeast, east, and southeast, the deficit reaches as high as 60-70 %. Notably, areas with SMD values below 20 % largely have AY>90 %. In other words, the water-limited yield gap less than 10 % of the potential yield achievable under unstressed moisture conditions (equivalent to fully irrigated system) can be attained in the south-central, southwestern, and eastern highland parts of the RFA region (Fig. 4.5b). As expected, low AY (mostly less than 40 %) is evident in the southern and southeastern semi-arid parts of the RFA region during the Meher growing season. In summary, the median Meher SMD values are 17 %, 30 %, 37 %, and 53 % in humid, sub-humid, dry sub-humid, and semi-arid climates, respectively, while the corresponding median AY values are 93 %, 80 %, 68 % and 46 % (Fig. 4.5e, f).

In the Belg season, the median SMD is mostly below 40% in the major Belg-producing areas in the south (see Fig. 4.5c), with AY of up to 80% in the humid areas in the southwestern regions (Fig. 4.5d). In the central and eastern parts of the RFA, which constitute other Belg regions, SMD is higher, reaching up to 60 %, resulting in a correspondingly lower AY of 40-60 %. The northern and northwestern parts of the RFA are dry during the Belg season, thus SMD is very high. Unlike in the Meher season, the differences in SMD among the climatic regimes are less pronounced, with median SMD ranging from 56 % in humid areas and 62 % in semi-arid regions (Fig. 4.5e).

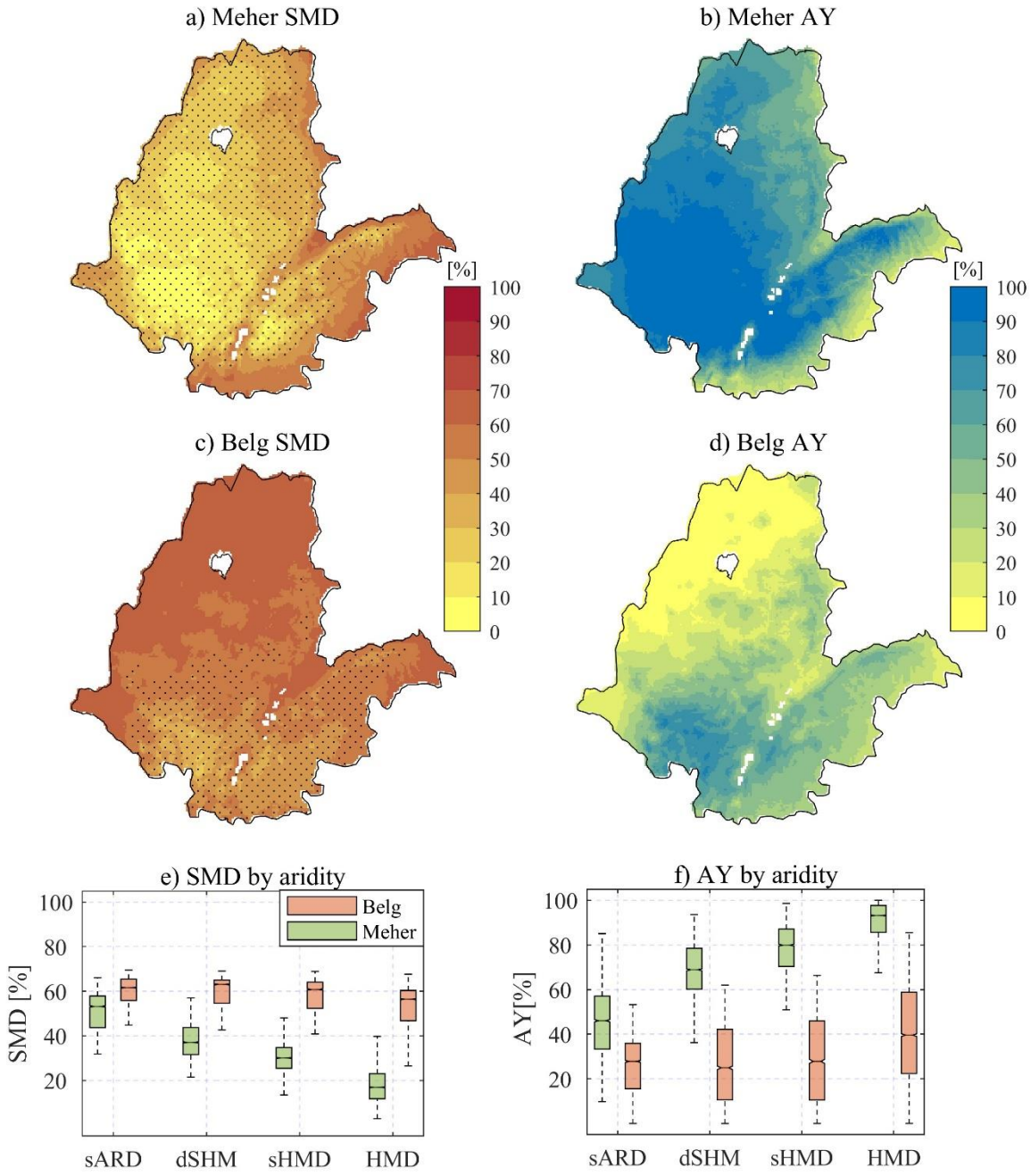

Fig. 4.5: Climatological soil moisture deficit (SMD) during Meher (a) and Belg (c), water-limited attainable yield (AY) for alfalfa (Ky = 1.1) during Meher (b) and Belg (d), SMD in different climatic regimes by aridity (e), AY in different climatic regimes during the two growing seasons for the period 1981-2010. Aridity classification is given in Fig. 4.1: sARD = semi-arid, dSMD = dry sub-humid, sHMD = sub-humid, HMD = humid. The dotted areas in (a) and (c) show the Meher- and Belg-producing regions respectively, delineated based on the Atlas of Ethiopian Rural Socioeconomy (IFPRI and CSA, 2006).

4.3.3. Future changes in GWA and AY

Projected changes in growing season rainfall and temperature

Based on the downscaled multiple GCM median projection, the growing season climate across the RFA regions is expected to become warmer and wetter in future periods (Fig. 4.6). The temperature increase is progressive over time, especially under the intermediate and high emission scenarios, and shows little spatial variability (e.g., Fig. 4.6c). However, changes in rainfall patterns vary across regions and depend on the growing seasons. For example, Meher-producing areas are likely to experience increased rainfall, while dry seasons are expected to remain unchanged or become even drier (e.g., Fig. 4.6a, b). Similarly, during the Belg season, the Belg-producing areas in the southern part of the RFA region are expected to become wetter under higher greenhouse gas emissions. In general, a rainfall increase of up to 250 mm is anticipated over a large part of the RFA region during the Meher season under the high emission scenario in the 2060s (Fig. 4.6a) and up to 300 mm in the 2080s (not shown). During the Belg season, rainfall increase could reach up to 150 mm under the high emission scenario in the 2060s. Additionally, the mean annual temperature is projected to rise by up to 3 °C in the 2060s and up to 5 °C by the end of the century.

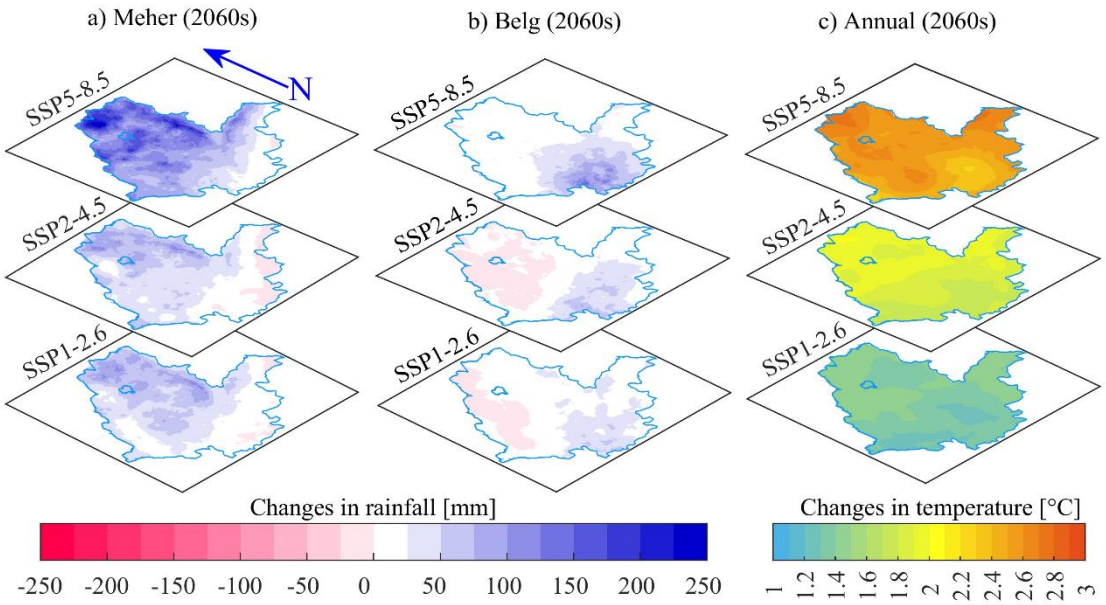

Fig. 4.6: Projected changes in seasonal rainfall in the 2060s during a) Meher (May-September), b) Belg (February-May), and c) changes in annual temperature under the three SSPs. The changes presented here are the median of 26 downscaled GCM projections for rainfall and 21 GCM projections for temperature.

Future changes in soil moisture deficit

In the face of the expected warmer and mostly wetter climate across the RFA region of Ethiopia, the GWA is likely to increase. In the main growing season, Meher, SMD is expected to decrease by up to 5 % over a large part of the region in the 2030s under all emission scenarios (Fig. 4.7). However, in the 2060s and 2080s, SMD is projected to increase by 3-15 % over the western, southwestern, and southern parts under the low and intermediate emission scenarios. This is expected, given the projected minimal change in rainfall under the warming climate over these regions, as shown in Fig. 4.6 in the 2060s, for example.

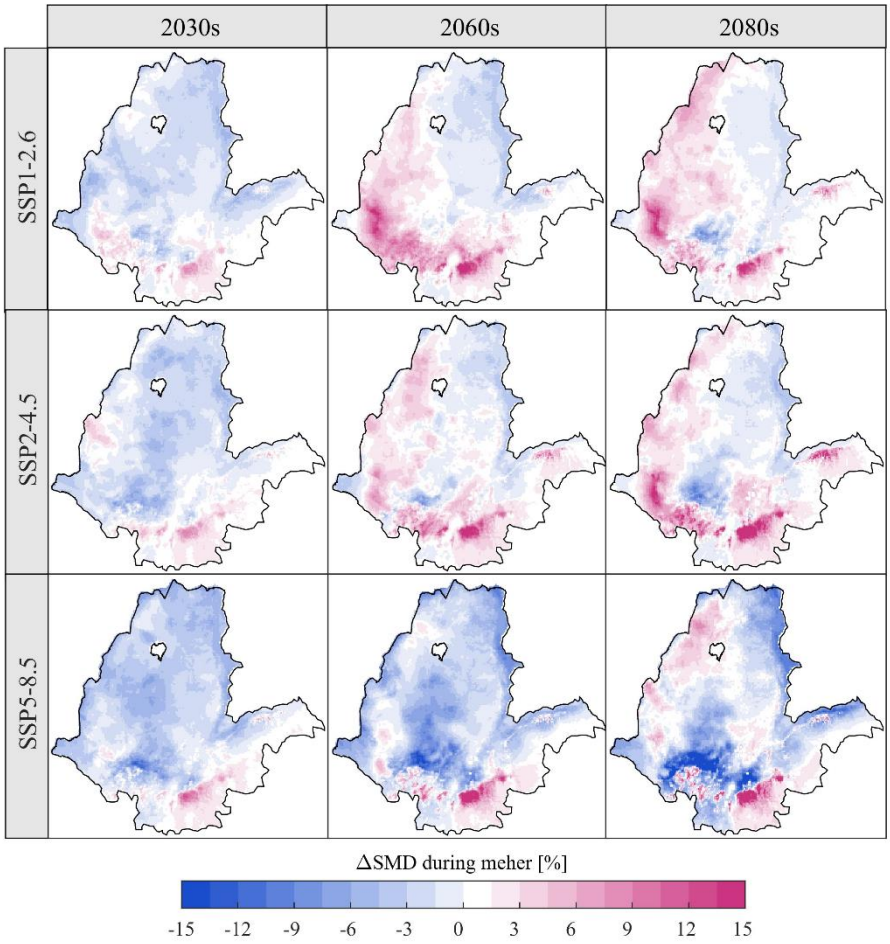

Fig. 4.7: Projected changes in soil moisture deficit (SMD) across the rainfed agricultural region of Ethiopia during the Meher growing season under the SSP1-2.6, SSP2-4.5, and SSP5-8.5 scenarios in the 2030s, 2060s, and 2080s

Under the high emission scenario, soil moisture deficit is likely to decrease over the majority of the region, following the increase in rainfall. The central and northeastern parts of the RFA regions are generally expected to experience a slight decrease in SMD and thus slightly higher

GWA under all scenarios in the future. The highest increase in SMD is observed in the southwestern and southern parts of the RFA region, where the Meher rainfall mostly remains unchanged (Fig. 4.6a).

In the Belg growing season, soil moisture deficit consistently decreases over the producing regions in the future periods under all scenarios (Fig. 4.8). These increases in GWA are particularly significant across the main Belg region in the southwestern parts of the RFA. In these areas, SMD is expected to decrease by up to 6 % in the 2030s (2020-2049) and by over 15 % in the 2080s under the low and intermediate emission scenarios.

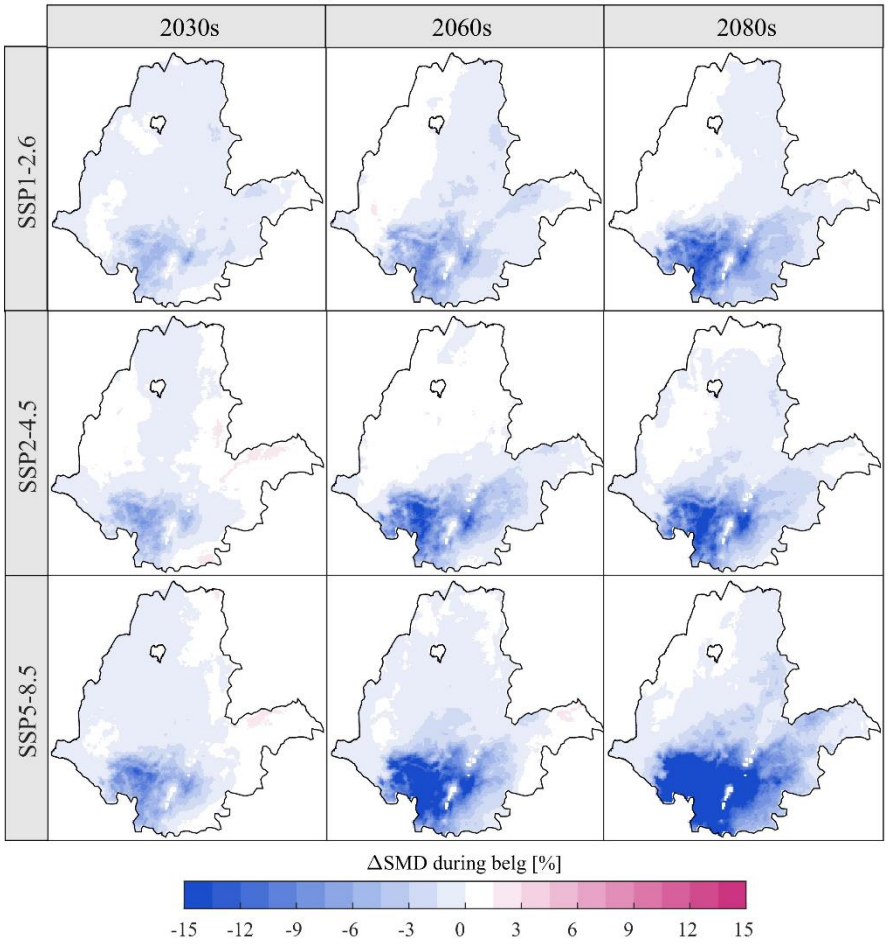

Fig. 4.8: Projected changes in soil moisture deficit (SMD) across the rainfed agricultural region of Ethiopia during the Belg growing season under the SSP1-2.6, SSP2-4.5, and SSP5-8.5 in the 2030s, 2060s, and 2080s

Under the high emission scenario, GWA across the primary Belg-producing regions in the south and southwest is expected to increase by up to 35 % by the end of the century. Overall, the projected changes in soil moisture deficit across the study area are largely consistent with

a recent global-scale assessment by Liu et al. (2022), which reported a decrease in agricultural water scarcity of up to 15 % in the RFA region for a comparable future period (2026-2050) and reference period (1981-2005) under the RCP2.6 scenario.

Future changes in water-limited crop yields

The likely implications of changes in SMD on attainable yields for the four major cereal crops (teff, maize, sorghum, wheat) cultivated in Ethiopia are presented next. We summarize the changes occurring during the two growing seasons in their respective producing regions and across the various climatic regimes of the RFA.

Meher season

In the Meher season, minor or no changes in AY are expected, although regional differences exist in both the magnitude and direction of these changes. For example, for the 2060s, the projected changes in AY for teff range from -7.8 % to 5.3 % under the low-emission scenario, and from -12.1 % to 10.7% under the high-emission scenario. Similarly, for maize, the expected changes range from -7.8 % to 4.7 % under the low emission scenario, and from -11.5 % to 6 % under the high emission scenario (Fig. 4.9a). Under the intermediate emission scenario, the changes are predominantly negative, ranging from -9.3 % to 1.8 % for teff and from -8.2 % to 1.2 % for maize. Similar order of magnitude and direction of changes were observed for sorghum and wheat crops (refer to Fig. S4.3-4.7).

Comparing the near- and long-term future changes, we note a decreasing trend in AY for all crops under all emission scenarios. During the 2030s, the northern parts of the RFA region are likely to experience increases, while decreases are mainly evident in the southern and southeastern parts of the Meher-producing areas. Notably, the marginal areas in the south and southeast are likely to experience the most significant decrease in AY for all crops and under all scenarios. By the 2080s, most Meher-producing areas are expected to witness either no change or a decrease in AY (Fig. S4.3-4.7).

We also examined the water-limited attainable yield responses in different climatic regimes (Fig. 4.10). In humid areas, the temporal changes and spatial variability in AY are small for all crops under all emission scenarios. This is because these areas rarely have moisture limitations, meaning that an increase in rainfall will have a minimal effect on yield improvement. In

contrast, in semi-arid, dry sub-humid, and sub-humid areas, AY is likely to increase in the 2030s and then consistently decrease in future periods under both low and high emission scenarios. Under the intermediate scenario, AY is expected to decrease in the 2060s and then increase in the 2080s. Spatial variations are particularly high for teff, especially in semi-arid areas with changes ranging from -10 % to +5 % in the 2060s.

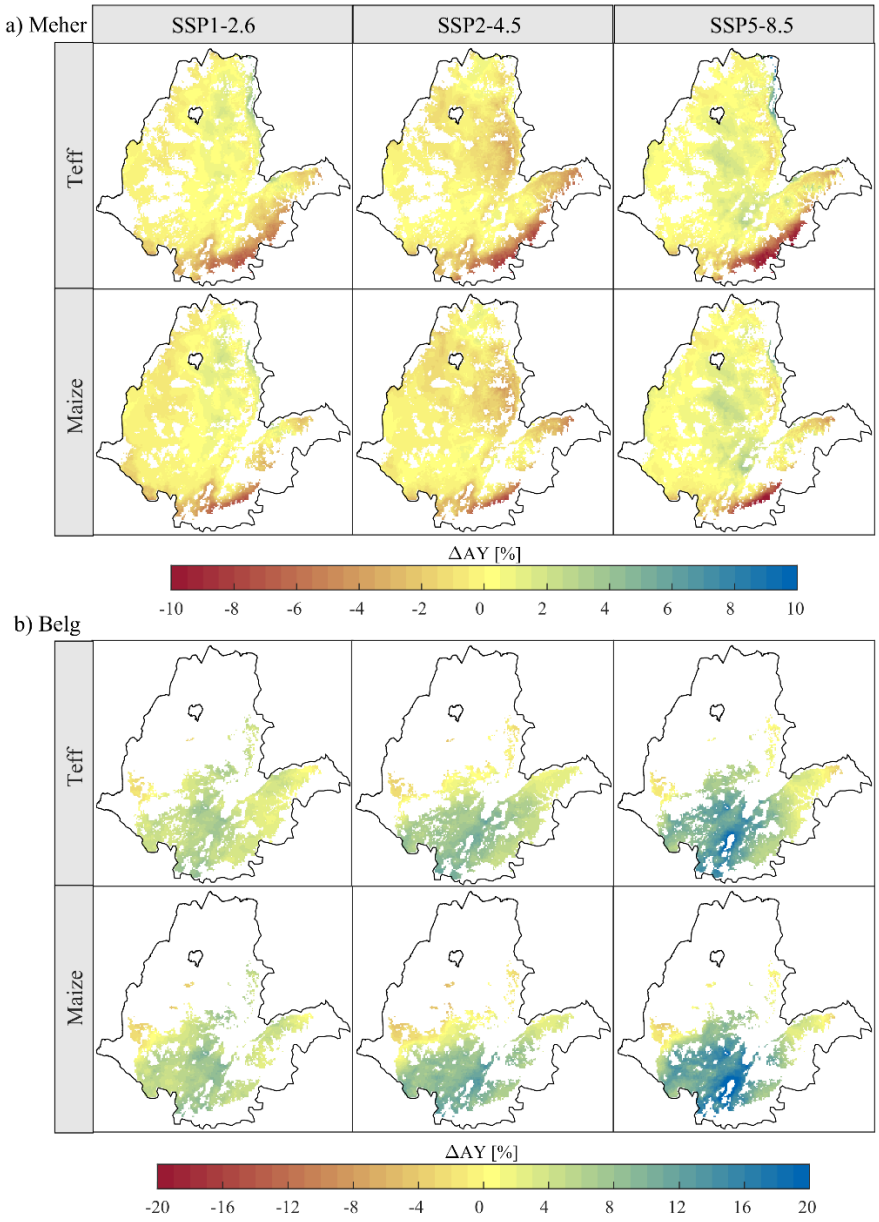

Fig. 4.9: Projected changes in water-limited attainable yield for teff and maize in Meher (a) and Belg (b) during the 2060s under the SSP1-2.6, SSP2-4.5, and SSP5-8.5. The RFA region was masked using cropland suitability maps (Wakjira et al., under review) to restrict the analysis to areas potentially suitable for each crop. The non-producing areas during both seasons were also masked out following the Atlas of Ethiopian Rural Socioeconomy (IFPRI and CSA, 2006).

Belg season

Following the increased rainfall and the subsequent rise in GWA, AY is projected to increase significantly and progressively over the major parts of the Belg-producing regions in future periods. However, a few areas will experience small decreases (Fig. 4.9b). For teff, the expected changes in the 2060s range from -3.5 % to 8.8 % under the low emission scenario and from -3.6 % to 21.7 % under the high emission scenario. Similarly, for maize, the changes range from -5.9 % to 10.6 % under the low-emission scenario and from -4.7 % to 27.6 % under the high-emission scenario. These positive changes are expected to intensify, particularly under the high emission scenario, with the majority of the Belg-producing region experiencing an increase in AY of over 20 % for all crops examined. The changes for all crops and future periods have been illustrated in the supplementary material appended to this paper (Fig. S4.7-4.10).

The changes in AY during the Belg season in different climatic regimes are illustrated in Fig. S4.11. The variations in overall changes in AY among these regimes depend on the emission scenario. Under the low emission scenario, median changes in AY do not significantly vary across climatic regimes, remaining positive throughout the three future periods for all crops examined. In contrast, under the intermediate and high emissions, AY tends to increase with climatic wetness (from semi-arid to humid climates).

Decreases in AY are mainly noticeable in semi-arid and dry sub-humid areas in the 2030s. However, during the 2060s and 2080s, median changes in AY are relatively consistent across climatic regimes for all crops. Spatial variability in changes generally increases with climatic wetness and into the future periods under the low emission scenario while a decreasing pattern rarely observed under the intermediate and high emission scenarios. In all cases, spatial variability of the changes is lower in the 2030s compared to the mid- and long-term future periods. Concerning the examined crops, it was observed that the projected increases in AY are higher for maize and wheat compared to teff and sorghum.

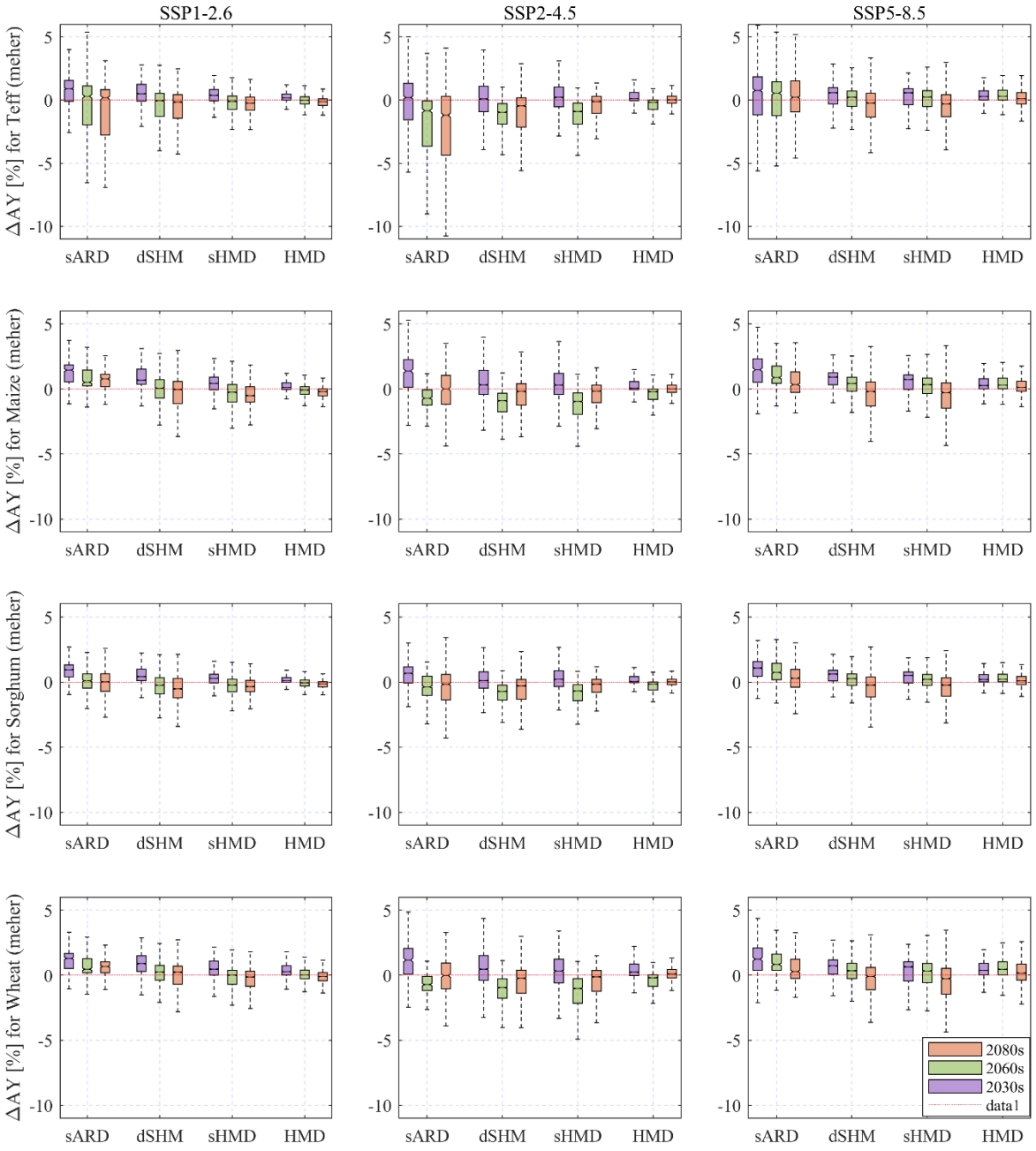

Fig. 4.10: Boxplots of the projected changes in water-limited yields (AY) of the four major cereal crops produced in Ethiopia in different climatic regimes under the three SSPs during the three future periods, during the Meher growing season. Each boxplot represents the distribution of AY changes within Meher-producing areas for all grid cells in the respective climatic regime. Outlier values have been excluded.

4.3.4. Climate sensitivity of attainable crop yields

The spatiotemporal average relative sensitivity (β_{ratio}) of AY to atmospheric evaporative demand (AED) and rainfall for the four crops under the three SSPs are presented in Fig. 4.11. The results are averaged for the three future periods for the main growing season Meher at the

administrative agricultural zones of Ethiopia. Results for the Belg short growing season are presented in Fig. S4.12. The climate sensitivity is reported at a zonal scale, rather than at the grid scale, to provide zone-specific insights into the relative importance of ETo and rainfall that determines future green water supply; this information is crucial for agricultural water management planning, service provision, and decision-making at the institutional scale. For the interpretation, we categorize the sensitivity of AY as AED-sensitive ($\beta_{\text{ratio}} \leq 0.8$), AED- and rainfall-sensitive ($0.8 < \beta_{\text{ratio}} < 1.2$), and rainfall-sensitive ($\beta_{\text{ratio}} \geq 1.2$).

During the Meher growing season, AY is predominantly AED-sensitive for all crops under all emission scenarios we considered (Fig. 4.11). The percentage of zones across which AY is, on average, AED-sensitive is 64 % for teff, 50 % for maize, 52 % for sorghum and 77 % for wheat under low emissions. The influences of AED on AY increase with GHG emissions. Under high emissions, AED dominates the changes in AY in 82 %, 65 %, 73 %, and 92 % of the zones for teff, maize, sorghum, and wheat respectively. In the remaining zones, the simultaneous influences of rainfall and AED are evident, except for maize, where rainfall has a more significant impact than AED. Notably, changes in rainfall have a low influence on teff and wheat, with AY being rainfall-sensitive in less than 5 % of the zones. These crops are exceptionally more sensitive to AED compared to maize and sorghum, as indicated earlier. Temporal changes in climate sensitivity of AY are also evident, but the spatial patterns do not change significantly in future periods.

The influences of changes in AED and rainfall on AY are primarily linked to the climatic regimes of the RFA region. In semi-arid and dry sub-humid climates, AY is predominantly AED-sensitive. This is particularly noticeable in the northeastern zones (covering the eastern parts of Tigray and Amhara, and western zones of Afar regions) and the central to eastern zones (including East Shoa, Arsi, and Hararge zones of the Oromia region) in the RFA region for all crops under low emissions (left panels in Fig. 4.11).

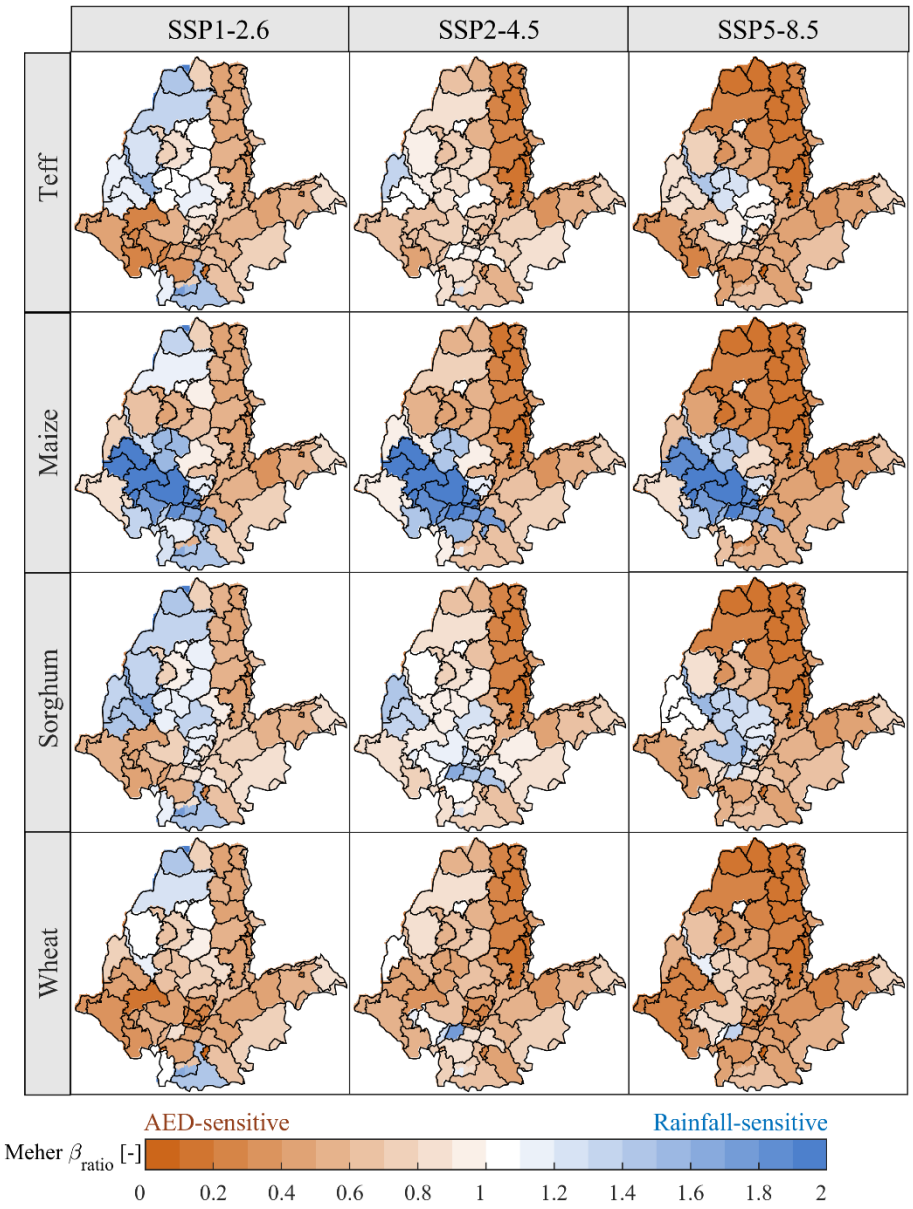

Fig. 4.11: Area-averaged relative sensitivity (β_{ratio}) of water-limited attainable yields (AY) to rainfall and atmospheric evaporative demand (AED) for the Meher growing season at the administrative zone level under the low, intermediate, and high emission scenarios. The mapped values represent the average of β_{ratio} of all grid cells within each zone, and all three future periods. The names of the administrative zones are indicated in Fig. 4.1 and Table S4.1.

This influence of AED intensifies to more zones in sub-humid and humid climates under the intermediate and high emissions. Rainfall-sensitivity is largely evident in humid climates, mostly in the central, western, and northwestern zones under low emissions for all crops except wheat, which is rainfall-sensitive only in the northwestern parts of the RFA region (Western Tigray and North Gonder zones). Maize AY is strongly rainfall-sensitive under all scenarios,

across the humid zones in the western part of Oromia (Wollega, Jimma, and Illubabor zones), Sidama region, and most of the zones of the SNNP region in the southwestern part.

In contrast to the main growing season, future changes in AY during the Belg growing season are primarily influenced by changes in rainfall, particularly in the main Belg-producing areas in the southwestern, southern, and southeastern parts of the RFA region for all crops under all SSPs (Fig. S4.11). There is less spatio-temporal change in the rainfall sensitivity of Belg AY. Only under the high emission scenario does the influence of changes in AED contribute to the influences of rainfall, primarily in the northern half of the RFA region, which remains dry during this season.

4.4. Discussion

4.4.1. Current water limitations and crop yield gaps

Achieving crop yield at its potential level is not only a matter of adaptation to climate variability and change, but it is also a key strategy for eradicating rural poverty and building resilience in heavily agricultural nations like Ethiopia (Abrams, 2018; Tittonell and Giller, 2013). In the effort to enhance crop yields, three levels of yields can be defined and targeted (van Ittersum et al., 2013): (i) potential yield (Yp), primarily defined by temperature, radiation, light, and cultivar; (ii) water-limited yield (Yw), determined by moisture availability and soil type, but within the constraints of Yp; and (iii) actual yield (Ya), which is dependent mainly on farm management practices including water, soil, nutrient, pest and weed management. In RFA systems water is a major limiting factor, and thus, Yw defines the rainfed crop yield potential (Dijk et al., 2017; van Ittersum et al., 2013), as Yp can be reached only by supplementing the green water through irrigation to fully meet the crop water demand.

Fig. 4.12 illustrates the current conditions of the three yield levels in a Budyko-like space (Budyko, 1958) and analyzes the yield gaps with AY. In the Meher season, green water has the potential to produce more than 80 % of Yp across 52 % of the Meher-producing regions of Ethiopia (highlighted by the shaded area in Fig. 4.12a). Only about 27 % of the Meher-producing region is moisture-limited (P/ETo < 1). However, there are areas where the seasonal rainfall is greater than the atmospheric evaporative demand, but AY is still low (e.g., shown by the red ellipse in Fig. 4.12a). This discrepancy is primarily linked to surface and soil characteristics that influence rainfall-runoff partitioning and green water storage capacity.

From a management perspective, there may be limited options to address inherent soil physical properties like textural composition, apart from measures such as amendment with organic matter, which might to some extent, improve infiltration and green water storage capacity (Hartmann and Six, 2023).

On the other hand, there is an extremely large yield gap between Ya (orange rectangle symbols) and Yw (blue diamond symbols) as shown in Fig. 4.12a, for maize for example. Our comparison of Yw from study results at 14 experimental case studies across the RFA region (see Table S4.4 of the supplementary material), and the corresponding zone-averaged Ya from the agricultural sample survey of Ethiopia (e.g., CSA, 2010) shows that the absolute yield gap at these sites ranges from 1.3 to 7 ton.ha^{-1} (Fig. 4.12b).

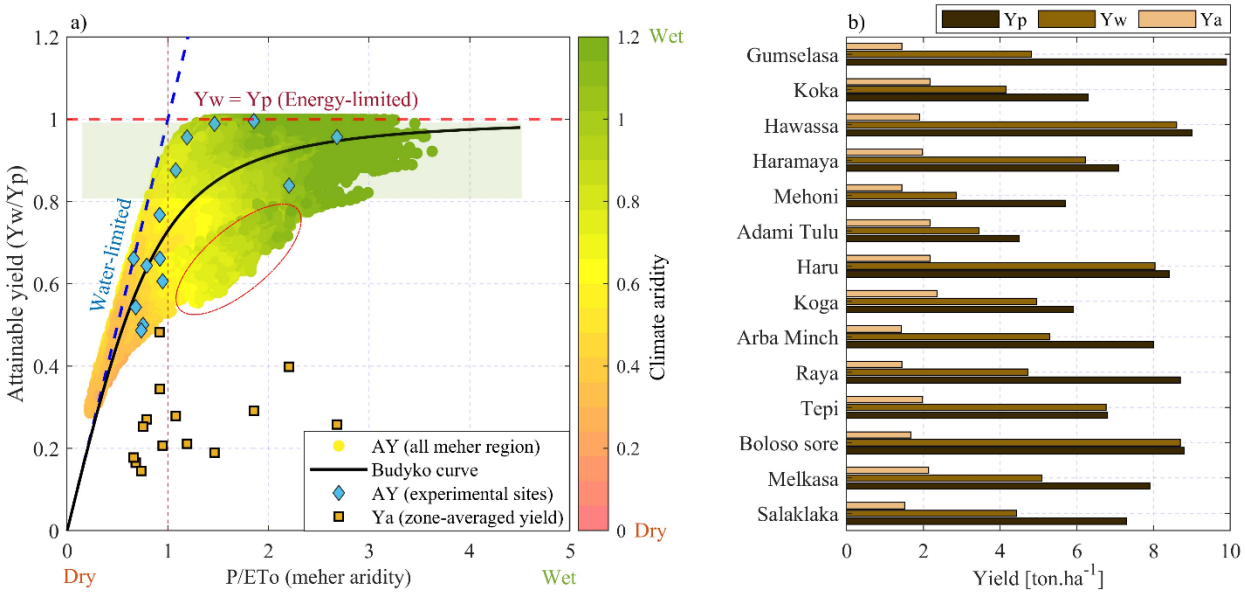

Fig. 4.12: a) Scatterplot of water-limited attainable maize yield fraction (Yw/Yp) against seasonal aridity showing the energy (dashed red line) and water limitations (dashed blue line). The color gradient shows the climatic aridity of each grid cell (different from the values on the x-axis, which are seasonal aridity). The solid line represents the parametric Budyko curve fitted to the point cloud. The blue diamonds show Yw at 14 locations across the RFA region, derived from published maize Yp data (fully irrigated, optimally fertilized). The orange squares are the corresponding average actual maize yield (Ya) in the administrative zone within which the experimental location is found. The shaded area indicates maize AY>80 %. b) Comparison of Yp (experimental), Yw (derived as a fraction of Yp using AY), and Ya (also as a fraction of Yp). The list of experimental locations is given in Table S4.4.

This gap should be reduced by addressing farm management actions, including tillage, resources use (green water and soil nutrient and fertility management, cultivar selection) and

crop protection (pest and weed management) (Lobell et al., 2009). Other limitations like soil salinity, acidity, and waterlogging are also among the yield-reducing factors that need a substantial amount of financial and technological investment. Our previous work has shown that actual crop yields are also greatly influenced by seasonal rainfall characteristics such as timing (onset and cessation) and seasonal distribution (Wakjira et al., 2021), which suggests that measures like onset-informed planting (Lala et al., 2021) could be beneficial to reduce the yield gaps associated with water stress in moisture limited areas.

4.4.2. Implications for agricultural water management

While the changes in water-limited attainable yield vary greatly across the RFA in terms of both magnitude and direction during the main growing season, the results show that semi-arid and dry sub-humid areas are most likely to experience a reduction in AY. On one hand, this is attributed to an intensified soil moisture deficit, as evident for example in the northwestern, western, southern, and southeastern semi-arid areas (with low and intermediate emissions in the 2060s and 2080s, in Fig. 4.7), and on the other hand, it is also a result of increases in AED-sensitivity (Fig. 4.11), particularly in the moisture-limited regions. In these regions, it would be beneficial to implement on-farm water management strategies that maximize green water availability and minimize non-productive green water flows.

Practices that aim to maximize GWA should focus on altering the rainfall-runoff partitioning processes by increasing the opportunity for infiltration during rainfall through various surface management practices. For example, tillage and physical measures like bunds, infiltration trenches, tied-ridge, and planting pits among others (Hurni, 2016; Makurira et al., 2009; Nyakudya et al., 2014) have been successfully evaluated in field experiments and on-farm practices. Other measures like residue retention and cover cropping not only enhance infiltration, but also suppress the non-productive evaporation from the soil surface. (Rockström, 2003). Additionally, measures that improve infiltration also offer the side benefit of reducing soil erosion by runoff, another critical challenge that contributes to the crop yield gap. Finally, we strongly suggest that the selection of water management practices should be carefully made by evaluating their need and suitability primarily based on climate and soil characteristics. For example, in humid climates with heavy clay soils, such practices may result in waterlogging problems, which is also a major yield-reducing factor in such environments (Manik et al., 2019; Pittelkow et al., 2015).

4.4.3. Intensification of the Belg season production

The projected increase in GWA and AY during the Belg season may provide an additional opportunity for farmers to intensify their production during this season. This, however, will need firm stakeholder commitment to plan and mobilize resources for action in the framework of National Adaptation Plans (NAP) and similar initiatives (Conway and Vincent, 2021). Long-term awareness of stakeholders, ranging from the institutional level to farm-level actors, on the expected challenges and opportunities of climate change, supported by climate information services for short-term decisions, is highly important to exploit such opportunities (Grossi and Dinku, 2022b). In addition to climate information like the forecast information of the expected onset and cessation of Belg rain, extensive support on proper selection of crop types compatible with the duration of the short growing season is vital to help farmers effectively plan and undertake bi-annual production without compromising the main growing season. Moreover, the high soil moisture deficit (Fig. 4.5) and high sensitivity of water-limited yield to rainfall during this season (Fig. S4.12) suggest that green water management practices are crucial for enhancing productivity.

4.5. Conclusions

We investigated the cascading effects of climate on green water availability and water-limited attainable yield (AY) in the context of the rainfed agricultural region of Ethiopia. We integrated hydroclimatic processes with crop yield response through an agrohydrological modelling framework to assess the current potential, future changes, and climate sensitivity of AY. The AY across the Ethiopian RFA region is 79 % of what could be produced under water-unlimited conditions during the main growing season (Meher) and 37 % during the shorter season (Belg) during the reference period, with regional variation depending on the climatic regimes. The soil moisture deficit (percent of soil moisture content at field capacity) during this period is on average about 29 % in Meher and 56 % in Belg.

The future climate over the RFA region is expected to be warmer and mostly wetter. Under these changes, future changes in green water availability and AY vary across regions, emission scenarios, future periods, and between the two growing seasons. In Meher, the expected changes in AY range largely in the ±5 % range under all scenarios and future periods. Changes during the 2030s are largely positive under all scenarios, but AY shows overall decreases in the 2060s and 2080s. Decreases in AY are mostly evident in semi-arid regions, with teff being

the most affected. These changes are dominantly driven by the atmospheric evaporative demand (AED), that is by temperature increase, especially in moisture-limited regions. The influence of AED increases under the intermediate and high emission scenarios, suggesting the need for due attention to management strategies that suppress evaporative losses in the future. In Belg, AY is expected to progressively increase by up to 20 % under the high emission scenario by the end of the century, providing an opportunity for farmers to expand crop production in this season. These changes are dominantly driven by increases in rainfall, implying that green water management practices that increase water availability would further improve crop yields during this season. Furthermore, our assessment of documented field experiment results and crop yield data from the RFA region reveals a large gap between the actual and water-limited yield. For example, for maize on average only 36 % of AY is actually realized under the current practices, suggesting that green water management practices should be combined with other measures that overcome the yield-reducing factors related to soil nutrient, tillage practices, plant protection, and cultivar improvement.

Finally, the CHC modeling framework developed in this study can be applied to conduct similar assessments in other regions. It can also be adopted for various agrometeorological applications, such as estimating seasonal water availability and crop water demand for both irrigated and rainfed systems, as well as predicting relative yields for management planning and decision-making. This framework minimizes dependence on process-based crop models for such analyses, which often require intensive measurement data for the calibration of several model parameters.

Chapter 5

Current and future cropland suitability for cereal production across the rainfed agricultural landscapes of Ethiopia

Author
Mosisa Tujuba Wakjira

Co-authors
Nadav Peleg, Johan Six and Peter Molnar

Submitted to Agricultural and Forest Meteorology
Submitted on 19 December 2023
Revised on 30 April 2024

Key finding

- Future changes in suitability involve altitudinal shifts and areal contraction
- Teff and wheat croplands are drastically affected in lowland agroecologies
- Cropland suitability is rainfall-sensitive in hyper-humid and semi-arid areas
- Suitability is temperature-sensitive especially at the lowest and highest altitudes

Author's contributions

Conceptualization, data collection and preprocessing, methodology, discussion, original draft preparation, revision.

Co-authors' contributions

N. Peleg: methodology, discussion, reviewing and editing. ***Johan Six***: discussion, review and editing. ***P. Molnar***: methodology, discussion, reviewing and editing, supervision.

5.1. Introduction

One of the major impacts of climate change globally is the disturbance it imposes on ecosystem functioning, which ultimately leads to redistribution and even irreversible losses of species (Pecl et al., 2017; Schmidhuber and Tubiello, 2007). The influences on crop species threaten human society as they may reduce global food production and affect the livelihoods of people involved in agriculture (Godfray et al., 2010). Global assessments show that the observed and projected changes in cropland distributions follow latitudinal patterns with temperate regions gaining cropland suitability (CLS), while in the tropical regions croplands are in general becoming less suitable (e.g. Kummu et al., 2021; Ramankutty et al., 2002; Rosenzweig et al., 2014; Zabel et al., 2014). At local and regional scales CLS changes with elevation, primarily decreasing in lowlands and increasing in highlands (Brusca et al., 2013; Castro-Llanos et al., 2019). Although climate-related changes lead to gains in suitability in some regions and losses in others, the overall global change in cropland suitability is projected to considerably decrease globally, as a warming temperature and uncertain rainfall patterns put future food production at high risk (FAO, 2022).

Regions like sub-Saharan Africa, where the national economies and livelihoods of citizens are strongly dependent on agriculture, are likely to face severe socioeconomic crises and increase in poverty due to the climate-induced shifts and reductions in CLS (e.g. De Souza et al., 2015; Tim Wheeler and Braun, 2013). Ethiopia is among the nations in which agriculture is an extremely important socio-economic sector. It contributes about 34% to the national GDP and 85% of the export revenues and supports the livelihoods of 85% of the population (Eshete et al., 2020; NBE, 2021). Because nearly 95% of the cropland is under smallholder rainfed practices (FAOSTAT, 2018), the farming system is highly prone to weather and climate variability and changes (Shukla et al., 2021) in multiple ways. For example, the productivity of the rainfed agriculture (RFA) is extremely sensitive to fluctuations in the timing and amount of rainfall (Grossi and Dinku, 2022b; Lala et al., 2021; Wakjira et al., 2021), agricultural drought risks are high in the country and the entire horn of Africa (Carrão et al., 2016; Chere et al., 2022; Eze et al., 2022; Mera, 2018; Meza et al., 2020; Philip et al., 2018; Viste et al., 2013), weather-triggered pest infestations are becoming more frequent and are disastrous to crops (Alemu and Neigh, 2022; W. Peng et al., 2020; Zeleke et al., 2023). While these events only occur irregularly and with different severity levels depending on the driving

agrometeorological conditions, the change in CLS is a continuous effect, and a critical challenge that fundamentally determines the long-term cropland availability (Ramirez-Cabral et al., 2017; Tim Wheeler and Braun, 2013).

In recent years, several global and continental-scale assessments and databases of CLS have been developed, highlighting the distribution of various crop species. For example, the Global Agro-Ecological Zone (GAEZ) database (Fischer et al., 2021), which was developed based on the fundamental principles of land evaluation recommended by the Food and Agriculture Organization (FAO), offers a range of agroecological information, including CLS for 50 crops. Schneider et al. (2022) compiled a global inventory of potentially suitable croplands for 26 crop species using a fuzzy logic land suitability model while Chemura et al. (2024) recently developed an Africa-wide CLS dataset for 23 major crops using the EcoCrop model (Ramirez-Villegas et al., 2013). These assessments are optimized for global and regional scales in terms of inputs and models considered, which to some extent limits their ability to represent local scale conditions. Country-specific assessments are necessary to incorporate these details by leveraging locally available inputs (e.g., crop yield data) and utilizing the best-performing gridded climatic inputs, to better inform planning and practical decisions at national and sub-national levels.

In this regard, a limited number of studies have assessed the impacts of climate change on future croplands in Ethiopia. Evangelista et al. (2013) examined the future spatiotemporal changes in the major crops (teff, maize, sorghum, and barley) over the country by applying the Maxent species distribution model (Phillips et al., 2004) with several bioclimatic variables and crop yield datasets and found an overall decrease in CLS for cereal crops. More recent country-level studies focused on the teff CLS using species distribution models (Alemayehu et al., 2020; Bezabih et al., 2020; Zewudie et al., 2021), while Gebresamuel et al. (2022) assessed the altitudinal shifts in the major crops in southern Tigray using a similar approach and found a considerable migration toward the highlands and a decline in the suitable area of crops like wheat and barley. Two major gaps are noticeable in the previous studies on CLS changes. First, the spatial predictions of the CLS are solely based on climatic variables and do not account for the effects of other important environmental factors such as soil properties. Second, future changes are assessed based on a few projections of general circulation models (GCM), making the results highly uncertain.

In this study, we aim to define more accurate CLS maps and climate-driven changes therein by addressing the gaps mentioned above. We tackled the first gap by using a combination of climatic and soil factors. We developed a model linking observed crop yields with these combined predictors and used it to provide reliable potential CLS maps of the four major cereal crops (i.e., teff, maize, sorghum, and wheat) across the RFA areas of Ethiopia under the current climate. We tackle the second gap by examining the future changes in the CLS of the crops considering multiple GCM projections, and by separating the influences of rainfall and temperature on these changes. Moreover, we provide an in-depth analysis of the implications of these changes on future food production, the livelihoods of farmers, as well as environmental sustainability. With that information, we demonstrate the need for context-based and appropriate climate actions, which is inadequately considered in the current national adaptation plan of Ethiopia (FDRE, 2019).

5.2. Materials and Methods

5.2.1. Study area

The rainfed agricultural region of Ethiopia (Fig. 5.1) covers ~667,000 km^2 making up 59% of the total landmass of the country (Kassawmar et al., 2018) where over 90% of the population is living (CSA, 2007). The elevation of the RFA region ranges from about 400 to 4500 m.a.s.l and spans arid (annual rainfall of about 270 mm y^{-1}) to hyper-humid (~2100 mm y^{-1}) climates (Wakjira et al., 2021). Crop production takes place largely between May and September, locally known as the 'Meher' production season that accounts for about 88% of the annual crop harvest. The shorter growing season 'Belg' from February to May provides a second production window in some regions (Taffesse et al., 2012). Cereals are the main crops produced under the RFA practices and comprise about 80% of the total crop production in the country, with the top four cereals being teff, maize, sorghum, and wheat (CSA, 2010).

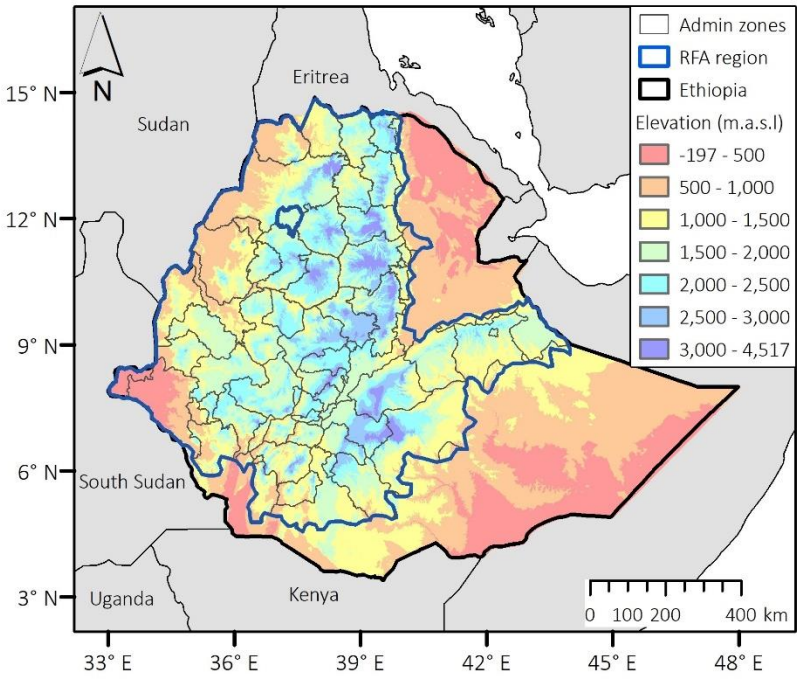

Fig. 5.1: Altitude and map of the rainfed agriculture (RFA) region (blue outline) in Ethiopia (Kassawmar et al., 2018). The inner polygons are the 62 administrative zones within the RFA region for which the annual crop production statistics are summarized (CSA, 2010).

5.2.2. Data

Gridded climate (precipitation and temperature) and soil properties (texture, pH, and organic carbon), along with national crop yield data, were used for the assessment of the CLS. The Climate Hazards Infrared Precipitation with Station (CHIRPS) rainfall (Funk et al., 2015), the bias-corrected and spatially disaggregated ERA5-Land maximum and minimum 2-m air temperature (BCE5) (Wakjira et al., 2023, 2022), and ERA5-Land surface net solar radiation (Muñoz-Sabater et al., 2021) datasets were used for the reference climate over the period 1981-2010. The future precipitation and temperature climates were retrieved from multiple GCMs (25 for precipitation and 21 for temperature) of the phase 6 Coupled Model Intercomparison Project (CMIP6) for three Shared Socioeconomic Pathways, (SSPs, Meinshausen et al., 2020; O'Neill et al., 2016), namely the SSP1-2.6 (low emission), SSP2-4.5 (intermediate emission), and SSP5-8.5 (high emission). The list of the considered CMIP6 GCMs is given in the supplementary material (Table S4.2). The GCM projections were downscaled to 0.05° x 0.05° resolution in space and bias-corrected using the change factor (delta) method (e.g., Anandhi et

al., 2011; Teutschbein and Seibert, 2012) for three future periods, i.e., 2020-2049, 2045-2074 and 2070-2099 (hereafter, 2030s, 2060s and 2080s respectively).

The change factor is a statistical downscaling technique. The underlying principle of this method is that the change factors that are determined from the Global and/or Regional Circulation Model (GCM or RCM) simulations of the current (reference) and future periods can be expressed as either relative or absolute changes, and are used to perturb the observed current climate to generate the future climate locally (Anandhi et al., 2011; Karger et al., 2020; Navarro-Racines et al., 2020; Teutschbein and Seibert, 2012). For precipitation, the change factors are typically computed as relative values, i.e., as ratios of the GCM simulations (under a given greenhouse gas emission scenario) to the GCM simulation for the current climate. The downscaled future precipitation is then derived by multiplying observed precipitation for the current (reference) period by the change factors. For temperature, absolute change factors are typically computed as the difference between the GCM simulations for the future periods and the reference period, and then added to the observed reference period temperature to determine the downscaled future temperature.

Soil properties were obtained from the SoilGrids dataset (Hengl et al., 2017; Poggio et al., 2021). SoilGrids contains various soil properties at a global 250 m x 250 m spatial resolution, interpolated from about 240,000 soil samples using machine-learning. The soil data were spatially averaged to re-grid them to a coarser spatial resolution of ~5 km x 5 km grid size (0.05° x 0.05°) to match the spatial resolution of the climate data. The Meher (May-Sep) growing season crop yield data for the four major crops (teff, maize, sorghum, and wheat) were obtained from the published Agricultural Sample Survey (AgSS) of seven years (2000, 2003, 2004, 2005, 2006, 2007 and 2010) for 62 administrative units, locally known as ‘zones’ (CSA, 2010). AgSS is an annual countrywide survey conducted by the Central Statistical Agency (CSA) of Ethiopia and is aimed at collecting and compiling agricultural (crop and livestock) production data from over 45,000 agricultural households across the country.

5.2.3. Modelling of cropland suitability

Climate, soil, and terrain slope are the major factors that determine cropland suitability (Akpoti et al., 2019; Suhairi et al., 2018; Zabel et al., 2014). We termed “cropland suitability” as the potential of an agroecological setting to provide optimal climatic and biophysical conditions

for the growth and productivity of a specific crop. We estimate the CLS by establishing mathematical (nonlinear) relationships between crop yields and climatic and soil factors. We haven't considered the terrain slope as its effect is obscured at the coarse resolution, i.e., grid-scale of 5 km. Three climatic factors: the total rainfall (RF), mean temperature (Tm), and solar radiation (Rs) during the growing season, and three soil factors: sand-to-clay ratio (S2C), pH, and soil organic carbon (SOC), were considered in the CLS modelling. The choice of these suitability factors is motivated by the need to better represent the crop growth defining factors (Tm and Rs), the limiting factors, and the reducing factors (S2C, pH, and SOC) (Ittersum et al., 2013; Lobell et al., 2009). Because the cessation dates of the Meher rainy season vary across the RFA region, ranging from September to November (Wakjira et al., 2021), and because the corresponding harvest season ranges from September to February depending on locations and crop types (CSA, 2010), RF, Tm, and Rs were also computed over the period from May to November to match the crop yield data. The seven years of crop yield data (see Section 5.2.2) and the growing season RF, Tm, and Rs of the corresponding yield years were averaged for each of the 62 zones. Similarly, average S2C, pH, and SOC were computed for each zone.

Partial suitability models

The CLS models were derived from the partial yield responses (PYR) of crops to each of the six individual factors (Fig. 5.2). We assume that high partial yield responses (hPYR), which represent the upper limit of the PYR for each factor (assuming all other factors remain optimal; Fig. 5.2), indicate the factor's potential impact on suitability. We sampled the hPYR data points from PYR across the range of observed values of each factor using the convex hull algorithm, which determines the smallest polygon that encloses the PYR scatter through geometric computations (e.g., Berg et al., 2008; Jarvis, 1973). We considered the data points on the upper envelope of the polygon as hPYR. The number of hPYR data points sampled by the algorithm is determined by the geometry of the polygon resulting from the PYR scatter. The fewer vertices the polygon has, the fewer hPYR data points will be picked. In cases where the algorithm picks a limited number of data points, like in S2C for wheat and SOC for maize (the green circles in Fig. 5.2) for example, we picked supplementary hPYR data points manually.

Table 5.1: Summary of the agroecological processes and plant growth mechanisms affected by the climatic and soil limiting conditions (very low and high values).

Factors	Low values	High values
RF	Low soil moisture, high plant water stress, low biomass production, and thus low crop yield (Kang et al., 2009; Rockström et al., 2010)	Soil saturation (waterlogging in clay soils), inhibition of aerobic plant metabolism, denitrification, soil nutrient leaching and erosion, plant growth inhibition, crop failure (Jørgensen et al., 2020; Kaur et al., 2020; Palmer et al., 2023; Pan et al., 2021)
Tm	Cold stress, frost damage, reduced water root water uptake, water stress, limited photosynthesis, low/no biomass productivity, and thus low crop yield (Hassan et al., 2021; Hussain et al., 2018)	Heat stress, inhibited/limited plant metabolic activities, limited evapotranspiration and photosynthesis, leading to lower crop yield (Hatfield and Prueger, 2015)
S2C	High clay content, poor soil internal drainage, waterlogging and nutrient deficiency, less crop yield (Manik et al., 2019)	Low clay content, poor water retention capacity and low fertility, less plant-available water, water and nutrient stress, less biomass productivity and low crop yield (Huang and Hartemink, 2020)
pH	Toxicity, limited root development, less ability to extract nutrients, and crop failure (Msimbira and Smith, 2020)	Poor nutrient recycling, nitrogen, phosphorous, potassium and zinc deficiencies, less infiltration and soil hydraulic conductivity, poor root development, toxicity, and crop failure (Marlet et al., 1998; Msimbira and Smith, 2020)
SOC	Low soil fertility (low dissolved organic carbon for soil microbes which are responsible for nutrient recycling), poor soil structure and moisture fluxes, and reduced crop growth and yield (Lehmann and Kleber, 2015)	Too much nutrients for soil microbes, increased respiration, enhanced nutrient recycling (e.g., nitrogen fixation), accelerated crop growth resulting in crop lodging (stem buckling and root anchorage failure) (Wu et al., 2022)
SLR	Low rate of photosynthesis, less biomass productivity and thus less crop yield (Hatfield and Dold, 2019; Muchow et al., 1990)	Increased evapotranspiration, high water stress and hence low yield under moisture limited conditions (Hatfield and Dold, 2019; Muchow et al., 1990)

The sampled hPYR data points were then used to build the partial suitability models by fitting polynomial functions:

$$Y(x_i) = p_1 x_i^n + p_2 x_i^{n-1} + \cdots + p_{n-1} x_i + p_n \quad (5.1)$$

where Y is the potential yield that is associated with factor x_i (x is the value of the hPYR data points for factor i, that is, RF, Tm, Rs, S2C, pH, or SOC), and $p_1, p_2, \ldots, p_n$ are the coefficients of the polynomial function of order n. The yield responses to the climatic and soil factors can be adequately explained by quadratic functions, except for the responses of teff, maize, and sorghum to soil texture (Fig. 5.2). These crops exhibited strong sensitivity to S2C values below approximately 0.5, while they were much less sensitive to higher values. These non-asymmetrical relations are better represented by fourth-degree polynomials. The influences of the factors on the partial suitability are related to the plant growth mechanisms and agroecological processes that are described in Table 5.1. High partial suitability is associated with optimum values depending on the crop types. It represents the highest (normalized) yield that can be achieved for each controlling factor.

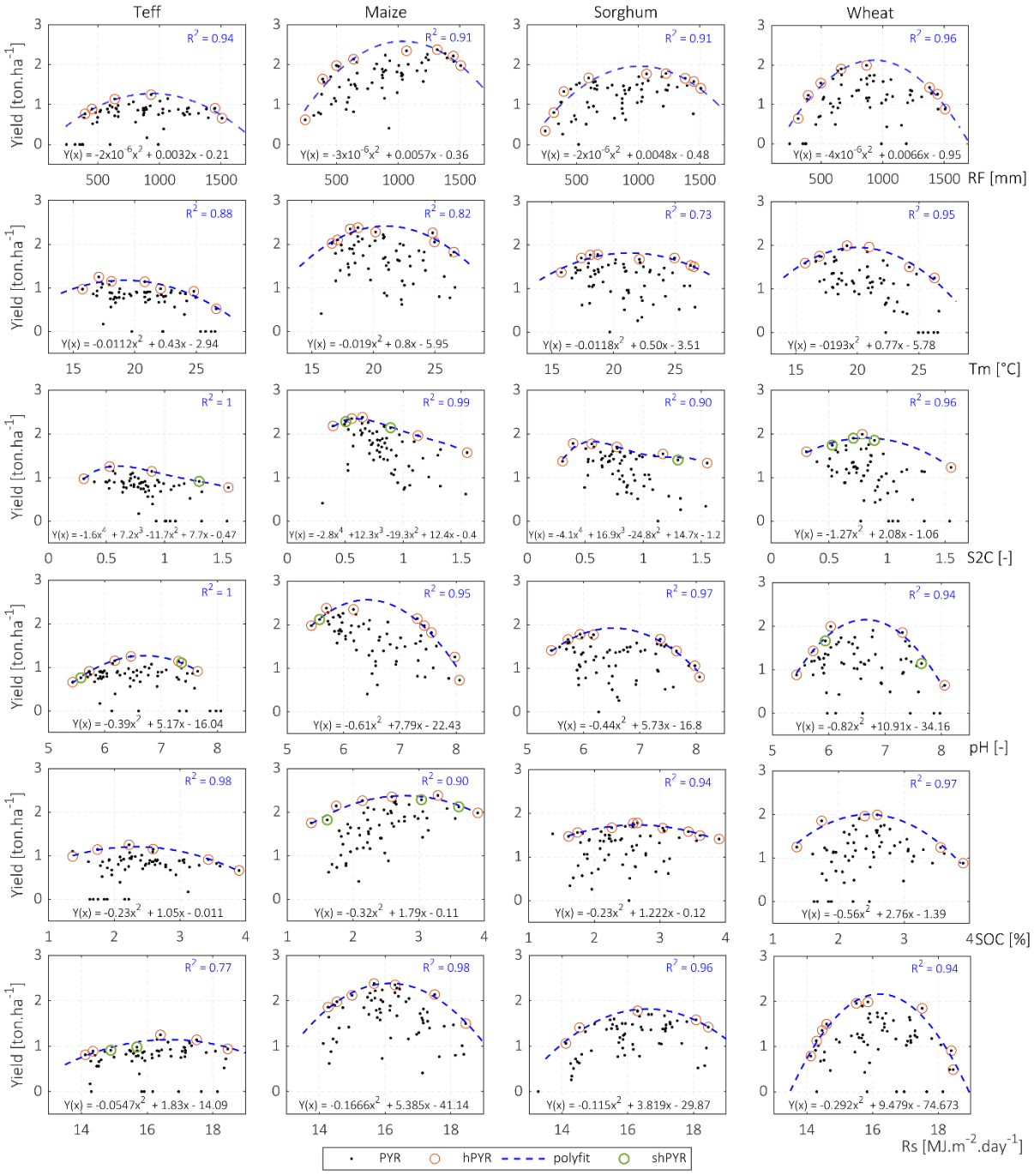

Fig. 5.2: Partial yield responses (PYR) of the four crops to individual climatic and soil factors. Each dot represents a zone. The orange circles are the hPYR picked automatically and the green circles (shPYR) are the supplementary hPYR picked manually that were used for the construction of the partial suitability models. The dashed lines are the fitted polynomial function (partial suitability model). RF is the May to November total rainfall, Tm and Rs are May to November mean temperature and mean solar radiation for each zone respectively.

CLS under the current climate

The partial suitability models $Y(x_i)$ were applied to the current growing season climate (the average over the reference period 1981-2010) and soil factors. Subsequently, the gridded PYR results were normalized to derive the partial suitability indices at each grid cell with values ranging from 0 (not suitable) to 1 (highly suitable). The max-min scaling approach given by Eq. (5.2) was used for the normalization.

$$y' = \frac{y - y_{min}}{y_{max} - y_{min}} \tag{5.2}$$

where y' is the normalized value of PYR, and y_{min} and y_{max} are the minimum and maximum PYR values across the entire RFA region. Then, the partial suitability indices from the six factors individually were combined to determine the overall CLS suitability index (SI) for each crop. In computing the SI, factors related to the climate and soil were not taken into consideration equally. The rainfall, temperature, and solar radiation as yield defining and limiting factors, were assumed as fundamental factors (Holzkämper et al., 2013), and thus they were considered independently as rainfall suitability (S_{RF}), temperature suitability (S_{Tm}), radiation suitability (S_{Rs}).

The soil factors (reducing factors) were combined on a weighted basis to define the soil suitability (S_{soil}). To determine the weights of the soil factors, quadratic functions of the form

$$y(x_i) = p_{1,i}x_i^2 + p_{2,i}x_i + p_{3,i} \tag{5.3}$$

where fitted to the normalized hPYR and factor x_i (i in this case is either S2C, pH, or SOC). The weight w for each soil factor i was then computed as:

$$w_i = \frac{|p_{1,i}|}{\sum|p_{1,i}|} \tag{5.4}$$

where p_1 is the coefficient of the second-degree term of y(xi), which is the measure of the concavity of the fitted curve and can be considered as an estimate of the average rate of change in soil suitability per unit absolute change in the soil factor under sub-optimal conditions. The

computed weights are given in We defined SI as a multiplicative combination of the partial suitabilities because the limitations of each factor, in most cases, cannot be compensated for by the optimality of the others. Instead, they have a scaling effect on each other. In other words, the suitability factors considered in the model are assumed independent.

Table 5.2. The soil suitability for each crop was computed using Eq. (5.5).

$$S_{soil} = w_{S2C}S_{S2C} + w_{pH}S_{pH} + w_{SOC}S_{SOC} \quad (5.5)$$

Finally, the overall potential cropland suitability index (SI) was computed for every grid cell and the four crops as a multiplicative combination of the climatic and soil factors (Eq. (5.6)).

$$SI = S_{RF}S_{Tm}S_{Rs}S_{soil} \quad (5.6)$$

We defined SI as a multiplicative combination of the partial suitabilities because the limitations of each factor, in most cases, cannot be compensated for by the optimality of the others. Instead, they have a scaling effect on each other. In other words, the suitability factors considered in the model are assumed independent.

Table 5.2: Computed weights of the soil factors for teff, maize, sorghum, and wheat

	Teff	Maize	Sorghum	Wheat
S2C	0.26	0.16	0.24	0.26
pH	0.42	0.37	0.37	0.42
SOC	0.32	0.47	0.39	0.32

Model performance evaluation

The CLS model we developed is conceptually similar to the fuzzy classification approach (Burrough et al., 1992), except that the classification membership functions (suitability curves) in our case are built based on ‘high’ crop yield responses (a proxy for best suitability, which represents maximum observed yield) across the range of the suitability factor instead of assuming hypothetical functions that define the yield responses. We evaluated the performance of our approach with independent data, i.e., all of the black data points (PYR) in Fig. 5.2, using the Receiver Operating Characteristics (ROC) analysis (Fawcett, 2006). The aim here is to

evaluate the model predictions against observations (normalized crop yield). We transformed the normalized crop yield into binary data using SI threshold of 0.4 (FAO, 1976). If SI is greater than or equal to 0.4, then a crop is considered to be present (1), otherwise absent (0) in a given zone. We evaluated the presence/absence of each crop in each zone using the binary data (observed suitability) and the corresponding modelled suitability, and summarized the results in a ROC plot.

The ROC analysis compares the tradeoffs between maximizing the correct detection of crop presence (true positives) and minimizing false detection of presence (false positives) at different SI thresholds. This done by computing True Positive Rate (TPR) and False Positive Rate (FPR) using Eq. (5.7) and (5.8).

$$\mathrm{TPR} = \frac{\mathrm{TP}}{\mathrm{TP} + \mathrm{FN}} \tag{5.7}$$

$$\mathrm{FPR} = \frac{\mathrm{FP}}{\mathrm{FP} + \mathrm{TN}} \tag{5.8}$$

where in the classification process, TP is true positive, FN is false negative (missed detection), FP is false positive and TN is true negative (correct rejection) as shown in Fig. 5.3a. The ROC curve is the plot of TPR on the y-axis and FPR on the x-axis (Fig. 5.3b). The area under the ROC curve (AUC) is used as a performance metric, where AUC = 0.5 shows the performance of a random prediction and AUC = 1 shows a perfect prediction.

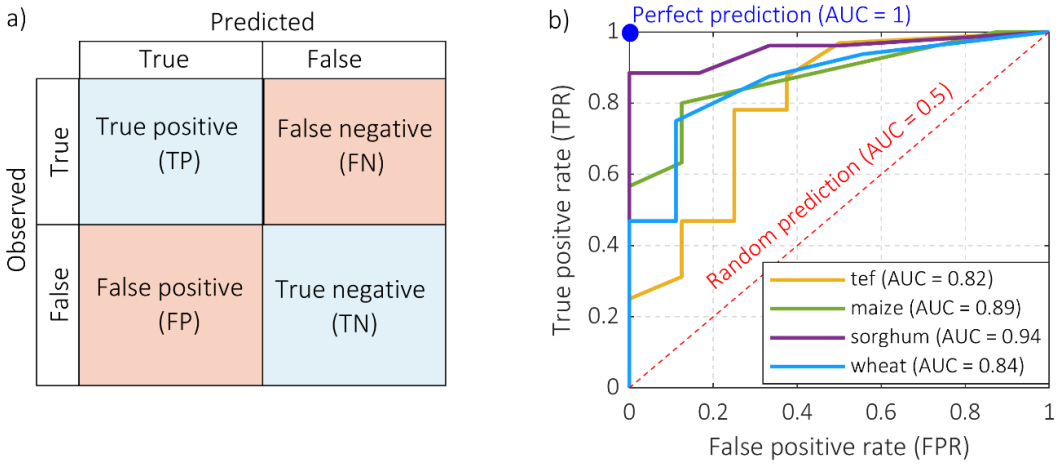

Fig. 5.3: a) Confusion matrix illustrating the possible prediction outcomes of CLS with SI > SI*, where SI* is a chosen threshold indicating crop presence/absence and, b) the resulting ROC curves for the four crops

5.2.4. Climate change impact and sensitivity analysis

Future CLS values for the four major crops in Ethiopia were computed by forcing the suitability models with projected climate scenarios. We took the multi-model median values of rainfall and temperature, computed from the downscaled CMIP6 ensemble described in Section 5.2.2. Three SSPs and three future periods (the 2030s, 2060s, and 2080s) were examined for which the May-November RF and Tm were computed. Only changes in rainfall and temperature were considered in the assessment of future changes in CLS. Solar radiation was not considered in the assessment of future changes in CLS because the projected future changes in this variable are small in magnitude, largely less than 3%, even under the extreme emission scenario by the end of the century. Similarly, soil factors were assumed to remain fixed in the computation of future CLS as their timescales of change are much longer.

The sensitivity of CLS to changes in RF and Tm was analyzed using the One-At-a-Time (OAT) sensitivity analysis (Hamby, 1994). OAT is a local sensitivity analysis method in which changes in the modelled quantities are examined by modifying one variable at a time. When the model is forced by continuous input variables, the sensitivity can be determined by taking the partial derivatives of the output with respect to the inputs (Bhatt and Abbassi, 2023). The suitability models were forced by discretized inputs, i.e., the future RF and Tm. We simplified the sensitivity analysis by assuming that the overall change in suitability associated with the combined effects of the changes in RF and Tm is equal to the weighted sum of the changes in partial suitability associated with the change in the corresponding factor when the other factor remains unaltered. This can be formulated as (Lobell and Burke, 2008):

$$\Delta SI = \beta_{RF}\Delta S_{RF} + \beta_{Tm}\Delta S_{Tm} \tag{5.9}$$

where β_{RF} is rainfall-sensitivity and β_{Tm} is temperature-sensitivity and were determined using the OAT approach. Note also that this assumption holds only when the factors (RF and Tm) are independent (Goodman, 1960). We tested this by correlating RF and Tm over the RFA region and found a statistically insignificant correlation (Pearson's r = -0.13) at a significance level of $\alpha = 0.05$. Similarly, we verified that the temporal changes in RF and Tm are uncorrelated. We then computed a sensitivity ratio (β_{ratio}) to identify the relative controls of RF and Tm on the changes in CLS.

$$\beta_{ratio} = \frac{\beta_{RF}}{\beta_{Tm}} \tag{5.10}$$

The condition $\beta_{ratio} > 1$ indicates that changes in CLS are rainfall-sensitive whereas $\beta_{ratio} < 1$ shows temperature-sensitivity.

5.3. Results

We first present the performance of the suitability models. From the ROC analysis, we conclude that the suitability models predict the CLS for all crops with AUC values of 0.82, 0.89, 0.94, and 0.84 for teff, maize, sorghum, and wheat respectively (see also Fig. 5.3b). In comparison with the other crops, the teff suitability model showed the least predictive power. This is most likely due to the socioeconomic dimension of teff production, which may have been reflected in the observed suitability, but is not represented in our model. Teff is a typical staple food crop and the most commercialized cereal in Ethiopia because it is a basic and traditional element of the food system for the entirety of the urban population and a significant part of the rural population (Tadele and Hibistu, 2022). As a result, depending on the climatic and biophysical suitability, teff is intensively cropped near cities and towns, and along major road networks that ease market access (Amede et al., 2017; Tadele and Hibistu, 2022). Teff is also the most labor-intensive crop (Hailu et al., 2017; Lee, 2018). In remote areas where access to market and transport infrastructure is limited, for example, in humid lowland agro-pastoral regions, farmers prefer growing less labor-intensive crops like sorghum and maize over teff (Amede et al., 2017), although the croplands are classified as suitable. The suitability models do not take into account these social and cultural dimensions since they were trained solely on climatic and soil factors. We note that our suitability models have higher predictive power for teff, maize and sorghum when compared to the Maxent-based suitability model performance presented by Evangelista et al. (2013), who reported AUC values of 0.79 for tef, 0.81 for maize, and 0.79 for sorghum. The improvements in predictive performance can be attributed to the robustness of the modelling framework we implemented, combined with the use of state-of-the-art climatic data (including solar radiation) and key soil properties, thus accounting for suitability-defining, limiting and reducing factors.

5.3.1. Current potential suitability

The derived CLS maps in Fig. 5.4 show the continuous suitability indices SI of the four cereal crops over the RFA area of Ethiopia. The Food and Agriculture Organization of the United Nations (FAO) provides guidelines for land suitability classification (FAO, 1976) as given in Table 5.3. Accordingly, we found that sorghum is the most suitable crop to be grown in the RFA area of Ethiopia (with moderate and high suitability of 63% of the grid cells), followed by teff (54%), maize (51%), and last but not least wheat (29%). Teff and wheat croplands mostly overlap, covering mainly the eastern half of the RFA region. Wheat is more limited to higher altitude regions (Fig. 5.4) while maize and sorghum are crops that are more versatile and grown also at lower elevations.

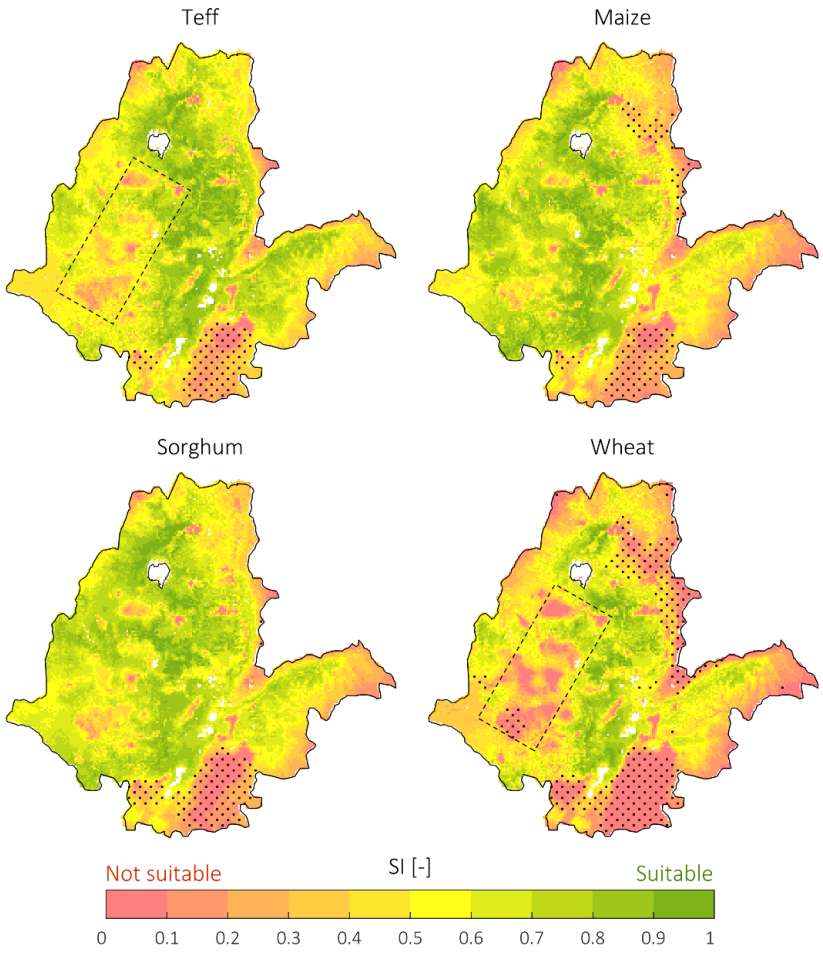

Fig. 5.4: Cropland suitability (CLS) maps for teff, maize, sorghum and wheat under the present climate (1981-2010). The dashed rectangles show the areas where waterlogging limits cropland suitability. The dots indicate regions where radiation-unlimited CLS is reduced by 50% or more under radiation-limited conditions.

The western humid areas (indicated by the dashed rectangles in Fig. 5.4) are characterized by high rainfall and clayey soils where waterlogging can be a major constraint. This low rainfall suitability (Fig. S5.1) together with high soil acidity (Fig. S5.2) are the main limitations, particularly for wheat and teff in this region. The low suitability for wheat, teff, and maize in the western and northwestern lowland areas is predominantly due to temperature limitations (Fig. S5.3). In the eastern and southeastern peripheries of the RFA region, suitability for all crops, especially wheat and maize, is low (Fig. 5.4); this is mainly due to low rainfall and high soil alkalinity (Fig. S5.1 and S5.2). Cropland suitability in the forest and Afro-alpine regions across the southern part of the RFA (the dotted areas in Fig. 5.4) is strongly limited by low solar radiation (Fig. S5.4) that results in low rate of photosynthesis for all crops, particularly wheat. Additionally, low suitability for wheat and maize is observed in the northeastern part of the RFA region. However, in this case, the limitation is due to high solar radiation, resulting in increased evapotranspiration and leading to crop water stress.

Table 5.3: Percent of grid cells in the RFA region corresponding to the FAO suitability classes (FAO, 1976). SI is the overall suitability index.

	Highly suitable (SI≥0.8) in %	Moderately suitable (0.6≤SI<0.8) in %	Marginally suitable (0.4≤SI<0.6) in %	Not suitable (SI<0.4) in %
Teff	19	35	30	16
Maize	19	32	26	23
Sorghum	21	42	21	17
Wheat	8	21	28	43

5.3.2. CLS under the future climate

Projected changes in the May-November season

The downscaled multi-model median projections show that the May-November season of the RFA regions of Ethiopia is likely to become warmer (Fig. 5.5b) and mostly wetter (Fig. 5.5a) under all emission scenarios. Under SSP1-2.6, the May-November RF is expected to increase by up to 100 mm, especially over the highlands in the 2030s without further changes into the mid- and end- of-the-century. However, incremental RF intensifications are expected in the future under SSP2-4.5 and SSP5-8.5, the latter is likely to increase by up to 300 mm by the end

of the century. Unlike the changes in RF, which vary significantly among regions, the projected changes in Tm has little spatial variability. Tm is expected to increase by up to 1.8 °C, 2.8 °C, and 4.6 °C under the low, intermediate, and high emission scenarios (respectively) by the end of the century (Fig. 5.5b).

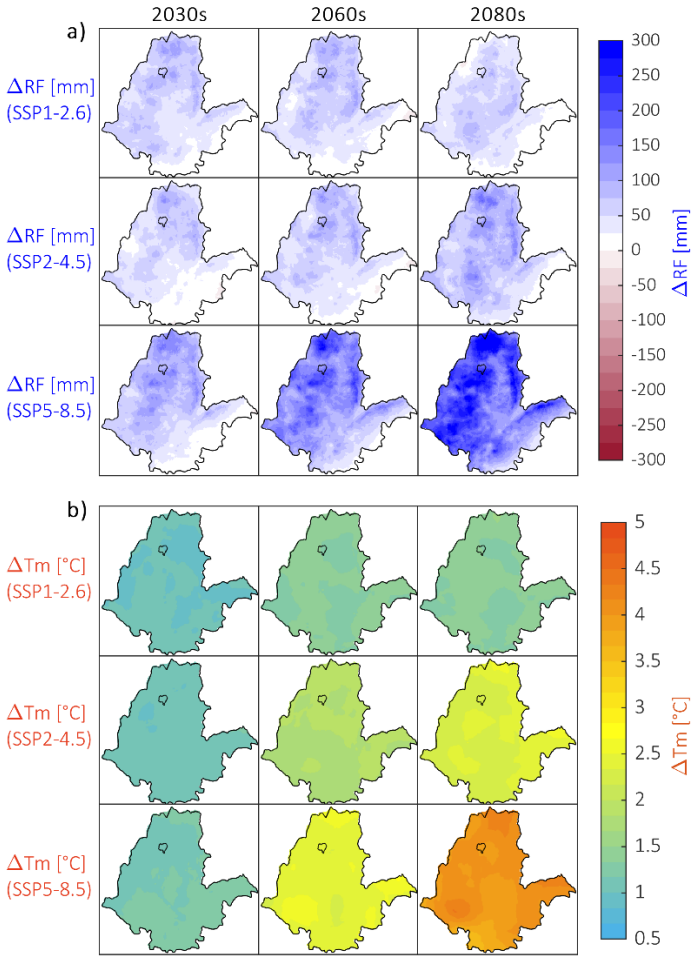

Fig. 5.5: The expected future changes in the May-Nov season climate: a) total rainfall (RF) and b) mean temperature (Tm) under three shared socioeconomic pathways. The indicated changes correspond to the median of 25 CMIP6 models for RF and 21 models for Tm.

Changes in cropland suitability

The future CLS across the RFA area of Ethiopia is strongly influenced by the projected future climates, i.e., total rainfall and mean temperature during the growing season (Fig. 5.6). Ethiopia's RFA areas are likely to become less suitable for teff and wheat production on average. This is evident even under the low emission scenario (SSP1-2.6) already in the near future (the 2030s) when the climate is less than 1°C warmer than the reference period. Under

the medium and high emission scenarios, substantial areas where teff and wheat are growing are likely to be at risk of abandonment. While teff and wheat croplands will mostly experience decreases in suitability, that of maize and sorghum will generally remain unchanged, as some areas will lose suitability while nearly comparable areas will gain suitability in the future. The exception is under the medium and high emission scenarios where the majority of the maize and sorghum areas are expected to lose suitability by the end of the century.

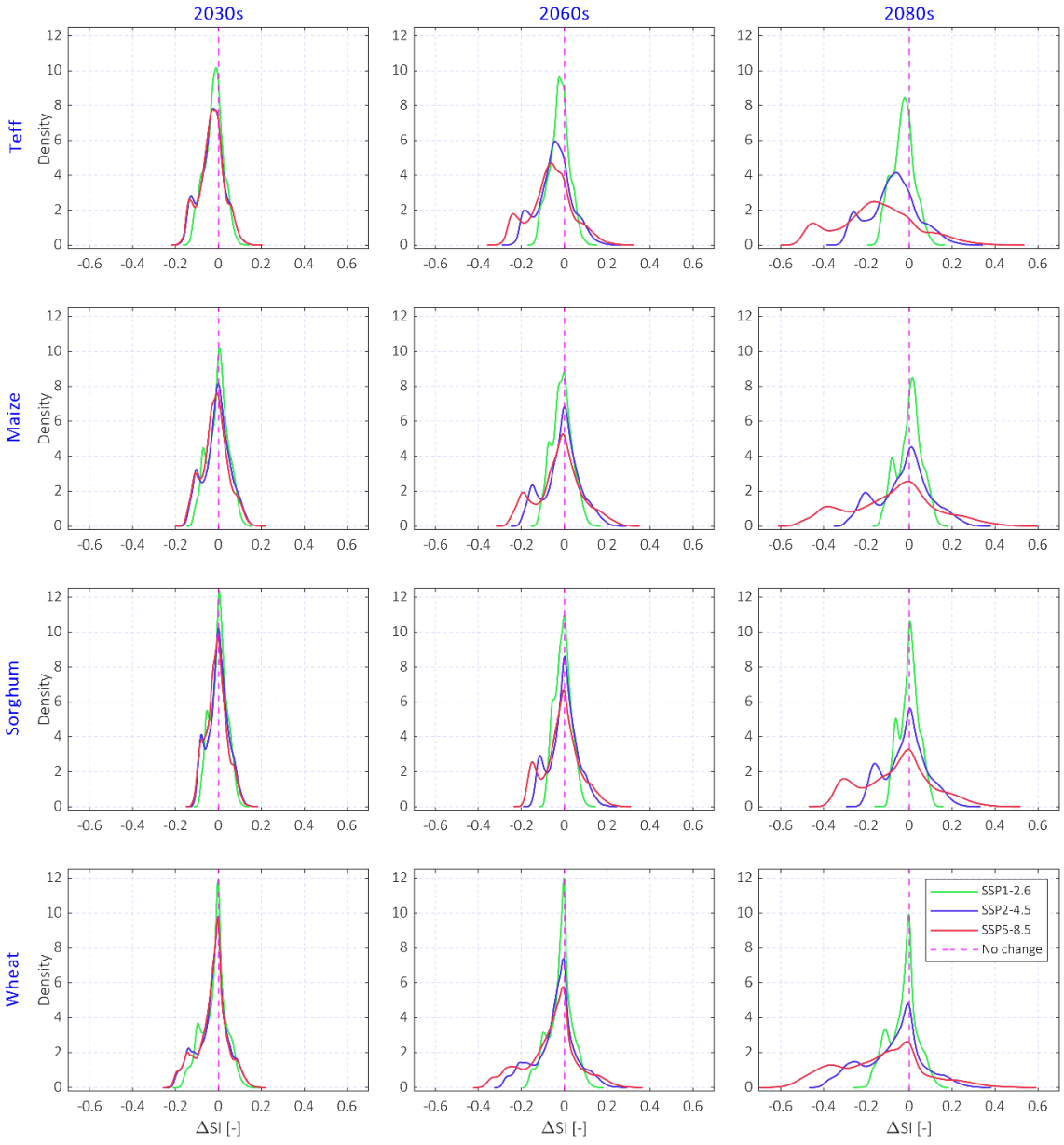

Fig. 5.6: Kernel-smoothed distributions of changes in the future cropland suitability (***ΔSI***) for teff, maize, sorghum, and wheat under SSP1-2.6, SSP2-4.5, and SSP5-8.5 across all grid cells within the RFA region for the 2030s, 2060s, 2080s, from left to right.

The spatial patterns of the changes in CLS under SSP2-4.5 are shown in Fig. 5.7, and the CLS changes for the other climate scenarios are presented in the supplementary material (Fig. S5.5-S5.8). Decreases in CLS are evident largely in the northwestern, western, and southwestern lowland parts of the RFA region for all crops under all climate scenarios and future periods. When comparing the crops, teff and wheat croplands are more affected with projected decreases in the suitability of up to 0.40 (on a scale of 0 – 1) compared to maize and sorghum (projected decreases of up to 0.25).

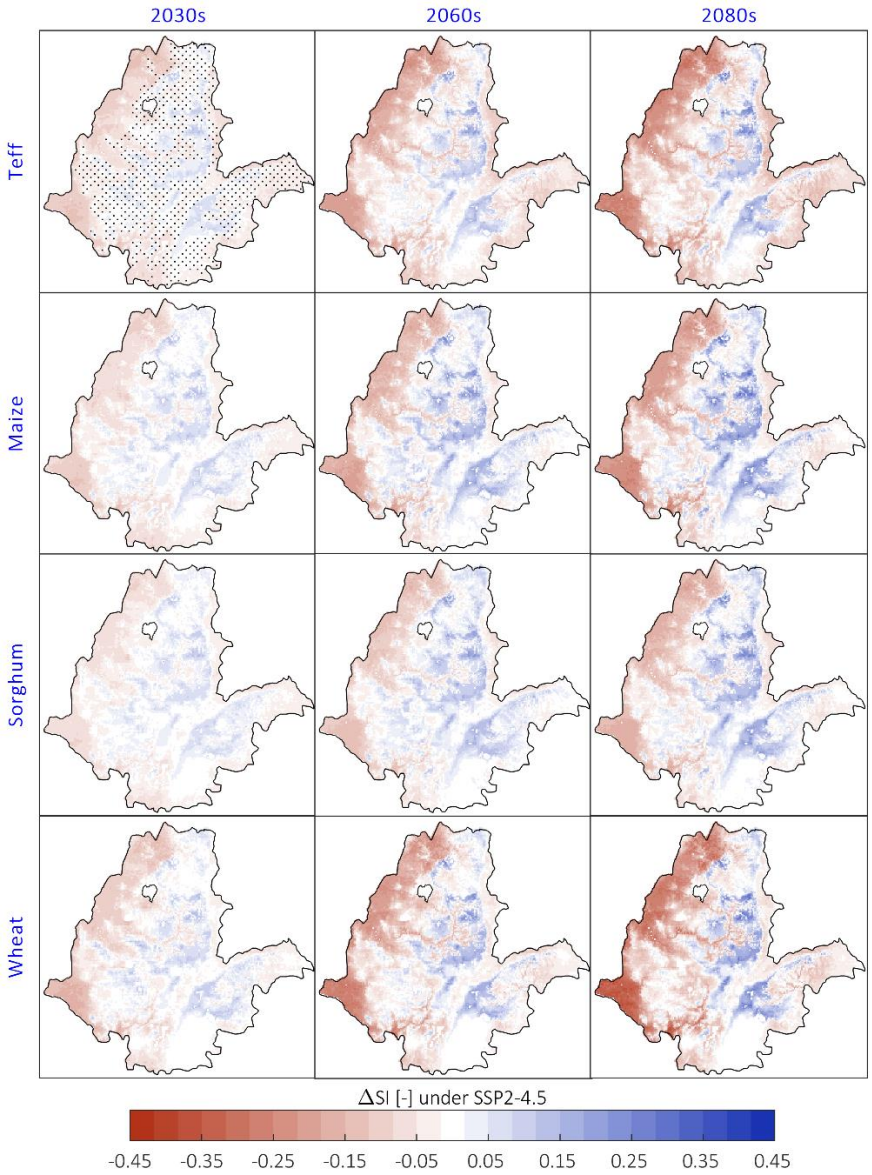

Fig. 5.7: Change maps of the cropland suitability for teff, maize, sorghum and wheat comparing SSP2-4.5 to the current climate during the three future periods. The dots in the first map show the midland areas (altitude range of 1300 – 2500 masl).

Suitable cropland areas in the lowland agroecologies (altitude <1300 masl), particularly that of teff and wheat, are expected to shrink considerably (Fig. S5.9a) under all scenarios. The expected decreases in the suitable cropland (SI > 0.6) area ranges from 21% and 34% (low emission, in the 2030s) to 87% and 96% (high emission, in the 2080s). The CLS in the midlands with an altitude range of about 1300 – 2500 masl (shown by dots in Fig. 5.7) are largely expected to remain unaffected or change only slightly. Only teff and wheat areas are expected to decrease significantly by 18% and 27% by the end of the century under SSP5-8.5 (Fig. S5.9b). In the highland regions (altitude above 2500 masl), on the other hand, the croplands will become more suitable under all emission scenarios (Fig. 5.7, Fig. S5.9c).

Altitudinal shifts and areal changes in CLS

The predicted changes in CLS suggest a shift in suitable croplands from lowland to highland regions. For example, the altitudes of the highly suitable croplands of the four cereal crops are predicted to shift by 85–135 m (depending on the crops) under SSP1-2.6 by 2080s (Fig. 5.8, left panels). The altitudinal shifts are relatively stable under SSP1-2.6 throughout the future periods for the four crops compared to SSP2-4.5 and SSP5-8.5, which are predicted to result in shifts by over 210 m and 390 m respectively by the end of the century. The average shifts under the intermediate and high emissions are projected to be similar in the 2030s but will diverge after that. Overall, the altitudinal shifts tend to be higher for maize and sorghum compared to teff and wheat, probably because teff and wheat are midland and upland crops, and further upward shifts are limited or slowed by environmental constraints.

The future changes in CLS are also accompanied by decreases in the area of the suitable croplands as indicated in the right panels of Fig. 5.8. In particular, the average area of suitable teff cropland is projected to decrease by 9% in the 2030s and by 12.5% in the 2080s under the low emission scenario. The intermediate and high emissions will exacerbate the impacts pushing about 17% and 22% of the teff area out of the suitable climate space in the 2060s, and 25% and 39.5% of the area by the end of the century. Wheat cropland is the second most affected among the four crops with projected decreases in area of about 2.5% and 5% under low emission by 2030s and 2080s respectively. Under the high emissions, wheat areas are likely to decrease by 16% and 32% by the mid and end of the century. Changes in maize and sorghum areas are generally small under the low and intermediate emission scenarios in the

2030s and 2060s, suggesting that the changes are largely dominated by shifts in the suitable croplands as mentioned earlier. However, over 7% and 24% of the suitable areas of both crops are projected to be lost under intermediate and high emission scenarios, during the 2080s.

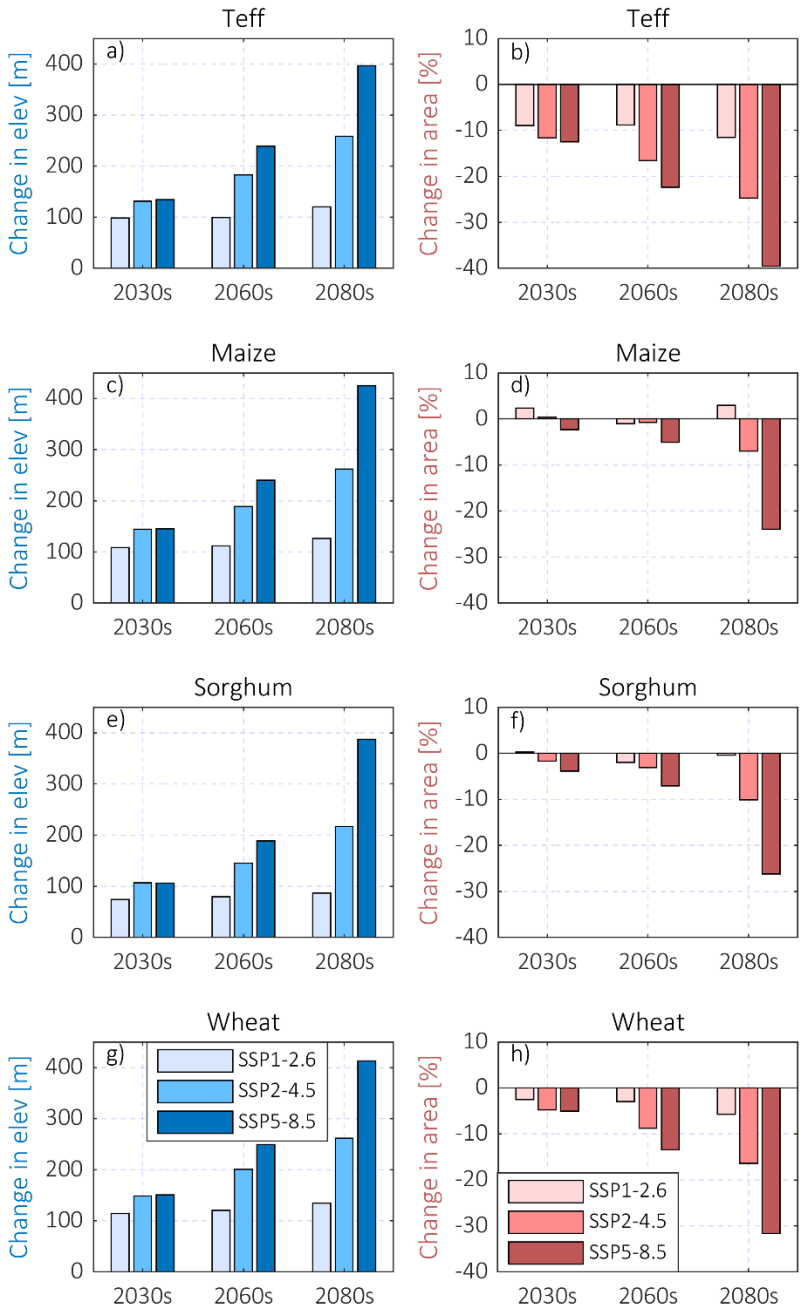

Fig. 5.8: Average changes in the altitudes (left) and average changes in the areas (right) of highly suitable teff, maize, sorghum, and wheat croplands in the RFA region of Ethiopia. The changes were calculated comparing the future versus current suitabilities considering all grid cells with $SI \geq 0.6$.

Future changes in the major producing zones

The CLS changes and their climatic drivers in the Ethiopia's major producing zones (ranked based on the observed yield data) in 2060s are summarized in Fig. 5.9, and altitudinal shifts and areal changes associated with the changes in suitability are presented in Fig. 5.10. The major teff producing zones considered here are likely to experience rather small changes ranging from -0.04 to +0.04 (on a scale of 0 to 1) under SSP5-8.5 during 2060s (Fig. 5.9a). As a result, the areas of teff croplands are likely to remain nearly stable in most of the zones with the exception of West Hararge where the teff area is projected to decrease by up to 13% under SSP5-8.5 in 2060s (Fig. 5.10b), and this decrease in suitability is linked to a decrease in temperature suitability (Fig. 5.9c). The slight increases in suitability in zones like Southwest Shoa and South Wollo is linked to an increase in temperature suitability (Fig. 5.9c) in the highland regions, which is also evident from the increases in the mean altitude Fig. 5.10a). Other major teff producing zones like North Shoa of the Amhara Regional State, and West Shoa are likely to experience altitudinal shifts of about 50 – 100 m, but with only slight or no changes in the suitable area.

CLS for maize is likely to decrease considerably in the major producing zones across the western part (East Gojam and East Wollega) and northwestern part (Awi and Metekel) of the RFA regions (Fig. 5.9d). In Awi and Metekel in particular, highly suitable (SI $\geq$ 0.8) maize cropland area is projected to decrease by about 48% and 69% under SSP5-8.5 by the mid of the century (Fig. 5.10d). A decrease in rainfall suitability is highly evident in the major producing zones in the western part of the RFA region (Fig. 5.9e). High altitudinal shifts are expected in Awi and Metekel zones suggesting rapid maize cropland retreats towards the highlands (Fig. 5.10c). Maize areas in West Shoa and Gurage zones in the central part of the RFA region on the other hand, are projected to expand by over 12% (SSP5-8.5) in 2060s, mainly due to an increase in temperature suitability.

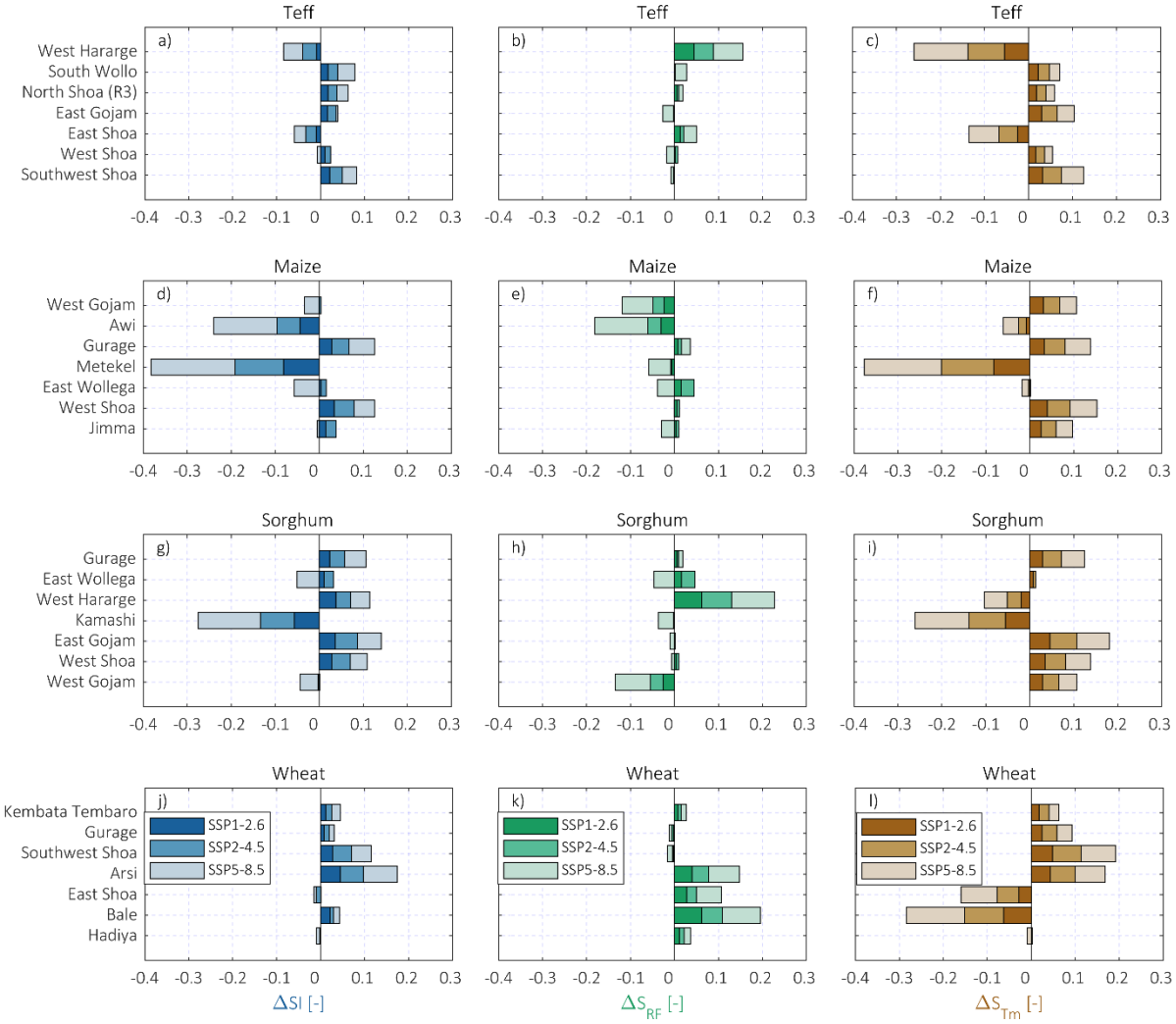

Fig. 5.9: Changes in overall cropland suitability (left), rainfall partial suitability (center), and temperature partial suitability (right), for teff, maize, sorghum, and wheat in the major producing zones (the y-tick labels) under the three SSP1-2.6, SSP2-4.5 and SSP5-8.5 by 2060s. The top-producing zones were identified based on the observed multi-year average crop yields. R3 stands for the Amhara Regional State in which the North Shoa zone is found.

The major sorghum-producing zones like West Shoa (central part), East Gojam (north central), and West Hararge (east) showed an increase in suitability under all SSPs in the mid of the century (Fig. 5.9g-i). In moisture-limited climates like in West Hararge, increases in rainfall suitability are likely to improve CLS, even by reversing the direction of the altitudinal shifts towards the lowlands. This is evident from the decreases in the average altitude and increases in the area (by about 4% under SSP5-8.5) of the suitable croplands in this zone (Fig. 5.10e-f). In West Shoa and East Gojam, an increase in suitability are associated with increases in temperature suitability for sorghum. On the contrary, negative impacts on the CLS for sorghum

are expected in the major producing zones such as Kamashi, East Wollega, and West Gojam in the western side of the RFA region, especially under the high emission scenario. Consequently, sorghum croplands are projected to decrease by about 21% in Kamashi, and 12% in East Wollega under SSP5-8.5.

Wheat CLS are projected to increase or remain nearly stable in the 2060s across the seven major-producing zones we examined as shown in Fig. 5.9j. In particular, in the wheat corridors of Ethiopia (Bale and Arsi), the wheat-suitable croplands are expected to expand by 41% and 49% respectively under SSP5-8.5 (Fig. 5.10h), mainly due to the projected increase in rainfall suitability in Bale and increases in both rainfall and temperature suitability in Arsi. Similarly, wheat areas are projected to expand in East Shoa, Southwest Shoa, and Gurage under all SSPs, for example by up to 11% under SSP5-8.5 by the mid of the century. Only in Hadiya and Kembata-Tembaro zones, the wheat-suitable areas are likely to decrease slightly by less than 5%. As one can expect, the increases in the suitable areas are largely associated with altitudinal shifts towards the higher elevations, especially in Arsi (~185 m) and East Shoa (~130 m) as shown in Fig. 5.10g. The exception is in Bale zone, where a decrease in the elevation of suitable croplands is projected, especially under the low emission scenario and this decrease is attributed to the projected increase in rainfall suitability (Fig. 9k), which in turn increases the overall suitability in the mid-altitude croplands.

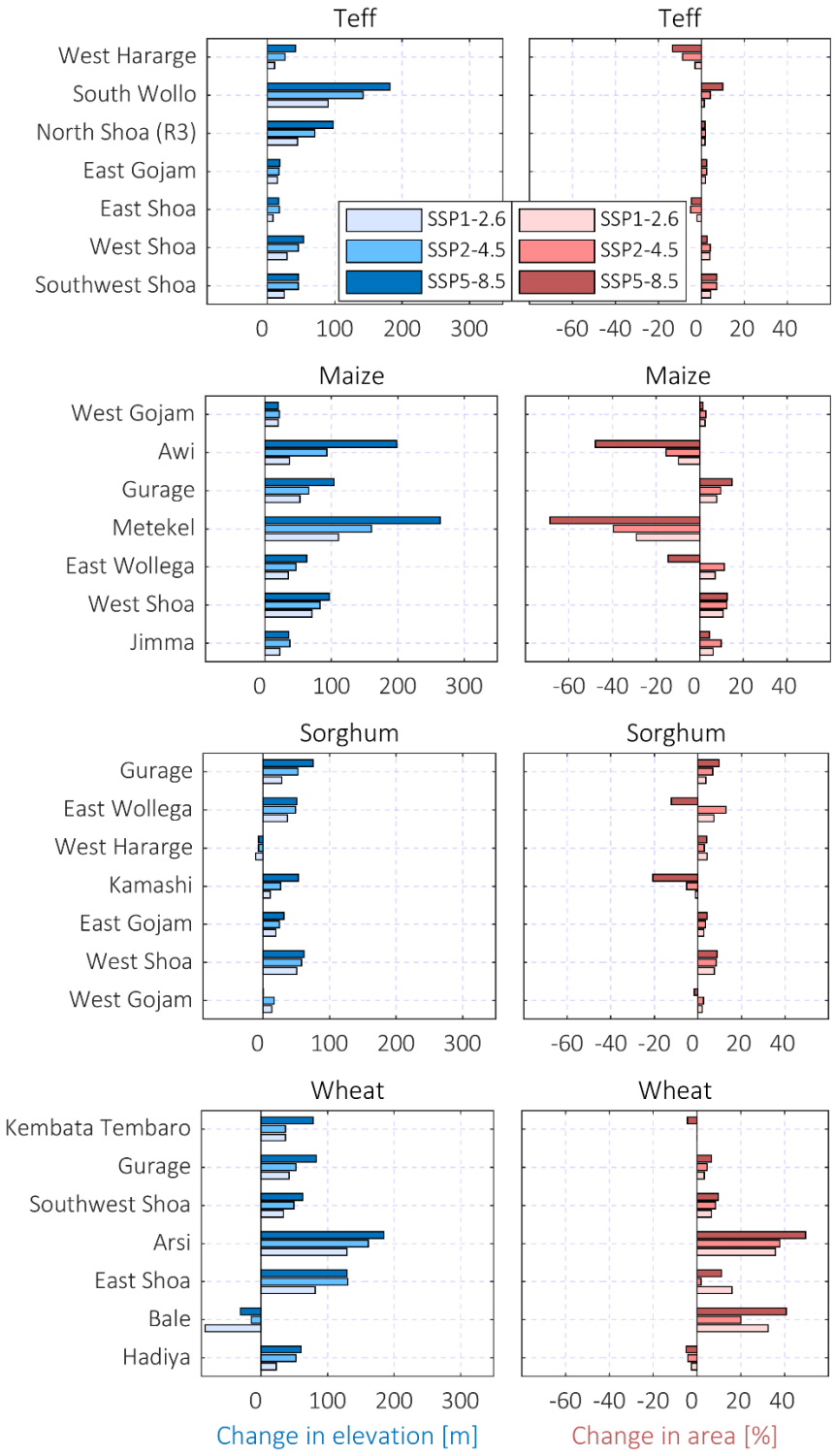

Fig. 5.10: Changes in mean elevation (left) and changes in area (right), of highly suitable croplands (SI ≥ 0.8) of teff, maize, sorghum and wheat in the major-producing zones under SSP1-2.6, SSP2-4.5, and SSP5-8.5 in the 2060s. The changes were computed considering all grid cells of each zone with SI ≥ 0.8.

5.3.3. Sensitivity of CLS to rainfall and temperature

The results suggest that Ethiopian RFA cropland suitability may be affected by rainfall and temperature changes in different ways. Therefore, it is important to examine the sensitivity of CLS to each factor. The OAT sensitivity analysis results in Fig. 5.11 show that the relative sensitivity β_{ratio} is high (blue) in semi-arid climates across the southern, southeastern, eastern, and northeastern margins, and in hyper-humid climates in the western parts of the RFA region. This indicates that changes in CLS in these regions are predominantly driven by changes in rainfall suitability. Changes in CLS in semi-arid and dry sub-humid climates of the Rift Valley corridor (dashed line in Fig. 5.11) are also sensitive to rainfall, especially for maize, sorghum, and wheat. The rainfall limitations in the dry climatic regions are linked to moisture deficit during the growing season that considerably reduces crop yields. In the hyper-humid regions, problems associated with excess rainfall including waterlogging and soil nutrient erosion (as discussed in Table 5.1) are the main constraints and are highly noticeable, especially for teff and wheat CLS. Clay soils like nitisols, luvisols, and vertisols are the dominant soils across the hyper-humid areas in the western part of the RFA region (Ali et al., 2022), making the region susceptible to waterlogging problems.

In the highland and lowland (western and northwestern) regions, on the other hand, the changes in CLS are highly sensitive to temperature. In the lowland areas, teff and wheat CLS are more sensitive to temperature compared to maize and sorghum. The temperature sensitivity of CLS can be attributed to two combined limitations of temperature, namely thermal stress and evaporative stress limitations. Thermal stress (cold and heat stress) tolerance is the genetic property of a crop that determines the geographic niche of that crop species (Sutherst, 2003). The thermal ranges in which a crop can survive are often given by low- and high-temperature thresholds. Under the projected warming climates, temperature converges to and eventually surpasses the high-temperature thresholds of crops in lowland regions, resulting in frequent heat stresses and gradual abandonment of crops. In the highland marginal agroecosystems, temperature instead exceeds the low-temperature thresholds reducing cold stress frequencies, and thus widening the crop niches toward high altitudes. The evaporative stress limitations are linked to temperature effects on crop evaporative moisture losses. Lowland regions are energy-excess (water-limited) systems where crops often suffer from high water stress due to high evaporative losses driven by high temperature under a given moisture-limited condition, thus

climate warming aggravates water stress conditions in lowlands. On the contrary, highland ecosystems tend to be energy-limited, thus crops transpire less due to stomatal closure under cold temperatures, which also means that CO_2 uptake and photosynthesis are limited. Climate warming overcomes the energy limits in the highland ecosystems, increasing photosynthesis and crop yields under available water conditions

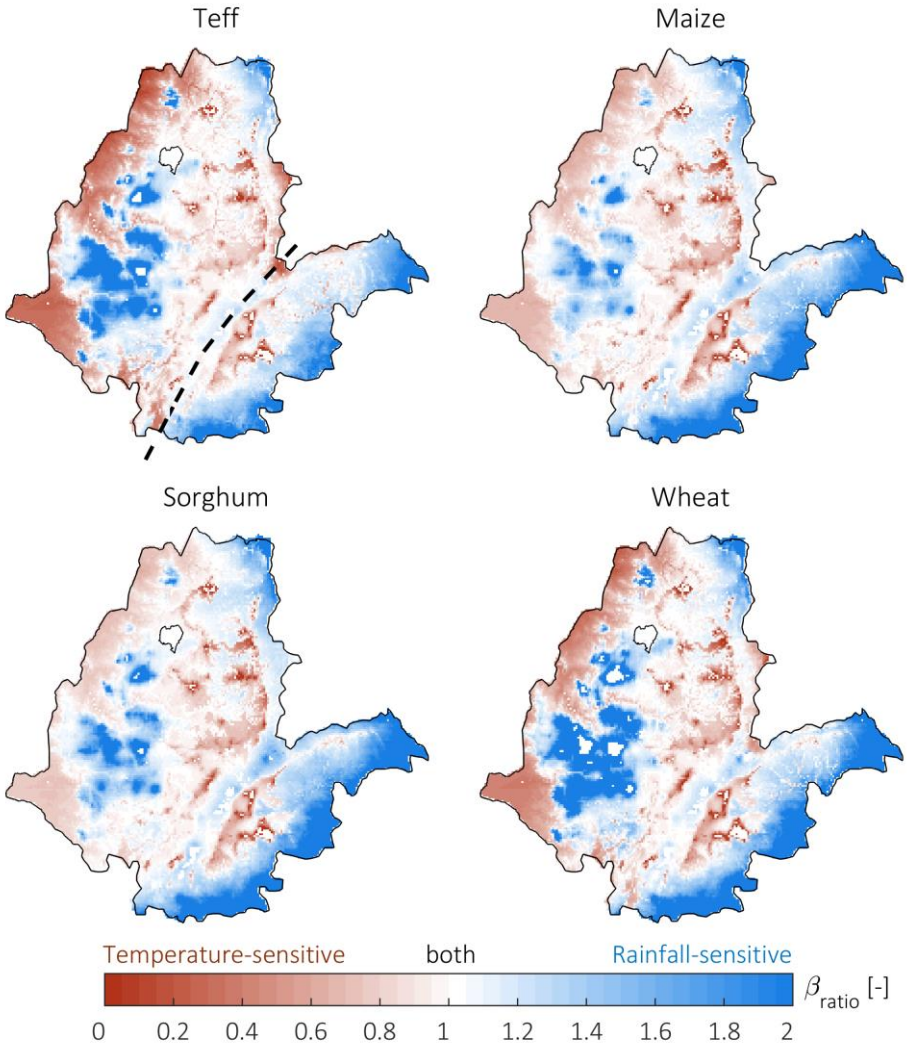

Fig. 5.11: Relative sensitivity (β_{ratio}) of cropland suitability to rainfall and temperature for teff, maize, sorghum and wheat. The β_{ratio} values mapped here are the average of nine OAT simulations – the combinations of three future periods (the 2030s, 2060s, and 2080s) under three SSPs (SSP1-2.6, SSP2-4.5, and SSP5-8.5).

5.4. Discussion

5.4.1. Socioeconomic and environmental implications

We have presented the possible future changes in CLS for the major staple food crops on climatological time scales in the RFA area of Ethiopia. It should be understood that these changes in CLS represent a response to climate change in the long term, which is different from responses to climatic extremes and interannual variability that often result in spontaneous short-term impacts on crop yield. While interannual variabilities in CLS are primarily driven by variabilities in rainfall suitability as illustrated in Fig. 5.12a, and temperature extremes (not shown here) the long-term changes in CLS are caused by both temperature and rainfall. In fact, temperature limitations are more severe in the long-term for the four crops, compared to rainfall limitations (Fig. 5.12b), which is also in agreement with the findings in previous studies (Akpoti et al., 2022; Holzkämper et al., 2013; Lobell and Burke, 2008; Schlenker and Lobell, 2010). The early sign of these changes can be a gradual decrease in the native crop productivity, as has already been witnessed by farmers across various regions in Ethiopia (Zenebe Adimassu et al., 2014; Destaw and Mekuyie, 2022; Megabia et al., 2022; Moroda et al., 2018; Tesfahunegn, 2021; Teshome et al., 2021; Tessema, 2021). This is followed by a phase of generally low productivity where the native (existing) crop species retreat and new crop species emerge (e.g., Abera and Tesema, 2019; Hameso, 2018; Tofu and Wolka, 2023). The final stage is when the native crop is abandoned and the new crop is adapted, for example as observed in sub-humid and humid areas in central and northern Ethiopia (Taye, 2021; Tessema et al., 2019).

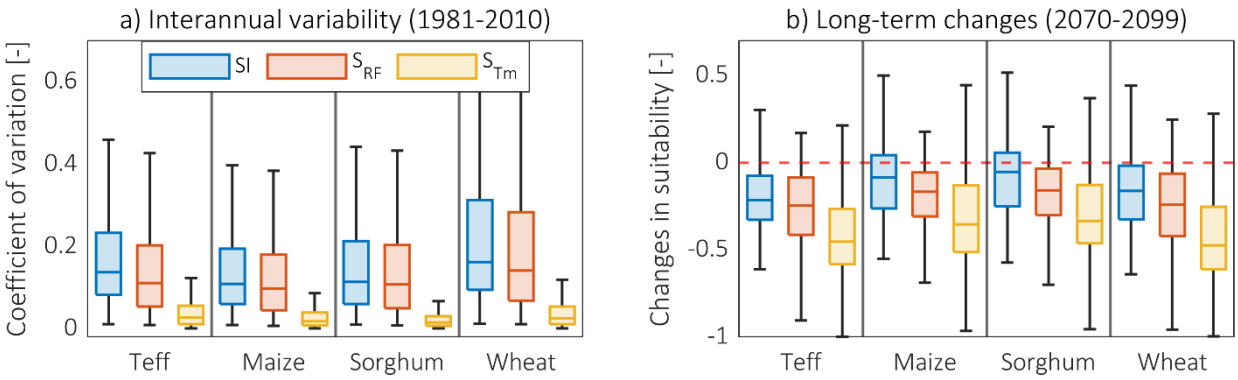

Fig. 5.12: (a) Interannual variability in suitability represented by boxplots of the coefficients of variation in the current climate , and (b) long-term changes in the suitability index (SI, blue boxes), rainfall suitability (S_{RF}, orange) and temperature suitability (S_{Tm}, yellow) under future climate. The boxplots represent variations among

the grid cells across the RFA region. The coefficients of variation were calculated from the annual SI, S_{RF} and S_{Tm} for the reference period (1981-2010). The long-term changes were computed as the differences between the future (2070-2099) suitability under SSP5-8.5, and the reference (present) suitability.

In marginal croplands, the changes in CLS are largely unidirectional. For example, in lowland areas the emergence of new crop species is constrained by warm temperature extremes, thus the croplands are abandoned once suitability for the native crop diminishes, while in highlands temperature becomes more suitable and new croplands emerge (Burke et al., 2009; Dendir and Simane, 2021; Sloat et al., 2020). However, expansions toward the highlands are not only limited by other environmental factors such as soil and slope, but they are also unsustainable as they trigger massive land conversion with serious environmental impacts including deforestation, biodiversity losses, and land degradation (Delelegn et al., 2018; Gidey et al., 2023; Moges, 2018), particularly in highly populated countries like Ethiopia. Since only a portion of the newly emerging croplands can realistically be exploited by farmers, our analysis represents a best-case scenario, which is unlikely to occur. Our analysis may therefore underestimate the overall negative impacts of climate change on future cropland areas in Ethiopia.

The contraction of suitable croplands will have adverse economic and food security implications in Ethiopia. A summary of the approximate changes in the annual production of the four crops in the 2060s under the intermediate emission scenario, assuming a linear relationship between production volume and cropped area is shown in Table 5.4. For example, under business-as-usual practices, i.e., rainfed small-scale farming practices with the same level of inputs, technologies, and services as present, the national teff production will decrease from the current volume of about 2.1 million tons to 1.8 million tons. Similarly, it is projected that maize production will fall from 2.8 million tons to 2.6 million tons due to the contractions of the suitable cropland areas (Fig. 5.8). On the contrary, Ethiopia's population is predicted to climb from 73.8 million (2007 census) to about 171.8 million in 2050 (Bekele and Lakew, 2014). These concurrent challenges add to the severe food security status in the country (GHI, 2022; Mohamed, 2017) exacerbating the level of poverty and the risks of hunger and malnutrition in the future.

Table 5.4: Comparison of the current and future cereal production associated with the projected changes in suitable cropland areas during the 2060s under the intermediate emission scenario. The present (reference) production was assumed comparable to the average of productions in the years 2000, 2003-2007 and 2010.

	Current		Future (2060s) under SSP2-4.5	
	Production (10^6 tons)	Cropped area (10^6 ha)	Production in (10^6 tons)	Crop area in (10^6 ha)
Teff	2.09	2.14	1.76	1.80
Maize	2.80	1.41	2.77	1.40
Sorghum	2.10	1.39	2.04	1.35
Wheat	1.99	1.29	1.81	1.17

5.4.2. Adaptation

Our results suggest that climate-driven changes in CLS are relatively small under sustainable development pathways that lead to low GHG emissions compared to the intermediate and high emissions, indisputably implying that global emission mitigation is vital. However, the impacts of these small changes even under the low emission targets are net negative and they can be impactful for society given the increasing food demand. For example, low emission pathways result in the reduction of teff cropland area by about 9% and that of wheat by 2.5% by 2060s (Fig. 5.8b, h), which can be a substantial limitation to the efforts towards meeting the 'zero hunger' sustainability goal (Tilman et al., 2011). Context-based adaptation and sustainable intensification measures are vital to reduce these impacts and meet the food demand of the growing population. Our sensitivity analysis results are useful in defining the objectives and the types of adaptation measures that can be implemented at a given location.

In rainfall-sensitive agroecosystems, water management practices aimed at reducing crop water stress in rainfall-deficit areas and waterlogging and nutrient losses in rainfall-excess areas are needed. In particular, reducing water stress in rainfed farming systems consists of several measures ranging from locating optimal planting dates that maximize the total available moisture during the growing season, to optimal on-farm management of rainwater that allows maximum infiltration, storage, and plant water availability, and minimum evaporative losses. In temperature-sensitive lowland areas, it is the management practices, which aim at reducing

evaporative losses that are important to alleviate evaporative stress, but only within the thermal stress limits of crops. Improving crop tolerance to harsh agroecological conditions like thermal and water stress through plant breeding is a viable and widely used strategy for climate adaptation and yield improvement (van Etten et al., 2019). Microclimate regulation is another adaptation strategy that can be implemented to reduce heat stress under warm climates. In this regard, agroforestry systems provide multiple benefits including microclimatic regulation, water conservation, soil fertility improvement, pest control, and farmers' income stabilization (Lasco et al., 2014). Under limited adaptive capacity, which is likely for example in Metekel and Awi zones for maize, Kamashi zone for sorghum in the western part, and West Hararge for teff in the eastern part of the RFA region, gradual switching to more resilient crops and/or smooth transition to a suitable farming system is needed.

Effective adaptation entails holistic measures including policy, appropriate technology, informed decisions, social transformation, and multi-stakeholder actions. These measures would unlock the untapped potential for adaptation and resilience by filling the current yield gaps thereby increasing production, for example by about 24 million tons (8 times more) for maize in Ethiopia (van Dijk et al., 2020). Institutional-level efforts are very crucial in Ethiopia to coordinate knowledge generation, evidence-based adaptation planning, decision-making, implementation, monitoring, and financing of climate adaptation. Because in Ethiopia climate change poses multiple impacts that differ in their types, occurrence probability, and severity, adaptation goals and plans need to be site-specific and comprehensive beyond the mostly climatic emergency responses (Conway and Schipper, 2011). Adaptation goals that target to improve resilience at farm and landscape levels considering interannual variability of rainfall, droughts as well as long-term changes in cropland suitability are necessary. Awareness of the diversity of future climate impacts should be created within the agricultural community to build readiness and flexibility for farmers to adjust to the changes and practice a diversified family economy.

5.4.3. Study limitations and future directions

The spatial maps presented here are limited by the spatial resolution of the climate data (0.05° x 0.05°), and thus sub-grid (e.g., landscape, farm, and field scale) details are not explicitly represented. In particular, terrain characteristics like slope and aspect have not been considered

in the suitability model, as their effects are impossible to capture at this coarse spatial resolution. As a result, the estimated potential suitability and projected cropland expansion toward highlands have not been topographically constrained and thus might be overestimated. Our framework however allows the inclusion of topographic limitations into the assessment of crop suitability and this could be a useful direction for future research. Ultimately, local scale plans and decisions, for example, cropland intensification should be based on future suitability assessments at a higher spatial resolution. Another limitation is that the effects of rainfall and temperature on crop suitability in our model were represented in a generalized way, i.e., as growing season total rainfall and mean temperature. The influences of other rainfall characteristics, such as the onset and duration of the rainy season, and additional temperature characteristics, such as cold and warm extremes, should be considered in future studies, also using process-based crop models in addition to statistical approaches. Future research in Ethiopia should also be extended to the Belg growing season, because the secondary rainy season may provide new opportunities as well. Despite these shortcomings, our analysis provides a valuable first-order assessment of the agroecological impacts of climate change on cereal crop production in the RFA area of Ethiopia, with a towards understanding the implications as well as adaptation actions that need to be taken especially at institutional level in the country.

5.5. Summary and Conclusions

The impact of climate change on rainfed agriculture poses a significant challenge to future food security and livelihoods, particularly in vulnerable countries like Ethiopia. We investigated the impacts on cropland availability by modelling cropland suitability under current and projected future climate conditions. We show that the warming climate and variable rainfall conditions in Ethiopia's rainfed agricultural area will cause suitable cropland areas to experience altitudinal shifts toward the highlands, leading to a loss of viable farming areas in the lowlands and a gain in the highlands as a result. However, due to strong evaporative and heat stresses in the moisture-limited lowland areas, it is expected that suitability losses in the lowlands will outweigh the gains in the highlands. Thus, even under the low-emission climate scenario, the net projected effects on cropland areas will be negative. This could have serious implications for food security in Ethiopia, especially given the expected high demographic growth in the

coming years. The impacts of intermediate and high emission scenarios are more severe, and cropland suitability conditions will worsen with time.

In some parts of the rainfed agricultural region, the current cropland suitability is constrained by low soil suitability, for example, due to high clay content (thus poor internal drainage) and acidity in the western humid agroecologies, and high soil alkalinity in the eastern and southeastern parts of the rainfed agricultural region. It is possible to increase productivity in these regions using effective management and technologies that can improve the suitability of the soil. The management and technologies that will help overcome climatic limitations can be selected based on the rainfall and temperature sensitivity of the croplands. Because lowland areas are more sensitive to temperature change, management interventions that reduce heat and evaporative stress are particularly necessary. In contrast, the management of excess rainwater in hyper-humid regions and the conservation of moisture in dry regions can significantly improve cropland suitability in these areas. The significant limitation of solar radiation in the forest-dominated southern part of the RFA region necessitates measures like selection of crop species with high radiation use efficiency, and proper choice of the growing season to ensure optimal radiation inputs, and moisture and temperature conditions. Our analysis provides a pioneer study and comprehensive information for guiding climate adaptation plans mainly at a national level. However, our work also stresses that reliable local adaptation plans should be based on high-resolution site-specific information about future climate, soil, and local farming contexts.

Chapter 6

Conclusions and Outlook

6.1. Summary

This thesis aimed to assess the climatic aspects of agro-environmental challenges and opportunities in rainfed agriculture (RFA), and their implications for future climate adaptation and resilience-building plans and decision-making in the context of Ethiopia. It begins by dealing with data limitations in the RFA region of Ethiopia (Chapter 2) and the utility of lower-quality scarce ground station observations to enhance the accuracy and spatial resolution of widely-available gridded climate datasets. Concretely, in this Chapter the ERA5-Land 2-m air temperature was de-biased and resampled to a higher spatial resolution over the Ethiopian domain (Wakjira et al., 2023, 2022). This new temperature dataset called BCE5, together with existing gridded precipitation datasets, and various spatial land cover and soil datasets, form the foundation of the analysis framework in this thesis. In the subsequent chapters 3-5, the thesis then assessed three aspects of climate-water-agriculture relations, quantifying their potential effects on crop distributions and yields, with a special view towards climate change impacts.

The first aspect, presented in Chapter 3, focused on the temporal attributes of rainfall that determine the timing and duration of the rainy season and the seasonality of rainfall (Wakjira et al., 2021), the features that critically define the optimal timing of seasonal crop planting that guarantees adequate moisture availability during the growing season in RFA systems. The second aspect, presented in Chapter 4, focused on quantifying growing season water availability and crop water demand, and on the implications for closing the water-limited yield gaps both under present and future climates. The third aspect, explored in Chapter 5, delved into changes in the agroecological suitability cropping areas, which is primarily defined by climate, soil and topographic factors. The focus here was on mapping potential cropland suitability and analyzing anticipated future changes under climate scenarios. In the following

sections, I summarize the *main insights* resulting from the research in view of the major research questions posed at the start of this thesis.

Insight 1: ***Low-quality ground station temperature observations can reliably be used for enhancing the quality of gridded global datasets through adoption of appropriate statistical methods that reduce local at-site uncertainty and account for external forcing, e.g. elevation*****.**

The first research question posed in this thesis was, "*how can we utilize low-quality station temperature observations for adjusting statistical biases and enhancing spatial details in gridded climate datasets for local applications?*" The answer to this question (Chapter 2) is based on the development of a workflow for bias-adjustment of the ERA5-Land maximum and minimum 2-m air temperature at an enhanced spatial resolution (0.05° x 0.05°) using spatial interpolation and quantile mapping (QM). The aim here was two-fold: first, to develop a framework for utilizing in-situ observed (IOBS) temperature data to de-bias and downscale gridded global datasets for local applications, and second, to produce a new high-quality gridded temperature dataset for Ethiopia. The fact that the IOBS temperature data that is needed to set up the QM in this thesis involves large data gaps, a sparse station network, measurement errors (outliers), and inhomogeneity, necessitates a careful adoption of a set of approaches. These approaches include preprocessing the IOBS data to address outliers and inhomogeneity issues, along with spatial interpolation and the QM technique. Three major issues needed to be resolved to enhance the local quality of the global temperature dataset in ERA5-Land using poor-quality IOBS data in Ethiopia (see section 2.2).

First, large data gaps imply that the IOBS data are not directly usable for robust time series-based QM model calibration. I instead proposed to use statistical parameters (mean and standard deviation) derived from the IOBS rather than the IOBS time series for the calibration of the QM model. The choice of the statistical parameters depends on which probability distributing function fits the IOBS data best. The idea of relying on temperature statistics triggered an important question: whether or not the statistics derived from observed data with large gaps are reliable. In the context of Ethiopia, it was found that maximum difference in the long-term mean of both maximum and minimum temperature statistics computed from full 30 year records and short 5 year records (25 years of gaps), is very low (less than 0.25°C) suggesting that reliable statistics can be obtained from measurements with large data gaps.

Second, despite the reliability of the estimated at-site temperature statistics, the sparse IOBS station network, particularly in remote parts of Ethiopia, introduces a significant problem for the spatial interpolation of IOBS statistics. To address this, a hybrid interpolation technique was applied. In this technique, background temperature statistics are modeled as a function of elevation and location, and the residual temperature statistics are interpolated using the Inverse Generalized (non-Euclidean) Distance Weighted (IGDW) approach (Frei, 2014). The use of non-Euclidean distance accounts for the effects of mountain barriers on temperature differences between two locations, which is particularly vital for capturing spatial variabilities in mountainous regions. The hybrid interpolation technique, combining regression-derived background and IGDW-interpolated residual IOBS temperature statistics, enabled the generation of the spatial field of IOBS statistics more accurately, which was then successfully used for the calibration of the QM model at every grid.

Third, in time series-based QM, non-stationarity (preservation of trends in the data) is ensured by calibrating the model dynamically along the data length, for example, on a moving window basis, which is impossible when relying only on the temperature statistics. To overcome this problem, a two-step QM procedure was introduced in this thesis. In the first step, bias adjustment is performed in a stationary setting (without preserving trends) using the climatology of monthly temperature statistics. Then, in the second step, non-stationary QM was applied to the monthly-corrected data in the first step, using annual temperature statistics to allow for interannual variability and trends along the data length. This two-step QM successfully produced the bias-adjusted dataset at the same accuracy that could be achieved with time series-based QM.

In summary, I showed that low-quality IOBS temperature data provides a sufficiently representative local temperature climate that can be incorporated into gridded global temperature datasets to de-bias and downscale them for local applications in data-scarce regions. However, this process requires an innovative combination of methods accounting for limitations regarding data gaps in time and space and nonstationarity. The final bias-corrected ERA5-Land dataset called BCE5 produced in this thesis demonstrates an approximately 68% greater accuracy in maximum air temperature and 25% greater accuracy in minimum air temperature compared to the original ERA5-Land 2-m air temperature dataset over Ethiopia.

It was published as an Open Access Dataset and is freely available to the scientific community (Wakjira et al. 2022).

Insight 2: ***The timing of the start of the rainy season and rainfall seasonality are significantly impacting crop yields in RFA regions, i.e. delays in rainfall onset dates under unimodal rainfall regimes, and changes in seasonality under bimodal rainfall regimes, are the main determinants of cereal crop production in Ethiopia***.

The second research question posed in this thesis was, "*What are the influences of rainfall timing and seasonality on seasonal crop production and what implications do they have for agronomic and water management decisions across the RFA region of Ethiopia*?" To answer this question, in Chapter 3 four key temporal attributes of rainfall -- seasonality, onset, cessation and duration of the rainy season -- were analyzed and associated with the June-September (meher) cereal crop production in the Ethiopian RFA region. Seasonality, representing the extent to which the annual rainfall is concentrated in the rainy (growing) season (Feng et al., 2013), was determined as a dimensionless index by combining the annual rainfall and its probabilistic monthly distribution for every year (see section 3.3.1). The timing and duration of the rainy season were computed by a method which identified the onset and cessation dates of the rainy season from daily gridded precipitation (CHIRPS), and the rainy season duration between the onset and cessation dates was considered as the length of the rainfed growing season (see section 3.3.2).

These analyses provided several very useful outputs about the rainfall regime in Ethiopia that significantly complement existing literature (Liebmann et al., 2012; MacLeod, 2018; Segele and Lamb, 2005). For example, with higher accuracy we can categorize the Ethiopian RFA region into northern and southern sub-regions that generally exhibit distinct temporal rainfall features. I showed that the major meher-producing *northern half* of the RFA region is characterized by highly seasonal rainfall (Fig. 3.6) and a unimodal rainfall regime (Fig. 3.3). The onset dates in this sub-region range from early May in the western humid areas (with season duration of ~180 days) to early July in the northeastern semi-arid areas, where the season duration is as short as ~60 days (Fig. 3.8). With the exception of the northeastern semi-arid areas, this sub-region shows low interannual variability in seasonality (Fig. 3.7), timing and duration (Fig. 3.9) of the rainy season. Correlation analyses between cereal production

reported by the Central Statistical Agency of Ethiopia and temporal attributes of the meher rain over this sub-region revealed a strong influence of the rainy season onset, with late-onset resulting in statistically significant decreases (on average by 1.5% for every 5-day delay) in cereal production. The influence of seasonality was weakly pronounced (Fig. 3.10). These findings emphasize the critical importance of rainfall onset-informed scheduling of planting operations in the main meher-producing region of Ethiopia.

In contrast, the *southern half* of the RFA region experience erratic (less seasonal) rainfall with transitional (year-round) and bimodal rainfall regimes peaking in March/April (belg), and August/September in the eastern, or September/October in the southern parts of this sub-region (Fig. 3.3). Both seasonality and timing (onset and cessation), and hence the duration of the wet seasons, vary highly from year to year. As a result, meher crop production shows a weak correlation with the timing and duration of the rainy season. Instead, it is meaningfully correlated with seasonality (Fig. 3.10). This is particularly evident in the eastern semi-arid part of the RFA region. The insight here was about the "curse of seasonality", meaning that where a small annual rainfall total comes in two seasons, this makes both seasons less reliable for crop production. The more the annual rainfall total is concentrated in one of the two seasons (either meher or belg), the more green water becomes available for crops, and hence the higher the crop production in that season. The water management implication of this is that water harvesting and vapor-shifting (from evaporative losses to transpiration gains) strategies should be prioritized to increase water-limited yields.

Insight 3: ***The median water-limited attainable yield (AY) during the meher growing season is approximately 80% of energy-limited potential yield, i.e., the water-limited yield gap is 20%. Climate change is expected to have minimal impact on AY in the major meher-producing regions, while it has a greater positive impact in the Belg-producing regions.***

The next research question was, "*What is the current climatology of water-limited attainable yield potential under RFA practices, and how is it expected to change under future climate conditions in Ethiopia?"* This was investigated in Chapter 4 by developing a modelling framework that utilizes climatic-hydrological-crop yield (CHC) relationships (section 4.2.3). The framework integrates the FAO Penman-Monteith algorithm (for estimating atmospheric evaporative demand), a conceptual hydrological model (for simulating key agronomic water

balance components), and a water production function (for determining water-limited yield). The CHC modelling framework is driven by gridded climatic data (temperature developed in Chapter 2 and precipitation studied in Chapter 3), and utilizes state-of-the-art topographic, land cover and soil data. The CHC modelling framework was applied to examine green water availability and to estimate attainable yield potential during the two growing seasons – meher and belg -- under both present and future climates in the RFA region of Ethiopia.

I showed that green water serves as a highly reliable source for meher (May – September) agricultural evapotranspiration across the majority of the RFA region. In over 50% of the region, AY exceeds 80% of the potential (fully irrigated) yield. The median climatological AY during meher, considering the period 1981-2010, ranges from 46% in highly moisture-limited dry semi-arid areas to 93% in humid areas (Fig. 4.1). During the belg season, which contributes to nearly 10% of the annual cereal crop production in Ethiopia (Taffesse et al., 2012), the median AY ranges from 40-60% across the respective producing region, primarily in the southern half of the RFA region. Spatial variations in AY are attributed not only to the spatial distribution of rainfall but also to the spatial variability of soil properties and surface conditions (e.g., slope, roughness), influencing surface and root zone hydrological fluxes and green water storage capacity. One main result of this Chapter was the systematic comparison of the AY and observed actual yield (Fig. 4.12), which helps us identify the crop yield gap that needs to be addressed through holistic agro-environmental resource management to enhance rainfed crop productivity in the face of climate change (see section 6.2).

Another important insight in this Chapter was related to the nature of climate change across Ethiopia. The downscaled multiple GCM projections of the future climate revealed warmer and largely wetter future climates during the growing seasons across the RFA region (Fig. 4.6). I showed with the CHC framework that this is likely to result in only slight changes (increases or decreases) in AY across the large parts of the meher-producing regions, particularly in humid and sub-humid areas. Relatively higher changes, mostly in the range of -5% to 5%, are expected in the southeastern and eastern semi-arid areas, especially for teff compared to maize, sorghum and wheat. The changes in meher AY are predominantly positive in the 2030s, and then decreases towards the end of the century (Fig. 4.10). In contrast, climate change is projected to result in an increase the belg AY in the future periods, for example by up to 20% in a large part

of the belg-producing regions by the end of the century, providing perhaps an additional opportunity for the intensification the belg season crop production by farmers.

Insight 4: ***A larger part of the RFA region is potentially suitable for the major cereal crops in Ethiopia, although soil-related limitations require management interventions. However, climate change is likely to have a serious impact in the future, resulting in altitudinal shifts and contraction of suitable croplands.***

The fourth research question of this thesis, "*What is the potential cropland suitability across the RFA region of Ethiopia, and how will it change under the projected future climate?*" was addressed in Chapter 5. This was approached through numerical modelling of cropland suitability (as detailed in section 5.2.3), considering key climatic (growing season temperature rainfall, and solar radiation) and soil factors (texture, pH and organic carbon). The modelling framework leverages a functional relationship between crop yield and the individual factors (Fig. 5.2) that was parameterized with yield observations and factor data at grid scale, and used for the simulation of the partial yield responses. The simulated (factor-specific) yield responses were post-processed to determine the partial suitability. The overall cropland suitability was obtained by combining the partial suitabilities. The framework was then applied to map the current potential cropland suitability and to assess future changes, considering the four major cereal crops produced in Ethiopia. Furthermore, relative sensitivity of cropland suitability to rainfall and temperature was analyzed using the one-at-time local sensitivity method.

The finding from this Chapter was that based on climatic and soil qualities, more than half of the cultivable areas of the RFA region are moderately and highly suitable for sorghum (63%), teff (54%) and maize (51%). Limited to mid- and highland agroecologies, wheat is the least versatile crop with only 29% of the region potentially suitable (Fig. 5.4). While climate plays a defining role, I also show that soil related limitations such as acidity, alkalinity and waterlogging could constrain present cropland suitability in some regions. Looking towards the future, climate change is expected to significantly impact cropland suitability in Ethiopia. The projections suggest that the areas suitable for teff and wheat will decrease, for example, by 18% and 27%, respectively, under SSP5-8.5 by the end of the century (Fig. 5.8). Maize and sorghum croplands will experience altitudinal shifts with relatively less areal losses compared to teff and wheat croplands.

The impacts of climate change on croplands become more pronounced with more extreme greenhouse gas emission scenarios, and as we move toward the end of the century. This is particularly evident in lowland agroecologies, where the changes are predominantly driven by increases in temperature. Highland agroecologies are also temperature-sensitive, but the impact there results in a gain in cropland suitability. On the other hand, hyper-humid and semi-arid agroecologies are more sensitive to rainfall. These regional differences in the climate sensitivity of croplands are crucial to guide the type of adaptation measures that are suitable, depending on the sensitivity. I argue in this work that this aspect of climate change will pose critical challenges to development targets like food security, poverty reduction, and economic resilience of the rural society, necessitating urgent adaptation and risk management strategies.

6.2. Scientific and practical relevance

This thesis provides novel quantitative insights into the agroclimatic, agrohydrological, and agroecological perspectives of the rainfed farming system in Ethiopia at a national scale using state-of-the-art datasets, models, and ground observations. During this research effort, new climate data have been produced, replicable analysis and modelling frameworks have been developed, and both scientific and practical information have been generated. These outcomes can serve as a foundation and input for future research in the field, as well as provide valuable information for practices, planning, and policy- and decision-making relevant to climate-smart agriculture in Ethiopia. Although the study was focused on Ethiopia, the vision was to create generalizable workflows that will be reproducible in other RFA regions worldwide. Here, the main methods and results are discussed with regard to their scientific and practical relevance and existing literature.

6.2.1. Data and methods for agrometeorological analyses

Climate-smart agricultural practice requires detailed agrometeorological elaborations of agricultural landscapes and effective monitoring of key state variables and their changes (Blaser et al., 2018; Lipper et al., 2014; Peng and Guan, 2021). This requires high-quality climate data with adequate spatial detail, sufficient duration, and reasonable accuracy (Tim Wheeler and Braun, 2013) -- a prerequisite historically lacking in wider sub-Saharan Africa and other parts of the developing world. Frameworks, such as the one employed here to de-bias and downscale globally available climate reanalysis data, applied to air temperature in

Chapter 2 can be reproduced in other regions. I believe such local calibration of a global dataset to a specific region/country is better than a globally adjusted dataset to fit local applications. The demonstrated performance in producing the BCE5 dataset can potentially serve as a showcase of the value of lower-quality in-situ observation data. This framework is versatile and can be adopted for other climate variables, with necessary considerations for the nature of the variable. For example, one must account for the probability distribution of the data, environmental covariates, and internal properties of the variable, such as intermittency and phase for precipitation, among others. In my opinion, BCE5 can serve as a reference temperature dataset for other agrometeorological and climate impact studies in Ethiopia that provide both scientific understanding and practical applications as presented in section 6.2.4.

The works undertaken in Chapters 3-5 represent examples of climate data applications in combination with soil, land cover and crop data, for a detailed agrometeorological characterization of locations. This includes defining the climatology of rainy season onset and cessation, potential rainwater productivity (water-limited yield potential), and climate-defined and soil-limited cropland suitability. These key agroecological characteristics can inform farm management practices and be used for detecting and monitoring ongoing environmental changes. The aim in my research was to develop analysis frameworks and workflows in Chapters 3-5 that can be replicated for similar scientific inquiries in other case studies, with context-specific adjustments as needed. The numerical modelling framework implemented in Chapter 5 overcomes some of the important drawbacks of existing land suitability models, such as those based on fuzzy logic (e.g., Feng et al., 2017; Schneider et al., 2022; Zabel et al., 2014) that are based on an empirical definition of suitability functions. In our case, the suitability functions derived from a mathematical relationship between crop yield and the suitability factor allow a more realistic and data-driven parametrization of suitability.

The CHC modelling framework applied in Chapter 4 is a simple but powerful tool that can be adopted for various agrometeorological applications such as estimation of water availability and crop water demand both for irrigated and rainfed systems, and relative yield prediction the purpose of management planning. This avoids the dependence on process-based crop models, which are often data-intensive and the require rigorous calibration of several parameters (Jägermeyr et al., 2021; Ramirez-Villegas et al., 2017; Steduto et al., 2009). Moreover, the

CHC modelling framework allows simulations at any scale from field scale to region and global scale.

6.2.2. Implications for yield forecast and decision-support for actors

Ideally, farmers make the right decisions when they have insights into the prospective yield in the upcoming season based on the onset of the rainy season. In this context, insights from Chapter 3 provide a concrete link between crop yield losses or gains and the onset of the rainy season. This linkage can serve as a foundation for extending rainfall onset forecasts to yield predictions (Rattalino Edreira et al., 2021), supporting farmers in making elementary agronomic and water management decisions, particularly in the main meher-region of Ethiopia. When the forecast of rainfall amount is available and sufficiently reliable (Diro et al., 2011b; Ehsan et al., 2021; Gissila et al., 2004; MacLeod et al., 2023), the agrohydrological modelling framework used for assessing water-limited yield in Chapter 4 can be employed to estimate the level of soil moisture limitations that farmers can expect during the forecast lead time. A late onset of the rainy season often signifies either drought onset or dry spell conditions that may necessitate the activation of risk management actions, where yield-based information is crucial for government agencies and non-governmental organizations.

6.2.3. Climate impact information for planning, policy design and decision-making

The primary practical significance of this thesis lies in providing information climate adaptation, resilience and risk management planning, policy design and decision-making in Ethiopia. The insights gained from the assessment of agroecological impacts of climate change in Chapter 5 sound an important alarm for urgent policy, regulatory and institutional responses to address the potential challenges of climate-driven future cropland abandonment and shifts – something that seems to have been underestimated in the current national adaptation plan of Ethiopia (FDRE, 2019). Insight from our climate sensitivity analysis in section 5.3.3, which is in contrast to other studies (Burke et al., 2009; Kummu et al., 2021; David B Lobell et al., 2011; Lobell and Burke, 2008) suggests that temperature increase predominantly drives the reductions in cropland availability necessitates holistic approaches to adaptation and mitigation solutions. Alongside well-established genetic modification of crop varieties (Gago et al., 2014; Hatfield and Dold, 2019; Porras et al., 2023), considering agroecological measures that can regulate the microclimates of croplands could be viewed as an alternative strategy in this

regard. Insights from Chapter 4 regarding the present and future green water yield potential, on the other hand, suggest largely minimal influence of climate change during the main growing season, but with untapped potential and positive impacts during the shorter growing season. This information is useful for setting agricultural intensification targets based on the available potential and planning how to reach these targets by closing yield gaps. Such planning is crucial in efforts to overcome the triple challenges -- food security, poverty, and climate vulnerability in agricultural nations like Ethiopia.

6.2.4. Major practical applications of the findings

In this section, I will present concrete examples of where and how agro-environmental insights from this thesis can be utilized to improve rainfed crop production for food security, poverty reduction, and climate resilience. As mentioned in earlier sections, these findings are relevant in both practical applications, such as farm-level management supported through agricultural extension services, and institutional applications, including planning, policy, and regulatory designs.

Water conservation in dryland area with bi-modal rainfall regime

The regional patterns of crop production responses to rainfall seasonality and timing presented in Chapter 3 can serve as a guide for agricultural extension and development agents in supporting farmers with strategies to minimize crop water stress during the growing season. In this regard, our findings (Fig. 3.10) point out which strategy is needed where, implicating two categories of possible management strategies: proper choice of optimal planting dates based on the rainfall onset under a unimodal rainfall regime, and rainwater water conservation in semi-arid bi-modal rainfall regimes. The latter is particularly crucial in the eastern part of the RFA region, where soil moisture deficit is high (Fig. 4.5a), necessitating soil and water conservation measures at field and farm scales. The established guidelines for soil and water conservation in Ethiopia, as suggested by Hurni (2016, 1998), can provide technical guidance for implementing water conservation measures effectively. While water conservation in this moisture-limited region should aim to maximize rainfall infiltration (*runoff retaining*), and minimize evaporative losses, achieving both simultaneously can be challenging due to the high labor requirements of these measures (Studer, 2021). Our analysis result (Fig. 5.12a) suggest

that rainfall variability is the main factor contributing to interannual variability in crop yields, emphasizing the need to prioritize conservation measures that maximize soil moisture.

Amelioration of soil-related limitations

In our assessment of cropland suitability, we have identified areas where soil conditions limit crop yields. One such limitation is the potential for waterlogging problems, affecting a substantial area of the RFA region in the western humid and sub-humid parts (Fig. S5.1). These areas are characterized by clayey soils, mainly nitisols and vertisols (Ali et al., 2024). Teff and wheat production in these areas are particularly hampered by this soil-climate interaction, leading to prolonged soil saturation. Addressing this issue requires the removal of excess water from agricultural fields (*runoff draining*) to overcome waterlogging-induced limitations. Locally developed soil drainage implements such as the Broad Bed Maker (BBM) (Rutherford, 2008) have been effectively used in Ethiopia. Several studies have demonstrated that runoff drainage practices like broad bed and furrow methods can increase crop yields by over 30 percent (Alemayehu et al., 2023; Lebay et al., 2021; Welderufael and Woyessa, 2009).

The pH partial suitability map (Fig. S5.2) provides indications of areas where soil pH limits crop yields. About 13% of the RFA region, particularly the western humid areas are identified as acidity-affected (the dotted areas in Fig. 6.1), significantly limiting land suitability for teff and wheat cultivation. Conversely, croplands in the northern parts (primarily in the Tigray Regional State) and eastern parts (accounting for about 11%) of the RFA region are limited by soil alkalinity (see the crosshatched areas in Fig. 6.1). These insights can guide planning technical advisory services for farmers and resource mobilization for soil amendment practices such as liming, organic amendment, and tillage management to address acidic soils in these regions (Gurmessa, 2021; Warner et al., 2023). Despite the significant limitations posed by soil alkalinity, soil treatment practices for alkaline soils have been limited in Ethiopia. Our findings highlight the urgent need for alkaline soil amendment in these vulnerable regions. Assessments show that practices such as amendment with gypsum, biochar, cow dung, and phosphate fertilizers hold promise for ameliorating alkaline soil conditions (Bello, 2012; Li-ping et al., 2015; Qayyum et al., 2017).

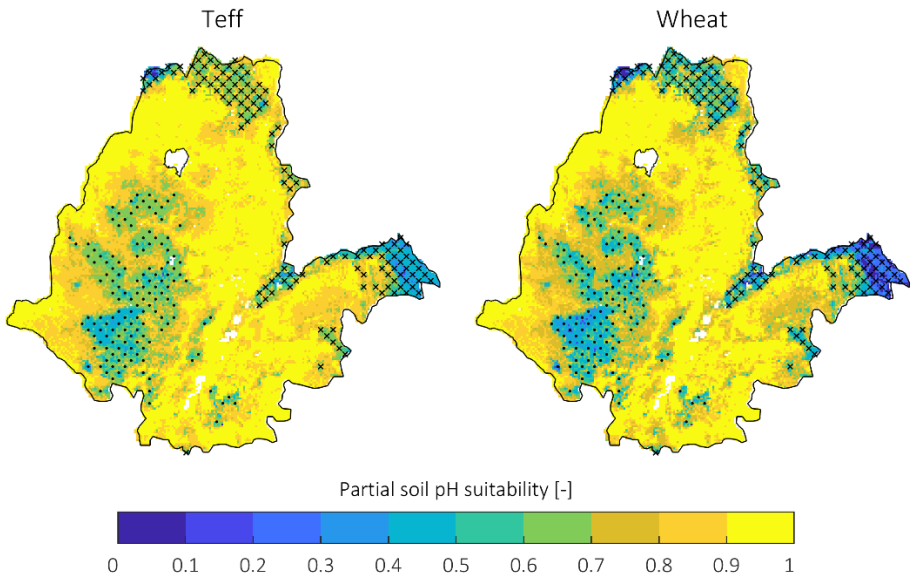

Fig. 6.1: Soil pH suitability for teff and wheat production across the rainfed agricultural region of Ethiopia. The dotted areas correspond to regions with soil pH < 6 (acidic), and the crosshatched areas correspond to soil pH > 8 (alkaline)

Policy and institutional implications

The comprehensive analysis of agro-environmental dimensions in smallholder rainfed farming systems undertaken in this thesis provides crucial information for policy and institutional considerations for the achievement of the food security, poverty reduction, and climate resilience goals. The main understanding from Chapter 4 is that under ideal input and management conditions, the regional average water-limited yield gap is 21% of the potential (fully irrigated) yield, while the actual yield gap (e.g., for maize) is about 73% of the fully irrigated yield or about 64% of the water-limited (rainfed) attainable yield. In other words, only 36% of what could be produced on average is achievable under prevailing agro-environmental conditions. This yield gap can be attributed to agricultural input and management limitations, which are determined by the underlying policy and institutional setting as summarized in Fig. 1.1. This implies that there should be fundamental reconsiderations of regulatory and institutional measures to ensure farmers have unlimited access to agricultural inputs (such as fertilizer, pesticides, and herbicides), appropriate technologies, extension services, access to markets and finance, and weather and climate services. The future changes in cropland suitability reported in Chapter 5 are also key inputs for long-term climate adaptation policies that need to be in place.

6.3. Limitations and Outlook

6.3.1. Limitations of the thesis

In this thesis, the research effort was driven by the development and use of a range of quantitative methods to contribute to our understanding of the climate, water, crop, and agroecological relationships and their changes with climate, primarily addressing the need for evidence-based policy- and decision-making (Fig. 1.1) at higher administrative level in Ethiopia. These quantitative estimations, which involved multi-year simulations at relatively high resolution covering the entire rainfed agricultural region (~667,000 sq.km), required assumptions and simplifications, leading to three key limitations that I highlight here.

The first one is related to the adequacy of the prediction scales. The analyses here were performed at a spatial resolution defined by the state-of-the art climate dataset used (0.05° x 0.05°), mainly CHIRPS rainfall (Funk et al., 2015) and BCE5 air temperature (Wakjira et al., 2023, 2022). Therefore, sub-grid landscape and farm scale details have not been represented. This limitation is particularly important, for example, in the context of our cropland suitability mapping in Chapter 5, in which the effects of terrain slope were masked out, and sub-grid variabilities in soil properties were not included. Consequently, not every piece of information presented in the thesis at grid scale is complete for landscape and farm level uses. Therefore, additional local assessments may be needed for (details in section 6.3.3).

The second limitation is related to the conceptual modelling of the climate-hydrology-crop relations. In order to optimize the handling of computations involving large data volumes, some methods used in this thesis have been simplified without significantly compromising the quality of the output. For example, the CHC modelling framework implemented in Chapter 4 involved a simplified crop response module in which water production function was used where the complex crop growth processes were represented by the yield response factor. This modelling framework can be categorized into crop coefficient models, which are types of crop models wherein the water production function is coupled with water balance models to estimate seasonal crop water use and crop yield (Foster and Brozović, 2018; He et al., 2022; Schwartz et al., 2020). In our case, this allows the simulation of relative yield (the ratio of water-limited and energy-limited yields).

The third important simplification concerns the climate downscaling method used, i.e. the delta change method in which the natural variability of the reference climate was assumed to remain unchanged (Navarro-Racines et al., 2020; Sarr et al., 2015). For the two applications in this thesis -- the analyses of changes in water-limited yield potential in Chapter 4, and changes in cropland suitability in Chapter 5, both of which focused on the changes at climatological time scale, this assumption does not pose major uncertainty (Glotter et al., 2014). However, assessments focusing on seasonal, interannual variability and trends under future climates need to account for changes in the natural variability of the future climate (Basche et al., 2016; Hoffmann et al., 2018; Williams and Falloon, 2015).

6.3.2. Uncertainties in inputs and model parameters

In addition to the limitations discussed in Section 6.3.1, uncertainties in input data and parameters also influence the model outputs. Here, I will elaborate the uncertainties in climate data, soil, and crop data and parameters, and their propagation through modelling cascades in the three major agro-environmental aspects covered in this thesis (Chapter 3-5).

Uncertainties in climatic inputs

Climatic inputs are the major sources of uncertainties in this thesis. These uncertainties fall under three categories (Deser et al., 2012; Fatichi et al., 2016a; Peleg et al., 2019): *climate model uncertainties* resulting from limitations in climate models and the algorithms used to produce the data, *climate scenario uncertainties* stemming from limited knowledge of future greenhouse gas emission pathways, and *stochastic uncertainties* arising from the random variability of the climate variables. In our analyses, the influence of stochastic uncertainties in the future climate datasets on our results is minimal, particularly at the climatological timescale, where they are averaged out.

Concerning climate model uncertainties in the current climate, we have significantly reduced uncertainties in temperature inputs through bias-correction (see Chapter 2). The CHIRPS rainfall data, used as the reference for rainfall climate, is considered the most suitable gridded rainfall data for agroclimatic monitoring in Ethiopia (Bayissa et al., 2017; Gebremicael et al., 2019; Musie et al., 2019). However, its performance tends to decline over the southern and southeastern parts of the RFA region (Fig. 3.2) where the station observation network is sparse

(Ahmed et al., 2024). Consequently, uncertainties arise in rainfall timing attributes over these regions, where predictability is naturally low due to the transitional or bimodal nature of the rainfall regime (Fig. 3.3). Moreover, uncertainties in rainfall across the southeastern part contribute to uncertainties in simulated agrohydrological fluxes and attainable yield potential, particularly during the Belg season. Water-limited attainable yield is sensitive to rainfall during Belg, as illustrated in Fig. 4.11. Cropland suitability in this region is also rainfall-sensitive (see Fig. 5.11), implying higher uncertainty in the suitability maps for this area.

The future climates (rainfall and temperature) carry both climate model and climate scenario uncertainties that could propagate to the analyses results in Chapters 4 and 5. In delta change downscaling approach that we employed, future climate is partitioned into the *natural climate*, and the *delta* (change). The propagation of climate model uncertainties in the natural climate is negligible because the uncertainties are similar in the future climate and current climate due to the stationarity assumption in the delta change downscaling method (see Section 5.2.2). The uncertainties in the delta (changes) are explained by the differences in the future changes projected by various GCMs or RCMs. As discussed in the earlier sections, we represented the future changes in the climate variables by the median of the changes derived from multiple model projections to keep the uncertainties at minimal. The largest source of uncertainty in future climates stems from scenario uncertainty (Hawkins and Sutton, 2011). In this regard, our results were presented based on three possible future climate trajectories, which correspond to low, intermediate, and high greenhouse gas emissions scenarios as defined by the Intergovernmental Panel on Climate Change (IPCC).

Uncertainties in soil data and parameters

Soil inputs introduce additional uncertainties that must be considered when interpreting and using the results related to water-limited attainable yields and cropland suitability presented in Chapters 4 and 5. Due to the inherently high spatial variability of soil properties, even the quality of the best available soil data, such as SoilGrids is limited. For this, further soil profile measurements are needed for better calibration of the spatial prediction models (Poggio et al., 2021). Specifically, SoilGrids utilized fewer than 2 soil profile measurements per 1000 km^2 area in Ethiopia (Batjes et al., 2020), highlighting the scarcity of observed soil data that can potentially lead to uncertainty in the spatial prediction model.

Uncertainties in soil texture, organic carbon content, and pH can influence the predicted crop suitability. In the case of water-limited attainable yields, uncertainties related to soil arise from soil texture, organic carbon, and the agrohydrological parameters derived from them. The determination of soil water retention at saturation, field capacity, and wilting point is based on pedotransfer functions, such as Saxton and Rawls, (2006) in our case, which are also affected by the spatial heterogeneity of the soil properties (Nasta et al., 2021; Van Looy et al., 2017). The uncertainties in the water retention characteristics affect soil water balance calculations, which in turn propagates to the green water availability and water-limited yield estimates.

Uncertainties in crop data

The crop data used in this thesis that is sourced from the statistical summaries of the annual Agricultural Sample Survey (AgSS) published by the Central Statistical Agency of Ethiopia (e.g., CSA, 2010). Consequently, there are obvious statistical uncertainties associated with this crop data. One such uncertainty arises from sampling, as these data are based on yield surveys and measurements from the sample households, which are then extrapolated to represent crop production data for entire administrative zones. Additionally, yield measurement errors and inconsistencies, in crop sample weight, sampled area, field size, cultivated area, and other involved measurements can introduce further uncertainties into the data.

The spatial downscaling of zonal average crop data to grid scale in Chapter 3 assumed the crop cover fraction retrieved from the Copernicus Land Services. This product is reported to have continental-scale accuracy of 80% at a 100 m spatial resolution (Buchhorn et al., 2020), implying some level of uncertainty in the spatial pattern of the disaggregated total cereal production. Consequently, this uncertainty can propagate to the correlation analysis results reported in the chapter.

Uncertainty and sensitivity analyses

In previous discussions, I have identified the main uncertainties arising from inputs, assumptions, and models and how they influence the model outputs. It is important to note that some of these uncertainties are masked due to the spatial and temporal aggregations involved. For instance, both the soil and cropland cover datasets were spatially aggregated from their original resolutions of 250 m and 100 m, respectively, to 5 km, which is the spatial scale

considered throughout this thesis. Our analyses in section 2.2.1 (see Fig. 2.7) demonstrated how uncertainties in climate data diminish upon temporal aggregation. Consequently, rainfall uncertainties in the analyses of rainfall temporal attributes (Chapter 3), which were carried out at pentadal (5-daily) are reduced. Similarly, in the assessments performed at climatological timescales, focusing on water-limited yields and cropland suitability, uncertainties in the climatic inputs as well as that of the agrohydrological and agroecological model outputs are significantly reduced, as mentioned earlier.

Quantification of uncertainties is crucial for guiding end-user decisions and understanding the associated risks. In this thesis, a local sensitivity analysis was conducted to focus on key drivers of changes, such as rainfall, temperature, and evapotranspiration, affecting water-limited attainable yield and cropland suitability. This method involves systematically analyzing output variability in response to individual changes in input variables. In future studies, this analysis can be extended to global sensitivity and uncertainty analyses, such as Sobol' method (Sobol' et al., 2007) to provide a more comprehensive understanding on the influences of input variabilities on model outputs. Sobol' method enables quantification and partitioning of uncertainties considering input and parameter variabilities across entire variable space (Hamby, 1994; Sobol' et al., 2007). It employs distribution-based sampling of variances mostly using Monte-Carlo simulations, to perturb the model with the sampled set of inputs (Fatichi et al., 2016a; Guo et al., 2017; Peleg et al., 2019). One main limitation of the Sobol' method can be its computational demand, especially when applied at the grid scale over a large geographical domain. This limitation becomes more pronounced with the number of input parameters for which sensitivity is analyzed.

6.3.3. Research Outlook

Climate-smart agriculture is founded on the application of practical information and technologies, considering the agroecological and socioeconomic contexts to enhance productivity, build resilience, and ensure environmental sustainability (FAO, 2022). In this sub-section, I will describe what I think are important future research topics that can overcome the limitations indicated in section 6.3.1, in order to enhance our understanding of the *landscape and farm-scale context*, and thus support smart farming practices.

Joint agrometeorological and agroecological elaborations

Soil properties, topographic characteristics, weather, land cover, and biodiversity vary over small horizontal distances, influencing agrohydrological and agronomic responses to weather and climate dynamics. These responses, in turn, shape farm management practices. The availability of high-resolution geospatial data from multiple sources, coupled with climate datasets, allows for detailed spatial elaboration (at sub-kilometer scale) of agroecologies. However, the spatial resolution of existing climate datasets is coarse compared to soil, elevation, and land cover datasets. Future efforts should therefore focus on enhancing climate data availability for local applications. For variables like temperature, frameworks such as the one implemented in Chapter 2, which enables the assimilation of local climate statistics can be utilized, leveraging the strong explanatory power of elevation. A similar approach can also be extended to rainfall and other climate data through a thorough selection of statistical parameters and environmental covariates. The potential of remote sensing observations such as cloud dynamics to be used as predictors of the local climate variables like rainfall can also be evaluated (Kumah et al., 2022; Wilson and Jetz, 2016). Alternatively, recently developed high-resolution global climate datasets like Climatologies at High resolution for the Earth's Land Surface Areas (CHELSA) (Karger et al., 2020) can be tested and used.

High-resolution cropland suitability mapping is essential for guiding cropland expansion without causing unsustainable land conversion. The numerical suitability-mapping framework implemented in this thesis (Chapter 5) can be utilized by incorporating additional factors, such as elevation, slope, and soil depth, while masking out non-agricultural land uses. Simultaneously, agrometeorological details of the suitable agroecologies need to be elaborated. These details may include the agrohydrological component responses (Chapter 4) of agricultural landscapes, such as rainfall-runoff, infiltration, green water storage capacity, evapotranspiration demand, erosion risks, waterlogging risks, and water-limited yield potential. These are vital to guide farmers in implementing appropriate soil, tillage, and water management strategies (Hurni, 2016).

Teleconnection-based prediction of rainfall timing

Forecast information on the timing of the growing season rainfall is of paramount importance for scheduling planting operations and water management to minimize the risks of crop failure associated with delays in the rainy season in rainfed systems. The teleconnection between Ethiopian rainfall and the dynamics of the SST over the Pacific, Atlantic, Indian Oceans, and the Red Sea region (Alhamshry et al., 2019; Segele and Lamb, 2005) as well as global atmospheric moisture circulations (see also section 1.2.2) can be utilized for predicting the arrival of rainy days over the meher region of Ethiopia. For example, in our exploratory data analysis (Fig. 6.2) of the linkage between rainfall onset and SST anomalies of the central Equatorial Pacific using NINO3.4 index in Chapter 3 demonstrate such potential. The analysis showed that 54% of the years with late meher rainfall onset during 1981-2010 were the years with a positive ENSO (NINO3.4 > 0.5°C is El Niño). Specifically, during El Niño years, 64% of the cases (7 out of 11) exhibited a late onset of the meher rainy season (see the green marks in Fig. 6.2b). Looking at the corresponding cereal production anomaly during the period 1995-2010 (Fig. 6.2c), it was found that 4 out of the 6 El Niño years (67%) had a negative cereal production anomaly, suggesting a meaningful linkage.

The utilization of these teleconnections entails further understanding on the dynamic aspects of these linkages that future research needs to solidify. For example, the choice of the optimal time scale and the lag between the relevant oceanic variable (e.g., SST) and the rainfall onset that maximizes that correlation, and the intensity of SST anomaly versus the intensity of the onset anomaly, are relevant information the prediction of the teleconnection-based rainfall onset. The joint influences of multiple SST-related phenomena, especially that of the ENSO, the Indian Ocean Dipole (Degefu et al., 2017; Dubache et al., 2019) and Madden Julian Oscillation (Berhane and Zaitchik, 2014; Zaitchik, 2017) can also have a significant influence on the prediction of the rainfall onset.

Atmospheric circulation, which is responsible for moisture transport from oceans to land, is also a key aspect that needs to be understood. As briefly touched in Chapter 3, the onset and cessation of the meher rainy season is largely controlled by the seasonal north-south oscillation of the Inter Tropical Convergence Zone (ITCZ). Consistent with this oscillation, the onset of the meher season rainfall follows a gradual movement from the southwestern part of the RFA

region where first onset is observed around early April toward the northeastern part where the last onset happens around early July (Fig. 3.8). This suggests that onset prediction can be improved through tracking the latitudinal location of the ITCZ, which needs to be further explored. Additionally, westerly and easterly winds also play an important role in moisture transport to Ethiopia (Gleixner et al., 2017; Viste and Sorteberg, 2013), thus their interaction with the ITCZ should be considered in the prediction of the rainfall onset.

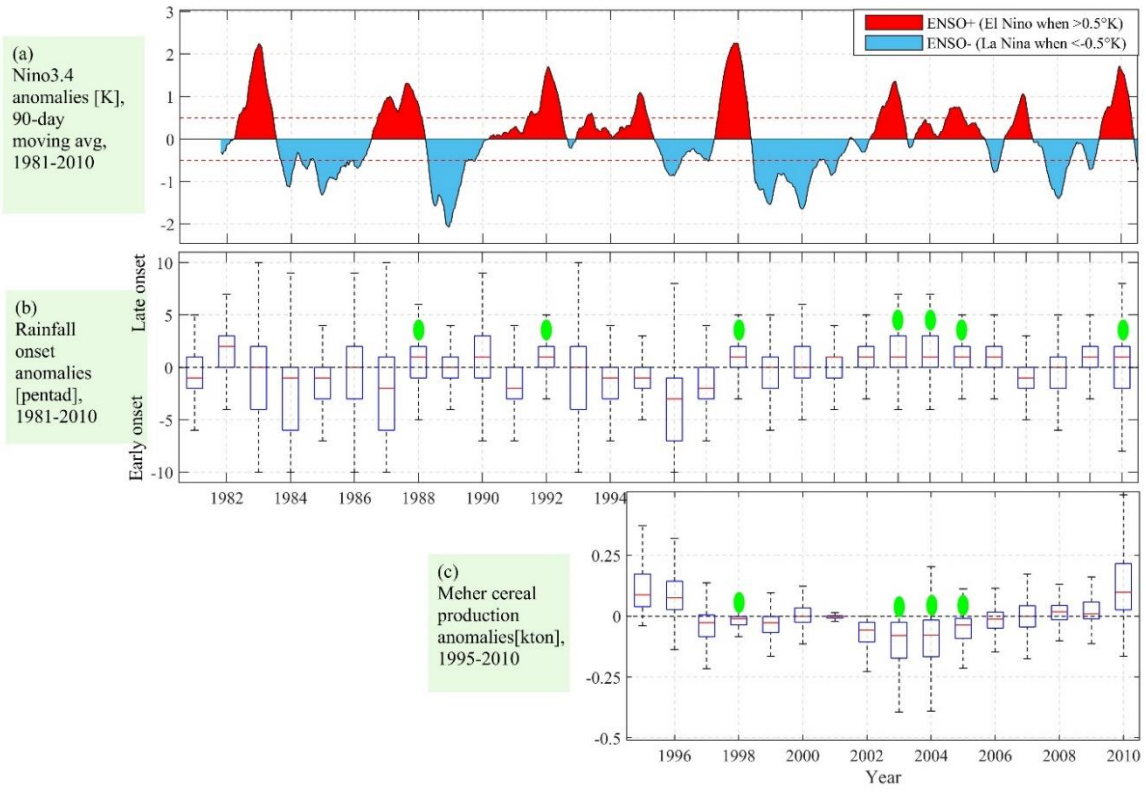

Fig. 6.2: Anomalies in the CHIRPS rainfall onset (panel b) and meher cereal production (c) over the entire rainfed agricultural area (see section 3.3.3) with respect to the NINO3.4 index from https://climexp.knmi.nl/ (a) for the period (1981-2010). Each boxplot considers the values at all grid cells in the study area. Outliers are not plotted. The green marks show the years of +ve ENSO phase (El Niño) with +ve rainfall onset anomaly (late-onset), and -ve cereal production anomaly.

Assessment of climate impact and adaptation strategies using mechanistic crop models

In the assessment of green water availability and water-limited attainable yield in Chapter 4 of this thesis, it was assumed that the crop response to climate was lumped into the yield response factor, Ky. Additionally, nutrient and crop management were assumed optimal so that the effects of changes in water availability under a changing climate can be detected. However,

impact assessments and adaptation evaluations for field application should be based on models that are more detailed.

One advantage of process-based crop models for climate impact studies is its ability to account for the positive gains of crops from the elevated CO_2 concentration through increase water use efficiency (Minoli et al., 2022; Zhao et al., 2017). The positive gains from elevated CO_2 are limited by soil nutrient availability (Fleischer and Terrer, 2022; Raes et al., 2021; Van Groenigen et al., 2006). In this regard, process-based crop models can be used to analyze fertilizer use scenarios and recommend optimal fertilizer application to maximize the benefits of crops from CO_2 fertilization. Crop models also consider the thermal stress effect of cold/warm temperature, which is another key aspect driven by climate change. Crop growth responses to various stresses (water, nutrient and thermal) at different growth stages have different implications for the final yield and these non-linear responses are only captured by process-based crop models.

Future studies should leverage crop modelling experiments to also analyze management scenarios aimed at improving agricultural resource use efficiencies for enhanced crop yields (Raes et al., 2021). This requires the further development of frameworks to evaluate the effectiveness of climate adaptation strategies. Specifically, agrohydrological feedbacks and processes associated with soil and water management-based adaptation strategies should be adequately represented in crop models (B. Peng et al., 2020; Siad et al., 2019; Zhang et al., 2021). Enhancing water use efficiency is the main priority in climate adaptation and resilience building. This ranges from strategies that maximize the seasonal water availability, for example, through optimal choice of planting date and measures to reduce runoff and increase infiltration, to measures that minimize evaporation losses. A wide range of such strategies have been recommended in previous research and field demonstrations (Hurni, 2016; Marval et al., 2022). However, their implementation remains limited, primarily focusing on community-based landscape and watershed development targets in Ethiopia (Siraw et al., 2020). On-farm water management should be promoted through collaborative research that involves farmers and on-farm trials. This approach not only facilitates the co-creation of knowledge but also allows for field data collection essential for modelling the system effectively.

Lastly, multi-objective practice like conservation agriculture seeks to maintain the agriculture-environment equilibrium through restoration of healthy agroecosystems and climate mitigation while ensuring sustainable food production. It is based on the principles of maintaining soil health by minimizing soil disturbance through reduced tillage, and increasing soil organic carbon through practices like residue retention, cover cropping and crop rotation (Giller et al., 2021; Wittwer et al., 2021). Such practices can potentially alter the agrohydrological responses and thus water availability, and are largely overlooked in the current research in the field (Lankford et al., 2022). Future studies should assess the effectiveness of conservation agriculture from water availability, and thus the climate adaptation perspective.

Bibliography

Abatzoglou, J.T., Dobrowski, S.Z., Parks, S.A., Hegewisch, K.C., 2017. Data Descriptor : TerraClimate , a high-resolution global dataset of monthly climate and climatic water balance from 1958 – 2015 1–12.

Abebe, S., Deribew, K.T., Alemu, G., Moisa, M.B., 2023. Modeling Eragrostis tef Zucc and Hordeum vulgare L cropland in response to food insecurity in the Southwestern parts of Ethiopia. Heliyon 9, e14535. https://doi.org/10.1016/j.heliyon.2023.e14535

Abera, K., Crespo, O., Seid, J., Mequanent, F., 2018. Simulating the impact of climate change on maize production in Ethiopia, East Africa. Environ. Syst. Res. 7. https://doi.org/10.1186/s40068-018-0107-z

Abera, N., Tesema, D., 2019. Perceptions and practices of climate change adaptation and mitigation strategies among farmers in the Konta Special District , Ethiopia 1–16. https://doi.org/10.2478/environ-2019-0019

Abiyu, A., Alamirew, T., 2015. Assessment of stage-wise deficit furrow irrigation application on maize production at Koga irrigation scheme, Blue Nile River Basin, Ethiopia. Assessment 6, 21–29.

Abrams, L., 2018. Unlocking the potential of enhanced rainfed agriculture. Stockholm.

Adam, M., Van Bussel, L.G.J., Leffelaar, P.A., Van Keulen, H., Ewert, F., 2011. Effects of modelling detail on simulated potential crop yields under a wide range of climatic conditions. Ecol. Modell. 222, 131–143. https://doi.org/10.1016/j.ecolmodel.2010.09.001

Ademe, F., Kibret, K., Beyene, S., Mitike, G., Getinet, M., 2020. Rainfall analysis for rain-fed farming in the great rift valley basins of Ethiopia. J. Water Clim. Chang. 11, 812–828. https://doi.org/10.2166/wcc.2019.242

Adimassu, Z., Alemu, G., Tamene, L., 2019. Effects of tillage and crop residue management on runoff, soil loss and crop yield in the Humid Highlands of Ethiopia. Agric. Syst. 168, 11–18. https://doi.org/10.1016/j.agsy.2018.10.007

Adimassu, Zenebe, Kessler, A., Stroosnijder, L., 2014. Farmers ' strategies to perceived trends of rainfall and crop productivity in the Central Rift Valley of Ethiopia. Environ. Dev. 11, 123–140. https://doi.org/10.1016/j.envdev.2014.04.004

Adimassu, Z., Mekonnen, K., Yirga, C., Kessler, A., 2014. Effect of soil bunds on runoff, soil and nutrient losses, and crop yield in the central highlands of ethiopia. L. Degrad. Dev. 25, 554–564. https://doi.org/10.1002/ldr.2182

Admasu, R., Tadesse, M., Shimbir, T., 2017. Effect of Growth Stage Moisture Stress on Maize (Zea Mays L .) Yield and Water Use Efficiency at West Wellaga , Ethiopia. J. Biol. Agric. Healthc. 7, 98–103.

Agutu, N.O., Awange, J.L., Ndehedehe, C., Mwaniki, M., 2020. Consistency of agricultural drought characterization over Upper Greater Horn of Africa (1982–2013): Topographical, gauge density, and model forcing influence. Sci. Total Environ. 709, 135149. https://doi.org/10.1016/j.scitotenv.2019.135149

Ahmadalipour, A., Moradkhani, H., Castelletti, A., Magliocca, N., 2019. Future drought risk in Africa: Integrating vulnerability, climate change, and population growth. Sci. Total Environ. 662, 672–686. https://doi.org/10.1016/j.scitotenv.2019.01.278

Ahmed, J.S., Buizza, R., Dell'Acqua, M., Demissie, T., Pè, M.E., 2024. Evaluation of ERA5 and CHIRPS rainfall estimates against observations across Ethiopia. Meteorol. Atmos. Phys. 136. https://doi.org/10.1007/s00703-024-01008-0

Akpoti, K., Groen, T., Dossou-Yovo, E., Kabo-bah, A.T., Zwart, S.J., 2022. Climate change-induced reduction in agricultural land suitability of West-Africa's inland valley landscapes. Agric. Syst. 200, 103429. https://doi.org/10.1016/j.agsy.2022.103429

Akpoti, K., Kabo-bah, A.T., Zwart, S.J., Rice, A., Ivoire, C., 2019. Agricultural land suitability analysis : State-of-the-art and outlooks for integration of climate change analysis. Agric. Syst. 173, 172–208. https://doi.org/10.1016/j.agsy.2019.02.013

Alasow, A.A., Hamed, M.M., Shahid, S., 2023. Spatiotemporal variability of drought and affected croplands in the horn of Africa. Stoch. Environ. Res. Risk Assess. 1. https://doi.org/10.1007/s00477-023-02575-1

Alemayehu, A.A., Getu, L.A., Samual, T., Ayalew, B., Addis, H.K., Feyisa, T., Worku, T., Tahir, M., Getu, E., 2023. Effects of tillage practices and planting techniques on crop yield and soil properties in northwestern lowlands of Ethiopia. J. Agric. Food Res. 14, 100852. https://doi.org/10.1016/j.jafr.2023.100852

Alemayehu, N., Masafu, M., Ebro, A., Tegegne, A., Gebru, G., 2020. Climate Change and Variability in the Mixed Crop/Livestock Production Systems of Central Ethiopian Highland, in: W. Leal Filho (Ed.), Handbook OfClimate Change Resilience. Springer Nature, pp. 1169–1192. https://doi.org/10.1007/978-3-319-93336-8_120

Alemu, W.G., Neigh, C.S.R., 2022. Desert Locust Cropland Damage Differentiated from Drought, with Multi-Source Remote Sensing in Ethiopia. Remote Sens. 14. https://doi.org/10.3390/rs14071723

Alhamshry, A., Fenta, A.A., Yasuda, H., Kimura, R., Shimizu, K., 2020. Seasonal rainfall variability in Ethiopia and its long-term link to global sea surface temperatures. Water (Switzerland) 12, 1–19. https://doi.org/10.3390/w12010055

Alhamshry, A., Fenta, A.A., Yasuda, H., Shimizu, K., Kawai, T., 2019. Prediction of summer rainfall over the source region of the Blue Nile by using teleconnections based on sea surface temperatures. Theor. Appl. Climatol. 137, 3077–3087. https://doi.org/10.1007/s00704-019-02796-x

Ali, A., Erkossa, T., Gudeta, K., Abera, W., Mesfin, E., Mekete, T., Haile, M., Haile, W., Abegaz, A., Tafesse, D., Belay, G., Getahun, M., Beyene, S., Assen, M., Regassa, A.,

Selassie, Y.G., Schulz, S., Tamene, L., Elias, E., Tadesse, S., Abebe, D., Wolde, Y., Hussien, N., Yirdaw, A., Mera, A., Gebremariam, S., Aregaw, Y., Abebaw, B., Bekele, D., Zewdie, E., Admas, T., Wakoya, F., Legesse, A., Tessema, N., Abebe, A., 2024. Reference soil groups map of Ethiopia based on legacy data and machine learning-technique: EthioSoilGrids 1.0. Soil 10, 189–209. https://doi.org/10.5194/soil-10-189-2024

Ali, A., Erkossa, T., Gudeta, K., Abera, W., Mesfin, E., Mekete, T., Haile, M., Haile, W., Abegaz, A., Tafesse, D., Belay, G., Getahun, M., Beyene, S., Assen, M., Regassa, A., Selassis, Y.G., Tadesse, S., Adebe, D., Walde, Y., Hussien, N., Yirdaw, A., Mera, A., Admas, T., Wakoya, F., Legesse, A., Tessema, N., Ababa, A., Gebremariam, S., Aregaw, Y., Abebaw, B., Bekele, D., Zewdie, E., Schulz, S., Temane, L., Eyasu, E., 2022. Reference Soil Groups Map of Ethiopia Based on Legacy Data and Machine Learning Technique : EthioSoilGrids 1 . 0. EGUsphere 1–40. https://doi.org/10.5194/egusphere-2022-301

Allen, R.G., Pereira, L.S., Raes, D., Smith, M., 1998. Crop Evapotranspiration, Irrigation and Drainage Paper No. 56. Rome.

Altchenko, Y., Villholth, K.G., 2015. Mapping irrigation potential from renewable groundwater in Africa-A quantitative hydrological approach. Hydrol. Earth Syst. Sci. 19, 1055–1067. https://doi.org/10.5194/hess-19-1055-2015

Amare, T., Zegeye, A.D., Yitaferu, B., Steenhuis, T.S., Hurni, H., Zeleke, G., 2014. Combined effect of soil bund with biological soil and water conservation measures in the northwestern Ethiopian highlands. Ecohydrol. Hydrobiol. 14, 192–199. https://doi.org/10.1016/j.ecohyd.2014.07.002

Amede, T., Auricht, C., Boffa, J., Dixon, J., Mallawaarachchi, T., Rukuni, M., Teklewold-deneke, T., 2017. A Farming System Framework for Investment Planning and Priority Setting in Ethiopia. Canberra, Australia.

Anandhi, A., Frei, A., Pierson, D.C., Schneiderman, E.M., Zion, M.S., Lounsbury, D., Matonse, A.H., 2011. Examination of change factor methodologies for climate change impact assessment 47, 1–10. https://doi.org/10.1029/2010WR009104

Anderson, R., Bayer, P.E., Edwards, D., 2020. Climate change and the need for agricultural adaptation, Current Opinion in Plant Biology. Elsevier Ltd. https://doi.org/10.1016/j.pbi.2019.12.006

Anderson, W., Taylor, C., McDermid, S., Ilboudo-Nébié, E., Seager, R., Schlenker, W., Cottier, F., de Sherbinin, A., Mendeloff, D., Markey, K., 2021. Violent conflict exacerbated drought-related food insecurity between 2009 and 2019 in sub-Saharan Africa. Nat. Food 2, 603–615. https://doi.org/10.1038/s43016-021-00327-4

Andrews, M.B., Ridley, J.K., Wood, R.A., Andrews, T., Blockley, E.W., Booth, B., Burke, E., Dittus, A.J., Florek, P., Gray, L.J., Haddad, S., Hardiman, S.C., Hermanson, L., Hodson, D., Hogan, E., Jones, G.S., Knight, J.R., Kuhlbrodt, T., Misios, S., Mizielinski, M.S., Ringer, M.A., Robson, J., Sutton, R.T., 2020. Historical Simulations With HadGEM3-GC3.1 for CMIP6. J. Adv. Model. Earth Syst. 12, 1–34.

https://doi.org/10.1029/2019MS001995

Antwi-Agyei, P., Dougill, A.J., Abaidoo, R.C., 2021. Opportunities and barriers for using climate information for building resilient agricultural systems in Sudan savannah agro-ecological zone of north-eastern Ghana. Clim. Serv. 22, 100226. https://doi.org/10.1016/j.cliser.2021.100226

Araya, A., Girma, A., Getachew, F., 2015. Exploring Impacts of Climate Change on Maize Yield in Two Contrasting Agro-Ecologies of Ethiopia. Asian J. Appl. Sci. Eng. 4, 2305–915.

Araya, A., Stroosnijder, L., 2011. Assessing drought risk and irrigation need in northern Ethiopia. Agric. For. Meteorol. 151, 425–436. https://doi.org/10.1016/j.agrformet.2010.11.014

Araya, A., Stroosnijder, L., Girmay, G., Keesstra, S.D., 2011. Crop coefficient, yield response to water stress and water productivity of teff (Eragrostis tef (Zucc.). Agric. Water Manag. 98, 775–783. https://doi.org/10.1016/j.agwat.2010.12.001

Asrat, P., Simane, B., 2018. Farmers' perception of climate change and adaptation strategies in the Dabus watershed, North-West Ethiopia. Ecol. Process. 7. https://doi.org/10.1186/s13717-018-0118-8

Ayanlade, A., Radeny, M., Morton, J.F., Muchaba, T., 2018. Rainfall variability and drought characteristics in two agro-climatic zones: An assessment of climate change challenges in Africa. Sci. Total Environ. 630, 728–737. https://doi.org/10.1016/j.scitotenv.2018.02.196

Bao, Y., Song, Z., Qiao, F., 2020. FIO-ESM Version 2.0: Model Description and Evaluation. J. Geophys. Res. Ocean. 125, 1–21. https://doi.org/10.1029/2019JC016036

Barron, J., Rockström, J., Gichuki, F., Hatibu, N., 2003. Dry spell analysis and maize yields for two semi-arid locations in east Africa. Agric. For. Meteorol. 117, 23–37. https://doi.org/10.1016/S0168-1923(03)00037-6

Basche, A.D., Archontoulis, S. V., Kaspar, T.C., Jaynes, D.B., Parkin, T.B., Miguez, F.E., 2016. Simulating long-term impacts of cover crops and climate change on crop production and environmental outcomes in the Midwestern United States. Agric. Ecosyst. Environ. 218, 95–106. https://doi.org/10.1016/j.agee.2015.11.011

Batjes, N.H., Ribeiro, E., Van Oostrum, A., 2020. Standardised soil profile data to support global mapping and modelling (WoSIS snapshot 2019). Earth Syst. Sci. Data 12, 299–320. https://doi.org/10.5194/essd-12-299-2020

Bayissa, Y., Tadesse, T., Demisse, G., Shiferaw, A., 2017. Evaluation of satellite-based rainfall estimates and application to monitor meteorological drought for the Upper Blue Nile Basin, Ethiopia. Remote Sens. 9, 1–17. https://doi.org/10.3390/rs9070669

Beck, H.E., Wood, E.F., Pan, M., Fisher, C.K., Miralles, D.G., Van Dijk, A.I.J.M., McVicar, T.R., Adler, R.F., 2019. MSWep v2 Global 3-hourly 0.1° precipitation: Methodology and

quantitative assessment. Bull. Am. Meteorol. Soc. 100, 473–500. https://doi.org/10.1175/BAMS-D-17-0138.1

Bekele, A., Lakew, Y., 2014. Projecting Ethiopian demographics from 2012–2050 using the spectrum suite of models, Policy brief. Addis Ababa, Ethiopia.

Bello, W., 2012. Greener Journal of Agricultural Sciences Influence of Gypsum application on Wheat (Triticum aestivum) yield and Components on Saline and Alkaline Soils of Tigray region, Ethiopia 2, 316–322. https://doi.org/10.15580/GJAS.2012.7.100912100

Benin, S., Wood, S., Nin-Pratt, A., 2016. In Agricultural productivity in Africa: Trends, patterns, and determinants, International Food Policy Research Institute.

Berg, M. de, Cheong, O., Kreveld, M. van, Overmars, M., 2008. Computational Geometry: Algorithms and Applications, Third. ed. Springer.

Berhane, F., Zaitchik, B., 2014. Modulation of daily precipitation over East Africa by the Madden-Julian oscillation. J. Clim. 27, 6016–6034. https://doi.org/10.1175/JCLI-D-13-00693.1

Bezabih, A., Accotto, C., Abate, E., Gebrehawaryat, Y., Fadda, C., Enrico, M., Dell, M., 2020. Agriculture , Ecosystems and Environment Current and projected eco-geographic adaptation and phenotypic diversity of Ethiopian te ff (Eragrostis te ff) across its cultivation range. Agric. Ecosyst. Environ. 300, 107020. https://doi.org/10.1016/j.agee.2020.107020

Bhatt, A., Abbassi, B., 2023. Life Cycle & Sustainability Relative sensitivity value (RSV): A metric for measuring input parameter in fl uence in life cycle assessment modeling 19, 547–555. https://doi.org/10.1002/ieam.4701

Bi, D., Dix, M., Marsland, S., O'farrell, S., Sullivan, A., Bodman, R., Law, R., Harman, I., Srbinovsky, J., Rashid, H.A., Dobrohotoff, P., Mackallah, C., Yan, H., Hirst, A., Savita, A., Dias, F.B., Woodhouse, M., Fiedler, R., Heerdegen, A., 2020. Configuration and spin-up of ACCESS-CM2, the new generation Australian Community Climate and Earth System Simulator Coupled Model. J. South. Hemisph. Earth Syst. Sci. 70, 225–251. https://doi.org/10.1071/ES19040

Blaser, W.J., Oppong, J., Hart, S.P., Landolt, J., Yeboah, E., Six, J., 2018. Climate-smart sustainable agriculture in low-to-intermediate shade agroforests. Nat. Sustain. 1, 234–239. https://doi.org/10.1038/s41893-018-0062-8

Bonetti, S., Wei, Z., Or, D., 2021. A framework for quantifying hydrologic effects of soil structure across scales. Commun. Earth Environ. 2. https://doi.org/10.1038/s43247-021-00180-0

Borchert, R., 1998. Responses of tropical trees to rainfall seasonality and its long-term changes, in: Potential Impacts of Climate Change on Tropical Forest Ecosystems. Springer, pp. 381–393.

Borgomeo, E., Khan, H.F., Heino, M., Zaveri, E., Kummu, M., Brown, C., Jägerskog, A., 2020.

Impact of green water anomalies on global rainfed crop yields. Environ. Res. Lett. 15. https://doi.org/10.1088/1748-9326/abc587

Boucher, O., Servonnat, J., Albright, A.L., Aumont, O., Balkanski, Y., Bastrikov, V., Bekki, S., Bonnet, R., Bony, S., Bopp, L., Braconnot, P., Brockmann, P., Cadule, P., Caubel, A., Cheruy, F., Codron, F., Cozic, A., Cugnet, D., D'Andrea, F., Davini, P., de Lavergne, C., Denvil, S., Deshayes, J., Devilliers, M., Ducharne, A., Dufresne, J.L., Dupont, E., Éthé, C., Fairhead, L., Falletti, L., Flavoni, S., Foujols, M.A., Gardoll, S., Gastineau, G., Ghattas, J., Grandpeix, J.Y., Guenet, B., Guez, L.E., Guilyardi, E., Guimberteau, M., Hauglustaine, D., Hourdin, F., Idelkadi, A., Joussaume, S., Kageyama, M., Khodri, M., Krinner, G., Lebas, N., Levavasseur, G., Lévy, C., Li, L., Lott, F., Lurton, T., Luyssaert, S., Madec, G., Madeleine, J.B., Maignan, F., Marchand, M., Marti, O., Mellul, L., Meurdesoif, Y., Mignot, J., Musat, I., Ottlé, C., Peylin, P., Planton, Y., Polcher, J., Rio, C., Rochetin, N., Rousset, C., Sepulchre, P., Sima, A., Swingedouw, D., Thiéblemont, R., Traore, A.K., Vancoppenolle, M., Vial, J., Vialard, J., Viovy, N., Vuichard, N., 2020. Presentation and Evaluation of the IPSL-CM6A-LR Climate Model. J. Adv. Model. Earth Syst. 12, 1–52. https://doi.org/10.1029/2019MS002010

Broman, D., Rajagopalan, B., Hopson, T., Gebremichael, M., 2020. Spatial and temporal variability of East African Kiremt season precipitation and large-scale teleconnections. Int. J. Climatol. 40, 1241–1254. https://doi.org/10.1002/joc.6268

Brusca, R.C., Wiens, J.F., Meyer, W.M., Eble, J., Franklin, K., Overpeck, J.T., Moore, W., 2013. Dramatic response to climate change in the Southwest: Robert Whittaker's 1963 Arizona Mountain plant transect revisited. Ecol. Evol. 3, 3307–3319. https://doi.org/10.1002/ece3.720

Buchhorn, M., Smets, B., Bertels, L., De Roo, B., Lesiv, M., Tsendbazar, Nandin-Erdene Tarko, A., 2020. Copernicus Global Land Operations "Vegetation and Energy" "CGLOPS-1." Copernicus Glob. L. Oper. 1–93. https://doi.org/10.5281/zenodo.3938963.PU

Budyko, M.I., 1958. The Heat Balance of the Earth's Surface.

Burke, M.B., Lobell, D.B., Guarino, L., 2009. Shifts in African crop climates by 2050, and the implications for crop improvement and genetic resources conservation. Glob. Environ. Chang. 19, 317–325. https://doi.org/10.1016/j.gloenvcha.2009.04.003

Burrough, P.A., Macmillan, R.A., van Deursen, W., 1992. Fuzzy classification methods for determining land suitability from soil profile observations and topography 193–210.

Byerlee, D., Spielman, D.J., Alemu, D., Gautam, M., 2007. Policies to Promote Cereal Intensification in Ethiopia: A Review of Evidence and Experience, IFPRI Discussion Paper.

Camberlin, P., 1997. Rainfall anomalies in the source region of the Nile and their connection with the Indian summer monsoon. J. Clim. 10, 1380–1392. https://doi.org/10.1175/1520-0442(1997)010<1380:RAITSR>2.0.CO;2

Cao, J., Wang, B., Yang, Y.M., Ma, L., Li, J., Sun, B., Bao, Y., He, J., Zhou, X., Wu, L., 2018.

The NUIST Earth System Model (NESM) version 3: Description and preliminary evaluation. Geosci. Model Dev. 11, 2975–2993. https://doi.org/10.5194/gmd-11-2975-2018

Carrão, H., Naumann, G., Barbosa, P., 2016. Mapping global patterns of drought risk: An empirical framework based on sub-national estimates of hazard, exposure and vulnerability. Glob. Environ. Chang. 39, 108–124. https://doi.org/10.1016/j.gloenvcha.2016.04.012

Castañeda, A., Doan, D., Newhouse, D., Nguyen, M.C., Uematsu, H., Azevedo, J.P., 2016. Poverty and Shared Prosperity Report 2016: Taking on Inequality Background Paper, Policy Research Working Paper 7844.

Castro-Llanos, F., Hyman, G., Rubiano, J., Ramirez-Villegas, J., Achicanoy, H., 2019. Climate change favors rice production at higher elevations in Colombia. Mitig. Adapt. Strateg. Glob. Chang. 24, 1401–1430. https://doi.org/10.1007/s11027-019-09852-x

Chaney, N.W., Sheffield, J., Villarini, G., Wood, E.F., 2014. Development of a high-resolution gridded daily meteorological dataset over sub-Saharan Africa: Spatial analysis of trends in climate extremes. J. Clim. 27, 5815–5835. https://doi.org/10.1175/JCLI-D-13-00423.1

Chemura, A., Gleixner, S., Gornott, C., 2024. Dataset of the suitability of major food crops in Africa under climate change. Sci. data 11, 294. https://doi.org/10.1038/s41597-024-03118-1

Cherchi, A., Fogli, P.G., Lovato, T., Peano, D., Iovino, D., Gualdi, S., Masina, S., Scoccimarro, E., Materia, S., Bellucci, A., Navarra, A., 2019. Global Mean Climate and Main Patterns of Variability in the CMCC-CM2 Coupled Model. J. Adv. Model. Earth Syst. 11, 185–209. https://doi.org/10.1029/2018MS001369

Chere, Z., Abegaz, A., Tamene, L., Abera, W., 2022. Modeling and mapping the spatiotemporal variation in agricultural drought based on a satellite-derived vegetation health index across the highlands of Ethiopia. Model. Earth Syst. Environ. 8, 4539–4552. https://doi.org/10.1007/s40808-022-01439-x

Cheung, W.H., Senay, G.B., Singh, A., 2008. Trends and spatial distribution of annual and seasonal rainfall in Ethiopia. Int. J. Climatol. 28, 1723–1734. https://doi.org/10.1002/joc

Chiarelli, D.D., Passera, C., Rosa, L., Davis, K.F., D'Odorico, P., Rulli, M.C., 2020. The green and blue crop water requirement WATNEEDS model and its global gridded outputs. Sci. Data 7, 1–9. https://doi.org/10.1038/s41597-020-00612-0

Chinasho, A., Bedadi, B., Lemma, T., Tana, T., Hordofa, T., Elias, B., 2023. Response of maize to irrigation and blended fertilizer levels for climate smart food production in Wolaita Zone, southern Ethiopia. J. Agric. Food Res. 12, 100551. https://doi.org/10.1016/j.jafr.2023.100551

Chiputwa, B., Blundo-Canto, G., Steward, P., Andrieu, N., Ndiaye, O., 2022. Co-production, uptake of weather and climate services, and welfare impacts on farmers in Senegal: A panel data approach. Agric. Syst. 195, 103309.

https://doi.org/10.1016/j.agsy.2021.103309

Christian, J.R., Denman, K.L., Hayashida, H., Holdsworth, A.M., Lee, W.G., Riche, O.G.J., Shao, A.E., Steiner, N., Swart, N.C., 2022. Ocean biogeochemistry in the Canadian Earth System Model version 5.0.3: CanESM5 and CanESM5-CanOE. Geosci. Model Dev. 15, 4393–4424. https://doi.org/10.5194/gmd-15-4393-2022

Cleveland, W.S., 1979. Robust locally weighted regression and smoothing scatterplots. J. Am. Stat. Assoc. 74, 829–836. https://doi.org/10.1080/01621459.1979.10481038

Collins, J.M., 2011. Temperature variability over Africa. J. Clim. 24, 3649–3666. https://doi.org/10.1175/2011JCLI3753.1

Conway, D., Schipper, E.L.F., 2011. Adaptation to climate change in Africa : Challenges and opportunities identified from Ethiopia. Glob. Environ. Chang. 21, 227–237. https://doi.org/10.1016/j.gloenvcha.2010.07.013

Conway, D., Vincent, K., 2021. Conversations About Climate Risk, Adaptation and Resilience in Africa, Climate Risk in Africa. https://doi.org/10.1007/978-3-030-61160-6_9

Cooper, P.J.M., Dimes, J., Rao, K.P.C., Shapiro, B., Shiferaw, B., Twomlow, S., 2008. Coping better with current climatic variability in the rain-fed farming systems of sub-Saharan Africa: An essential first step in adapting to future climate change? Agric. Ecosyst. Environ. 126, 24–35. https://doi.org/10.1016/j.agee.2008.01.007

Cover, T.M., Thomas, J.A., 2005. Elements of Information Theory, Elements of Information Theory. https://doi.org/10.1002/047174882X

CSA, 2023. Population size by region, zone and woreda: July 2023.

CSA, 2016. Agricultural Sample Survery 2015/16 (2008 E.C): Report on Area, Production and Farm Management Practice of Belg Season Crops for Private Peasant Holdings, Statistical Bulletin.

CSA, 2010. Agricultural sample survey (2010/2011): Report on area and production of crops, Central Statistical Agency. Addis Ababa, Ethiopia.

CSA, 2007. Summary and statistical report of the 2007 population and housing census. Addis Ababa.

Danabasoglu, G., Lamarque, J.F., Bacmeister, J., Bailey, D.A., DuVivier, A.K., Edwards, J., Emmons, L.K., Fasullo, J., Garcia, R., Gettelman, A., Hannay, C., Holland, M.M., Large, W.G., Lauritzen, P.H., Lawrence, D.M., Lenaerts, J.T.M., Lindsay, K., Lipscomb, W.H., Mills, M.J., Neale, R., Oleson, K.W., Otto-Bliesner, B., Phillips, A.S., Sacks, W., Tilmes, S., van Kampenhout, L., Vertenstein, M., Bertini, A., Dennis, J., Deser, C., Fischer, C., Fox-Kemper, B., Kay, J.E., Kinnison, D., Kushner, P.J., Larson, V.E., Long, M.C., Mickelson, S., Moore, J.K., Nienhouse, E., Polvani, L., Rasch, P.J., Strand, W.G., 2020. The Community Earth System Model Version 2 (CESM2). J. Adv. Model. Earth Syst. 12, 1–35. https://doi.org/10.1029/2019MS001916

David A., R., J., S., Ravi S., N., Parthasarrathi, M., 2019. Current Trends in the Representation of Physical Processes in Weather and Climate Models, Current Trends in the Representation of Physical Processes in Weather and Climate Models.

De Souza, K., Kituyi, E., Harvey, B., Leone, M., Murali, K.S., Ford, J.D., 2015. Vulnerability to climate change in three hot spots in Africa and Asia: key issues for policy-relevant adaptation and resilience-building research. Reg. Environ. Chang. 15, 747–753. https://doi.org/10.1007/s10113-015-0755-8

Degefu, M.A., Bewket, W., 2023. Drought monitoring performance of global precipitation products in three wet seasons in Ethiopia: Part I—Quasi-objective examination. Meteorol. Appl. 30, 1–28. https://doi.org/10.1002/met.2143

Degefu, M.A., Bewket, W., Amha, Y., 2022. Evaluating performance of 20 global and quasi-global precipitation products in representing drought events in Ethiopia I: Visual and correlation analysis. Weather Clim. Extrem. 35, 100416. https://doi.org/10.1016/j.wace.2022.100416

Degefu, M.A., Rowell, D.P., Bewket, W., 2017. Teleconnections between Ethiopian rainfall variability and global SSTs: observations and methods for model evaluation. Meteorol. Atmos. Phys. 129, 173–186. https://doi.org/10.1007/s00703-016-0466-9

Degife, A.W., Zabel, F., Mauser, W., 2021. Climate change impacts on potential maize yields in Gambella Region, Ethiopia. Reg. Environ. Chang. 21. https://doi.org/10.1007/s10113-021-01773-3

Delelegn, Y.T., Purahong, W., Sandén, H., Yitaferu, B., Godbold, D.L., 2018. Transition of Ethiopian highland forests to agriculture - dominated landscapes shifts the soil microbial community composition. BMC Ecol. 1–14. https://doi.org/10.1186/s12898-018-0214-8

Dembele, M., Schaefli, B., Van De Giesen, N., 2020. Suitability of 17 gridded rainfall and temperature datasets for large-scale hydrological modelling in West Africa. Hydrol. Earth Syst. Sci. 24, 5379–5406. https://doi.org/10.5194/hess-24-5379-2020

Dendir, Z., Simane, B., 2021. Farmers ' perceptions about changes in climate variables : Perceived risks and household responses in different agro-ecological communities ,. Clim. Serv. 22, 100236. https://doi.org/10.1016/j.cliser.2021.100236

Descheemaeker, K., 2020. Limits of conservation agriculture in Africa. Nat. Food. https://doi.org/10.1038/s43016-020-0119-5

Deser, C., Phillips, A., Bourdette, V., Teng, H., 2012. Uncertainty in climate change projections: The role of internal variability. Clim. Dyn. 38, 527–546. https://doi.org/10.1007/s00382-010-0977-x

Desta, G., Kassawmar, T., Tadesse, M., Zeleke, G., 2021. Extent and distribution of surface soil acidity in the rainfed areas of Ethiopia 5348–5359. https://doi.org/10.1002/ldr.4113

Destaw, F., Mekuyie, M., 2022. Farmers ' Perception on Climate Variability and its Effects in Ambassel District , Northern Ethiopia. Agric. Res. 11, 539–548.

https://doi.org/10.1007/s40003-021-00573-9

Dijk, M. Van, Morley, T., Jongeneel, R., Ittersum, M. Van, Reidsma, P., Ruben, R., 2017. Disentangling agronomic and economic yield gaps : An integrated framework and application. Agric. Syst. 154, 90–99. https://doi.org/10.1016/j.agsy.2017.03.004

Dinku, T., Block, P., Sharoff, J., Hailemariam, K., Osgood, D., del Corral, J., Cousin, R., Thomson, M.C., 2014. Bridging critical gaps in climate services and applications in africa. Earth Perspect. 1, 15. https://doi.org/10.1186/2194-6434-1-15

Dinku, T., Chidzambwa, S., Ceccato, P., Connor, S.J., Ropelewski, C.F., 2008. Validation of high-resolution satellite rainfall products over complex terrain. Int. J. Remote Sens. 29, 4097–4110. https://doi.org/10.1080/01431160701772526

Dinku, T., Faniriantsoa, R., Cousin, R., Khomyakov, I., Vadillo, A., Hansen, J.W., Grossi, A., 2022. ENACTS: Advancing Climate Services Across Africa. Front. Clim. 3. https://doi.org/10.3389/fclim.2021.787683

Dinku, T., Funk, C., Peterson, P., Maidment, R., Tadesse, T., Gadain, H., Ceccato, P., 2018a. Validation of the CHIRPS satellite rainfall estimates over eastern Africa. Q. J. R. Meteorol. Soc. 144, 292–312. https://doi.org/10.1002/qj.3244

Dinku, T., Thomson, M.C., Cousin, R., del Corral, J., Ceccato, P., Hansen, J., Connor, S.J., 2018b. Enhancing National Climate Services (ENACTS) for development in Africa. Clim. Dev. 10, 664–672. https://doi.org/10.1080/17565529.2017.1405784

Diro, G.T., Grimes, D.I.F., Black, E., 2011a. Teleconnections between Ethiopian summer rainfall and sea surface temperature: Part II. Seasonal forecasting. Clim. Dyn. 37, 121–131. https://doi.org/10.1007/s00382-010-0896-x

Diro, G.T., Grimes, D.I.F., Black, E., 2011b. Teleconnections between Ethiopian summer rainfall and sea surface temperature: Part I-observation and modelling. Clim. Dyn. 37, 103–119. https://doi.org/10.1007/s00382-010-0837-8

Dodd, D.E.S., Jolliffe, I.T., 2001. Early detection of the start of the wet season in semiarid tropical climates of Western Africa. Int. J. Climatol. 21, 1251–1262. https://doi.org/10.1002/joc.640

Donat, M.G., Alexander, L. V., Yang, H., Durre, I., Vose, R., Dunn, R.J.H., Willett, K.M., Aguilar, E., Brunet, M., Caesar, J., Hewitson, B., Jack, C., Klein Tank, A.M.G., Kruger, A.C., Marengo, J., Peterson, T.C., Renom, M., Oria Rojas, C., Rusticucci, M., Salinger, J., Elrayah, A.S., Sekele, S.S., Srivastava, A.K., Trewin, B., Villarroel, C., Vincent, L.A., Zhai, P., Zhang, X., Kitching, S., 2013. Updated analyses of temperature and precipitation extreme indices since the beginning of the twentieth century: The HadEX2 dataset. J. Geophys. Res. Atmos. 118, 2098–2118. https://doi.org/10.1002/jgrd.50150

Doorenbos, J., Kassam, A.H., 1979. Paper 33. Yield Response to water, FAO Irrigation and Drainage Paper.

Döscher, R., Acosta, M., Alessandri, A., Anthoni, P., Arsouze, T., Bergman, T., Bernardello,

R., Boussetta, S., Caron, L.P., Carver, G., Castrillo, M., Catalano, F., Cvijanovic, I., Davini, P., Dekker, E., Doblas-Reyes, F.J., Docquier, D., Echevarria, P., Fladrich, U., Fuentes-Franco, R., Gröger, M., Hardenberg, J. V., Hieronymus, J., Karami, M.P., Keskinen, J.P., Koenigk, T., Makkonen, R., Massonnet, F., Ménégoz, M., Miller, P.A., Moreno-Chamarro, E., Nieradzik, L., Van Noije, T., Nolan, P., O'donnell, D., Ollinaho, P., Van Den Oord, G., Ortega, P., Prims, O.T., Ramos, A., Reerink, T., Rousset, C., Ruprich-Robert, Y., Le Sager, P., Schmith, T., Schrödner, R., Serva, F., Sicardi, V., Sloth Madsen, M., Smith, B., Tian, T., Tourigny, E., Uotila, P., Vancoppenolle, M., Wang, S., Wårlind, D., Willén, U., Wyser, K., Yang, S., Yepes-Arbós, X., Zhang, Q., 2022. The EC-Earth3 Earth system model for the Coupled Model Intercomparison Project 6. Geosci. Model Dev. 15, 2973–3020. https://doi.org/10.5194/gmd-15-2973-2022

Dubache, G., Ogwang, B.A., Ongoma, V., Towfiqul Islam, A.R.M., 2019. The effect of Indian Ocean on Ethiopian seasonal rainfall. Meteorol. Atmos. Phys. 131, 1753–1761. https://doi.org/10.1007/s00703-019-00667-8

Dubois, N., Oppo, D.W., Galy, V. V., Mohtadi, M., Van Der Kaars, S., Tierney, J.E., Rosenthal, Y., Eglinton, T.I., Lückge, A., Linsley, B.K., 2014. Indonesian vegetation response to changes in rainfall seasonality over the past 25,000 years. Nat. Geosci. 7, 513–517. https://doi.org/10.1038/ngeo2182

Dunne, J.P., Horowitz, L.W., Adcroft, A.J., Ginoux, P., Held, I.M., John, J.G., Krasting, J.P., Malyshev, S., Naik, V., Paulot, F., Shevliakova, E., Stock, C.A., Zadeh, N., Balaji, V., Blanton, C., Dunne, K.A., Dupuis, C., Durachta, J., Dussin, R., Gauthier, P.P.G., Griffies, S.M., Guo, H., Hallberg, R.W., Harrison, M., He, J., Hurlin, W., McHugh, C., Menzel, R., Milly, P.C.D., Nikonov, S., Paynter, D.J., Ploshay, J., Radhakrishnan, A., Rand, K., Reichl, B.G., Robinson, T., Schwarzkopf, D.M., Sentman, L.T., Underwood, S., Vahlenkamp, H., Winton, M., Wittenberg, A.T., Wyman, B., Zeng, Y., Zhao, M., 2020. The GFDL Earth System Model Version 4.1 (GFDL-ESM 4.1): Overall Coupled Model Description and Simulation Characteristics. J. Adv. Model. Earth Syst. 12, 1–56. https://doi.org/10.1029/2019MS002015

Dunning, C.M., Black, E., Allan, R.P., 2018. Later wet seasons with more intense rainfall over Africa under future climate change. J. Clim. 31, 9719–9738. https://doi.org/10.1175/JCLI-D-18-0102.1

Dunning, C.M., Black, E.C.L., Allan, R.P., 2016. The onset and cessation of seasonal rainfall over Africa. J. Geophys. Res. 121, 11405–11424. https://doi.org/10.1002/2016JD025428

Durre, I., Menne, M.J., Gleason, B.E., Houston, T.G., Vose, R.S., 2010. Comprehensive automated quality assurance of daily surface observations. J. Appl. Meteorol. Climatol. 49, 1615–1633. https://doi.org/10.1175/2010JAMC2375.1

Ebabu, K., Taye, G., Tsunekawa, A., Haregeweyn, N., Adgo, E., Tsubo, M., Fenta, A.A., Meshesha, D.T., Sultan, D., Aklog, D., Admasu, T., van Wesemael, B., Poesen, J., 2023. Land use, management and climate effects on runoff and soil loss responses in the highlands of Ethiopia. J. Environ. Manage. 326, 116707. https://doi.org/10.1016/j.jenvman.2022.116707

Ehsan, M.A., Tippett, M.K., Robertson, A.W., Almazroui, M., Ismail, M., Dinku, T., Acharya,

N., Siebert, A., Ahmed, J.S., Teshome, A., 2021. Seasonal predictability of Ethiopian Kiremt rainfall and forecast skill of ECMWF's SEAS5 model. Clim. Dyn. 57, 3075–3091. https://doi.org/10.1007/s00382-021-05855-0

Erkossa, T., Stahr, K., Gaiser, T., 2006. Effect of different methods of land preparation on runoff, soil and nutrient losses from a Vertisol in the Ethiopian highlands. Soil Use Manag. 21, 253–259. https://doi.org/10.1111/j.1475-2743.2005.tb00132.x

Eshete, G., Assefa, B., Lemma, E., Kibret, G., Ambaw, G., Samuel, S., Seid, J., Tesfaye, K., Tamene, L., Haile, A., Asnake, A., Mengiste, A., Hailemariam, S., Ericksen, P., Mekonnen, K., Amede, T., Hailesilassie, A., Hadgu, K., Woldemeskel, E., Solomon, D., 2020. Ethiopia climate-smart agriculture roadmap 2020 to 2030. Ministry of Agriculture, Addis Ababa, Ethiopia.

Evangelista, P., Young, N., Burnett, J., 2013. How will climate change spatially affect agriculture production in Ethiopia? Case studies of important cereal crops. Clim. Change 119, 855–873. https://doi.org/10.1007/s10584-013-0776-6

Eweg, H.P.A., Van Lammeren, R., Deurloo, H., Woldu, Z., 1998. Analysing degradation and rehabilitation for sustainable land management in the highlands of Ethiopia. L. Degrad. Dev. 9, 529–542. https://doi.org/10.1002/(SICI)1099-145X(199811/12)9:6<529::AID-LDR313>3.0.CO;2-O

Eyshi Rezaei, E., Webber, H., Gaiser, T., Naab, J., Ewert, F., 2015. Heat stress in cereals: Mechanisms and modelling. Eur. J. Agron. 64, 98–113. https://doi.org/10.1016/j.eja.2014.10.003

Eze, E., Girma, A., Zenebe, A., Okolo, C.C., Kourouma, J.M., Negash, E., 2022. Predictors of drought-induced crop yield/losses in two agroecologies of southern Tigray, Northern Ethiopia. Sci. Rep. 12, 1–14. https://doi.org/10.1038/s41598-022-09862-x

Falkenmark, M., 2013. Growing water scarcity in agriculture: Future challenge to global water security. Philos. Trans. R. Soc. A Math. Phys. Eng. Sci. 371. https://doi.org/10.1098/rsta.2012.0410

Falkenmark, M., 2006. The New Blue and Green Water Paradigm : Breaking New Ground for Water Resources Planning and Management 132, 129–132. https://doi.org/10.1061/(ASCE)0733-9496(2006)132

Falkenmark, M., Rockström, J., 2004. Balancing water for humans and nature: The new approach in ecoydrology.

Fan, J., McConkey, B., Wang, H., Janzen, H., 2016. Root distribution by depth for temperate agricultural crops. F. Crop. Res. 189, 68–74. https://doi.org/10.1016/j.fcr.2016.02.013

FAO, 2023. The future of food and agriculture: Drivers and triggers for transformation. Rome.

FAO, 2022. Crops and climate change impact briefs. Climate-smart agriculture for more sustainable, resilient, and equitable food systems, Food and Agriculture Organization of the United Nations. Rome. https://doi.org/10.4060/cb8030en

FAO, 2018. Sustainable food systems: Concept and framework. Rome.

FAO, 2015a. FAO and the Sustainable Development Goals, FAO and the Sustainable Development Goals. https://doi.org/10.4060/cc2063en

FAO, 2015b. The economic lives of smallholder farmers, Food And Agriculture Organization of the United Nations. Rome.

FAO, 2008. Climate change, water and food security.

FAO, 1986. Irrigation Water Management: Irrigation Water Needs [WWW Document]. URL http://www.fao.org/3/S2022E/s2022e06.htm#2.1 major climatic zones (accessed 2.13.21).

FAO, 1976. Framework of land evaluation [WWW Document]. Food Agric. Organ. United Nations, Rome, Italy. URL https://www.fao.org/3/x5310e/x5310e00.htm

FAOSTAT, 2018. Land use indicators [WWW Document]. URL http://www.fao.org/faostat/en/#data/EL (accessed 10.21.20).

Fatichi, S., Ivanov, V.Y., Paschalis, A., Peleg, N., Molnar, P., Rimkus, S., Kim, J., Burlando, P., Caporali, E., 2016a. Uncertainty partition challenges the predictability of vital details of climate change. Earth's Futur. 4, 240–251. https://doi.org/10.1002/2015EF000336

Fatichi, S., Pappas, C., Ivanov, V.Y., 2016b. Modeling plant–water interactions: an ecohydrological overview from the cell to the global scale. Wiley Interdiscip. Rev. Water 3, 327–368. https://doi.org/10.1002/wat2.1125

Fatima, Z., Ahmed, M., Hussain, M., Abbas, G., Ul-Allah, S., Ahmad, S., Ahmed, N., Ali, M.A., Sarwar, G., Haque, E. ul, Iqbal, P., Hussain, S., 2020. The fingerprints of climate warming on cereal crops phenology and adaptation options. Sci. Rep. 10, 1–21. https://doi.org/10.1038/s41598-020-74740-3

Fawcett, T., 2006. An introduction to ROC analysis 27, 861–874. https://doi.org/10.1016/j.patrec.2005.10.010

FDRE, 2019. Ethiopia's Climate Resilient Green Economy: National Adaptation Plan. Addis Ababa, Ethiopia.

Feng, Q., Chaubey, I., Engel, B., Cibin, R., Sudheer, K.P., Volenec, J., 2017. Marginal land suitability for switchgrass, Miscanthus and hybrid poplar in the Upper Mississippi River Basin (UMRB). Environ. Model. Softw. 93, 356–365. https://doi.org/10.1016/j.envsoft.2017.03.027

Feng, X., Porporato, A., Rodriguez-Iturbe, I., 2013. Changes in rainfall seasonality in the tropics. Nat. Clim. Chang. 3. https://doi.org/10.1038/NCLIMATE1907

Fischer, G., Nachtergaele, F., Velthuizen, H. van, Chiozza, F., Franceschini, G., Hnery, M., Muchoney, D., Tramberend, S., 2021. Global agro-ecological zone V4 – Model documentation, Global agro-ecological zone V4 – Model documentation. https://doi.org/10.4060/cb4744en

Fleischer, K., Terrer, C., 2022. Estimates of soil nutrient limitation on the CO2 fertilization effect for tropical vegetation. Glob. Chang. Biol. 28, 6366–6369. https://doi.org/10.1111/gcb.16377

Foster, T., Brozović, N., 2018. Simulating Crop-Water Production Functions Using Crop Growth Models to Support Water Policy Assessments. Ecol. Econ. 152, 9–21. https://doi.org/10.1016/j.ecolecon.2018.05.019

Frei, C., 2014. Interpolation of temperature in a mountainous region using nonlinear profiles and non-Euclidean distances. Int. J. Climatol. 34, 1585–1605. https://doi.org/10.1002/joc.3786

Funk, C., Asfaw, A., Phil, S., Gabriel, S., Jim, R., 2003. Estimating Meher Crop Production Using Rainfall in the ' Long Cycle ' Statistical Estimates of Meher Yields Based on April-May Rainfall Totals. Addis Ababa.

Funk, C., Peterson, P., Landsfeld, M., Pedreros, D., Verdin, J., Shukla, S., Husak, G., Rowland, J., Harrison, L., Hoell, A., Michaelsen, J., 2015. The climate hazards infrared precipitation with stations - A new environmental record for monitoring extremes. Nat. Sci. Data 2. https://doi.org/10.1038/sdata.2015.66

Funk, C., Senay, G., Asfaw, A., Verdin, J., Rowland, J., Michaelson, J., Eilerts, G., Korecha, D., Choularton, R., 2005. Recent drought tendencies in Ethiopia and equatorial-subtropical eastern Africa. Famine Early Warning System Network. U.S. Agency Int. Dev. 11.

Furgassa, Z.S., 2017. Zelalem Shelemew Furgassa. The Effect of Deficit Irrigation on Maize Crop Under Conventional Furrow Irrigation in Adami Tulu Central Rift Valley of Ethiopia. Appl. Eng. 1, 1–12. https://doi.org/10.11648/j.ae.20170101.11

Gaetani, M., Janicot, S., Vrac, M., Famien, A.M., Sultan, B., 2020. Robust assessment of the time of emergence of precipitation change in West Africa. Sci. Rep. 10, 1–10. https://doi.org/10.1038/s41598-020-63782-2

Gago, J., Douthe, C., Florez-Sarasa, I., Escalona, J.M., Galmes, J., Fernie, A.R., Flexas, J., Medrano, H., 2014. Opportunities for improving leaf water use efficiency under climate change conditions. Plant Sci. 226, 108–119. https://doi.org/10.1016/j.plantsci.2014.04.007

Gebeyehu, M.G., 2016. The Impact of Technology Adoption on Agricultural Productivity and Production Risk in Ethiopia: Evidence from Rural Amhara Household Survey. OALib 03, 1–14. https://doi.org/10.4236/oalib.1102369

Gebrechorkos, S.H., Hülsmann, S., Bernhofer, C., 2020. Analysis of climate variability and droughts in East Africa using high-resolution climate data products. Glob. Planet. Change 186, 103130. https://doi.org/10.1016/j.gloplacha.2020.103130

Gebrechorkos, S.H., Hülsmann, S., Bernhofer, C., 2018. Evaluation of multiple climate data sources for managing environmental resources in East Africa. Hydrol. Earth Syst. Sci 22, 4547–4564. https://doi.org/10.5194/hess-22-4547-2018

Gebreigziabher, E.T., 2020. Effect of Deficit Irrigation on Yield and Water Use Efficiency of Maize at Selekleka District, Ethiopia. J. Nepal Agric. Res. Counc. 6, 127–135. https://doi.org/10.3126/jnarc.v6i0.28124

Gebremeskel Haile, G., Tang, Q., Leng, G., Jia, G., Wang, J., Cai, D., Sun, S., Baniya, B., Zhang, Q., 2020. Long-term spatiotemporal variation of drought patterns over the Greater Horn of Africa. Sci. Total Environ. 704, 135299. https://doi.org/10.1016/j.scitotenv.2019.135299

Gebremicael, T.G., Mohamed, Y.A., Zaag, P. van der, Gebremedhin, A., Gebremeskel, G., Yazew, E., Kifle, M., 2019. Evaluation of multiple satellite rainfall products over the rugged topography of the Tekeze-Atbara basin in Ethiopia. Int. J. Remote Sens. 40, 4326–4345. https://doi.org/10.1080/01431161.2018.1562585

Gebresamuel, G., Abrha, H., Hagos, H., Elias, E., Haile, M., 2022. Empirical modeling of the impact of climate change on altitudinal shift of major cereal crops in South Tigray, Northern Ethiopia. J. Crop Improv. 36, 169–192. https://doi.org/10.1080/15427528.2021.1931608

Getnet, M., Descheemaeker, K., van Ittersum, M.K., Hengsdijk, H., 2022. Narrowing crop yield gaps in Ethiopia under current and future climate: A model-based exploration of intensification options and their trade-offs with the water balance. F. Crop. Res. 278, 108442. https://doi.org/10.1016/j.fcr.2022.108442

GHI, 2022. Global hunger index: Ethiopia Policy Brief.

Gidey, E., Dikinya, O., Sebego, R., Segosebe, E., Zenebe, A., Mussa, S., Mhangara, P., Birhane, E., 2023. Land Use and Land Cover Change Determinants in Raya Valley , Tigray , Northern Ethiopian Highlands 1–15.

Giller, K.E., Hijbeek, R., Andersson, J.A., Sumberg, J., 2021. Regenerative Agriculture: An agronomic perspective. Outlook Agric. 50, 13–25. https://doi.org/10.1177/0030727021998063

Gissila, T., Black, E., Grimes, D.I.F., Slingo, J.M., 2004. Seasonal forecasting of the Ethiopian summer rains. Int. J. Climatol. 24, 1345–1358. https://doi.org/10.1002/joc.1078

Gleixner, S., Keenlyside, N., Viste, E., Korecha, D., 2017. The El Niño effect on Ethiopian summer rainfall. Clim. Dyn. 49, 1865–1883. https://doi.org/10.1007/s00382-016-3421-z

Glotter, M., Elliott, J., McInerney, D., Best, N., Foster, I., Moyer, E.J., 2014. Evaluating the utility of dynamical downscaling in agricultural impacts projections. Proc. Natl. Acad. Sci. U. S. A. 111, 8776–8781. https://doi.org/10.1073/pnas.1314787111

Glover, D., Sumberg, J., Ton, G., Andersson, J., Badstue, L., 2019. Rethinking technological change in smallholder agriculture. Outlook Agric. 48, 169–180. https://doi.org/10.1177/0030727019864978

Godfray, H.C.J., Beddington, J.R., Crute, I.R., Haddad, L., Lawrence, D., Muir, J.F., Pretty, J., Robinson, S., Thomas, S.M., Toulmin, C., 2010. Food Security: The Challenge of

Feeding 9 Billion People. Science 327:812-818. Science (80-.). 327, 812–818.

González, M., Vera, C.S., Liebmann, B., Marengo, J.A., Kousky, V., Allured, D., 2007. The nature of the rainfall onset over central South America. Atmosfera 20, 377–394.

Goodman, L.A., 1960. On the Exact Variance of Products 55, 708–713. https://doi.org/10.1080/01621459.1960.10483369

Grossi, A., Dinku, T., 2022a. Enhancing national climate services: How systems thinking can accelerate locally led adaptation. One Earth 5, 74–83. https://doi.org/10.1016/j.oneear.2021.12.007

Grossi, A., Dinku, T., 2022b. From research to practice: Adapting agriculture to climate today for tomorrow in Ethiopia. Front. Clim. https://doi.org/10.3389/fclim.2022.931514

Guan, K., Sultan, B., Biasutti, M., Baron, C., Lobell, D.B., 2015. What aspects of future rainfall changes matter for crop yields in West Africa? Geophys. Res. Lett. 42, 8001–8010. https://doi.org/10.1002/2015GL063877

Guhathakurta, P., Saji, E., 2013. Detecting changes in rainfall pattern and seasonality index vis-à-vis increasing water scarcity in Maharashtra. J. Earth Syst. Sci. 122, 639–649. https://doi.org/10.1007/s12040-013-0294-y

Guido, Z., Zimmer, A., Lopus, S., Hannah, C., Gower, D., Waldman, K., Krell, N., Sheffield, J., Caylor, K., Evans, T., 2020. Farmer forecasts: Impacts of seasonal rainfall expectations on agricultural decision-making in Sub-Saharan Africa. Clim. Risk Manag. 30, 100247. https://doi.org/10.1016/j.crm.2020.100247

Guo, D., Westra, S., Maier, H.R., 2017. Sensitivity of potential evapotranspiration to changes in climate variables for different Australian climatic zones. Hydrol. Earth Syst. Sci. 21, 2107–2126. https://doi.org/10.5194/hess-21-2107-2017

Gurmessa, B., 2021. Soil acidity challenges and the significance of liming and organic amendments in tropical agricultural lands with reference to Ethiopia. Environ. Dev. Sustain. 23, 77–99. https://doi.org/10.1007/s10668-020-00615-2

Gutjahr, O., Putrasahan, D., Lohmann, K., Jungclaus, J.H., Von Storch, J.S., Brüggemann, N., Haak, H., Stössel, A., 2019. Max Planck Institute Earth System Model (MPI-ESM1.2) for the High-Resolution Model Intercomparison Project (HighResMIP). Geosci. Model Dev. 12, 3241–3281. https://doi.org/10.5194/gmd-12-3241-2019

Habtemariam, L.T., Gandorfer, M., Kassa, G.A., Heissenhuber, A., 2016. Factors Influencing Smallholder Farmers' Climate Change Perceptions: A Study from Farmers in Ethiopia. Environ. Manage. 58, 343–358. https://doi.org/10.1007/s00267-016-0708-0

Hadgu, G., Tesfaye, K., Mamo, G., 2015. Analysis of climate change in Northern Ethiopia: implications for agricultural production. Theor. Appl. Climatol. 121, 733–747. https://doi.org/10.1007/s00704-014-1261-5

Haile, G.G., Tang, Q., Hosseini-Moghari, S.M., Liu, X., Gebremicael, T.G., Leng, G., Kebede,

A., Xu, X., Yun, X., 2020. Projected Impacts of Climate Change on Drought Patterns Over East Africa. Earth's Futur. 8, 1–23. https://doi.org/10.1029/2020EF001502

Hailu, G., Weersink, A., Minten, B., 2017. Determinants of the Productivity of Teff in Ethiopia. Eur. J. Dev. Res. 29, 866–892. https://doi.org/10.1057/s41287-016-0065-0

Hajima, T., Watanabe, M., Yamamoto, A., Tatebe, H., Noguchi, M.A., Abe, M., Ohgaito, R., Ito, Akinori, Yamazaki, D., Okajima, H., Ito, Akihiko, Takata, K., Ogochi, K., Watanabe, S., Kawamiya, M., 2020. Development of the MIROC-ES2L Earth system model and the evaluation of biogeochemical processes and feedbacks. Geosci. Model Dev. 13, 2197–2244. https://doi.org/10.5194/gmd-13-2197-2020

Hamby, D.., 1994. A review of techniques for parameter sensitivity analysis of environmental models. Environ. Monit. Assess. 32, 135–154. https://doi.org/10.1007/BF00547132

Hameso, S., 2018. Farmers and policy-makers ' perceptions of climate change in Ethiopia. Clim. Dev. 10, 347–359. https://doi.org/10.1080/17565529.2017.1291408

Hampf, A.C., Stella, T., Berg-Mohnicke, M., Kawohl, T., Kilian, M., Nendel, C., 2020. Future yields of double-cropping systems in the Southern Amazon, Brazil, under climate change and technological development. Agric. Syst. 177. https://doi.org/10.1016/j.agsy.2019.102707

Hao, F., Chen, S., Ouyang, W., Shan, Y., Qi, S., 2013. Temporal rainfall patterns with water partitioning impacts on maize yield in a freeze – thaw zone. J. Hydrol. 486, 412–419. https://doi.org/10.1016/j.jhydrol.2013.02.008

Harris, I., Osborn, T.J., Jones, P., Lister, D., 2020. Version 4 of the CRU TS monthly high-resolution gridded multivariate climate dataset. Sci. Data 7, 1–18. https://doi.org/10.1038/s41597-020-0453-3

Hartmann, M., Six, J., 2023. Soil structure and microbiome functions in agroecosystems. Nat. Rev. Earth Environ. 4, 4–18. https://doi.org/10.1038/s43017-022-00366-w

Hassan, M.A., Xiang, C., Farooq, M., Muhammad, N., Yan, Z., Hui, X., Yuanyuan, K., Bruno, A.K., Lele, Z., Jincai, L., 2021. Cold Stress in Wheat: Plant Acclimation Responses and Management Strategies. Front. Plant Sci. 12, 1–15. https://doi.org/10.3389/fpls.2021.676884

Hatfield, J.L., Dold, C., 2019. Water-use efficiency: Advances and challenges in a changing climate. Front. Plant Sci. 10, 1–14. https://doi.org/10.3389/fpls.2019.00103

Hatfield, J.L., Prueger, J.H., 2015. Temperature extremes: Effect on plant growth and development. Weather Clim. Extrem. 10, 4–10. https://doi.org/10.1016/j.wace.2015.08.001

Hawkins, E., Sutton, R., 2011. The potential to narrow uncertainty in projections of regional precipitation change. Clim. Dyn. 37, 407–418. https://doi.org/10.1007/s00382-010-0810-6

Hawkins, R.H., Moglen, G.E., Ward, T.J., Woodward, D.E., 2020. Watershed Management 2020 99, in: Watershed Management 2020. pp. 301–340.

He, J., Ma, B., Tian, J., 2022. Water production function and optimal irrigation schedule for rice (Oryza sativa L.) cultivation with drip irrigation under plastic film-mulched. Sci. Rep. 12, 1–12. https://doi.org/10.1038/s41598-022-20652-3

Hengl, T., De Jesus, J.M., Heuvelink, G.B.M., Gonzalez, M.R., Kilibarda, M., Blagotić, A., Shangguan, W., Wright, M.N., Geng, X., Bauer-Marschallinger, B., Guevara, M.A., Vargas, R., MacMillan, R.A., Batjes, N.H., Leenaars, J.G.B., Ribeiro, E., Wheeler, I., Mantel, S., Kempen, B., 2017. SoilGrids250m: Global gridded soil information based on machine learning. PLoS One 12. https://doi.org/10.1371/journal.pone.0169748

Hersbach, H., Bell, B., Berrisford, P., Hirahara, S., Horányi, A., Muñoz-Sabater, J., Nicolas, J., Peubey, C., Radu, R., Schepers, D., Simmons, A., Soci, C., Abdalla, S., Abellan, X., Balsamo, G., Bechtold, P., Biavati, G., Bidlot, J., Bonavita, M., De Chiara, G., Dahlgren, P., Dee, D., Diamantakis, M., Dragani, R., Flemming, J., Forbes, R., Fuentes, M., Geer, A., Haimberger, L., Healy, S., Hogan, R.J., Hólm, E., Janisková, M., Keeley, S., Laloyaux, P., Lopez, P., Lupu, C., Radnoti, G., de Rosnay, P., Rozum, I., Vamborg, F., Villaume, S., Thépaut, J.N., 2020. The ERA5 global reanalysis. Q. J. R. Meteorol. Soc. 146, 1999–2049. https://doi.org/10.1002/qj.3803

Herweg, K., Stillhardt, B., 1999. The variability of soil erosion in the highlands of Ethiopia and Eritrea: Average and extreme erosion patterns. Bern, Switzerland.

Hiebl, J., Frei, C., 2016. Daily temperature grids for Austria since 1961—concept, creation and applicability. Theor. Appl. Climatol. 124, 161–178. https://doi.org/10.1007/s00704-015-1411-4

Hillocks, R.J., 2014. Addressing the yield gap in sub-Saharan Africa. Outlook Agric. 43, 85–90. https://doi.org/10.5367/oa.2014.0163

Hills, R.C., 1979. The structure of the inter-tropical convergence zone in equatorial Africa and its relationship to east African rainfall. Trans. Inst. Br. Geogr. 4, 329–352. https://doi.org/10.2307/622055

Hirons, M., Beauchamp, E., Whitfield, S., Conway, D., Asare, R., Malhi, Y., 2020. Resilience to climate shocks in the tropics. Environ. Res. Lett. 15. https://doi.org/10.1088/1748-9326/abb156

Hoffmann, M.P., Haakana, M., Asseng, S., Höhn, J.G., Palosuo, T., Ruiz-Ramos, M., Fronzek, S., Ewert, F., Gaiser, T., Kassie, B.T., Paff, K., Rezaei, E.E., Rodríguez, A., Semenov, M., Srivastava, A.K., Stratonovitch, P., Tao, F., Chen, Y., Rötter, R.P., 2018. How does inter-annual variability of attainable yield affect the magnitude of yield gaps for wheat and maize? An analysis at ten sites. Agric. Syst. 159, 199–208. https://doi.org/10.1016/j.agsy.2017.03.012

Holzkämper, A., Calanca, P., Fuhrer, J., 2013. Identifying climatic limitations to grain maize yield potentials using a suitability evaluation approach. Agric. For. Meteorol. 168, 149–159. https://doi.org/10.1016/j.agrformet.2012.09.004

Holzworth, D.P., Huth, N.I., deVoil, P.G., Zurcher, E.J., Herrmann, N.I., McLean, G., Chenu, K., van Oosterom, E.J., Snow, V., Murphy, C., Moore, A.D., Brown, H., Whish, J.P.M., Verrall, S., Fainges, J., Bell, L.W., Peake, A.S., Poulton, P.L., Hochman, Z., Thorburn, P.J., Gaydon, D.S., Dalgliesh, N.P., Rodriguez, D., Cox, H., Chapman, S., Doherty, A., Teixeira, E., Sharp, J., Cichota, R., Vogeler, I., Li, F.Y., Wang, E., Hammer, G.L., Robertson, M.J., Dimes, J.P., Whitbread, A.M., Hunt, J., van Rees, H., McClelland, T., Carberry, P.S., Hargreaves, J.N.G., MacLeod, N., McDonald, C., Harsdorf, J., Wedgwood, S., Keating, B.A., 2014. APSIM - Evolution towards a new generation of agricultural systems simulation. Environ. Model. Softw. 62, 327–350. https://doi.org/10.1016/j.envsoft.2014.07.009

Howden, S.M., Soussana, J.F., Tubiello, F.N., Chhetri, N., Dunlop, M., Meinke, H., 2007. Adapting agriculture to climate change. Proc. Natl. Acad. Sci. U. S. A. 104, 19691–19696. https://doi.org/10.1073/pnas.0701890104

Huang, J., Hartemink, A.E., 2020. Soil and environmental issues in sandy soils. Earth-Science Rev. 208, 103295. https://doi.org/10.1016/j.earscirev.2020.103295

Hundera, H., Mpandeli, S., Bantider, A., 2019. Smallholder farmers' awareness and perceptions of climate change in Adama district, central rift valley of Ethiopia. Weather Clim. Extrem. 26, 100230. https://doi.org/10.1016/j.wace.2019.100230

Hurni, H., 2016. Soil and Water Conservation in Ethiopia: Guidlines for Development Agents. Bern Open Publishing (BOP). https://doi.org/10.7892/boris.80013

Hurni, H., 1998. Agroecologial belts of Ethiopia: Explanatory notes on three maps at a scale of 1:1,000,000. Res. Report, Soil Conserv. Res. program, Addis Ababa 43.

Hurni, Hans, Abate, S., Bantider, A., Debele, B., Ludi, E., Portner, B., Yitaferu, B., Zeleke, G., 2010. Land Degradation and Sustainable Land Management in the Highlands of Ethiopia, in: Hurni, H, Wiesmann, U. (Eds.), Global Change and Sustainable Development: A Synthesis of Regional Experiences from Research Partnerships. Perspectives of the Swiss National Centre of Competence in Research (NCCR) North-South. Geographica Bernensia, Bern, pp. 187–207. https://doi.org/10.1002/(SICI)1099-145X(199811/12)9:6<529::AID-LDR313>3.0.CO;2-O

Hussain, H.A., Hussain, S., Khaliq, A., Ashraf, U., Anjum, S.A., Men, S., Wang, L., 2018. Chilling and drought stresses in crop plants: Implications, cross talk, and potential management opportunities. Front. Plant Sci. 9, 1–21. https://doi.org/10.3389/fpls.2018.00393

IFPRI, CSA, 2006. Atlas of the Ethiopian Rural Economy, Atlas of the Ethiopian Rural Economy. International Food Policy Research Institute, Washinton DC. https://doi.org/10.2499/0896291545

IPCC, 2021. Annex II: Models [Gutiérrez, J M., A.-M. Tréguier (eds.)], Climate Change 2021: The Physical Science Basis. Contribution of Working Group I to the Sixth Assessment Report of the Intergovernmental Panel on Climate Change. https://doi.org/10.1017/9781009157896.016.2087

Ittersum, M.K. Van, Cassman, K.G., Grassini, P., Wolf, J., Tittonell, P., Hochman, Z., 2013. Field Crops Research Yield gap analysis with local to global relevance — A review. F. Crop. Res. 143, 4–17. https://doi.org/10.1016/j.fcr.2012.09.009

Ivushkin, K., Bartholomeus, H., Bregt, A.K., Pulatov, A., Kempen, B., de Sousa, L., 2019. Global mapping of soil salinity change. Remote Sens. Environ. 231, 111260. https://doi.org/10.1016/j.rse.2019.111260

Jägermeyr, J., Müller, C., Ruane, A.C., Elliott, J., Balkovic, J., Castillo, O., Faye, B., Foster, I., Folberth, C., Franke, J.A., Fuchs, K., Guarin, J.R., Heinke, J., Hoogenboom, G., Iizumi, T., Jain, A.K., Kelly, D., Khabarov, N., Lange, S., Lin, T.S., Liu, W., Mialyk, O., Minoli, S., Moyer, E.J., Okada, M., Phillips, M., Porter, C., Rabin, S.S., Scheer, C., Schneider, J.M., Schyns, J.F., Skalsky, R., Smerald, A., Stella, T., Stephens, H., Webber, H., Zabel, F., Rosenzweig, C., 2021. Climate impacts on global agriculture emerge earlier in new generation of climate and crop models. Nat. Food 2, 873–885. https://doi.org/10.1038/s43016-021-00400-y

Jarvis, R.A., 1973. On the identification of the convex hull of a finite set of points in the plane 2, 18–21. https://doi.org/10.1016/0020-0190(73)90020-3

Jemal, K., Berhanu, S., 2020. Effect of Water Application Methods in Furrow Irrigation Along with Different Types of Mulches on Yield and Water Productivity of Maize (Zea mays l.) at Hawassa, Ethiopia. J. Nat. Sci. Res. 10, 1–14. https://doi.org/10.7176/jnsr/10-5-01

Jiang, Y., Zhou, L., Tucker, C.J., Raghavendra, A., Hua, W., Liu, Y.Y., Joiner, J., 2019. Widespread increase of boreal summer dry season length over the Congo rainforest. Nat. Clim. Chang. 9, 617–622. https://doi.org/10.1038/s41558-019-0512-y

Jones, J.W., Hoogenboom, G., Porter, C.H., Boote, K.J., Batchelor, W.D., Hunt, L.A., Wilkens, P.W., Singh, U., Gijsman, A.J., Ritchie, J.T., 2003. The DSSAT cropping system model, European Journal of Agronomy. https://doi.org/10.1016/S1161-0301(02)00107-7

Jørgensen, M., Torp, T., Alexander, J., Mølmann, B., 2020. Impact of waterlogging and temperature on autumn growth , hardening and freezing tolerance of timothy (Phleum pratense) 242–251. https://doi.org/10.1111/jac.12385

Joseph, J.., Akinrotimi, O.O., Rao, K.P.C., Ramaraj, A.P., Traore, P.S.C., Sujatha, P., Whitbread, A.., 2020. The Usefulness of Gridded Climate Data Products in Characterizing Climate Variability and Assessing Crop Production The Usefulness of Gridded Climate Data Products in Characterizing Climate Variability and Assessing Crop Production, CGIAR Research Program on Climate Change, Agriculture and Food Security (CCAFS).

Kahsay, H.T., Guta, D.D., Birhanu, B.S., Gidey, T.G., Routray, J.K., 2019. Farmers' Perceptions of Climate Change Trends and Adaptation Strategies in Semiarid Highlands of Eastern Tigray, Northern Ethiopia. Adv. Meteorol. 2019. https://doi.org/10.1155/2019/3849210

Kamali, B., Abbaspour, K.C., Lehmann, A., Wehrli, B., Yang, H., 2018a. Spatial assessment

of maize physical drought vulnerability in sub-Saharan Africa: Linking drought exposure with crop failure. Environ. Res. Lett. 13. https://doi.org/10.1088/1748-9326/aacb37

Kamali, B., Abbaspour, K.C., Wehrli, B., Yang, H., 2018b. Drought vulnerability assessment of maize in Sub-Saharan Africa: Insights from physical and social perspectives. Glob. Planet. Change 162, 266–274. https://doi.org/10.1016/j.gloplacha.2018.01.011

Kamali, B., Jahanbakhshi, F., Dogaru, D., Dietrich, J., Nendel, C., Aghakouchak, A., 2022. Probabilistic modeling of crop-yield loss risk under drought: A spatial showcase for sub-Saharan Africa. Environ. Res. Lett. 17. https://doi.org/10.1088/1748-9326/ac4ec1

Kang, Y., Khan, S., Ma, X., 2009. Climate change impacts on crop yield, crop water productivity and food security - A review. Prog. Nat. Sci. 19, 1665–1674. https://doi.org/10.1016/j.pnsc.2009.08.001

Karger, D.N., Schmatz, D.R., Dettling, G., Zimmermann, N.E., 2020. High-resolution monthly precipitation and temperature time series from 2006 to 2100. Sci. Data 7, 1–10. https://doi.org/10.1038/s41597-020-00587-y

Kassawmar, T., Zeleke, G., Bantider, A., Gessesse, G.D., Abebe, S., Abraha, L., Tadesse, M., 2019. State of cropland availability in rainfed farming systems in Ethiopia: Alternative pathways to address landlessness and food insecurity. In: Ethiopia: Social and Political Issues, in: Ethiopia: Social and Political Issues. NOVA, pp. 228–260.

Kassawmar, T., Zeleke, G., Bantider, A., Gessesse, G.D., Abraha, L., 2018. A synoptic land change assessment of Ethiopia's Rainfed Agricultural Area for evidence-based agricultural ecosystem management. Heliyon 4, e00914. https://doi.org/10.1016/j.heliyon.2018.e00914

Kassie, B.T., Rötter, R.P., Hengsdijk, H., Asseng, S., Van Ittersum, M.K., Kahiluoto, H., Van Keulen, H., 2014. Climate variability and change in the Central Rift Valley of Ethiopia: Challenges for rainfed crop production. J. Agric. Sci. 152, 58–74. https://doi.org/10.1017/S0021859612000986

Kaur, G., Singh, G., Motavalli, P.P., Nelson, K.A., Orlowski, J.M., Golden, B.R., 2020. Impacts and management strategies for crop production in waterlogged or flooded soils: A review. Agron. J. 112, 1475–1501. https://doi.org/10.1002/agj2.20093

Kazemi, H., Akinci, H., 2018. A land use suitability model for rainfed farming by Multi-criteria Decision-making Analysis (MCDA) and Geographic Information System (GIS). Ecol. Eng. 116, 1–6. https://doi.org/10.1016/j.ecoleng.2018.02.021

Kebede, A., Diekkrüger, B., Edossa, D.C., 2017. Dry spell, onset and cessation of the wet season rainfall in the Upper Baro-Akobo Basin, Ethiopia. Theor. Appl. Climatol. 129, 849–858. https://doi.org/10.1007/s00704-016-1813-y

Kendall, M.G., 1975. Ranked Correlation Methods, 4th ed, Behavior Research Methods, Instruments, & Computers. Charles Griffin, London. https://doi.org/10.3758/bf03202470

Kimutai, J., Barnes, C., Zachariah, M., Philip, S., Kew, S., Pinto, I., Wolski, P., Koren, G.,

Vecchi, G., Yang, W., Li, S., Vahlberg, M., Singh, R., Heinrich, D., Pereira, C.M., Arrighi, J., Thalheimer, L., Kane, C., Otto, F.E.L., 2022. Human-induced climate change increased drought severity in Horn of Africa. Julie Arrighi 16. https://doi.org/10.25561/103482

Korecha, D., Barnston, A.G., 2007. Predictability of June-September rainfall in Ethiopia. Mon. Weather Rev. 135, 628–650. https://doi.org/10.1175/MWR3304.1

Kukal, M.S., Irmak, S., 2018. Climate-Driven Crop Yield and Yield Variability and Climate Change Impacts on the U.S. Great Plains Agricultural Production. Nat. Sci. Rep. 8, 1–18. https://doi.org/10.1038/s41598-018-21848-2

Kumah, K.K., Maathuis, B.H.P., Hoedjes, J.C.B., Su, Z., 2022. Near real-time estimation of high spatiotemporal resolution rainfall from cloud top properties of the MSG satellite and commercial microwave link rainfall intensities. Atmos. Res. 279. https://doi.org/10.1016/j.atmosres.2022.106357

Kummu, M., Heino, M., Taka, M., Varis, O., Viviroli, D., 2021. Climate change risks pushing one-third of global food production outside the safe climatic space. One Earth 4, 720–729. https://doi.org/10.1016/j.oneear.2021.04.017

Laderach, P., Ramirez-Villegas, J., Prager, S.D., Osorio, D., Krendelsberger, A., Zougmore, R.B., Charbonneau, B., Van Dijk, H., Madurga-Lopez, I., Pacillo, G., 2021. The importance of food systems in a climate crisis for peace and security in the Sahel. Int. Rev. Red Cross 103, 995–1028. https://doi.org/10.1017/S1816383122000170

Lala, J., Tilahun, S., Block, P., 2020. Predicting rainy season onset in the ethiopian highlands for agricultural planning. J. Hydrometeorol. 21, 1675–1688. https://doi.org/10.1175/JHM-D-20-0058.1

Lala, J., Yang, M., Wang, G., Block, P., 2021. Utilizing rainy season onset predictions to enhance maize yields in Ethiopia. Environ. Res. Lett. 16. https://doi.org/10.1088/1748-9326/abf9c9

Lankford, B., Orr, S., Lankford, B., 2022. Exploring the Critical Role of Water in Regenerative Agriculture; Building Promises and Avoiding Pitfalls. Front. Sustain. Food Syst. 6, 1–17. https://doi.org/10.3389/fsufs.2022.891709

Lasco, R.D., Delfino, R.J.P., Espaldon, M.L.O., 2014. Agroforestry systems: Helping smallholders adapt to climate risks while mitigating climate change. Wiley Interdiscip. Rev. Clim. Chang. 5, 825–833. https://doi.org/10.1002/wcc.301

Leal Filho, W., Totin, E., Franke, J.A., Andrew, S.M., Abubakar, I.R., Azadi, H., Nunn, P.D., Ouweneel, B., Williams, P.A., Simpson, N.P., 2022. Understanding responses to climate-related water scarcity in Africa. Sci. Total Environ. 806, 150420. https://doi.org/10.1016/j.scitotenv.2021.150420

Lebay, M., Abiye, W., Taye, T., Belay, S., 2021. Evaluation of Soil Drainage Methods for the Productivity of Waterlogged Vertisols in Jama District , Eastern Amhara Region , Ethiopia 2021.

Lee, H., 2018. Teff, A Rising Global Crop: Current Status of Teff Production and Value Chain. Open Agric. J. 12, 185–193. https://doi.org/10.2174/1874331501812010185

Lehmann, J., Kleber, M., 2015. The contentious nature of soil organic matter. Nature 528, 60–68. https://doi.org/10.1038/nature16069

Lesk, C., Anderson, W., Rigden, A., Coast, O., Jägermeyr, J., McDermid, S., Davis, K.F., Konar, M., 2022. Compound heat and moisture extreme impacts on global crop yields under climate change. Nat. Rev. Earth Environ. 3, 872–889. https://doi.org/10.1038/s43017-022-00368-8

Li-ping, L., Xiao-hua, L., Hong-bo, S., Zhao-Pu, L., Ya, T., Quan-suo, Z., Jun-qin, Z., 2015. Ameliorants improve saline-alkaline soils on a large scale in northern Jiangsu Province, China. Ecol. Eng. 81, 328–334. https://doi.org/10.1016/j.ecoleng.2015.04.032

Li, L., Yu, Y., Tang, Y., Lin, P., Xie, J., Song, M., Dong, L., Zhou, T., Liu, L., Wang, Lu, Pu, Y., Chen, X., Chen, L., Xie, Z., Liu, Hongbo, Zhang, L., Huang, X., Feng, T., Zheng, W., Xia, K., Liu, Hailong, Liu, J., Wang, Y., Wang, Longhuan, Jia, B., Xie, F., Wang, B., Zhao, S., Yu, Z., Zhao, B., Wei, J., 2020. The Flexible Global Ocean-Atmosphere-Land System Model Grid-Point Version 3 (FGOALS-g3): Description and Evaluation. J. Adv. Model. Earth Syst. 12, 1–28. https://doi.org/10.1029/2019MS002012

Liebmann, B., Bladé, I., Kiladis, G.N., Carvalho, L.M.V., Senay, G.B., Allured, D., Leroux, S., Funk, C., 2012. Seasonality of African precipitation from 1996 to 2009. J. Clim. 25, 4304–4322. https://doi.org/10.1175/JCLI-D-11-00157.1

Liebmann, B., Marengo, J.A., 2001. Interannual variability of the rainy season and rainfall in the Brazilian Amazon Basin. J. Clim. 14, 4308–4318. https://doi.org/10.1175/1520-0442(2001)014<4308:IVOTRS>2.0.CO;2

Lin, Y., Huang, X., Liang, Y., Qin, Y., Xu, S., Huang, W., Xu, F., Liu, L., Wang, Y., Peng, Y., Wang, L., Xue, W., Fu, H., Zhang, G.J., Wang, B., Li, R., Zhang, C., Lu, H., Yang, K., Luo, Yong, Bai, Y., Song, Z., Wang, M., Zhao, W., Zhang, F., Xu, J., Zhao, X., Lu, C., Chen, Y., Luo, Yiqi, Hu, Y., Tang, Q., Chen, D., Yang, G., Gong, P., 2020. Community Integrated Earth System Model (CIESM): Description and Evaluation. J. Adv. Model. Earth Syst. 12, 1–29. https://doi.org/10.1029/2019MS002036

Lipper, L., Thornton, P., Campbell, B.M., Baedeker, T., Braimoh, A., Bwalya, M., Caron, P., Cattaneo, A., Garrity, D., Henry, K., Hottle, R., Jackson, L., Jarvis, A., Kossam, F., Mann, W., McCarthy, N., Meybeck, A., Neufeldt, H., Remington, T., Sen, P.T., Sessa, R., Shula, R., Tibu, A., Torquebiau, E.F., 2014. Climate-smart agriculture for food security. Nat. Clim. Chang. 4, 1068–1072. https://doi.org/10.1038/nclimate2437

Liu, J., Yang, H., Gosling, S.N., Kummu, M., Flörke, M., Pfister, S., Hanasaki, N., Wada, Y., Zhang, X., Zheng, C., Alcamo, J., Oki, T., 2017. Water scarcity assessments in the past, present, and future. Earth's Futur. 5, 545–559. https://doi.org/10.1002/2016EF000518

Liu, M., Wang, D., Chen, X., Chen, Y., Gao, L., Deng, H., 2022. Impacts of climate variability and land use on the blue and green water resources in a subtropical basin of China. Sci. Rep. 12, 1–11. https://doi.org/10.1038/s41598-022-21880-3

Liu, X., Liu, W., Tang, Q., Liu, B., Wada, Y., Yang, H., 2022. Global Agricultural Water Scarcity Assessment Incorporating Blue and Green Water Availability Under Future Climate Change. Earth's Futur. 10. https://doi.org/10.1029/2021EF002567

Lobell, David B, Bänziger, M., Magorokosho, C., Vivek, B., 2011. Nonlinear heat effects on African maize as evidenced by historical yield trials. Nat. Clim. Chang. 1. https://doi.org/10.1038/nclimate1043

Lobell, D.B., Burke, M.B., 2008. Why are agricultural impacts of climate change so uncertain? the importance of temperature relative to precipitation. Environ. Res. Lett. 3. https://doi.org/10.1088/1748-9326/3/3/034007

Lobell, D.B., Cassman, K.G., Field, C.B., 2009. Crop yield gaps: Their importance, magnitudes, and causes. Annu. Rev. Environ. Resour. 34, 179–204. https://doi.org/10.1146/annurev.environ.041008.093740

Lobell, David B., Schlenker, W., Costa-Roberts, J., 2011. Climate Trends and Global crop production since 1980 1980 333, 1186–1189. https://doi.org/10.1126/science.1206376

Lovato, T., Peano, D., Butenschön, M., Materia, S., Iovino, D., Scoccimarro, E., Fogli, P.G., Cherchi, A., Bellucci, A., Gualdi, S., Masina, S., Navarra, A., 2022. CMIP6 Simulations With the CMCC Earth System Model (CMCC-ESM2). J. Adv. Model. Earth Syst. 14. https://doi.org/10.1029/2021MS002814

MacLeod, D., 2018. Seasonal predictability of onset and cessation of the east African rains. Weather Clim. Extrem. 21, 27–35. https://doi.org/10.1016/j.wace.2018.05.003

MacLeod, D., Quichimbo, E.A., Michaelides, K., Asfaw, D.T., Rosolem, R., Cuthbert, M.O., Otenyo, E., Segele, Z., Rigby, J.M., Otieno, G., Hassaballah, K., Tadege, A., Singer, M.B., 2023. Translating seasonal climate forecasts into water balance forecasts for decision making. PLOS Clim. 2, e0000138. https://doi.org/10.1371/journal.pclm.0000138

Makurira, H., Savenije, H.H.G., Uhlenbrook, S., Rockström, J., Senzanje, A., 2009. Investigating the water balance of on-farm techniques for improved crop productivity in rainfed systems: A case study of Makanya catchment, Tanzania. Phys. Chem. Earth 34, 93–98. https://doi.org/10.1016/j.pce.2008.04.003

Manaye, A., Afewerk, A., Manjur, B., Solomon, N., 2023. The Effect of the war on smallholder agriculture in Tigray, Northern Ethiopia. Cogent Food Agric. 9. https://doi.org/10.1080/23311932.2023.2247696

Manik, S.M.N., Pengilley, G., Dean, G., Field, B., Shabala, S., Zhou, M., 2019. Soil and crop management practices to minimize the impact of waterlogging on crop productivity. Front. Plant Sci. 10, 1–23. https://doi.org/10.3389/fpls.2019.00140

Mann, H.B., 1945. H.B. Mann Nonparametric tests against trend Econometrica. Econometrica 245–259.

Maraun, D., 2013. Bias correction, quantile mapping, and downscaling: Revisiting the inflation

issue. J. Clim. 26, 2137–2143. https://doi.org/10.1175/JCLI-D-12-00821.1

Marengo, J.A., Liebmann, B., Kousky, V.E., Filizola, N.P., Wainer, I.C., 2001. Onset and end of the rainy season in the Brazilian Amazon Basin. J. Clim. 14, 833–852. https://doi.org/10.1175/1520-0442(2001)014<0833:OAEOTR>2.0.CO;2

Markos, D., Worku, W., Mamo, G., 2023. Exploring adaptation responses of maize to climate change scenarios in southern central Rift Valley of Ethiopia. Sci. Rep. 13, 1–18. https://doi.org/10.1038/s41598-023-39795-y

Marlet, S., Barbiero, L., Valles, V., 1998. Soil Alkalinization and irrigation in the Sahelian zone of Niger II: Agronomic consequences of alkalinity and sodicity. Arid Soil Res. Rehabil. 12, 139–152. https://doi.org/10.1080/15324989809381504

Marteau, R., Moron, V., Philippon, N., 2009. Spatial coherence of Monsoon onset over Western and Central Sahel (1950-2000). J. Clim. 22, 1313–1324. https://doi.org/10.1175/2008JCLI2383.1

Marteau, R., Sultan, B., Moron, V., Alhassane, A., Baron, C., Traoré, S.B., 2011. The onset of the rainy season and farmers' sowing strategy for pearl millet cultivation in Southwest Niger. Agric. For. Meteorol. 151, 1356–1369. https://doi.org/10.1016/j.agrformet.2011.05.018

Marval, A.Š., Vumop, P.F., Natalja, C.-A., Ku, Č., Strauch, M., Ufz, F.W., Wu, S.P., Farkas, C., 2022. SWAT + and SWAP retention measure implementation handbook.

Masih, I., Maskey, S., Mussá, F.E.F., Trambauer, P., 2014. A review of droughts on the African continent: A geospatial and long-term perspective. Hydrol. Earth Syst. Sci. https://doi.org/10.5194/hess-18-3635-2014

Mbow, C., Rosenzweig, C., Barioni, L.G., Benton, T.G., Herrero, M., Krishnapillai, M., Liwenga, E., Pradhan, P., Rivera-Ferre, M.G., Sapkota, T., Tubiello, F.N., Xu, Y., 2019. Food Security. In: Climate Change and Land: an IPCC special report on climate change, desertification, land degradation, sustainable land management, food security, and greenhouse gas fluxes in terrestrial ecosystems.

Mebrahtu, Y., Mehamed, A., 2019. Effect of Different Type of Mulching and Furrow Irrigation Methods on Maize (Zea mays L.) Yield and Water Productivity at Raya Valley, Northern Ethiopia. J. Biol. Agric. Healthc. 6–13. https://doi.org/10.7176/jbah/9-20-02

Megabia, T.T., Amare, Z.Y., Asmare, A.M., 2022. Rural household perception and adaptation strategies to climate change and variability : in the case of Libo - kemkem Woreda , Ethiopia. Environ. Syst. Res. https://doi.org/10.1186/s40068-022-00270-8

Mehari, H., Bedadi, B., Abegaz, F., 2020. Maximizing Water Productivity of Maize using Alternate Furrow Irrigation at Clay-loam Soil, Raya valley, Ethiopia. Int. J. Plant Breed. Crop Sci. 7, 771–778.

Meinshausen, M., Nicholls, Z.R.J., Lewis, J., Gidden, M.J., Vogel, E., Freund, M., Beyerle, U., Gessner, C., Nauels, A., Bauer, N., Canadell, J.G., Daniel, J.S., John, A., Krummel,

P.B., Luderer, G., Meinshausen, N., Montzka, S.A., Rayner, P.J., Reimann, S., Smith, S.J., Van Den Berg, M., Velders, G.J.M., Vollmer, M.K., Wang, R.H.J., 2020. The shared socio-economic pathway (SSP) greenhouse gas concentrations and their extensions to 2500. Geosci. Model Dev. 13, 3571–3605. https://doi.org/10.5194/gmd-13-3571-2020

Mekonnen, M.M., Hoekstra, A.Y., 2011. The green, blue and grey water footprint of crops and derived crop products. Hydrol. Earth Syst. Sci. 15, 1577–1600. https://doi.org/10.5194/hess-15-1577-2011

Meng, M., Pu, X., Li, S., Zhang, Y., Wang, Jian, Xu, H., Hu, Y., Wang, Junjie, Wang, Y., 2023. Sensitivities of rainfed maize production to root zone soil water , air temperature and shortwave radiation in the Sanjiang Plain under sub- humid cool-temperate climates. Water-Energy Nexus 6, 131–136. https://doi.org/10.1016/j.wen.2023.09.003

Mengiste, Y., Tilahun, K., 2009. Yield and water use efficiency of deficit-irrigated maize in semi-arid region of Ethiopia. African J. Food, Agric. Nutr. Dev. 9, 1635–1651. https://doi.org/10.4314/ajfand.v9i8.48403

Mengistu, D.K., Mekonnen, L.S., 2012. Integrated Agronomic Crop Managements to Improve Tef Productivity Under Terminal Drought, in: Rahman, P.I.M.M. (Ed.), Water Stress. pp. 235–254.

Menne, M.J., Durre, I., Vose, R.S., Gleason, B.E., Houston, T.G., 2012. An overview of the global historical climatology network-daily database. J. Atmos. Ocean. Technol. 29, 897–910. https://doi.org/10.1175/JTECH-D-11-00103.1

Mera, G.A., 2018. Drought and its impacts in Ethiopia. Weather Clim. Extrem. 22, 24–35. https://doi.org/10.1016/j.wace.2018.10.002

Mesgaran, M.B., Madani, K., Hashemi, H., Azadi, P., 2017. Iran's Land Suitability for Agriculture. Sci. Rep. 7, 1–12. https://doi.org/10.1038/s41598-017-08066-y

Meskelu, E., Tesfaye, H., Debebe, A., Mohammed, M., 2018. Integrated Effect of Mulching and Furrow Methods on Maize Yield and Water Productivity at Koka, Ethiopia. Irrig. Drain. Syst. Eng. 07, 1–7. https://doi.org/10.4172/2168-9768.1000207

Meza, I., Siebert, S., Döll, P., Kusche, J., Herbert, C., Rezaei, E.E., Nouri, H., Gerdener, H., Popat, E., Frischen, J., Naumann, G., Vogt, J. V., Walz, Y., Sebesvari, Z., Hagenlocher, M., 2020. Global-scale drought risk assessment for agricultural systems. Nat. Hazards Earth Syst. Sci. 20, 695–712. https://doi.org/10.5194/nhess-20-695-2020

Minoli, S., Jägermeyr, J., Asseng, S., Urfels, A., Müller, C., 2022. Global crop yields can be lifted by timely adaptation of growing periods to climate change. Nat. Commun. 13, 1–10. https://doi.org/10.1038/s41467-022-34411-5

Mintesinot, B., Verplancke, H., Van Ranst, E., Mitiku, H., 2004. Examining traditional irrigation methods, irrigation scheduling and alternate furrows irrigation on vertisols in northern Ethiopia. Agric. Water Manag. 64, 17–27. https://doi.org/10.1016/S0378-3774(03)00194-X

Moges, D.M., 2018. An insight into land use and land cover changes and their impacts in Rib watershed , north - western highland Ethiopia 3317–3330. https://doi.org/10.1002/ldr.3091

Moges, D.M., Gangadhara, B.H., 2021. Climate change and its implications for rainfed agriculture in Ethiopia. J. Water Clim. Chang. 12, 1229–1244. https://doi.org/10.2166/wcc.2020.058

Mohamed, A.A., 2017. Food Security Situation in Ethiopia: A Review Study. Int. J. Heal. Econ. Policy 2, 86–96. https://doi.org/10.11648/j.hep.20170203.11

Mohammadi, S., Rydgren, K., Bakkestuen, V., Gillespie, M.A.K., 2023. Impacts of recent climate change on crop yield can depend on local conditions in climatically diverse regions of Norway. Sci. Rep. 13, 1–12. https://doi.org/10.1038/s41598-023-30813-7

Molden, D., 2007a. Water for food, water for agriculture: A Comprehensive Assessment of Water Management in Agriculture, First. ed. London.

Molden, D., 2007b. A Comprehensive Assessment of Water Management in Agriculture; Summary, Water Management.

Molden, D., Vithanage, M., de Fraiture, C., Faures, J.M., Gordon, L., Molle, F., Peden, D., 2011. Water Availability and Its Use in Agriculture. Treatise Water Sci. 4, 707–732. https://doi.org/10.1016/B978-0-444-53199-5.00108-1

Moroda, G.T., Tolossa, D., Semie, N., 2018. Perception and adaptation strategies of rural people against the adverse e ff ects of climate variability : A case study of Boset District, East Shewa, Ethiopia. Environ. Dev. 27, 2–13. https://doi.org/10.1016/j.envdev.2018.07.005

Msimbira, L.A., Smith, D.L., 2020. The Roles of Plant Growth Promoting Microbes in Enhancing Plant Tolerance to Acidity and Alkalinity Stresses. Front. Sustain. Food Syst. 4, 1–14. https://doi.org/10.3389/fsufs.2020.00106

Mthandi, J., Kahimba, F.C., Tarimo, A.K.P.R., Salim, B.A., Lowole, M.W., 2013. Root zone soil moisture redistribution in maize (<i>Zea mays</i> L.) under different water application regimes. Agric. Sci. 04, 521–528. https://doi.org/10.4236/as.2013.410070

Mu, Q., Zhao, M., Running, S.W., 2019. MODIS Global Terrestrial Evapotranspiration (ET) Product (NASA MOD16A2/A3) Algorithm Theoretical Basis Document Collection 5.

Muchow, R.C., Sinclair, T.R., Bennett, J.M., 1990. Temperature and Solar Radiation Effects on Potential Maize Yield across Locations. Agron. J. 82, 338–343. https://doi.org/10.2134/agronj1990.00021962008200020033x

Mugalavai, E.M., Kipkorir, E.C., Raes, D., Rao, M.S., 2008. Analysis of rainfall onset, cessation and length of growing season for western Kenya. Agric. For. Meteorol. 148, 1123–1135. https://doi.org/10.1016/j.agrformet.2008.02.013

Muir, C., Smith, A.C., 2023. Climate change , degradation , and land acquisitions : evaluating inequalities among competing interests for suitable cropland in Ethiopia 28.

Müller, C., Cramer, W., Hare, W.L., Lotze-Campen, H., 2011. Climate change risks for African agriculture. Proc. Natl. Acad. Sci. U. S. A. 108, 4313–4315. https://doi.org/10.1073/pnas.1015078108

Muñoz-Sabater, J., Dutra, E., Agustí-Panareda, A., Albergel, C., Arduini, G., Balsamo, G., Boussetta, S., Choulga, M., Harrigan, S., Hersbach, H., Martens, B., Miralles, D.G., Piles, M.M., Rodríguez-Fernández, N.J., Zsoter, E., Buontempo, C., Thépaut, J.-N.N., 2021. ERA5-Land: A state-of-the-art global reanalysis dataset for land applications. Earth Syst. Sci. Data 13, 4349–4383. https://doi.org/10.5194/essd-13-4349-2021

Musie, M., Sen, S., Srivastava, P., 2019. Comparison and evaluation of gridded precipitation datasets for streamflow simulation in data scarce watersheds of Ethiopia. J. Hydrol. 579, 124168. https://doi.org/10.1016/j.jhydrol.2019.124168

Mutimura, M., Guthiga, P., Haug, R., Dechassa, N., Ketema, M., Hundessa, F., Tegegne, B., Kibret, K., Tana, T., Murage, A., Nyamu, G., Mburu, M., Katundu, M., Ndolo, V., Tuyisenge, J., Dusengemungu, L., Nyiransengimana, E., Myeni, L., Moeletsi, M.E., Mphephu, M., Modiselle, S., Mapunda, K., Athman, A.K., Selemani, I., Mwaseba, D., 2018. Socio-economic status affecting smallholder farming and food security : A study from six case countries in Africa.

Mutsaers, H.J.W., 1979. An agricultural analysis of rainfall reliability for Cameroon. Netherlands J. Agric. Sci. 27, 67–78. https://doi.org/10.18174/njas.v27i1.17072

Nash, J.E., Sutcliffe, J. V., 1970. River flow forecasting through conceptual models part I - A discussion of principles. J. Hydrol. 10, 282–290. https://doi.org/10.1016/0022-1694(70)90255-6

Nasta, P., Szabó, B., Romano, N., 2021. Evaluation of pedotransfer functions for predicting soil hydraulic properties: A voyage from regional to field scales across Europe. J. Hydrol. Reg. Stud. 37. https://doi.org/10.1016/j.ejrh.2021.100903

Navarro-Racines, C., Tarapues, J., Thornton, P., Jarvis, A., Ramirez-Villegas, J., 2020. High-resolution and bias-corrected CMIP5 projections for climate change impact assessments. Sci. Data 7, 1–14. https://doi.org/10.1038/s41597-019-0343-8

NBE, 2021. National Bank of Ethiopia Annual Bulletin. Addis Ababa, Ethiopia.

Nyakudya, I.W., Stroosnijder, L., Nyagumbo, I., 2014. Infiltration and planting pits for improved water management and maize yield in semi-arid Zimbabwe. Agric. Water Manag. 141, 30–46. https://doi.org/10.1016/j.agwat.2014.04.010

O'Neill, B.C., Tebaldi, C., Van Vuuren, D.P., Eyring, V., Friedlingstein, P., Hurtt, G., Knutti, R., Kriegler, E., Lamarque, J.F., Lowe, J., Meehl, G.A., Moss, R., Riahi, K., Sanderson, B.M., 2016. The Scenario Model Intercomparison Project (ScenarioMIP) for CMIP6. Geosci. Model Dev. 9, 3461–3482. https://doi.org/10.5194/gmd-9-3461-2016

OECD, 2023. Agricultural Policy Monitoring and Evaluation, OECD Publishing. OECD Publishing, Paris. https://doi.org/10.1787/b14de474-en

OECD, FAO, 2016. Agriculture in Sub-Saharan Africa : Prospects and challenges, OECD-FAO Agricultural Outlook 2016-2025.

Ofori, S.A., Cobbina, S.J., Obiri, S., 2021. Climate Change, Land, Water, and Food Security: Perspectives From Sub-Saharan Africa. Front. Sustain. Food Syst. 5, 1–9. https://doi.org/10.3389/fsufs.2021.680924

Omay, P.O., Muthama, N.J., Oludhe, C., Kinama, J.M., Artan, G., Atheru, Z., 2023. Changes and variability in rainfall onset, cessation, and length of rainy season in the IGAD region of Eastern Africa. Theor. Appl. Climatol. 152, 871–893. https://doi.org/10.1007/s00704-023-04433-0

Omotosho, J.B., Balogun, A.A., Ogunjobi, K., 2000. Predicting monthly and seasonal rainfall, onset and cessation of the rainy season in West Africa using only surface data. Int. J. Climatol. 20, 865–880. https://doi.org/10.1002/1097-0088(20000630)20:8<865::AID-JOC505>3.0.CO;2-R

Paff, K., Asseng, S., 2018. A review of tef physiology for developing a tef crop model. Eur. J. Agron. 94, 54–66. https://doi.org/10.1016/j.eja.2018.01.008

Palmer, P.I., Wainwright, C.M., Dong, B., Maidment, R.I., Wheeler, K.G., Gedney, N., Hickman, J.E., Madani, N., Folwell, S.S., Abdo, G., Allan, R.P., Black, E.C.L., Feng, L., Gudoshava, M., Haines, K., Huntingford, C., Kilavi, M., Lunt, M.F., Shaaban, A., Turner, A.G., 2023. Drivers and impacts of Eastern African rainfall variability. Nat. Rev. Earth Environ. 4. https://doi.org/10.1038/s43017-023-00397-x

Pan, J., Sharif, R., Xu, X., Chen, X., 2021. Mechanisms of Waterlogging Tolerance in Plants: Research Progress and Prospects. Front. Plant Sci. 11. https://doi.org/10.3389/fpls.2020.627331

Park, S., Chun, J.A., Kim, D., Sitthikone, M., 2022. Climate risk management for the rainfed rice yield in Lao PDR using APCC MME seasonal forecasts. Agric. Water Manag. 274, 107976. https://doi.org/10.1016/j.agwat.2022.107976

Pascale, S., Lucarini, V., Feng, X., Porporato, A., ul Hasson, S., 2016. Projected changes of rainfall seasonality and dry spells in a high greenhouse gas emissions scenario. Clim. Dyn. 46, 1331–1350. https://doi.org/10.1007/s00382-015-2648-4

Pecl, G.T., Araújo, M.B., Bell, J.D., Blanchard, J., Bonebrake, T.C., Chen, I.C., Clark, T.D., Colwell, R.K., Danielsen, F., Evengård, B., Falconi, L., Ferrier, S., Frusher, S., Garcia, R.A., Griffis, R.B., Hobday, A.J., Janion-Scheepers, C., Jarzyna, M.A., Jennings, S., Lenoir, J., Linnetved, H.I., Martin, V.Y., McCormack, P.C., McDonald, J., Mitchell, N.J., Mustonen, T., Pandolfi, J.M., Pettorelli, N., Popova, E., Robinson, S.A., Scheffers, B.R., Shaw, J.D., Sorte, C.J.B., Strugnell, J.M., Sunday, J.M., Tuanmu, M.N., Vergés, A., Villanueva, C., Wernberg, T., Wapstra, E., Williams, S.E., 2017. Biodiversity redistribution under climate change: Impacts on ecosystems and human well-being. Science (80-.). 355. https://doi.org/10.1126/science.aai9214

Peleg, N., Molnar, P., Burlando, P., Fatichi, S., 2019. Exploring stochastic climate uncertainty in space and time using a gridded hourly weather generator. J. Hydrol. 571, 627–641. https://doi.org/10.1016/j.jhydrol.2019.02.010

Peng, B., Guan, K., 2021. Harmonizing climate-smart and sustainable agriculture. Nat. Food 2, 853–854. https://doi.org/10.1038/s43016-021-00407-5

Peng, B., Guan, K., Tang, J., Ainsworth, E.A., Asseng, S., Bernacchi, C.J., Cooper, M., Delucia, E.H., Elliott, J.W., Ewert, F., Grant, R.F., Gustafson, D.I., Hammer, G.L., Jin, Z., Jones, J.W., Kimm, H., Lawrence, D.M., Li, Y., Lombardozzi, D.L., Marshall-Colon, A., Messina, C.D., Ort, D.R., Schnable, J.C., Vallejos, C.E., Wu, A., Yin, X., Zhou, W., 2020. Towards a multiscale crop modelling framework for climate change adaptation assessment. Nat. Plants 6, 338–348. https://doi.org/10.1038/s41477-020-0625-3

Peng, W., Ma, N.L., Zhang, D., Zhou, Q., Yue, X., Khoo, S.C., Yang, H., Guan, R., Chen, H., Zhang, X., Wang, Y., Wei, Z., Suo, C., Peng, Y., Yang, Y., Lam, S.S., Sonne, C., 2020. A review of historical and recent locust outbreaks: Links to global warming, food security and mitigation strategies. Environ. Res. 191, 110046. https://doi.org/10.1016/j.envres.2020.110046

Philip, S., Kew, S.F., van Oldenborgh, G.J., Otto, F., O'Keefe, S., Haustein, K., King, A., Zegeye, A., Eshetu, Z., Hailemariam, K., Singh, R., Jjemba, E., Funk, C., Cullen, H., 2018. Attribution analysis of the Ethiopian drought of 2015. J. Clim. 31, 2465–2486. https://doi.org/10.1175/JCLI-D-17-0274.1

Pierce, D.W., Cayan, D.R., Maurer, E.P., Abatzoglou, J.T., Hegewisch, K.C., 2015. Improved bias correction techniques for hydrological simulations of climate change. J. Hydrometeorol. 16, 2421–2442. https://doi.org/10.1175/JHM-D-14-0236.1

Pittelkow, C.M., Linquist, B.A., Lundy, M.E., Liang, X., van Groenigen, K.J., Lee, J., van Gestel, N., Six, J., Venterea, R.T., van Kessel, C., 2015. When does no-till yield more? A global meta-analysis. F. Crop. Res. 183, 156–168. https://doi.org/10.1016/j.fcr.2015.07.020

Poggio, L., De Sousa, L.M., Batjes, N.H., Heuvelink, G.B.M., Kempen, B., Ribeiro, E., Rossiter, D., 2021. SoilGrids 2.0: Producing soil information for the globe with quantified spatial uncertainty. Soil 7, 217–240. https://doi.org/10.5194/soil-7-217-2021

Poore, J., Nemecek, T., 2018. Reducing food's environmental impacts through producers and consumers. Science (80-.). 360, 987–992. https://doi.org/10.1126/science.aaq0216

Porkka, M., Wang-Erlandsson, L., Destouni, G., Ekman, A.M.L., Rockström, J., Gordon, L.J., 2021. Is wetter better? Exploring agriculturally-relevant rainfall characteristics over four decades in the Sahel. Environ. Res. Lett. 16. https://doi.org/10.1088/1748-9326/abdd57

Porporato, A., Daly, E., Rodriguez-Iturbe, I., 2004. Soil water balance and ecosystem response to climate change. Am. Nat. 164, 625–632. https://doi.org/10.1086/424970

Porras, R., Miguel-Rojas, C., Lorite, I.J., Pérez-de-Luque, A., Sillero, J.C., 2023. Characterization of Durum Wheat Resistance against Septoria Tritici Blotch under

Climate Change Conditions of Increasing Temperature and CO2 Concentration. Agronomy 13, 1–14. https://doi.org/10.3390/agronomy13102638

Potter, N.J., Zhang, L., Milly, P.C.D., McMahon, T.A., Jakeman, A.J., 2005. Effects of rainfall seasonality and soil moisture capacity on mean annual water balance for Australian catchments. Water Resour. Res. 41, 1–11. https://doi.org/10.1029/2004WR003697

Pradhan, R.K., Markonis, Y., Vargas Godoy, M.R., Villalba-Pradas, A., Andreadis, K.M., Nikolopoulos, E.I., Papalexiou, S.M., Rahim, A., Tapiador, F.J., Hanel, M., 2022. Review of GPM IMERG performance: A global perspective. Remote Sens. Environ. 268, 112754. https://doi.org/10.1016/j.rse.2021.112754

Prasad, P.V.V., Djanaguiraman, M., Stewart, Z.P., Ciampitti, I.A., 2018. Agroclimatology of maize, sorghum, and pearl millet. Agroclimatology 201–241. https://doi.org/10.2134/agronmonogr60.2016.0005

Prăvălie, R., Patriche, C., Borrelli, P., Panagos, P., Roșca, B., Dumitrașcu, M., Nita, I.A., Săvulescu, I., Birsan, M.V., Bandoc, G., 2021. Arable lands under the pressure of multiple land degradation processes. A global perspective. Environ. Res. 194. https://doi.org/10.1016/j.envres.2020.110697

Qayyum, M.F., Liaquat, F., Rehman, R.A., Gul, M., ul Hye, M.Z., Rizwan, M., Rehaman, M.Z. ur, 2017. Effects of co-composting of farm manure and biochar on plant growth and carbon mineralization in an alkaline soil. Environ. Sci. Pollut. Res. 24, 26060–26068. https://doi.org/10.1007/s11356-017-0227-4

Qureshi, A.S., Mohammed, M., Daba, A.W., Hailu, B., Belay, G., Tesfaye, A., Ertebo, T.M., 2019. Improving agricultural productivity on salt-affected soils in Ethiopia: Farmers perceptions and proposals. African J. Agric. Res. 14, 897–906. https://doi.org/10.5897/AJAR2019.14077

Radeny, M., Desalegn, A., Mubiru, D., Kyazze, F., Mahoo, H., Recha, J., Kimeli, P., Solomon, D., 2019. Indigenous knowledge for seasonal weather and climate forecasting across East Africa. Clim. Change 156, 509–526. https://doi.org/10.1007/s10584-019-02476-9

Raes, D., Sithole, A., Makarau, A., Milford, J., 2004. Evaluation of first planting dates recommended by criteria currently used in Zimbabwe. Agric. For. Meteorol. 125, 177–185. https://doi.org/10.1016/j.agrformet.2004.05.001

Raes, D., Steduto, P., Hsiao, T.C., Fereres, E., 2022. AquaCrop Version 7.1 Reference manual. Rome.

Raes, D., Steduto, P., Hsiao, T.C., Fereres, E., 2009. Aquacrop-The FAO crop model to simulate yield response to water: II. main algorithms and software description. Agron. J. 101, 438–447. https://doi.org/10.2134/agronj2008.0140s

Raes, D., Waongo, M., Vanuytrecht, E., Mejias Moreno, P., 2021. Improved management may alleviate some but not all of the adverse effects of climate change on crop yields in smallholder farms in West Africa. Agric. For. Meteorol. 308–309, 108563. https://doi.org/10.1016/j.agrformet.2021.108563

Rajczak, J., Kotlarski, S., Schär, C., 2016. Does quantile mapping of simulated precipitation correct for biases in transition probabilities and spell lengths? J. Clim. 29, 1605–1615. https://doi.org/10.1175/JCLI-D-15-0162.1

Raleigh, C., Kniveton, D., 2012. Come rain or shine: An analysis of conflict and climate variability in East Africa. J. Peace Res. 49, 51–64. https://doi.org/10.1177/0022343311427754

Ramankutty, N., Foley, J.A., Norman, J., McSweeney, K., 2002. The global distribution of cultivable lands: Current patterns and sensitivity to possible climate change. Glob. Ecol. Biogeogr. 11, 377–392. https://doi.org/10.1046/j.1466-822x.2002.00294.x

Ramirez-Cabral, N.Y.Z., Kumar, L., Shabani, F., 2017. Global alterations in areas of suitability for maize production from climate change and using a mechanistic species distribution model (CLIMEX). Sci. Rep. 7, 1–13. https://doi.org/10.1038/s41598-017-05804-0

Ramirez-Villegas, J., Jarvis, A., Läderach, P., 2013. Empirical approaches for assessing impacts of climate change on agriculture: The EcoCrop model and a case study with grain sorghum. Agric. For. Meteorol. 170, 67–78. https://doi.org/10.1016/j.agrformet.2011.09.005

Ramirez-Villegas, J., Koehler, A.K., Challinor, A.J., 2017. Assessing uncertainty and complexity in regional-scale crop model simulations. Eur. J. Agron. 88, 84–95. https://doi.org/10.1016/j.eja.2015.11.021

Rattalino Edreira, J.I., Andrade, J.F., Cassman, K.G., van Ittersum, M.K., van Loon, M.P., Grassini, P., 2021. Spatial frameworks for robust estimation of yield gaps. Nat. Food 2, 773–779. https://doi.org/10.1038/s43016-021-00365-y

Rezaei, E.E., Webber, H., Asseng, S., Boote, K., Durand, J.L., Ewert, F., Martre, P., MacCarthy, D.S., 2023. Climate change impacts on crop yields. Nat. Rev. Earth Environ. 4, 16. https://doi.org/10.1038/s43017-023-00491-0

RICCAR, 2022. Guidelines on the use of climate data for improving agricultural productivity. Lebanon.

Ringersma, J., Batjes, N., Dent, D., 2003. Green Water: definitions and data for assessment, ISRIC – World Soil Information.

Ritchie, H., Rosado, P., Roser, M., 2023. Agricultural Production [WWW Document]. Our World Data. URL https://ourworldindata.org/agricultural-production

Rockström, J., 2003. Water for food and nature in drought-prone tropics: Vapour shift in rain-fed agriculture. Philos. Trans. R. Soc. B Biol. Sci. 358, 1997–2009. https://doi.org/10.1098/rstb.2003.1400

Rockström, J., 1999. On-farm green water estimates as a tool for increased food production in water scarce regions. Phys. Chem. Earth, Part B Hydrol. Ocean. Atmos. 24, 375–383. https://doi.org/10.1016/S1464-1909(99)00016-7

Rockström, J., Falkenmark, M., 2000. Semiarid crop production from a hydrological perspective: Gap between potential and actual yields. CRC. Crit. Rev. Plant Sci. 19, 319–346. https://doi.org/10.1080/07352680091139259

Rockström, J., Falkenmark, M., Karlberg, L., Hoff, H., Rost, S., Gerten, D., 2009. Future water availability for global food production: The potential of green water for increasing resilience to global change. Water Resour. Res. 45, 1–16. https://doi.org/10.1029/2007WR006767

Rockström, J., Gordon, L., 2001. Assessment of Green Water Flows to Sustain Major Biomes of the World: Implications for Future Ecohydrological Landscape Management. Phys. Chem. Earth, Part B Hydrol. Ocean. Atmos. 26, 843–851. https://doi.org/10.1016/S1464-1909(01)00096-X

Rockström, J., Karlberg, L., Wani, S.P., Barron, J., Hatibu, N., Oweis, T., Bruggeman, A., Farahani, J., Qiang, Z., 2010. Managing water in rainfed agriculture-The need for a paradigm shift. Agric. Water Manag. 97, 543–550. https://doi.org/10.1016/j.agwat.2009.09.009

Rohr, T., Manzoni, S., Feng, X., Menezes, R.S.C., Porporato, A., 2013. Effect of rainfall seasonality on carbon storage in tropical dry ecosystems. J. Geophys. Res. Biogeosciences 118, 1156–1167. https://doi.org/10.1002/jgrg.20091

Rong, L. bing, Gong, K. yuan, Duan, F. ying, Li, S. kun, Zhao, M., He, J., Zhou, W. bin, Yu, Q., 2021. Yield gap and resource utilization efficiency of three major food crops in the world – A review. J. Integr. Agric. 20, 349–362. https://doi.org/10.1016/S2095-3119(20)63555-9

Rosa, L., Chiarelli, D.D., Rulli, M.C., Dell'Angelo, J., D'Odorico, P., 2020. Global agricultural economic water scarcity. Sci. Adv. 6, 1–11. https://doi.org/10.1126/sciadv.aaz6031

Rosa, L., Rulli, M.C., Davis, K.F., Chiarelli, D.D., Passera, C., D'Odorico, P., 2018. Closing the yield gap while ensuring water sustainability. Environ. Res. Lett. 13. https://doi.org/10.1088/1748-9326/aadeef

Rosenzweig, C., Elliott, J., Deryng, D., Ruane, A.C., Müller, C., Arneth, A., Boote, K.J., Folberth, C., Glotter, M., Khabarov, N., Neumann, K., Piontek, F., Pugh, T.A.M., Schmid, E., Stehfest, E., Yang, H., Jones, J.W., 2014. Assessing agricultural risks of climate change in the 21st century in a global gridded crop model intercomparison. Proc. Natl. Acad. Sci. U. S. A. 111, 3268–3273. https://doi.org/10.1073/pnas.1222463110

Ross, C.W., Prihodko, L., Anchang, J., Kumar, S., Ji, W., Hanan, N.P., 2018. HYSOGs250m, global gridded hydrologic soil groups for curve-number-based runoff modeling. Sci. data 5, 180091. https://doi.org/10.1038/sdata.2018.91

Ruffault, J., Martin-StPaul, N.K., Duffet, C., Goge, F., Mouillot, F., 2013. Projecting future drought in Mediterranean forests: Bias correction of climate models matters! Theor. Appl. Climatol. 117, 113–122. https://doi.org/10.1007/s00704-013-0992-z

Rui, H.L., Beaudoing, H., 2020. README Document for NASA GLDAS Version 2 Data

Products. Goddard Earth Sci. Data Inf. Serv. Cent. (GES DISC).

Rutherford, A.S., 2008. Broad bed maker technology package innovations in Ethiopian farming systems: An. Nairobi.

Sadiq, A.A., 2020. An estimation of rainfall seasonality index of Yola south LGA and its effects on agriculture and environment. African J. Environ. Nat. Sci. Res. 3, 57–72.

Saha, S., Moorthi, S., Pan, H.L., Wu, X., Wang, J.J., Nadiga, S., Tripp, P., Kistler, R., Woollen, J., Behringer, D., Liu, H., Stokes, D., Grumbine, R., Gayno, G., Wang, J.J., Hou, Y.T., Chuang, H.Y., Juang, H.M.H., Sela, J., Iredell, M., Treadon, R., Kleist, D., Van Delst, P., Keyser, D., Derber, J., Ek, M., Meng, J., Wei, H., Yang, R., Lord, S., Van Den Dool, H., Kumar, A., Wang, W., Long, C., Chelliah, M., Xue, Y., Huang, B., Schemm, J.K., Ebisuzaki, W., Lin, R., Xie, P., Chen, M., Zhou, S., Higgins, W., Zou, C.Z., Liu, Q., Chen, Y., Han, Y., Cucurull, L., Reynolds, R.W., Rutledge, G., Goldberg, M., 2010. The NCEP climate forecast system reanalysis. Bull. Am. Meteorol. Soc. 91, 1015–1057. https://doi.org/10.1175/2010BAMS3001.1

Sarr, M.A., Seidou, O., Tramblay, Y., El Adlouni, S., 2015. Comparison of downscaling methods for mean and extreme precipitation in Senegal. J. Hydrol. Reg. Stud. 4, 369–385. https://doi.org/10.1016/j.ejrh.2015.06.005

Saxton, K.E., Rawls, W.J., 2006. Soil Water Characteristic Estimates by Texture and Organic Matter for Hydrologic Solutions. Soil Sci. Soc. Am. J. 70, 1569–1578. https://doi.org/10.2136/sssaj2005.0117

Schlenker, W., Lobell, D.B., 2010. Robust negative impacts of climate change on African agriculture. Environ. Res. Lett. 5. https://doi.org/10.1088/1748-9326/5/1/014010

Schmidhuber, J., Tubiello, F.N., 2007. Global food security under climate change. Proc. Natl. Acad. Sci. U. S. A. 104, 19703–19708. https://doi.org/10.1073/pnas.0701976104

Schneider, J.M., Zabel, F., Mauser, W., 2022a. Global inventory of suitable, cultivable and available cropland under different scenarios and policies. Sci. Data 9, 1–14. https://doi.org/10.1038/s41597-022-01632-8

Schneider, J.M., Zabel, F., Schünemann, F., Delzeit, R., Mauser, W., 2022b. Global cropland could be almost halved: Assessment of land saving potentials under different strategies and implications for agricultural markets. PLoS One 17, 1–26. https://doi.org/10.1371/journal.pone.0263063

Schneider, L., Rebetez, M., Rasmann, S., 2022. The effect of climate change on invasive crop pests across biomes. Curr. Opin. Insect Sci. 50, 1–5. https://doi.org/10.1016/j.cois.2022.100895

Schuol, J., Abbaspour, K.C., Yang, H., Srinivasan, R., Zehnder, A.J.B., 2008. Modeling blue and green water availability in Africa. Water Resour. Res. 44, 1–18. https://doi.org/10.1029/2007WR006609

Schwartz, R.C., Domínguez, A., Pardo, J.J., Colaizzi, P.D., Baumhardt, R.L., Bell, J.M., 2020.

A crop coefficient –based water use model with non-uniform root distribution. Agric. Water Manag. 228, 105892. https://doi.org/10.1016/j.agwat.2019.105892

Segele, Z.T., Lamb, P.J., 2005. Characterization and variability of Kiremt rainy season over Ethiopia. Meteorol. Atmos. Phys. 89, 153–180. https://doi.org/10.1007/s00703-005-0127-x

Segele, Z.T., Lamb, P.J., Leslie, L.M., 2009a. Seasonal-to-interannual variability of Ethiopia/horn of Africa monsoon. Part I: Associations of wavelet-filtered large-scale atmospheric circulation and global sea surface temperature. J. Clim. 22, 3396–3421. https://doi.org/10.1175/2008JCLI2859.1

Segele, Z.T., Lamb, P.J., Leslie, L.M., 2009b. Large-scale atmospheric circulation and global sea surface temperature associations with Horn of Africa June–September rainfall. Int. J. Climatol. 29, 1075–1100. https://doi.org/DOI: 10.1002/joc.1751

Segele, Z.T., Richman, M.B., Leslie, L.M., Lamb, P.J., 2015. Seasonal-to-interannual variability of ethiopia/horn of Africa monsoon. Part II: Statistical multimodel ensemble rainfall predictions. J. Clim. 28, 3511–3536. https://doi.org/10.1175/JCLI-D-14-00476.1

Seid, Mulugeta M; Narayanan, K., 2015. Effect of Deficit Irrigation on Maize under Conventional, Fixed and Alternate Furrow Irrigation Systems at Melkassa, Ethiopia. Int. J. Eng. Res. V4, 119–126. https://doi.org/10.17577/ijertv4is110178

Seland, Ø., Bentsen, M., Olivié, D., Toniazzo, T., Gjermundsen, A., Graff, L.S., Debernard, J.B., Gupta, A.K., He, Y.C., Kirkeväg, A., Schwinger, J., Tjiputra, J., Schanke Aas, K., Bethke, I., Fan, Y., Griesfeller, J., Grini, A., Guo, C., Ilicak, M., Karset, I.H.H., Landgren, O., Liakka, J., Moseid, K.O., Nummelin, A., Spensberger, C., Tang, H., Zhang, Z., Heinze, C., Iversen, T., Schulz, M., 2020. Overview of the Norwegian Earth System Model (NorESM2) and key climate response of CMIP6 DECK, historical, and scenario simulations, Geoscientific Model Development. https://doi.org/10.5194/gmd-13-6165-2020

Seleshi, Y., Camberlin, P., 2006. Recent changes in dry spell and extreme rainfall events in Ethiopia. Theor. Appl. Climatol. 83, 181–191. https://doi.org/10.1007/s00704-005-0134-3

Seleshi, Y., Zanke, U., 2004. Recent changes in rainfall and rainy days in Ethiopia. Int. J. Climatol. 24, 973–983. https://doi.org/10.1002/joc.1052

Sellar, A.A., Jones, C.G., Mulcahy, J.P., Tang, Y., Yool, A., Wiltshire, A., O'Connor, F.M., Stringer, M., Hill, R., Palmieri, J., Woodward, S., de Mora, L., Kuhlbrodt, T., Rumbold, S.T., Kelley, D.I., Ellis, R., Johnson, C.E., Walton, J., Abraham, N.L., Andrews, M.B., Andrews, T., Archibald, A.T., Berthou, S., Burke, E., Blockley, E., Carslaw, K., Dalvi, M., Edwards, J., Folberth, G.A., Gedney, N., Griffiths, P.T., Harper, A.B., Hendry, M.A., Hewitt, A.J., Johnson, B., Jones, A., Jones, C.D., Keeble, J., Liddicoat, S., Morgenstern, O., Parker, R.J., Predoi, V., Robertson, E., Siahaan, A., Smith, R.S., Swaminathan, R., Woodhouse, M.T., Zeng, G., Zerroukat, M., 2019. UKESM1: Description and Evaluation of the U.K. Earth System Model. J. Adv. Model. Earth Syst. 11, 4513–4558. https://doi.org/10.1029/2019MS001739

Semmler, T., Danilov, S., Gierz, P., Goessling, H.F., Hegewald, J., Hinrichs, C., Koldunov, N., Khosravi, N., Mu, L., Rackow, T., Sein, D. V., Sidorenko, D., Wang, Q., Jung, T., 2020. Simulations for CMIP6 With the AWI Climate Model AWI-CM-1-1. J. Adv. Model. Earth Syst. 12, 1–34. https://doi.org/10.1029/2019MS002009

Sen, P.K., 1968. Estimates of the Regression Coefficient Based on Kendall's Tau. J. Am. Stat. Assoc. 63, 1379–1389. https://doi.org/10.1080/01621459.1968.10480934

Senay, G.B., Kagone, S., Velpuri, N.M., 2020. Operational Global Actual Evapotranspiration : Sensors.

Setu, T., Legese, T., Teklie, G., Gebeyhu, B., 2023. Effect of furrow irrigation systems and irrigation levels on maize agronomy and water use efficiency in Arba Minch, Southern, Ethiopia. Heliyon 9, e17833. https://doi.org/10.1016/j.heliyon.2023.e17833

Shanko, D., Camberlin, P., 1998. The effects of the southwest Indian ocean tropical cyclones on Ethiopian drought. Int. J. Climatol. 18, 1373–1388. https://doi.org/10.1002/(SICI)1097-0088(1998100)18:12<1373::AID-JOC313>3.0.CO;2-K

Sheffield, J., Goteti, G., Wood, E.F., 2006. Development of a 50-year high-resolution global dataset of meteorological forcings for land surface modeling. J. Clim. 19, 3088–3111. https://doi.org/10.1175/JCLI3790.1

Sheffield, J., Wood, E.F., Pan, M., Beck, H., Coccia, G., Serrat-Capdevila, A., Verbist, K., 2018. Satellite Remote Sensing for Water Resources Management: Potential for Supporting Sustainable Development in Data-Poor Regions. Water Resour. Res. 54, 9724–9758. https://doi.org/10.1029/2017WR022437

Shikur, Z.H., 2020. Agricultural policies, agricultural production and rural households' welfare in Ethiopia. J. Econ. Struct. 9. https://doi.org/10.1186/s40008-020-00228-y

Shukla, R., Gleixner, S., Yalew, A.W., Schauberger, B., Sietz, D., Gornott, C., 2021. Dynamic vulnerability of smallholder agricultural systems in the face of climate change for Ethiopia. Environ. Res. Lett. 16. https://doi.org/10.1088/1748-9326/abdb5c

Siad, S.M., Iacobellis, V., Zdruli, P., Gioia, A., Stavi, I., Hoogenboom, G., 2019. A review of coupled hydrologic and crop growth models. Agric. Water Manag. 224, 105746. https://doi.org/10.1016/j.agwat.2019.105746

Simpson, N.P., Andrews, T.M., Krönke, M., Lennard, C., Odoulami, R.C., Ouweneel, B., Steynor, A., Trisos, C.H., 2021. Climate change literacy in Africa. Nat. Clim. Chang. 11, 937–944. https://doi.org/10.1038/s41558-021-01171-x

Singh, B.K., Delgado-Baquerizo, M., Egidi, E., Guirado, E., Leach, J.E., Liu, H., Trivedi, P., 2023. Climate change impacts on plant pathogens, food security and paths forward. Nat. Rev. Microbiol. 21, 640–656. https://doi.org/10.1038/s41579-023-00900-7

Siraw, Z., Bewket, W., Adnew Degefu, M., 2020. Assessment of livelihood benefits of community-based watershed development in northwestern highlands of Ethiopia. Int. J.

River Basin Manag. 18, 395–405. https://doi.org/10.1080/15715124.2018.1505733

Sloat, L.L., Davis, S.J., Gerber, J.S., Moore, F.C., Ray, D.K., West, P.C., Mueller, N.D., 2020. Climate adaptation by crop migration. Nat. Commun. 11, 1–9. https://doi.org/10.1038/s41467-020-15076-4

Smedema, L.K., Rycroft, D.W., 1983. Land drainage: planning and design of agricultural drainage systems. 0, 183–184. https://doi.org/10.1016/0378-3774(85)90006-x

Sobol', I.M., Tarantola, S., Gatelli, D., Kucherenko, S.S., Mauntz, W., 2007. Estimating the approximation error when fixing unessential factors in global sensitivity analysis. Reliab. Eng. Syst. Saf. 92, 957–960. https://doi.org/10.1016/j.ress.2006.07.001

Souza, R., Feng, X., Antonino, A., Montenegro, S., Souza, E., Porporato, A., 2016. Vegetation response to rainfall seasonality and interannual variability in tropical dry forests. Hydrol. Process. 30, 3583–3595. https://doi.org/10.1002/hyp.10953

Spinoni, J., Vogt, J., Naumann, G., Carrao, H., Barbosa, P., 2015. Towards identifying areas at climatological risk of desertification using the Köppen-Geiger classification and FAO aridity index. Int. J. Climatol. 35, 2210–2222. https://doi.org/10.1002/joc.4124

Sposito, G., 2013. Green Water and Global Food Security. Vadose Zo. J. 12, 1–6. https://doi.org/10.2136/vzj2013.02.0041

Steduto, P., Hsiao, T.C., Fereres, E., Raes, D., 2012. Crop yield response to water (No. 66), FAO Irrigation and Drainage paper.

Steduto, P., Hsiao, T.C., Raes, D., Fereres, E., 2009. Aquacrop-the FAO crop model to simulate yield response to water: I. concepts and underlying principles. Agron. J. 101, 426–437. https://doi.org/10.2134/agronj2008.0139s

Stöckle, C.O., Donatelli, M., Nelson, R., 2003. CropSyst, a cropping systems simulation model. Eur. J. Agron. 18, 289–307. https://doi.org/10.1016/S1161-0301(02)00109-0

Studer, C., 2021. Water management for rainfed smallholder farming, in: The Sustainable Intensification of Smallholder Farming Systems. Burleigh Dodds Science Publishing Limited, pp. 67–131. https://doi.org/10.19103/AS.2020.0080.09

Suepa, T., Qi, J., Lawawirojwong, S., Messina, J.P., 2016. Understanding spatio-temporal variation of vegetation phenology and rainfall seasonality in the monsoon Southeast Asia. Environ. Res. 147, 621–629. https://doi.org/10.1016/j.envres.2016.02.005

Suhairi, T.A.S.T.M., Jahanshiri, E., Nizar, N.M.M., 2018. Multicriteria land suitability assessment for growing underutilised crop, bambara groundnut in Peninsular Malaysia. IOP Conf. Ser. Earth Environ. Sci. 169. https://doi.org/10.1088/1755-1315/169/1/012044

Sutherst, R.W., 2003. Prediction of species geographical ranges. J. Biogeogr. 30, 805–816. https://doi.org/10.1046/j.1365-2699.2003.00861.x

Tadele, E., Hibistu, T., 2022. Spatial production distribution, economic viability and value chain features of teff in Ethiopia: Systematic review. Cogent Econ. Financ. 10.

https://doi.org/10.1080/23322039.2021.2020484

Taffesse, A.S., Dorosh, P., Gemessa, S.A., 2012. Crop Production in Ethiopia: Regional Patterns and Trends. Summary of Report Ethiopian Strategy Support Program (ESSP II), Research Note 11, IFPRI and EDRI, Addis Ababa, Ethiopia (No. 16).

Tall, A., Coulibaly, J.Y., Diop, M., 2018. Do climate services make a difference? A review of evaluation methodologies and practices to assess the value of climate information services for farmers: Implications for Africa. Clim. Serv. 11, 1–12. https://doi.org/10.1016/j.cliser.2018.06.001

Tang, G., Clark, M.P., Papalexiou, S.M., 2022. EM-Earth: The Ensemble Meteorological Dataset for Planet Earth. Bull. Am. Meteorol. Soc. 103, E996–E1018. https://doi.org/10.1175/bams-d-21-0106.1

Tatebe, H., Ogura, T., Nitta, T., Komuro, Y., Ogochi, K., Takemura, T., Sudo, K., Sekiguchi, M., Abe, M., Saito, F., Chikira, M., Watanabe, S., Mori, M., Hirota, N., Kawatani, Y., Mochizuki, T., Yoshimura, K., Takata, K., O'Ishi, R., Yamazaki, D., Suzuki, T., Kurogi, M., Kataoka, T., Watanabe, M., Kimoto, M., 2019. Description and basic evaluation of simulated mean state, internal variability, and climate sensitivity in MIROC6. Geosci. Model Dev. 12, 2727–2765. https://doi.org/10.5194/gmd-12-2727-2019

Taye, M.A., 2021. Heliyon Agro – ecosystem sensitivity to climate change over the Ethiopian highlands in a watershed of Lake Tana sub – basin. Heliyon 7, e07454. https://doi.org/10.1016/j.heliyon.2021.e07454

Taye, M.T., Dyer, E., Charles, K.J., Hirons, L.C., 2021. Potential predictability of the Ethiopian summer rains: Understanding local variations and their implications for water management decisions. Sci. Total Environ. 755, 142604. https://doi.org/10.1016/j.scitotenv.2020.142604

Tefera, T., 2012. Post-harvest losses in African maize in the face of increasing food shortage. Food Secur. 4, 267–277. https://doi.org/10.1007/s12571-012-0182-3

Temam, D., Uddameri, V., Mohammadi, G., Hernandez, E.A., Ekwaro-Osire, S., 2019. Long-term drought trends in Ethiopia with implications for dryland agriculture. Water (Switzerland) 11, 1–22. https://doi.org/10.3390/w11122571

Temesgen, M., Rockstrom, J., Savenije, H.H.G., Hoogmoed, W.B., Alemu, D., 2008. Determinants of tillage frequency among smallholder farmers in two semi-arid areas in Ethiopia. Phys. Chem. Earth 33, 183–191. https://doi.org/10.1016/j.pce.2007.04.012

Tenzing, J.D., Conway, D., 2023. Does the geographical footprint of Ethiopia ' s flagship social protection programme align with climatic and conflict risks ?

Tesfahunegn, G.B., 2021. Climate change effects on agricultural production : insights for adaptation strategy from the context of smallholder farmers in Dura catchment , northern Ethiopia. GeoJournal 86, 417–430. https://doi.org/10.1007/s10708-019-10077-3

Tesfahunegn, G.B., Mekonen, K., Tekle, A., 2016. Farmers' perception on causes, indicators

and determinants of climate change in northern Ethiopia: Implication for developing adaptation strategies. Appl. Geogr. 73, 1–12. https://doi.org/10.1016/j.apgeog.2016.05.009

Tesfaye, W., Seifu, L., 2016. Climate change perception and choice of adaptation strategies: Empirical evidence from smallholder farmers in east Ethiopia. Int. J. Clim. Chang. Strateg. Manag. 8, 253–270. https://doi.org/10.1108/IJCCSM-01-2014-0017

Teshome, H., Tesfaye, K., Dechassa, N., Tana, T., Huber, M., 2021. Smallholder Farmers ' Perceptions of Climate Change and Adaptation Practices for Maize Production in Eastern Ethiopia 1–21.

Tessema, I., 2021. Smallholder Farmers ' perception and adaptation to climate variability and change in Fincha sub-basin of the Upper Blue Nile River Basin of Ethiopia. GeoJournal 86, 1767–1783. https://doi.org/10.1007/s10708-020-10159-7

Tessema, Y.A., Joerin, J., Patt, A., 2019. Crop switching as an adaptation strategy to climate change: the case of Semien Shewa Zone of Ethiopia. Int. J. Clim. Chang. Strateg. Manag. 11, 358–371. https://doi.org/10.1108/IJCCSM-05-2018-0043

Teutschbein, C., Seibert, J., 2012. Bias correction of regional climate model simulations for hydrological climate-change impact studies: Review and evaluation of different methods. J. Hydrol. 456–457, 12–29. https://doi.org/10.1016/j.jhydrol.2012.05.052

Tierney, J.E., Ummenhofer, C.C., DeMenocal, P.B., 2015. Past and future rainfall in the Horn of Africa. Sci. Adv. 1, 1–9. https://doi.org/10.1126/sciadv.1500682

Tilman, D., Balzer, C., Hill, J., Befort, B.L., 2011. Global food demand and the sustainable intensification of agriculture. Proc. Natl. Acad. Sci. U. S. A. 108, 20260–20264. https://doi.org/10.1073/pnas.1116437108

Tim Wheeler, Braun, J. von, 2013. Climate Change Impacts on Global Food Security. Science (80-.). 341, 1773–1775. https://doi.org/10.1126/science.1237190

Tittonell, P., Giller, K.E., 2013. When yield gaps are poverty traps: The paradigm of ecological intensification in African smallholder agriculture. F. Crop. Res. 143, 76–90. https://doi.org/10.1016/j.fcr.2012.10.007

Torres, M., Howitt, R., Rodrigues, L., 2019. Analyzing rainfall effects on agricultural income: Why timing matters. EconomiA 20, 1–14. https://doi.org/10.1016/j.econ.2019.03.006

Trisos, C.H., Adelekan, I.O., Totin, E., Ayanlade, A., Efitre, J., Gemeda, A., Kalaba, K., Lennard, C., Masao, C., Mgaya, Y., Ngaruiya, G., Olago, D., Simpson, N.P., Zakieldeen, S., 2022. Africa, in: Climate Change 2022: Impacts, Adaptation and Vulnerability. pp. 1285–1455. https://doi.org/10.1017/9781009325844.011.1286

UN, 2015. Transforming our world: the 2030 Agenda for Sustainable Development (No. A/RES/70/1). New York.

UNDP, OPHI, 2023. Global multi-dimensional poverty index 2023 Unstacking global

poverty : Data for high impact action. Oxford Poverty Hum. Dev. Initiat. 1–2.

UNFCCC, 2021. Progress in the Formulation and Implementation of Naps.

USDA, 1985. Urban Hydrology for Small Watersheds.

van Diepen, C.A., Wolf, J., van Keulen, H., Rappoldt, C., 1989. WOFOST: a simulation model of crop production. Soil Use Manag. 5, 16–24. https://doi.org/10.1111/j.1475-2743.1989.tb00755.x

van Dijk, M., Morley, T., van Loon, M., Reidsma, P., Tesfaye, K., van Ittersum, M.K., 2020. Reducing the maize yield gap in Ethiopia: Decomposition and policy simulation. Agric. Syst. 183. https://doi.org/10.1016/j.agsy.2020.102828

van Etten, J., de Sousa, K., Aguilar, A., Barrios, M., Coto, A., Dell'Acqua, M., Fadda, C., Gebrehawaryat, Y., van de Gevel, J., Gupta, A., Kiros, A.Y., Madriz, B., Mathur, P., Mengistu, D.K., Mercado, L., Mohammed, J.N., Paliwal, A., Pè, M.E., Quirós, C.F., Rosas, J.C., Sharma, N., Singh, S.S., Solanki, I.S., Steinke, J., 2019. Crop variety management for climate adaptation supported by citizen science. Proc. Natl. Acad. Sci. U. S. A. 116, 4194–4199. https://doi.org/10.1073/pnas.1813720116

Van Groenigen, K.J., Six, J., Hungate, B.A., De Graaff, M.A., Van Breemen, N., Van Kessel, C., 2006. Element interactions limit soil carbon storage. Proc. Natl. Acad. Sci. U. S. A. 103, 6571–6574. https://doi.org/10.1073/pnas.0509038103

van Ittersum, M.K., Cassman, K.G., Grassini, P., Wolf, J., Tittonell, P., Hochman, Z., 2013. Yield gap analysis with local to global relevance-A review. F. Crop. Res. 143, 4–17. https://doi.org/10.1016/j.fcr.2012.09.009

Van Ittersum, M.K., Van Bussel, L.G.J., Wolf, J., Grassini, P., Van Wart, J., Guilpart, N., Claessens, L., De Groot, H., Wiebe, K., Mason-D'Croz, D., Yang, H., Boogaard, H., Van Oort, P.A.J., Van Loon, M.P., Saito, K., Adimo, O., Adjei-Nsiah, S., Agali, A., Bala, A., Chikowo, R., Kaizzi, K., Kouressy, M., Makoi, J.H.J.R., Ouattara, K., Tesfaye, K., Cassman, K.G., 2016. Can sub-Saharan Africa feed itself? Proc. Natl. Acad. Sci. U. S. A. 113, 14964–14969. https://doi.org/10.1073/pnas.1610359113

Van Looy, K., Bouma, J., Herbst, M., Koestel, J., Minasny, B., Mishra, U., Montzka, C., Nemes, A., Pachepsky, Y.A., Padarian, J., Schaap, M.G., Tóth, B., Verhoef, A., Vanderborght, J., van der Ploeg, M.J., Weihermüller, L., Zacharias, S., Zhang, Y., Vereecken, H., 2017. Pedotransfer Functions in Earth System Science: Challenges and Perspectives. Rev. Geophys. 55, 1199–1256. https://doi.org/10.1002/2017RG000581

Verdin, A., Funk, C., Peterson, P., Landsfeld, M., Tuholske, C., Grace, K., 2020. Development and validation of the CHIRTS-daily quasi-global high-resolution daily temperature data set. Sci. Data 7, 1–14. https://doi.org/10.1038/s41597-020-00643-7

Victor, U.S., Srivastava, N.N., Subba Rao, A.V.M., Ramana Rao, B. V., 1996. Managing the impact of seasonal rainfall variability through response farming at a semi-arid tropical location. Curr. Sci. 71, 392–397.

Viste, E., Korecha, D., Sorteberg, A., 2013. Recent drought and precipitation tendencies in Ethiopia. Theor. Appl. Climatol. 112, 535–551. https://doi.org/10.1007/s00704-012-0746-3

Viste, E., Sorteberg, A., 2013. Moisture transport into the Ethiopian highlands. Int. J. Climatol. 33, 249–263. https://doi.org/10.1002/joc.3409

Vogel, C., Steynor, A., Manyuchi, A., 2019. Climate services in Africa: Re-imagining an inclusive, robust and sustainable service. Clim. Serv. 15, 100107. https://doi.org/10.1016/j.cliser.2019.100107

Voldoire, A., Saint-Martin, D., Sénési, S., Decharme, B., Alias, A., Chevallier, M., Colin, J., Guérémy, J.F., Michou, M., Moine, M.P., Nabat, P., Roehrig, R., Salas y Mélia, D., Séférian, R., Valcke, S., Beau, I., Belamari, S., Berthet, S., Cassou, C., Cattiaux, J., Deshayes, J., Douville, H., Ethé, C., Franchistéguy, L., Geoffroy, O., Lévy, C., Madec, G., Meurdesoif, Y., Msadek, R., Ribes, A., Sanchez-Gomez, E., Terray, L., Waldman, R., 2019. Evaluation of CMIP6 DECK Experiments With CNRM-CM6-1. J. Adv. Model. Earth Syst. 11, 2177–2213. https://doi.org/10.1029/2019MS001683

Volodin, E.M., Mortikov, E. V., Kostrykin, S. V., Galin, V.Y., Lykossov, V.N., Gritsun, A.S., Diansky, N.A., Gusev, A. V., Iakovlev, N.G., Shestakova, A.A., Emelina, S. V., 2018. Simulation of the modern climate using the INM-CM48 climate model. Russ. J. Numer. Anal. Math. Model. 33, 367–374. https://doi.org/10.1515/rnam-2018-0032

von Braun, J., Birner, R., 2017. Designing Global Governance for Agricultural Development and Food and Nutrition Security. Rev. Dev. Econ. 21, 265–284. https://doi.org/10.1111/rode.12261

Wakjira, M.T., Peleg, N., Anghileri, D., Molnar, D., Alamirew, T., Six, J., Molnar, P., 2021. Rainfall seasonality and timing: implications for cereal crop production in Ethiopia. Agric. For. Meteorol. 310, 108633. https://doi.org/10.1016/J.AGRFORMET.2021.108633

Wakjira, M.T., Peleg, N., Burlando, P., Molnar, P., 2023. Gridded daily 2-m air temperature dataset for Ethiopia derived by debiasing and downscaling ERA5-Land for the period 1981–2010. Data Br. 46, 108844. https://doi.org/10.1016/j.dib.2022.108844

Wakjira, M.T., Peleg, N., Molnar, P., Burlando, P., 2022. Bias-corrected and downscaled ERA5-Land 2-m air temperature dataset for Ethiopia for the period 1981-2010. https://doi.org/10.3929/ethz-b-000546574

Walsh, R.P.D., Lawler, D.M., 1981. Rainfall Seasonality: Description, Spatial Patterns and Change Through Time. Weather 36, 201–208. https://doi.org/10.1002/j.1477-8696.1981.tb05400.x

Wang, Y.C., Hsu, H.H., Chen, C.A., Tseng, W.L., Hsu, P.C., Lin, C.W., Chen, Y.L., Jiang, L.C., Lee, Y.C., Liang, H.C., Chang, W.M., Lee, W.L., Shiu, C.J., 2021. Performance of the Taiwan Earth System Model in Simulating Climate Variability Compared With Observations and CMIP6 Model Simulations. J. Adv. Model. Earth Syst. 13, 1–28. https://doi.org/10.1029/2020MS002353

Wani, S.P., Rockström, J., Oweis, T., 2009. Rain-fed Agriculture: Unlocking the Potential, CAB International. CABI, London.

Warner, J.M., Mann, M.L., Chamberlin, J., Tizale, C.Y., 2023. Estimating acid soil effects on selected cereal crop productivities in Ethiopia: Comparing economic cost-effectiveness of lime and fertilizer applications. PLoS One 18, 1–19. https://doi.org/10.1371/journal.pone.0280230

Warren, R.F., Wilby, R.L., Brown, K., Watkiss, P., Betts, R.A., Murphy, J.M., Lowe, J.A., 2018. Advancing national climate change risk assessment to deliver national adaptation plans. Philos. Trans. R. Soc. A Math. Phys. Eng. Sci. 376. https://doi.org/10.1098/rsta.2017.0295

Webb, N.P., Marshall, N.A., Stringer, L.C., Reed, M.S., Chappell, A., Herrick, J.E., 2017. Land degradation and climate change: building climate resilience in agriculture. Front. Ecol. Environ. 15, 450–459. https://doi.org/10.1002/fee.1530

Welderufael, W.A., Le Roux, P.A.L., Hensley, M., 2008. Quantifying rainfall-runoff relationships on the Dera Calcic Fluvic Regosol ecotope in Ethiopia. Agric. Water Manag. 95, 1223–1232. https://doi.org/10.1016/j.agwat.2008.04.007

Welderufael, W.A., Woyessa, Y.E., 2009. Evaluation of surface water drainage systems for cropping in the Central Highlands of Ethiopia. Agric. Water Manag. 96, 1667–1672. https://doi.org/10.1016/j.agwat.2009.07.001

Williams, A.P., Funk, C., Michaelsen, J., Rauscher, S.A., Robertson, I., Wils, T.H.G., Koprowski, M., Eshetu, Z., Loader, N.J., 2012. Recent summer precipitation trends in the Greater Horn of Africa and the emerging role of Indian Ocean sea surface temperature. Clim. Dyn. 39, 2307–2328. https://doi.org/10.1007/s00382-011-1222-y

Williams, J.., 1990. The erosion-productivity impact calculator (EPIC) model: a case history. Philos. Trans. R. Soc. London. Ser. B Biol. Sci. 329, 421–428. https://doi.org/10.1098/rstb.1990.0184

Williams, K.E., Falloon, P.D., 2015. Sources of interannual yield variability in JULES-crop and implications for forcing with seasonal weather forecasts. Geosci. Model Dev. 8, 3987–3997. https://doi.org/10.5194/gmd-8-3987-2015

Wilson, A.M., Jetz, W., 2016. Remotely Sensed High-Resolution Global Cloud Dynamics for Predicting Ecosystem and Biodiversity Distributions. PLoS Biol. 14, 1–20. https://doi.org/10.1371/journal.pbio.1002415

Wittwer, R.A., Bender, S.F., Hartman, K., Hydbom, S., Lima, R.A.A., Loaiza, V., Nemecek, T., Oehl, F., Olsson, P.A., Petchey, O., Prechsl, U.E., Schlaeppi, K., Scholten, T., Seitz, S., Six, J., Van Der Heijden, M.G.A., 2021. Organic and conservation agriculture promote ecosystem multifunctionality. Sci. Adv. 7, 1–13. https://doi.org/10.1126/sciadv.abg6995

WMO, 2020. Guidelines on Homogenization. Geneva.

WMO, 2017. Guidelines on the Calculation of Climate Normals, WMO-No. 1203. Geneva.

World Bank, 2022. Poverty and shared prosperity 2022: Correcting course, Managing Automation.

World Bank, 2020. Harnessing Continued Growth for Accelerated Poverty Reduction. Washington DC.

World Bank, 2003. Reaching the rural poor, Development Policy Review. https://doi.org/10.1111/1467-7679.00153

Wu, T., Lu, Y., Fang, Y., Xin, X., Li, L., Li, W., Jie, W., Zhang, J., Liu, Y., Zhang, L., Zhang, F., Zhang, Yanwu, Wu, F., Li, J., Chu, M., Wang, Z., Shi, X., Liu, Xiangwen, Wei, M., Huang, A., Zhang, Yaocun, Liu, Xiaohong, 2019. The Beijing Climate Center Climate System Model (BCC-CSM): The main progress from CMIP5 to CMIP6. Geosci. Model Dev. 12, 1573–1600. https://doi.org/10.5194/gmd-12-1573-2019

Wu, W., Shah, F., Ma, B., 2022. Understanding of crop lodging and agronomic strategies to improve the resilience of rapeseed production to climate change. Crop Environ. 1, 133–144. https://doi.org/10.1016/j.crope.2022.05.005

Yengoh, G.T., Armah, F.A., Onumah, E.E., Odoi, J.O., 2010. Trends in Agriculturally-Relevant Rainfall Characteristics for Small-scale Agriculture in Northern Ghana. J. Agric. Sci. 2, 3–16. https://doi.org/10.5539/jas.v2n3p3

YIN, H., SUN, Y., 2018. Characteristics of extreme temperature and precipitation in China in 2017 based on ETCCDI indices. Adv. Clim. Chang. Res. 9, 218–226. https://doi.org/10.1016/j.accre.2019.01.001

You, L., Ringler, C., Wood-Sichra, U., Robertson, R., Wood, S., Zhu, T., Nelson, G., Guo, Z., Sun, Y., 2011. What is the irrigation potential for Africa? A combined biophysical and socioeconomic approach. Food Policy 36, 770–782. https://doi.org/10.1016/j.foodpol.2011.09.001

Zabel, F., Putzenlechner, B., Mauser, W., 2014. Global agricultural land resources - A high resolution suitability evaluation and its perspectives until 2100 under climate change conditions. PLoS One 9, 1–12. https://doi.org/10.1371/journal.pone.0107522

Zaitchik, B.F., 2017. Madden-Julian Oscillation impacts on tropical African precipitation. Atmos. Res. 184, 88–102. https://doi.org/10.1016/j.atmosres.2016.10.002

Zeleke, G., Teshome, M., Ayele, L., 2023. Environmental and Sustainability Indicators Farmers ' livelihood vulnerability to climate-related risks in the North Wello. Environ. Sustain. Indic. 17, 100220. https://doi.org/10.1016/j.indic.2022.100220

Zeleke, Z.A., 2020. Effect of Different Levels of Supplementary Irrigation on Yield and Yield Component of Maize (zea mays L) at Teppi, South West Ethiopia. Int. J. Res. Stud. Agric. Sci. 6, 4–9. https://doi.org/10.20431/2454-6224.0611002

Zewudie, D., Ding, W., Rong, Z., Zhao, C., Chang, Y., 2021. Spatiotemporal dynamics of habitat suitability for the Ethiopian staple crop, Eragrostis tef (teff), under changing climate. PeerJ 9, 1–25. https://doi.org/10.7717/peerj.10965

Zhang, W., Brandt, M., Tong, X., Tian, Q., Fensholt, R., 2018. Impacts of the seasonal distribution of rainfall on vegetation productivity across the Sahel. Biogeosciences 15, 319–330. https://doi.org/10.5194/bg-15-319-2018

Zhang, Y., Kong, D., Gan, R., Chiew, F.H.S., McVicar, T.R., Zhang, Q., Yang, Y., 2019. Coupled estimation of 500 m and 8-day resolution global evapotranspiration and gross primary production in 2002–2017. Remote Sens. Environ. 222, 165–182. https://doi.org/10.1016/j.rse.2018.12.031

Zhang, Yuliang, Wu, Z., Singh, V.P., He, H., He, J., Yin, H., Zhang, Yaxin, 2021. Coupled hydrology-crop growth model incorporating an improved evapotranspiration module. Agric. Water Manag. 246, 106691. https://doi.org/10.1016/j.agwat.2020.106691

Zhao, C., Liu, B., Piao, S., Wang, X., Lobell, D.B., Huang, Y., Huang, M., Yao, Y., Bassu, S., Ciais, P., Durand, J.L., Elliott, J., Ewert, F., Janssens, I.A., Li, T., Lin, E., Liu, Q., Martre, P., Müller, C., Peng, S., Peñuelas, J., Ruane, A.C., Wallach, D., Wang, T., Wu, D., Liu, Z., Zhu, Y., Zhu, Z., Asseng, S., 2017. Temperature increase reduces global yields of major crops in four independent estimates. Proc. Natl. Acad. Sci. U. S. A. 114, 9326–9331. https://doi.org/10.1073/pnas.1701762114

Appendix A: Supplementary materials for Chapter 4

Table S4.1: List of the administrative zones within the nine regional states of Ethiopia based on pre-2010 divisions. The short names are arbitrary designations used in Fig. 4.1.

Short name	Long name	Region
NWT	North West Tigray	Tigray
CTI	Central Tigray	
ETI	Eastern Tigray	
STI	Southern Tigray	
WTI	Western Tigray	
ZO1	Zone 1	Afar
ZO2	Zone 2	
ZO3	Zone 3	
ZO4	Zone 4	
ZO5	Zone 5	
NGO	North Gondar	Amhara
SGO	South Gondar	
NWO	North Wello	
SWO	South Wello	
aNSH	North Shewa	
EGO	East Gojam	
WGO	West Gojam	
WAG	Wag Himra	
AWI	Awi	
ORO	Oromia	
WWL	West Wellega	Oromia
EWL	East Wellega	
ILU	Ilu Aba Bora	
JIM	Jimma	
WSH	West Shewa	
oNSH	North Shewa	
ESH	East Shewa	
ARS	Arsi	
WHA	West Hararge	
EHA	East Hararge	
BAL	Bale	
BOR	Borena	
SWS	South West Shewa	
GUJ	Guji	
wARS	West Arsi	

Short name	Long name	Region
SHI	Shinile	Somali
FAF	Fafan	
LIB	Liben	
AFD	Afder	
DOL	Dolo	
JAR	Jarar	
SHB	Shabelle	
KOR	Korahe	
SIT	Siti	
NOG	Nogob	
MET	Metekel	Benishangul-gumz
ASO	Asosa	
KEM	Kemashi	
GUR	Gurage	SNNPR
HAD	Hadiya	
KET	Kembata Tibaro	
SID	Sidama	
KEF	Kefa	
GGO	Gamo Gofa	
BMJ	Bench Maji	
YEM	Yem Special	
AMA	Amaro Special	
BUR	Burji Special	
KONs	Konso Speicial	
DER	Derashe Special	
DAW	Dawuro	
BAS	Basketo Special	
KON	Konta Special	
SIL	Siltie	
ALB	Alaba Special	
ALL	Alle	
WOL	Wolaita	
SOM	South Omo	
AGN	Agnuak	Gambela
MAJ	Majang	
NUE	Nuer	

Table S4.2: List of the CMIP6 model projections used for the projection of the precipitation, maximum and minimum temperature and incoming short wave radiation over Ethiopia. The 'x' marks shows the datasets that were used from the indicated model.

Model	Institution (country/region)[1]	Precip	Tmax	Tmin	Rsw	Reference
ACCESS-CM2	CSIRO (Australia)	x	x	x	x	(Bi et al., 2020)
AWI-CM-1-1-MR	AWI (Germany)	x	x	x	x	(Semmler et al., 2020)
BCC-CSM2-MR	BCC (Asia)	x			x	(Wu et al., 2019)
CAMS-CSM1-0	CAMS (China)	x			x	(Rong et al., 2019)
CanESM5-CanOE	CCCma (Canada)	x	x	x	x	(Christian et al., 2022)
CESM2	NCAR (USA)	x			x	(Danabasoglu et al., 2020)
CIESM	THU (China)		x	x		(Lin et al., 2020)
CMCC-CM2-SR5	CMCC (Italy)	x			x	(Cherchi et al., 2019)
CMCC-ESM2		x	x	x	x	(Lovato et al., 2022)
CNRM-CM6-1	CNRM (France)	x	x	x	x	(Voldoire et al., 2019)
CNRM-CM6-1-HR		x	x	x	x	
CNRM-ESM2-1		x	x	x	x	
EC-Earth3-Veg-LR	EC-Earth (Europe)		x	x		(Döscher et al., 2022)
FGOALS-g3	CAS (China)	x	x	x	x	(Li et al., 2020)
FIO-ESM-2-0	FIO-QNLM (China)	x	x	x	x	(Bao et al., 2020)
GFDL-ESM4	NOAA-GFDL (USA)	x	x	x	x	(Dunne et al., 2020)
HadGEM3-GC31-LL	MOHC (UK)	x	x	x	x	(Andrews et al., 2020)
IITM-ESM	CCCR-IITM (India)	x	x	x	x	(David A. et al., 2019)
INM-CM4-8	INM (Russia)		x	x		(Volodin et al., 2018)
INM-CM5-0		x	x	x	x	
IPSL-CM6A-LR	IPSL (France)	x	x	x	x	(Boucher et al., 2020)
MIROC6	MIROC (Japan)	x	x	x	x	(Tatebe et al., 2019)
MIROC-ES2L		x	x	x	x	(Hajima et al., 2020)
MPI-ESM1-2-LR	MPI (Germany)	x	x	x	x	(Gutjahr et al., 2019)
NESM3	NUIST (China)	x			x	(Cao et al., 2018)
NorESM2-MM	NCC (Norway)	x			x	(Seland et al., 2020)
TaiESM1	AS-RCEC (Taiwan)	x			x	(Wang et al., 2021)
UKESM1-0-LL	MOHC (UK)	x	x	x	x	(Sellar et al., 2019)

[1] The full names of the institutions can be found in (IPCC, 2021)

Table S4.3: List of the nine surface runoff measurement sites and measurement periods collected from published literature for validation of the simulated surface runoff.

Measurement site	Lat (° N)	Lon (° E)	Measurement periods (Values used in the evaluation)	Reference
Maybar	11.02	39.67	1982-1993 (mean)	(Herweg and Ludi, 1999; Herweg and Stillhardt, 1999)
Hunde lafto	9.07	41.00	1983-1993 (mean)	
Andit Tid	9.80	39.72	1982-1992 (mean)	
Anjeni	10.81	37.57	1985-1993 (mean)	
Gununo	6.92	37.65	1982-1992 (mean)	
Dendi	9.13	37.12	2007-2009 (annual)	(Adimassu et al., 2014)
Holeta	9.07	38.48	2009-2010 (annual)	(Adimassu et al., 2019)
Debre Mawi	11.33	37.43	2008-2009 (annual)	(Amare et al., 2014)
Chefe donsa	8.96	39.11	2001-2002 (annual)	(Erkossa et al., 2006)
Dera	8.36	39.34	2004 (annual)	(Welderufael et al., 2008)
Yeku	12.52	39.07	2003 (annual)	(Collick et al., 2009)
Guder*	9.84	36.67	2003 (annual)	(Tumsa et al., 2022)
Dodota*	11.50	39.92	1994-2000 (mean)	(Teso et al., 2010)
Keleta	8.12	39.46	1981, 1990 (annual)	(Tibebe and Bewket, 2011)
Suluh*	13.80	39.50	1992-2003 (mean)	(Abebe, 2014)
Hare*	6.25	37.55	1990-1999 (mean)	(Wagesho et al., 2013)
Bilate*	7.50	37.94	1990-1999 (mean)	

*These are model-calibrated surface runoff data: Guder (SWAT+), Dodota (SWAT), Suluh (HEC-HMS), Hare and Bilate (SWAT)

Table S4.4: Published potential (fully irrigated, optimally fertilized) yield measured at 14 experimental sites across the RFA region of Ethiopia.

Experimental site	Potential yield, Yp (ton/ha)	Lat (°N)	Lon (°E)	Reference
Salaklaka, Northwest Tigray	7.3	14.3	38.72	(Gebreigziabher, 2020)
Melkasa, East Shoa	7.9	8.4	39.35	(Seid, Mulugeta M; Narayanan, 2015)
Boloso Sore, Wolayta	8.8	7.0	37.75	(Chinasho et al., 2023)
Tepi, SW Ethiopia	6.8	7.187	35.42	(Zeleke, 2020)
Raya, South Tigray	8.7	12.7	39.7	(Mehari et al., 2020)
Arba Minch, Gamo Gofa	8.0	6.08	37.58	(Setu et al., 2023)
Koga, West Gojam	5.9	11.37	37.12	(Abiyu and Alamirew, 2015)
Haru ARC, West Wollega	8.4	8.90	35.87	(Admasu et al., 2017)
Adami Tulu, East Shoa	4.5	7.75	38.65	(Furgassa, 2017)
Mehoni, South Tigray	5.7	12.87	39.64	(Mebrahtu and Mehamed, 2019)
Haramaya, East Hararge	7.1	9.417	42.04	(Mengiste and Tilahun, 2009)
Hawassa, Sidama	9.0	7	38	(Jemal and Berhanu, 2020)
Koka, East Shoa	6.29	8.43	39	(Meskelu et al., 2018)
Gumselasa, South Tigray	9.9	13.25	39.51	(Mintesinot et al., 2004)

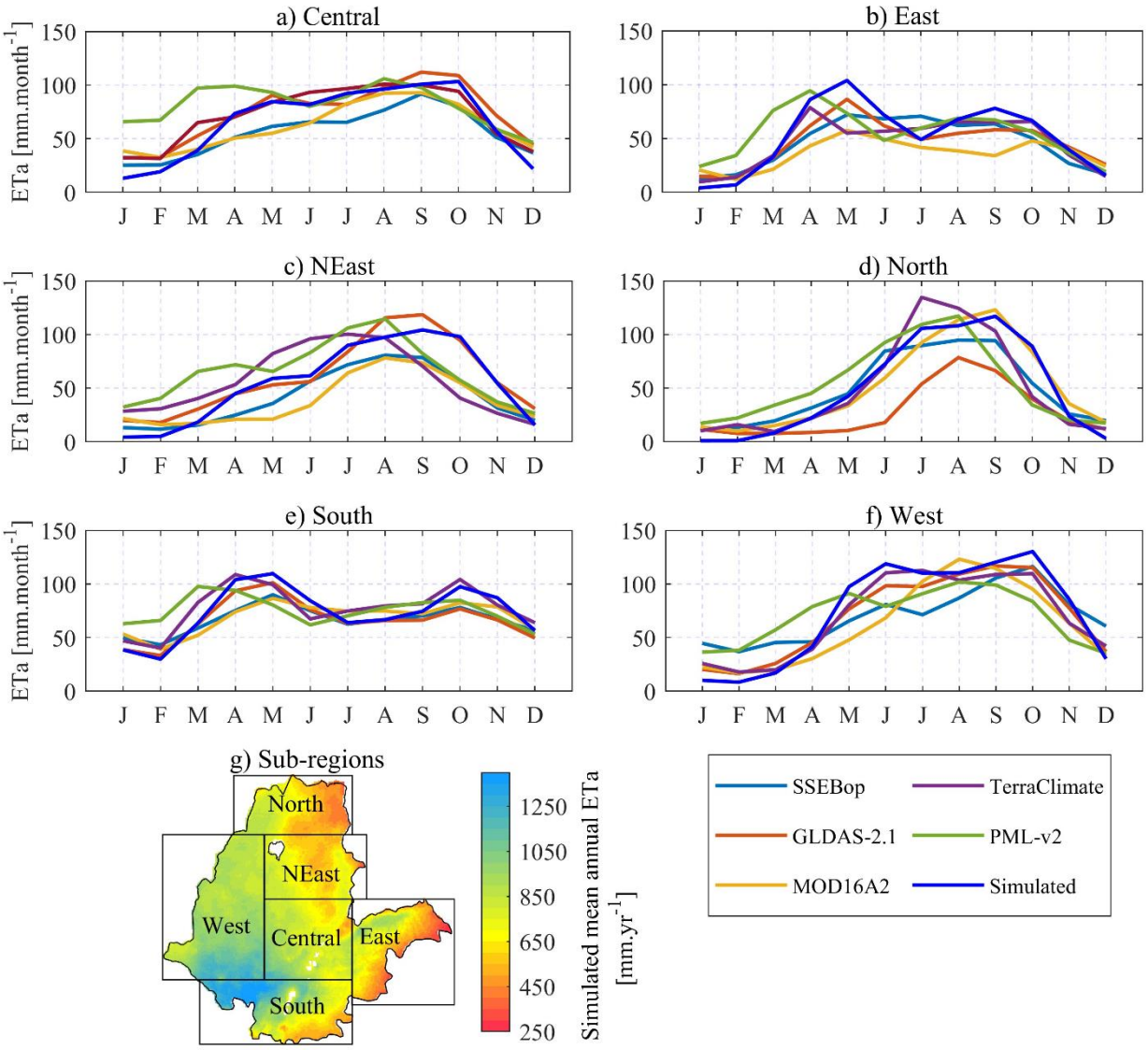

Fig. S4.1: Comparison of area-averaged monthly cycles of the simulated ETa and other independent ETa products (a-f) at six arbitrarily clustered sub-regions (g) for the record period 2003-2010.

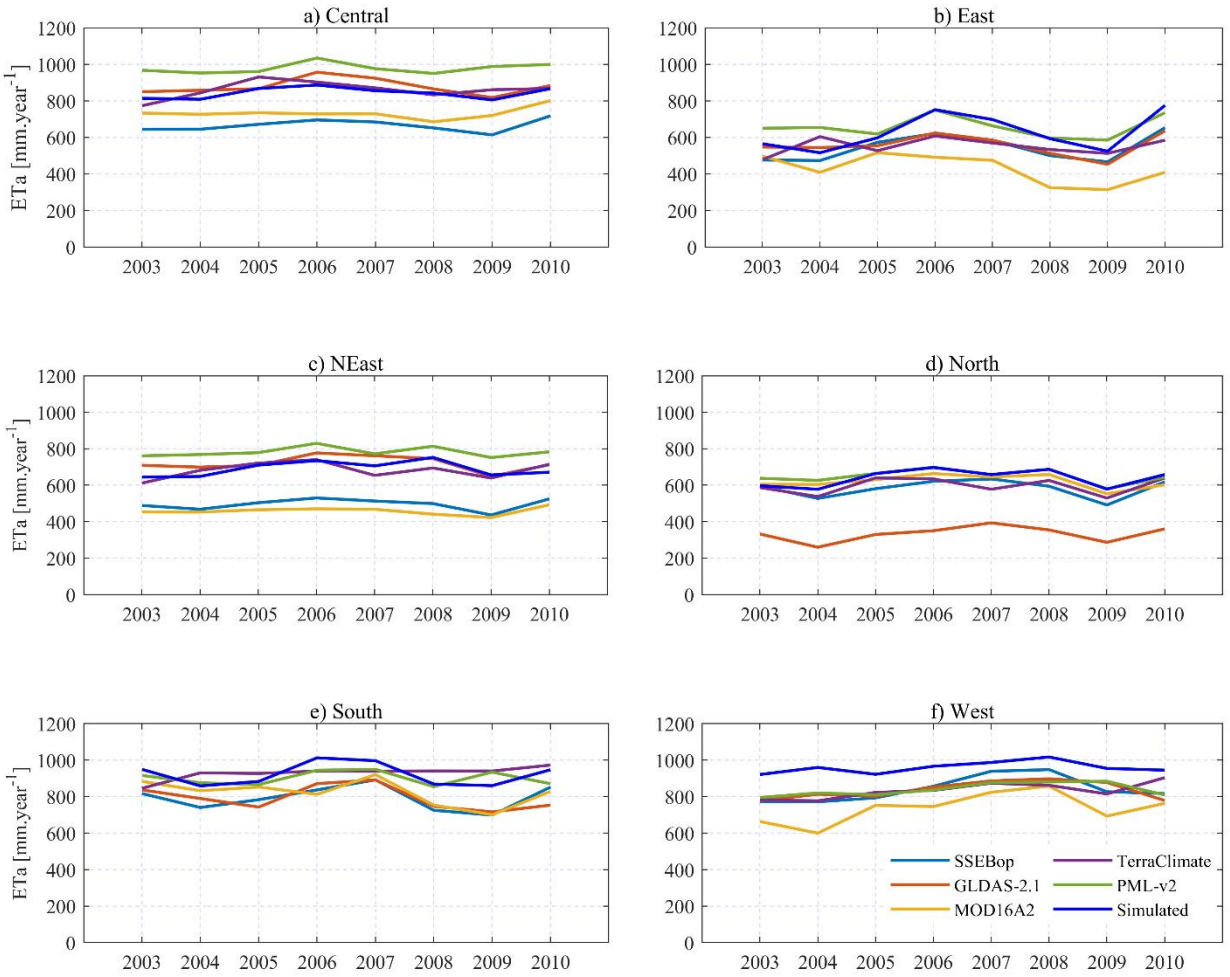

Fig. S4.2: Comparison of simulated and independent (observed) annual ETa (a-f) at the six sub-regions (see Fig. S1g) for the record period 2003-2010.

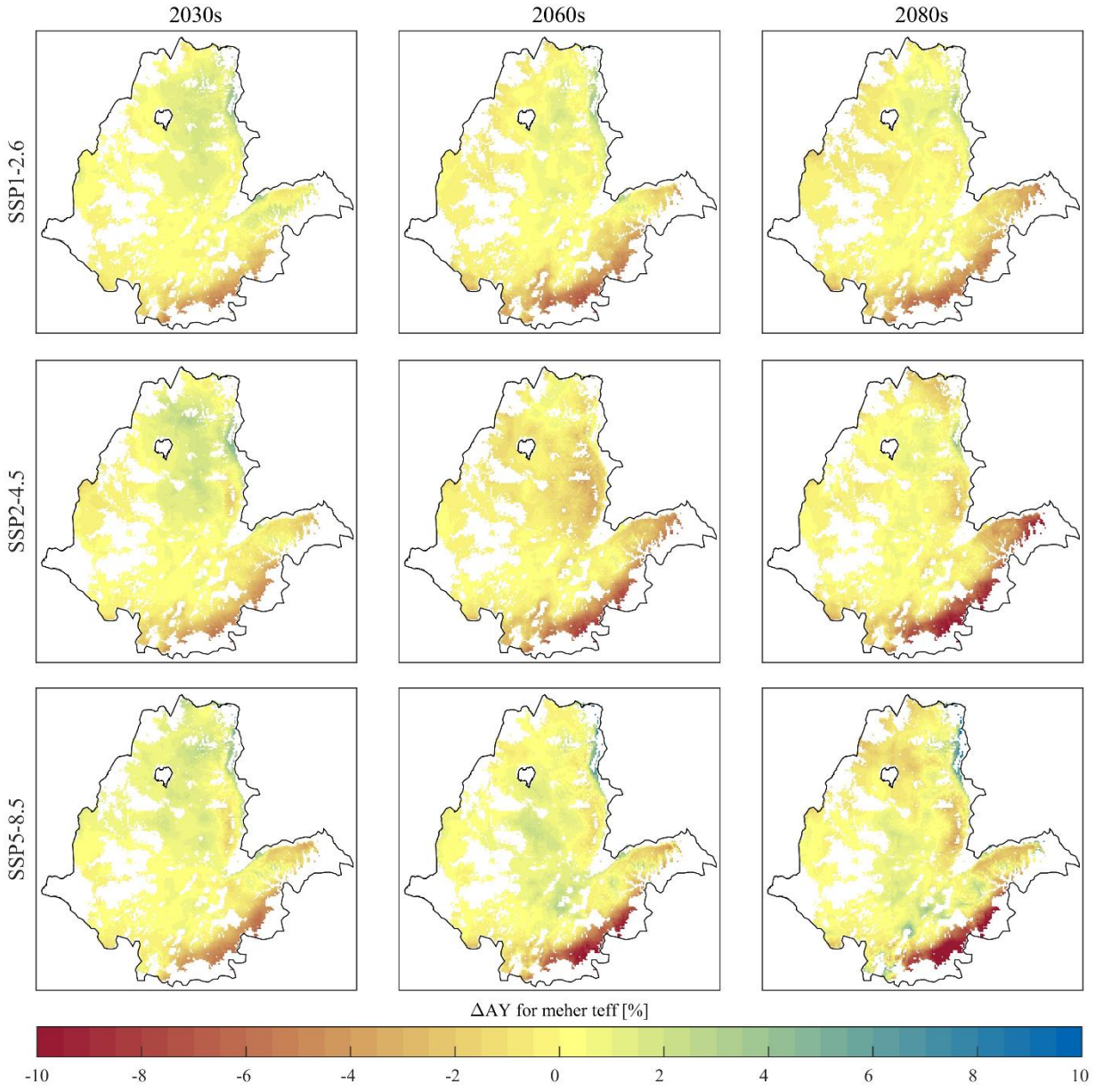

Fig. S4.3: Projected changes in Meher water-limited attainable yield (AY) for teff under the SSP1-2.6, SSP2-4.5, and SSP5-8.5. The RFA region was masked using cropland suitability maps (Wakjira et al., under review) to restrict the analysis to areas potentially suitable for each crop. The non-producing areas during both seasons were also masked out as mapped in the Atlas of Ethiopian Rural Socioeconomy (IFPRI and CSA, 2006).

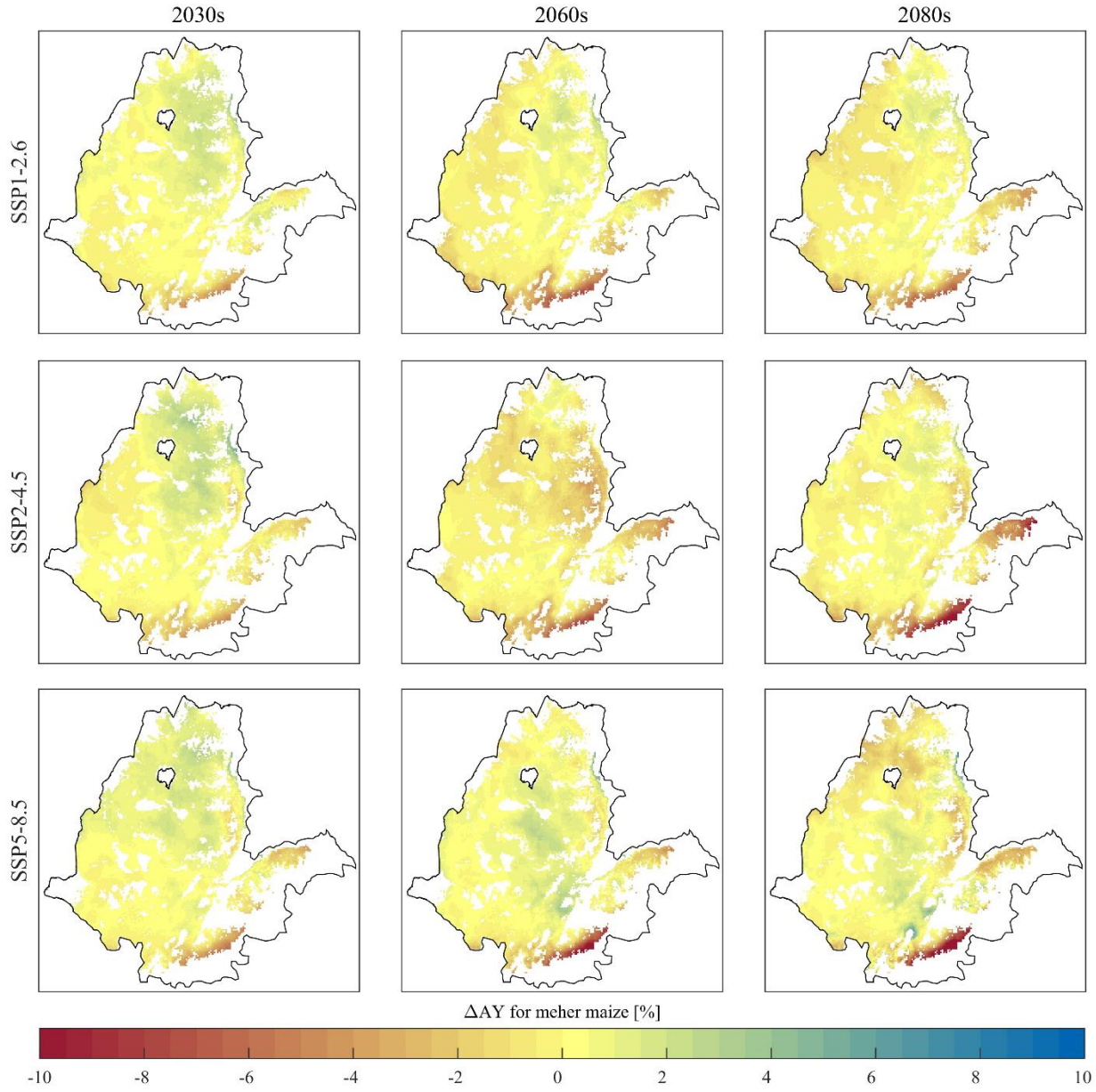

Fig. S4.4: Projected changes in Meher water-limited attainable yield (AY) for maize under the SSP1-2.6, SSP2-4.5, and SSP5-8.5. The RFA region was masked using cropland suitability maps (Wakjira et al., under review) to restrict the analysis to areas potentially suitable for each crop. The non-producing areas during both seasons were also masked out as mapped in the Atlas of Ethiopian Rural Socioeconomy (IFPRI and CSA, 2006).

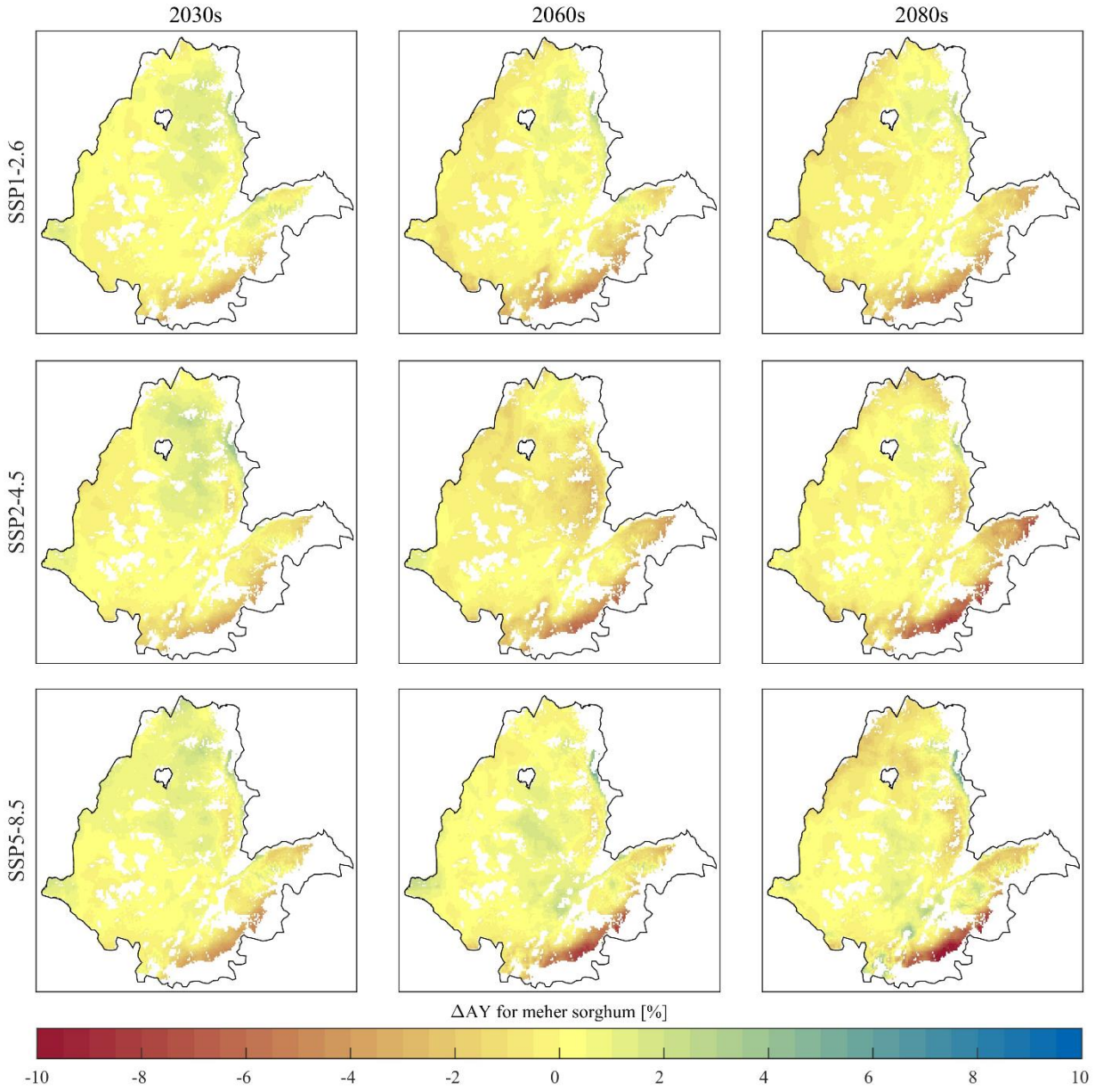

Fig. S4.5: Projected changes in Meher water-limited attainable yield (AY) for sorghum under the SSP1-2.6, SSP2-4.5, and SSP5-8.5. The RFA region was masked using cropland suitability maps (Wakjira et al., under review) to restrict the analysis to areas potentially suitable for each crop. The non-producing areas during both seasons were also masked out as mapped in the Atlas of Ethiopian Rural Socioeconomy (IFPRI and CSA, 2006)

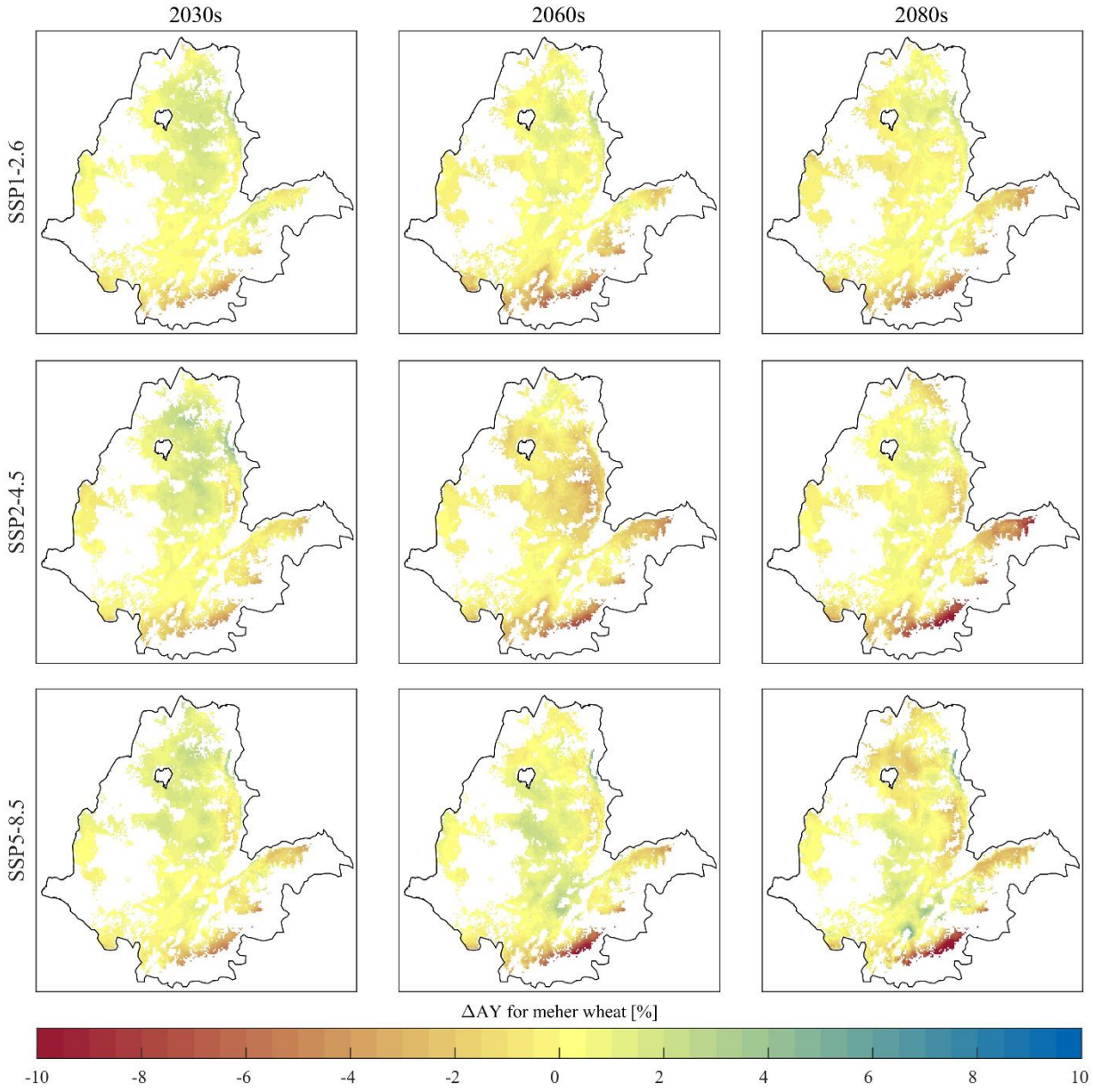

Fig. S4.6: Projected changes in Meher water-limited attainable yield (AY) for wheat under the SSP1-2.6, SSP2-4.5, and SSP5-8.5. The RFA region was masked using cropland suitability maps (Wakjira et al., under review) to restrict the analysis to areas potentially suitable for each crop. The non-producing areas during both seasons were also masked out as mapped in the Atlas of Ethiopian Rural Socioeconomy (IFPRI and CSA, 2006)

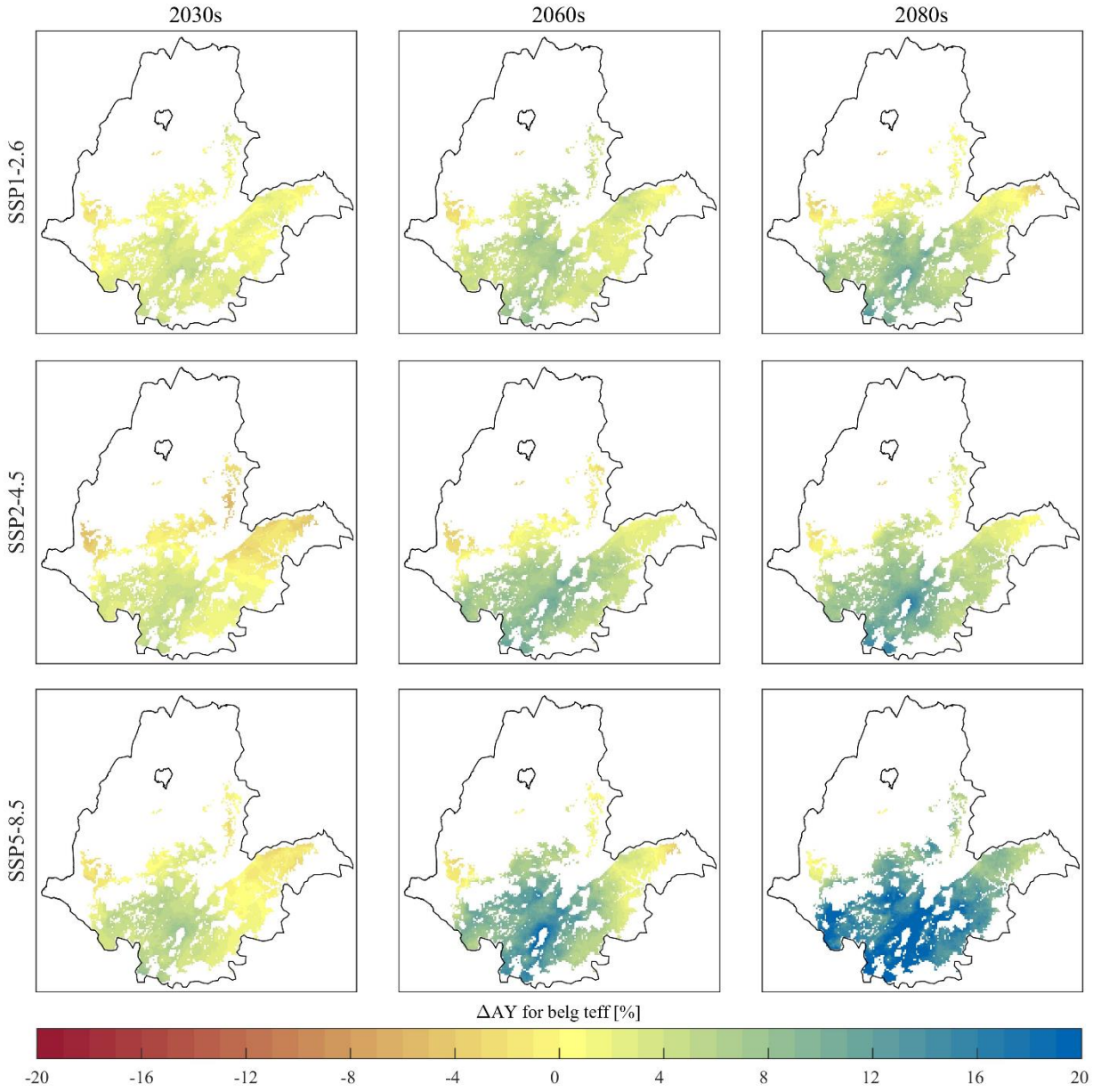

Fig. S4.7: Projected changes in Belg water-limited attainable yield (AY) for teff under the SSP1-2.6, SSP2-4.5, and SSP5-8.5. The RFA region was masked using cropland suitability maps (Wakjira et al., under review) to restrict the analysis to areas potentially suitable for each crop. The non-producing areas during both seasons were also masked out as mapped in the Atlas of Ethiopian Rural Socioeconomy (IFPRI and CSA, 2006).

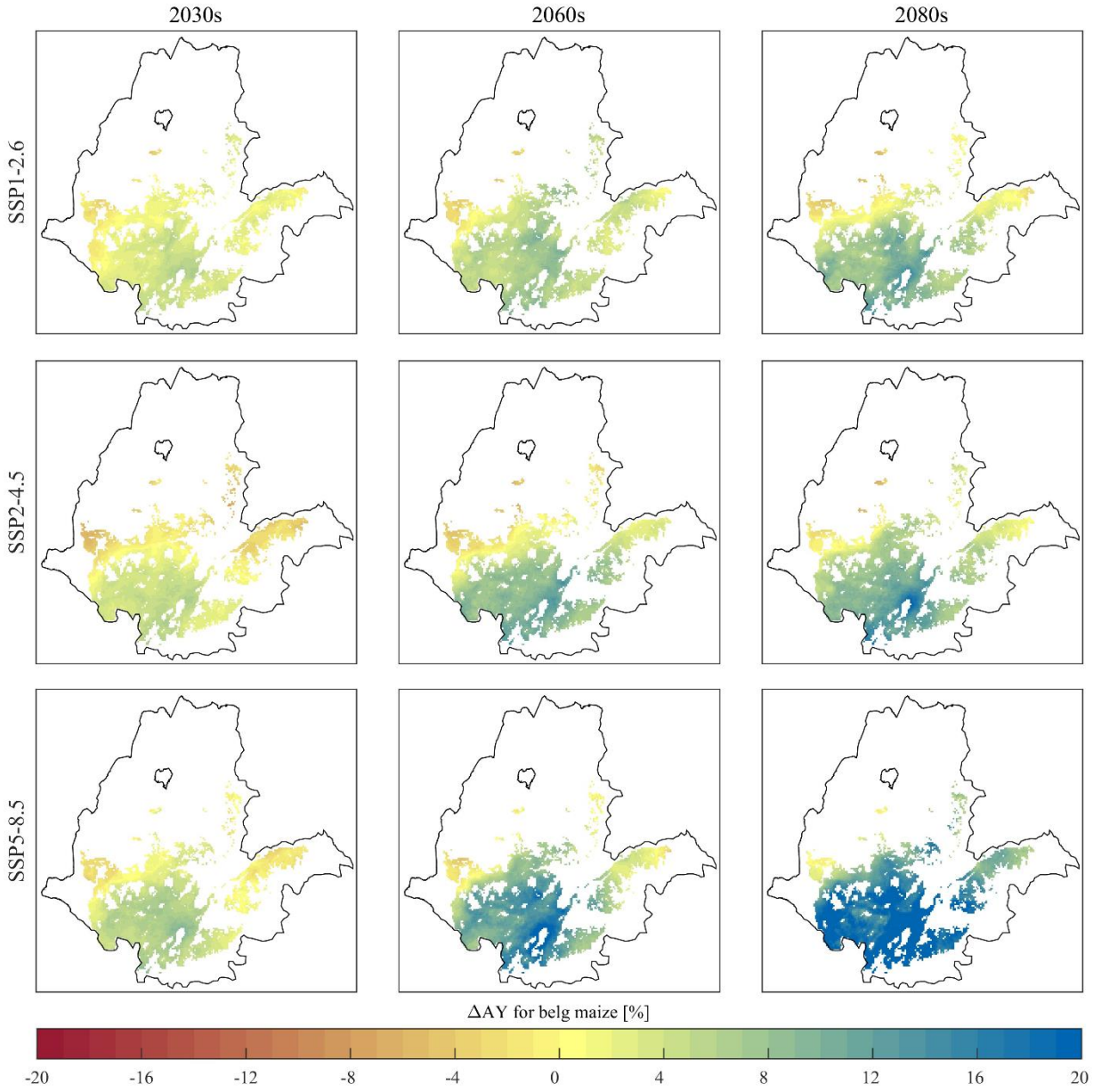

Fig. S4.8: Projected changes in Belg water-limited attainable yield (AY) for maize under the SSP1-2.6, SSP2-4.5, and SSP5-8.5. The RFA region was masked using cropland suitability maps (Wakjira et al., under review) to restrict the analysis to areas potentially suitable for each crop. The non-producing areas during both seasons were also masked out as mapped in the Atlas of Ethiopian Rural Socioeconomy (IFPRI and CSA, 2006).

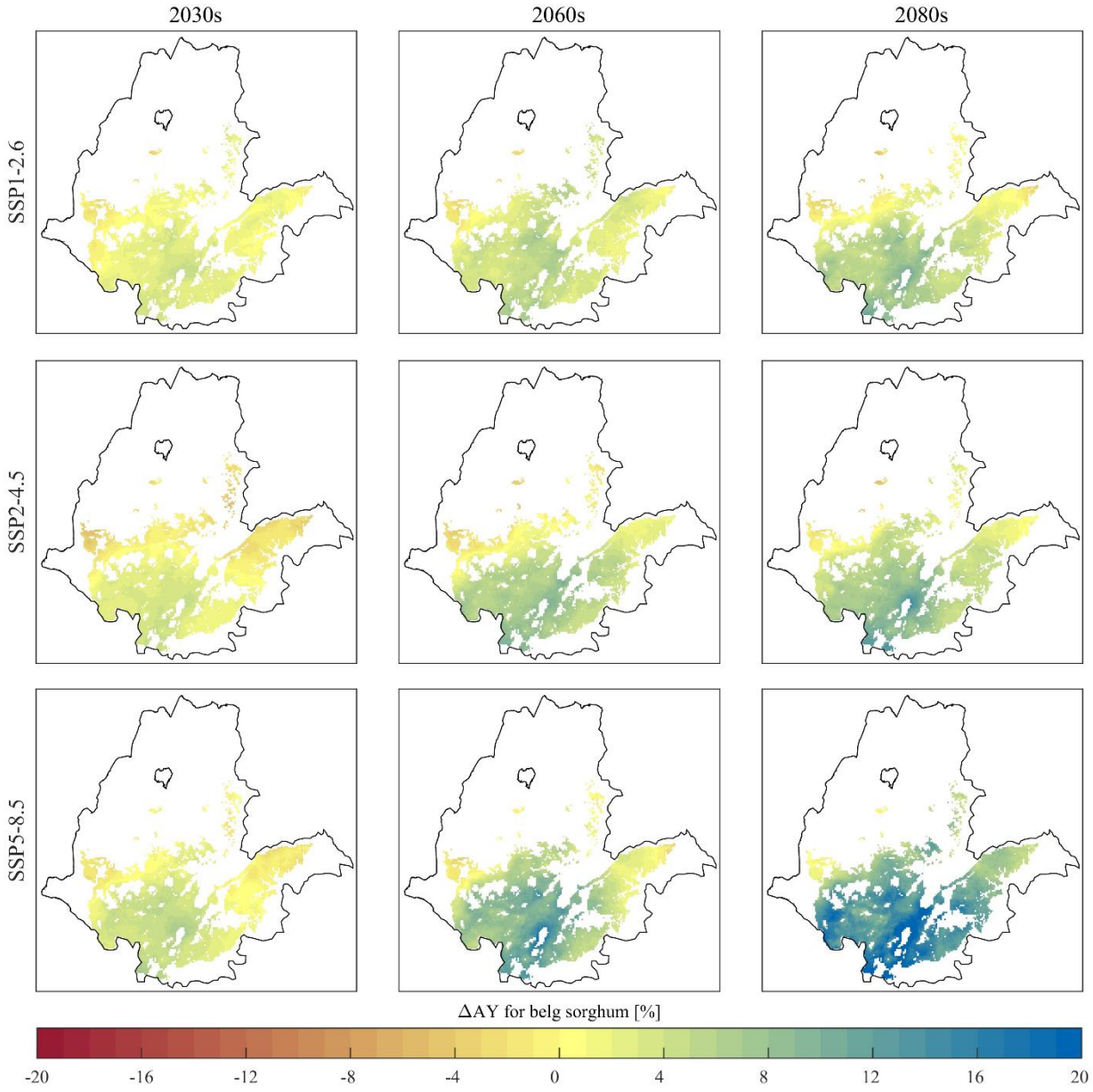

Fig. S4.9: Projected changes in Belg water-limited attainable yield (AY) for sorghum under the SSP1-2.6, SSP2-4.5, and SSP5-8.5. The RFA region was masked using cropland suitability maps (Wakjira et al., under review) to restrict the analysis to areas potentially suitable for each crop. The non-producing areas during both seasons were also masked out as mapped in the Atlas of Ethiopian Rural Socioeconomy (IFPRI and CSA, 2006).

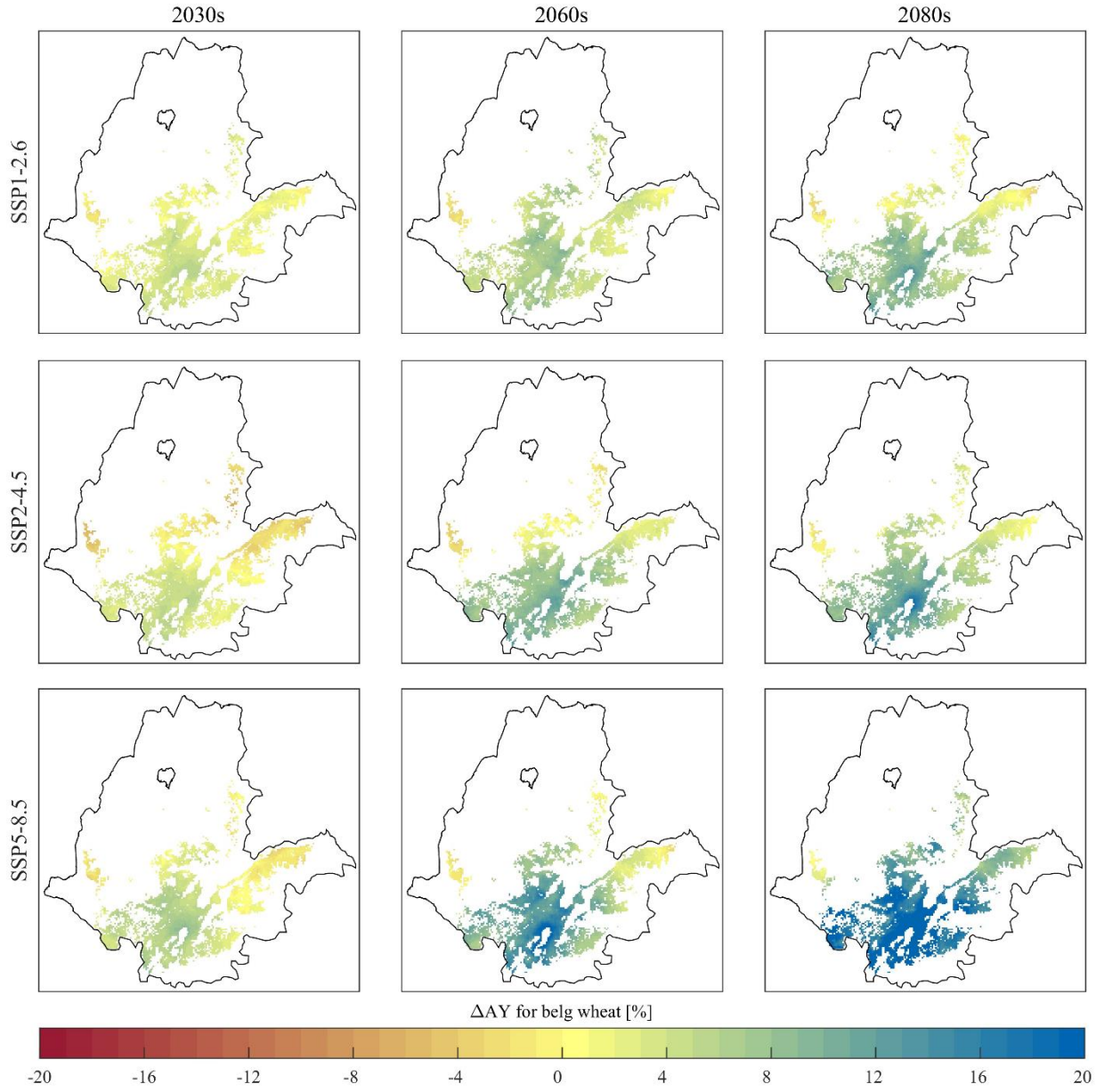

Fig. S4.10: Projected changes in Belg water-limited attainable yield (AY) for wheat under the SSP1-2.6, SSP2-4.5, and SSP5-8.5. The RFA region was masked using cropland suitability maps (Wakjira et al., under review) to restrict the analysis to areas potentially suitable for each crop. The non-producing areas during both seasons were also masked out as mapped in the Atlas of Ethiopian Rural Socioeconomy (IFPRI and CSA, 2006).

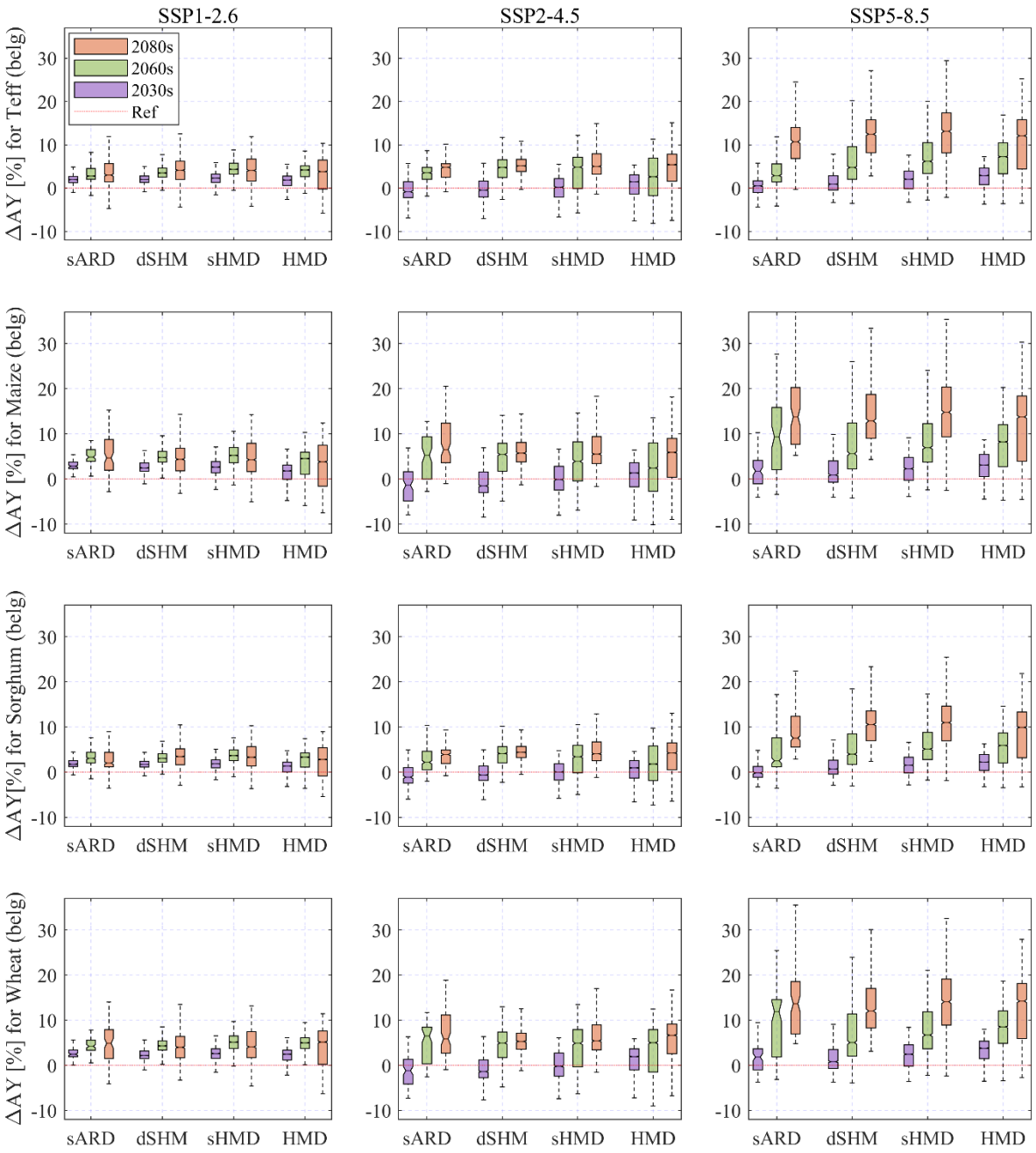

Fig. S4.11: Boxplots of the projected changes in water-limited yields (AY) of the four major cereal crops produced in Ethiopia in different climatic regimes under the three SSPs during the three future periods, during the Meher growing season. Each boxplot represents the distribution of AY changes within Belg-producing areas for all grid cells in the respective climatic regime. Outlier values have been excluded.

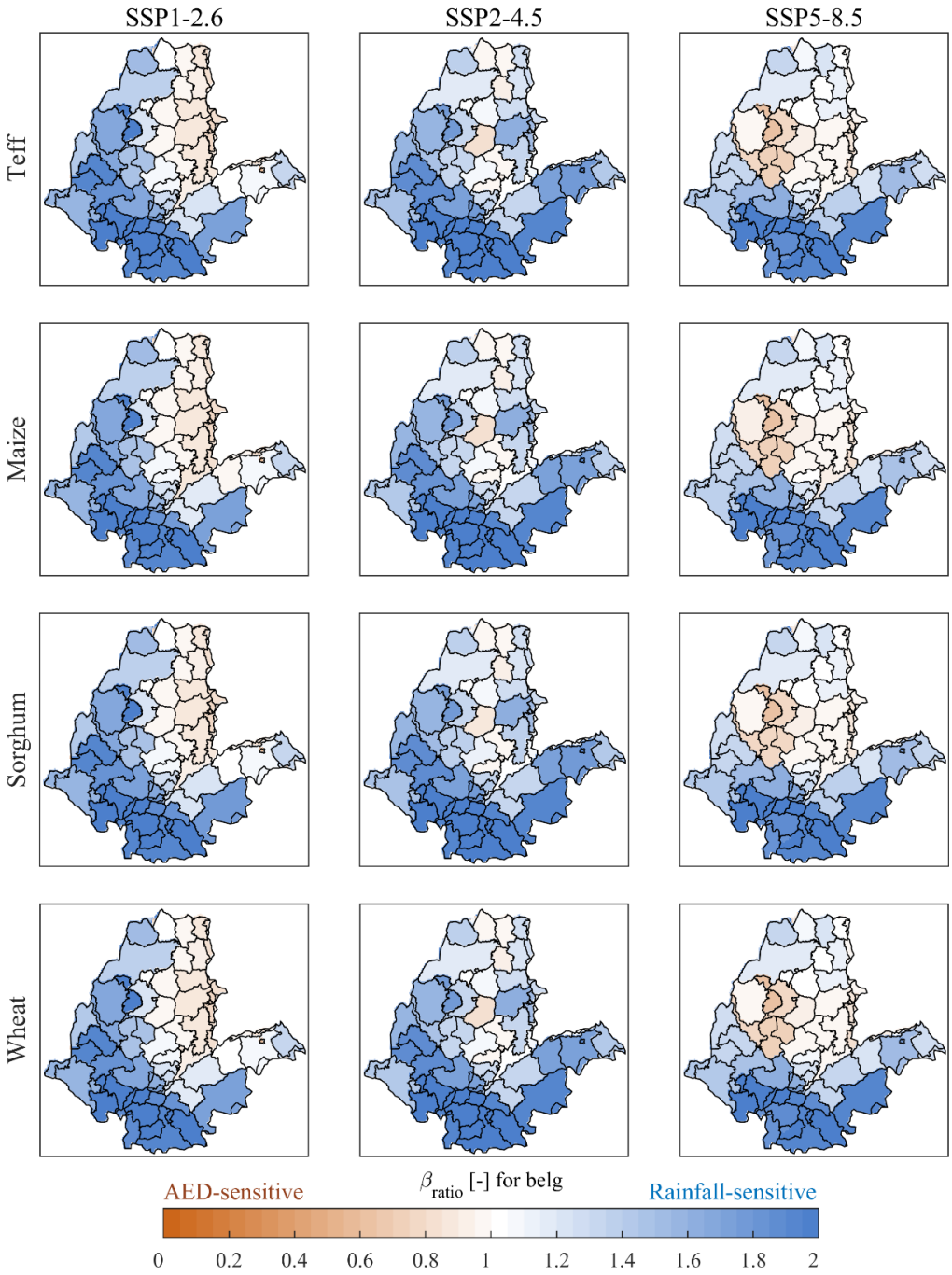

Fig. S4.12: Area-averaged relative sensitivity ($\boldsymbol{\beta_{ratio}}$) of water-limited attainable yields (AY) to rainfall and atmospheric evaporative demand (AED) for the Belg growing season at the administrative zone level under the low, intermediate and high emission scenarios for teff, maize, sorghum and wheat. The mapped values represent the average of $\boldsymbol{\beta_{ratio}}$ of all grid cells within each zone, and all three future periods. The short names of the 62 administrative zones within the RFA region of Ethiopia are indicated in Fig. 4.1. The long names are listed in Table S1 of the supplementary material.

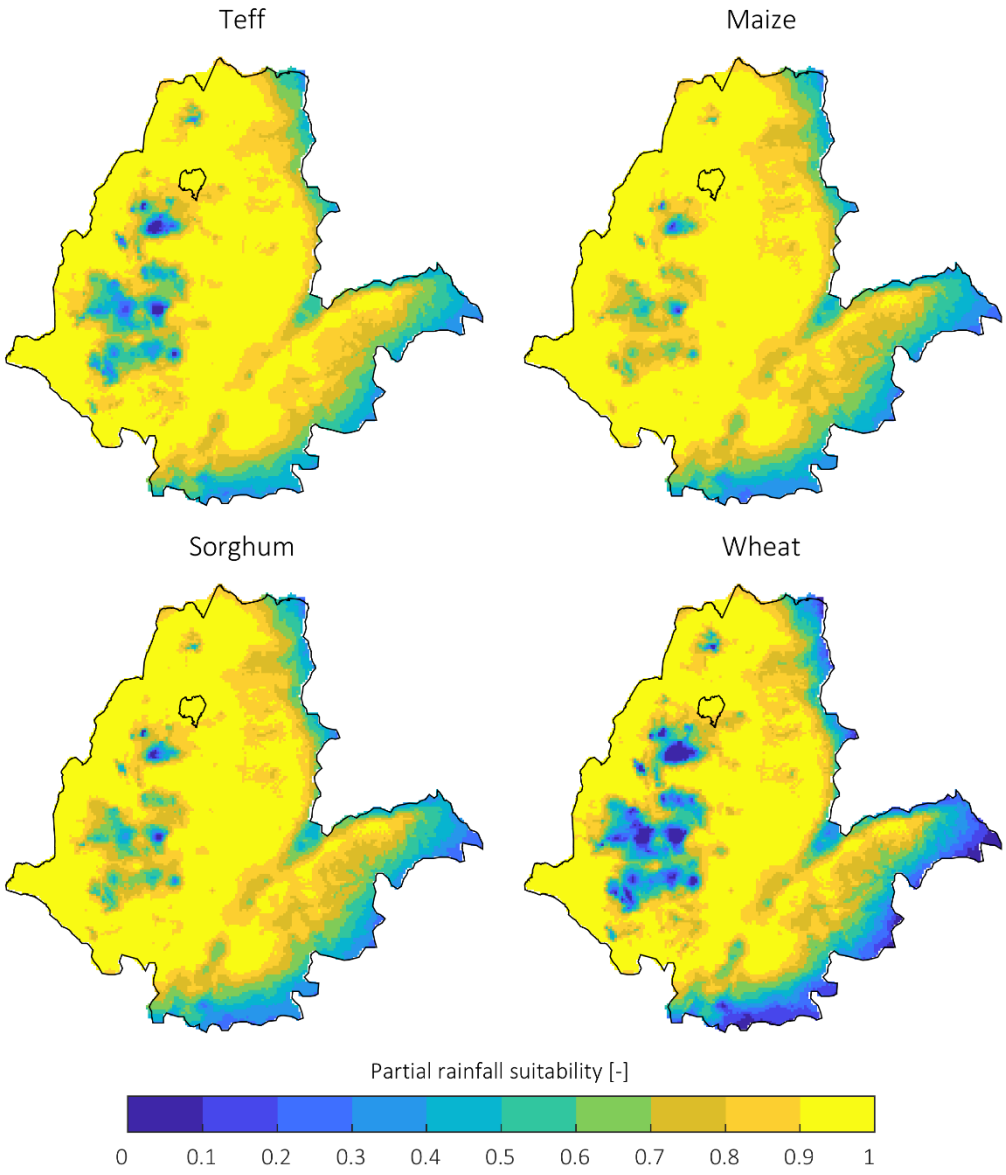

Fig. S5.1: Partial rainfall suitability for teff, maize, sorghum and wheat based on the total May-November rainfall climatology of the period 1981-2010.

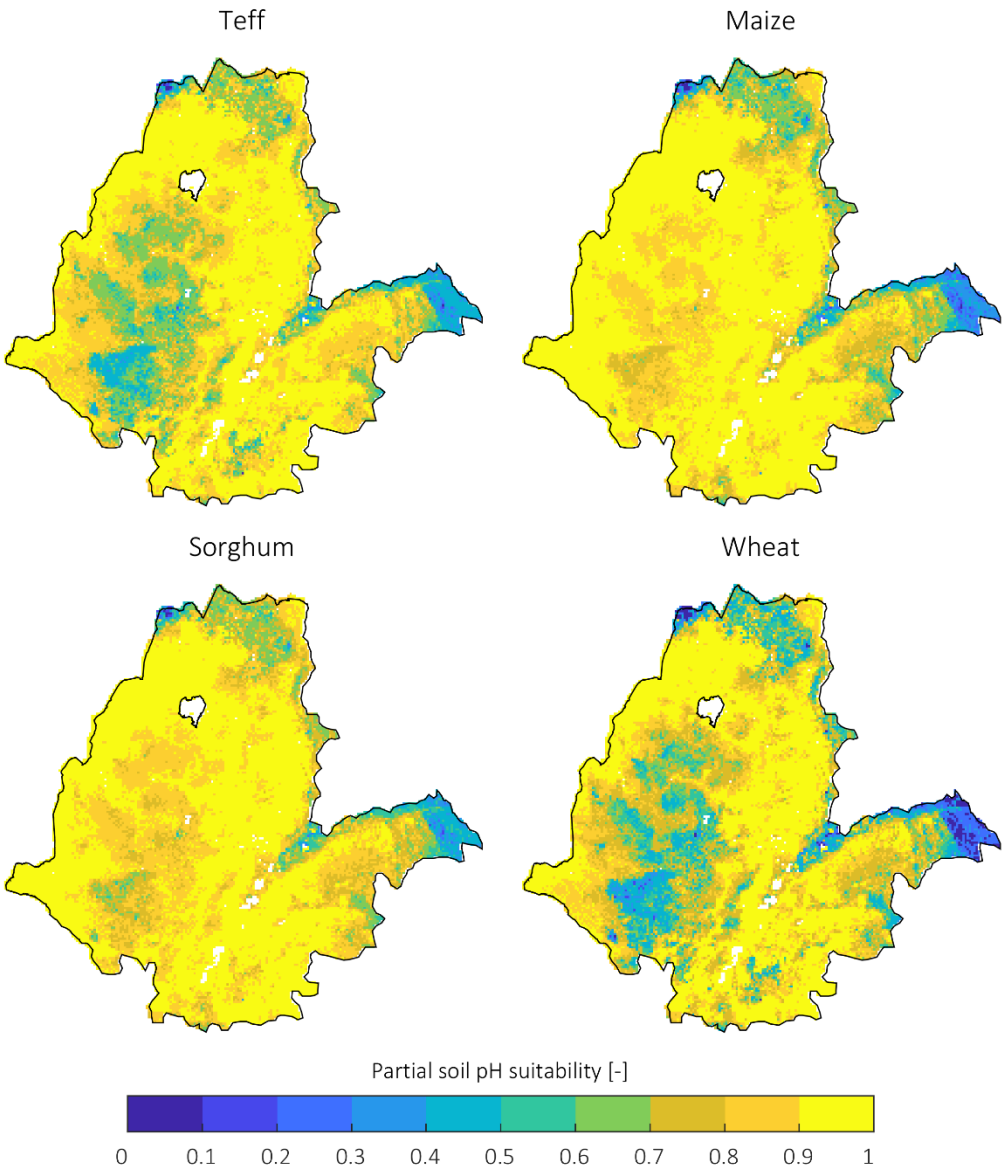

Fig. S5.2: Partial soil pH suitability for teff, maize, sorghum, wheat.

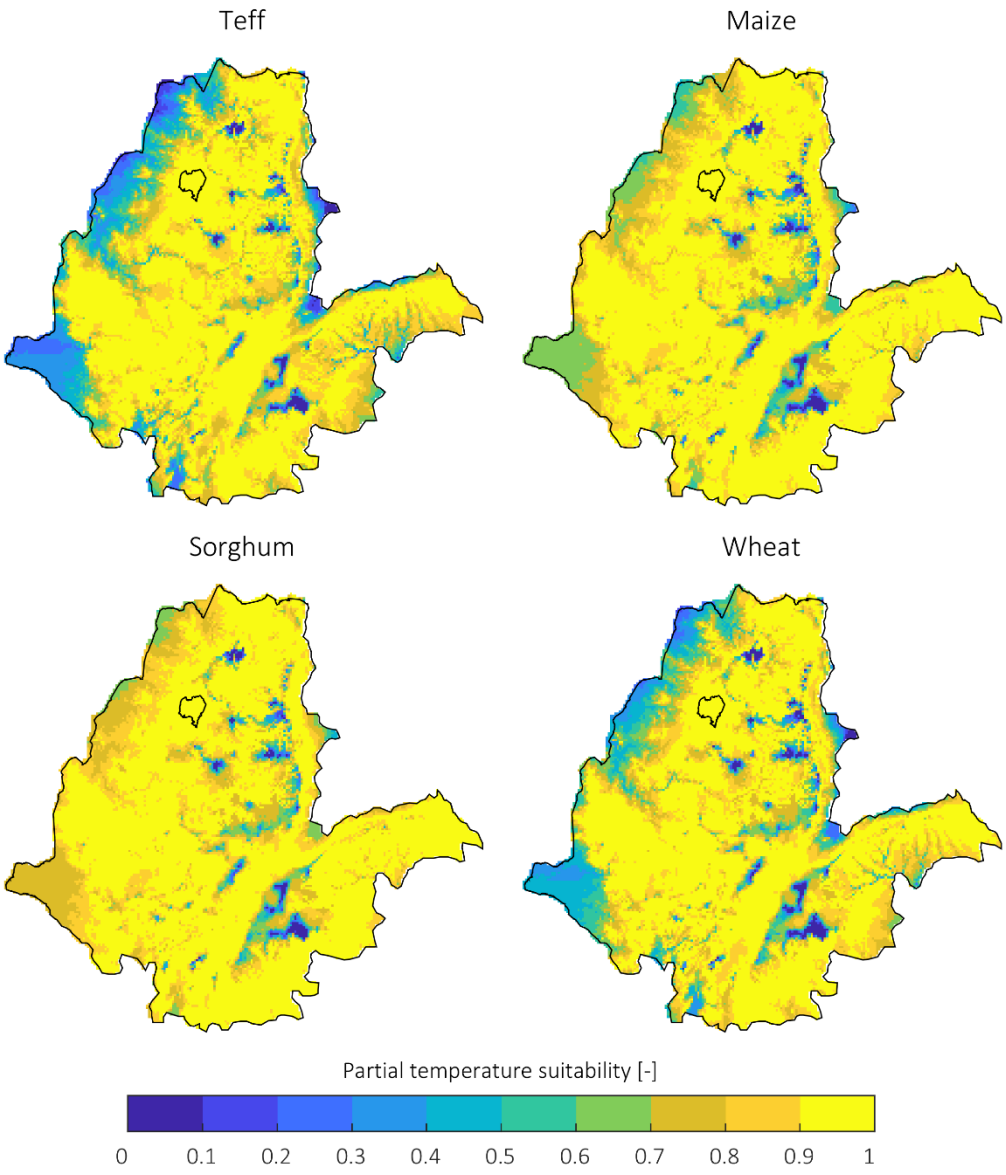

Fig. S5.3: Partial temperature suitability for teff, maize, sorghum and wheat based on the mean May-Nov temperature climatology of the period 1981-2010.

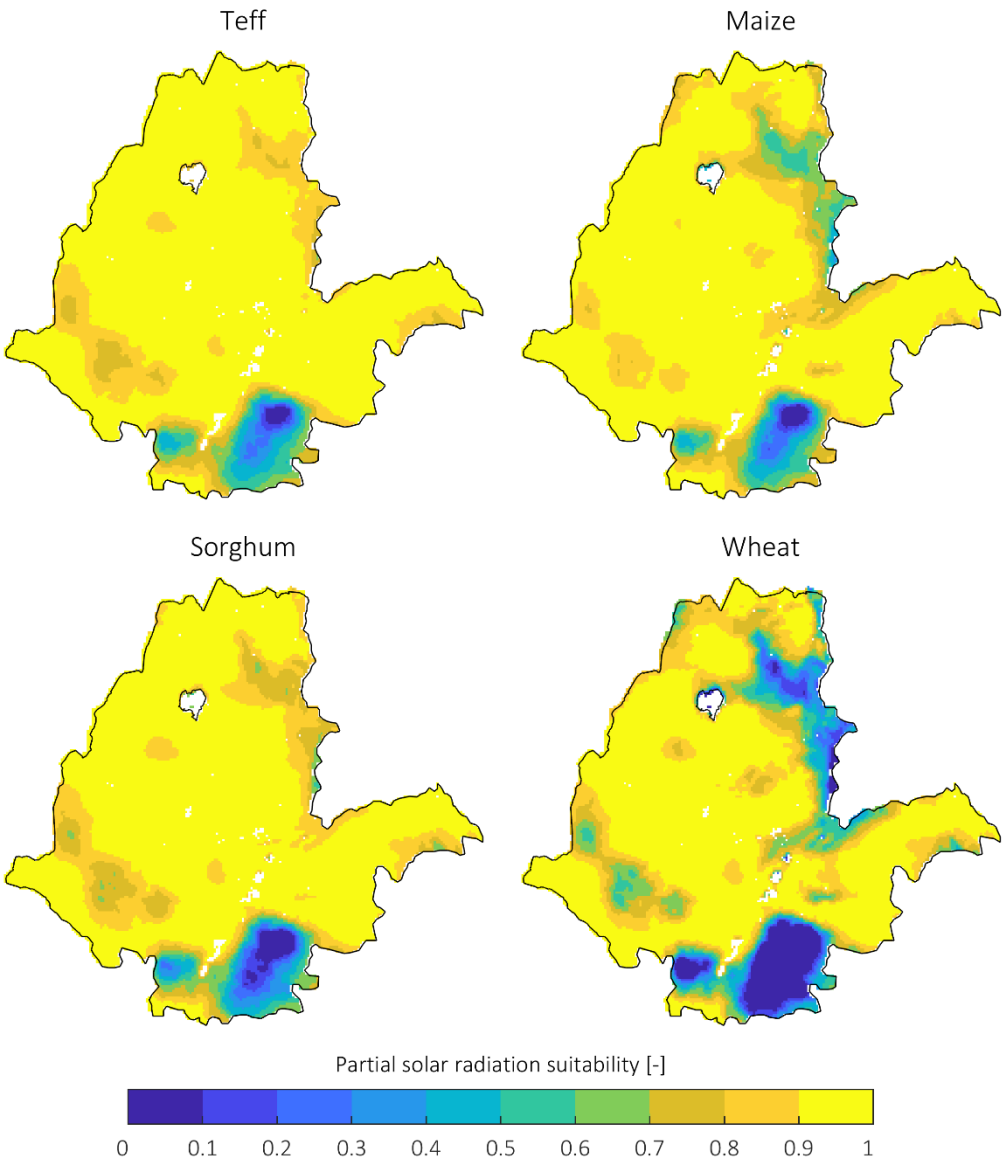

Fig. S5.4: Partial solar radiation suitability for teff, maize, sorghum and wheat based on the mean May-Nov temperature climatology of the period 1981-2010.

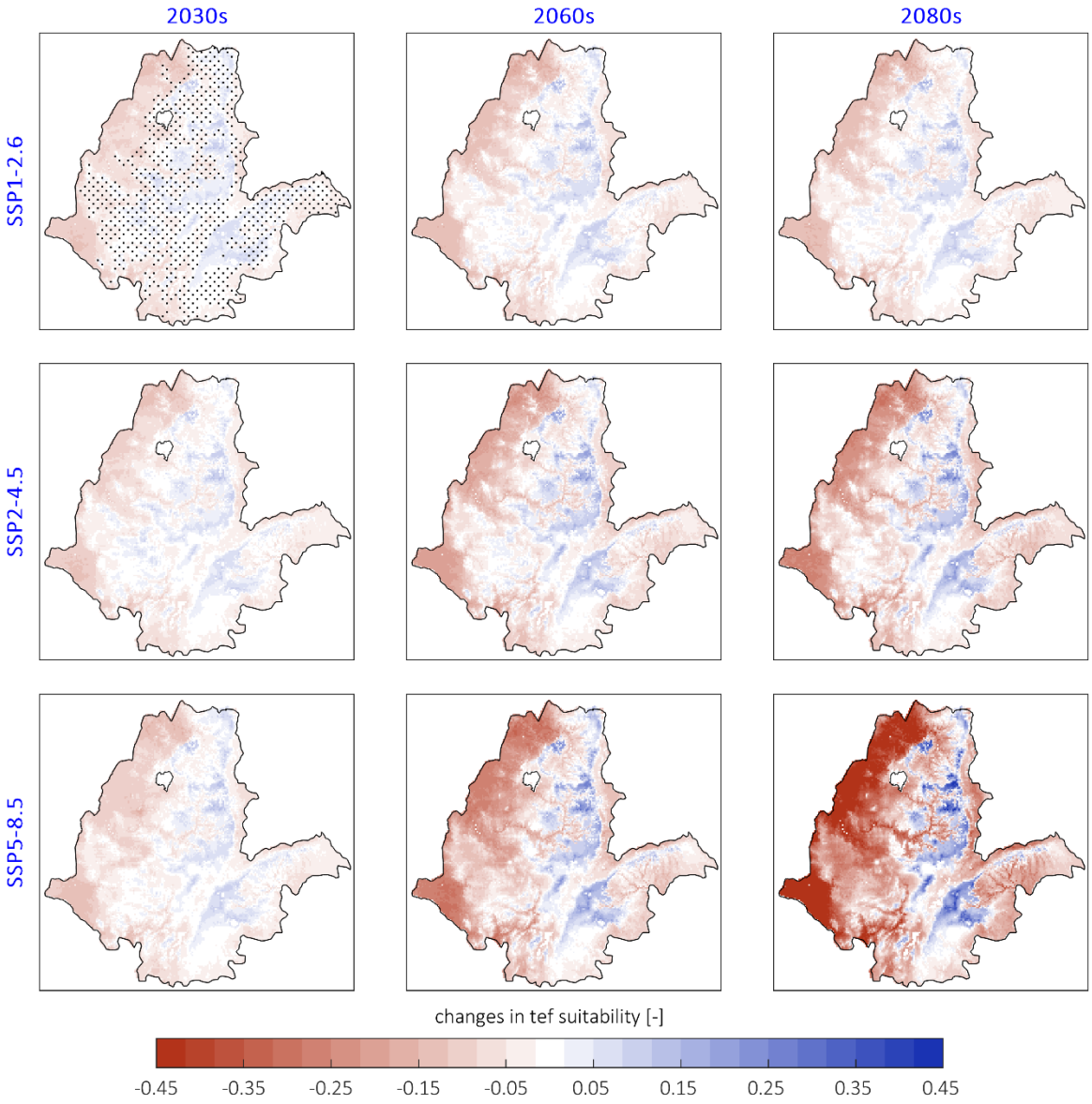

Fig. S5.5: Change maps of the cropland suitability for teff for emission scenarios (rows) and periods (columns).

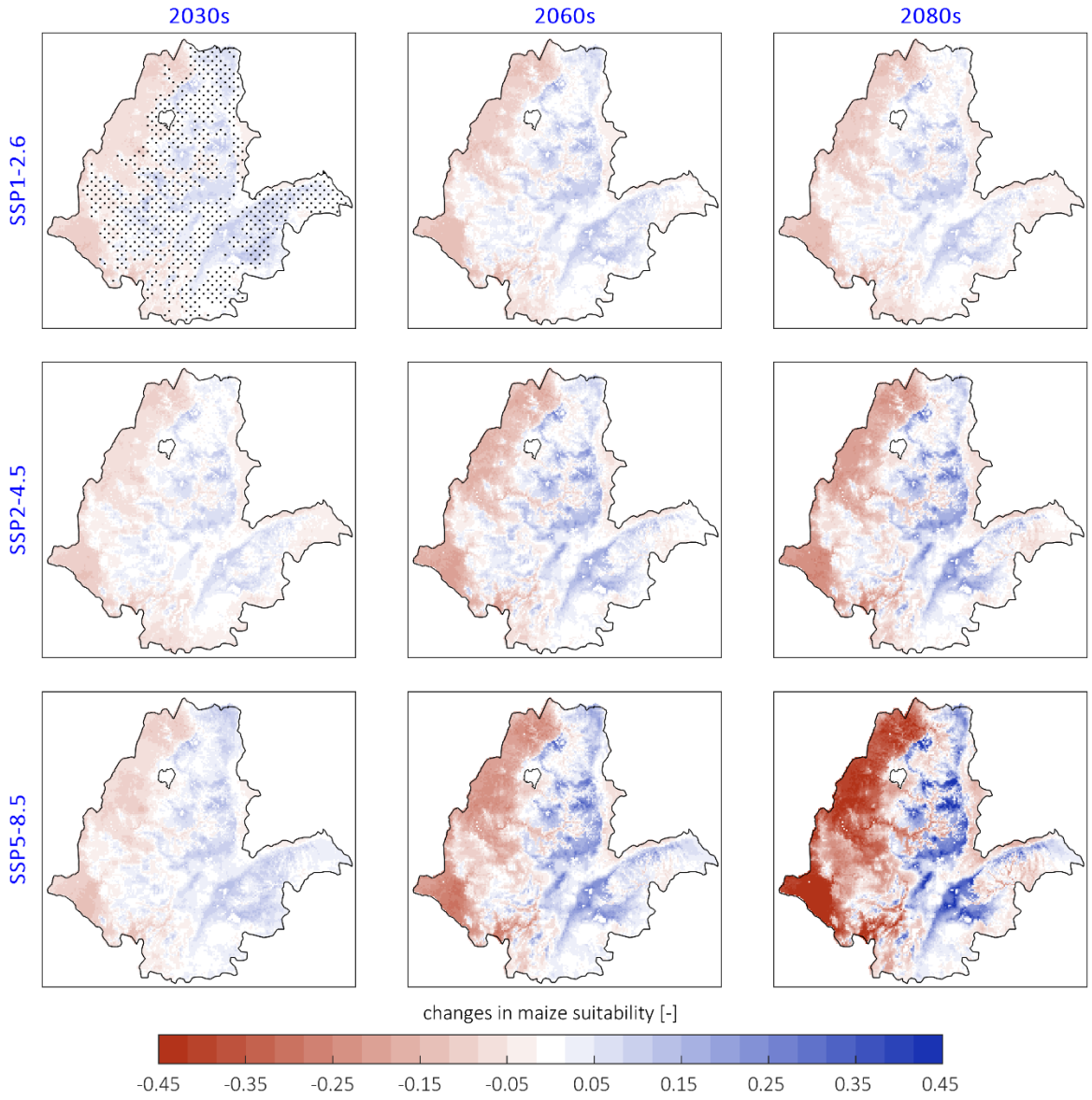

Fig. S5.6: Change maps of the cropland suitability for maize for emission scenarios (rows) and periods (columns).

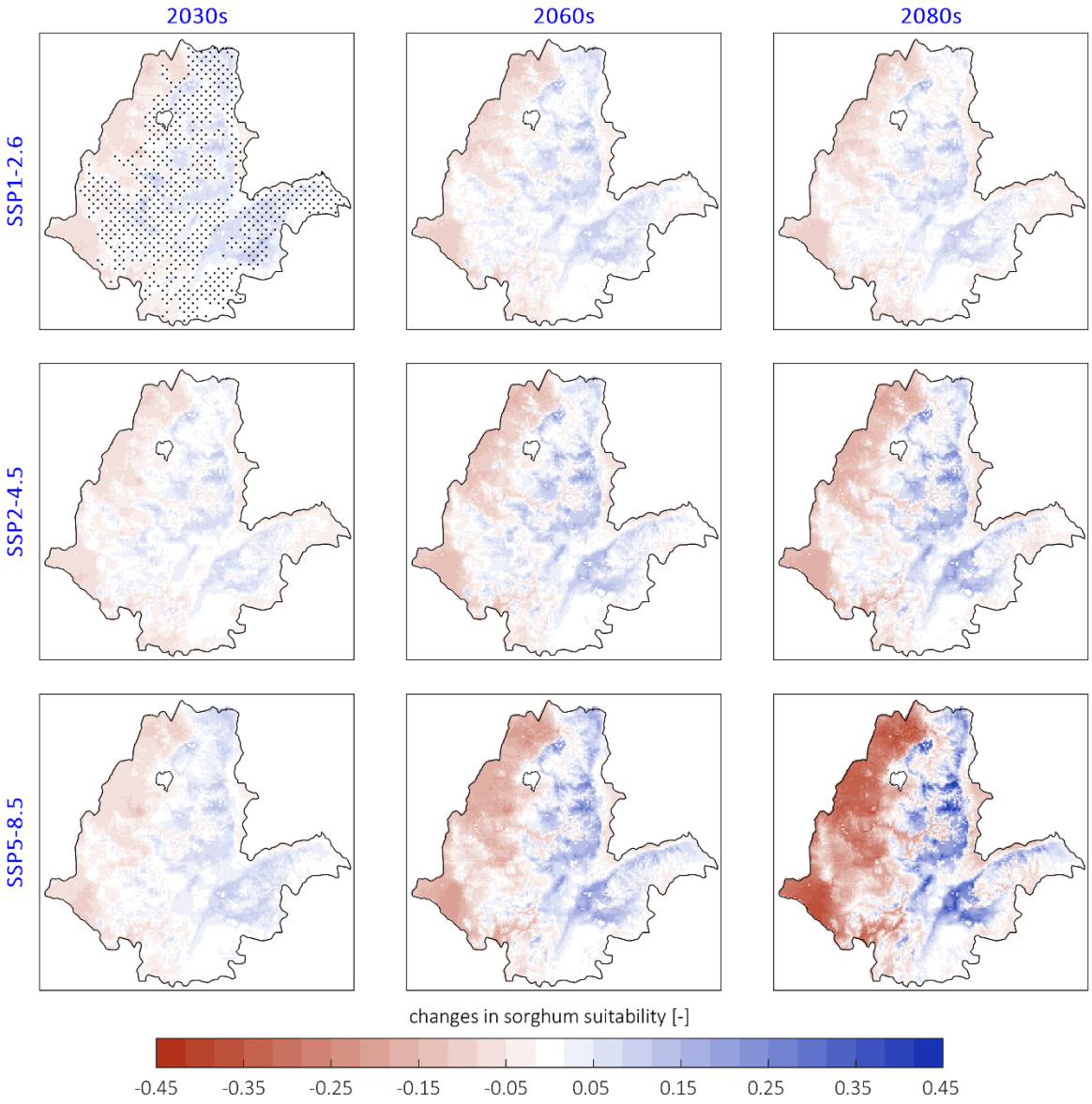

Fig. S5.7: Change maps of the cropland suitability for sorghum for emission scenarios (rows) and periods (columns).

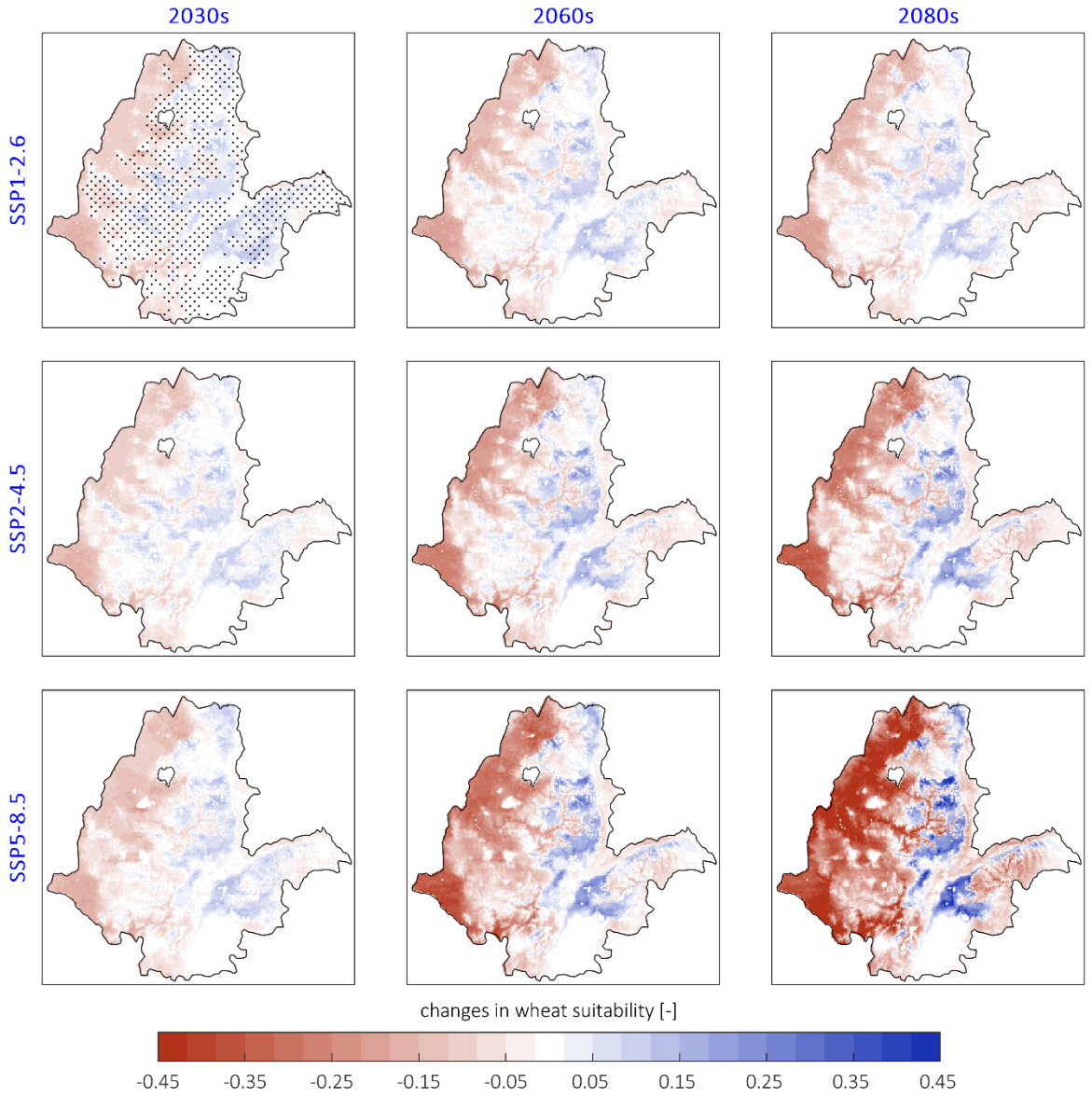

Fig. S5.8: Change maps of the cropland suitability for wheat for emission scenarios (rows) and periods (columns).

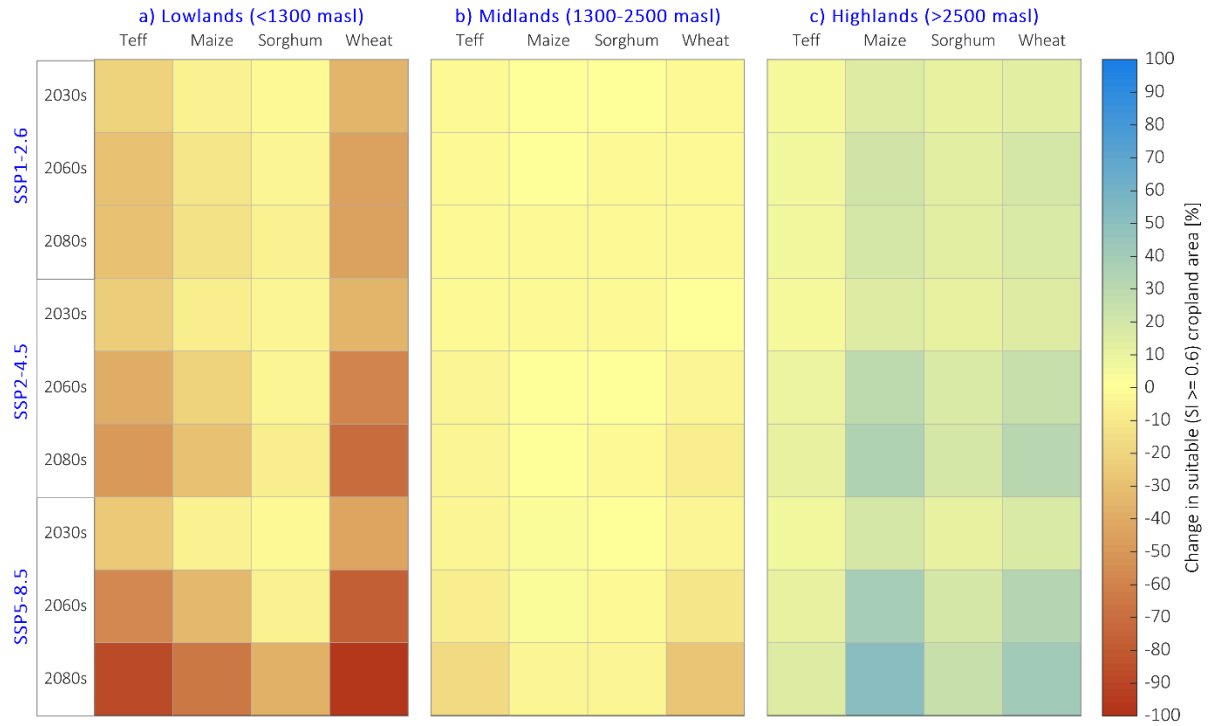

Fig. S5.9: Percent changes in suitable cropland areas for teff, maize, sorghum and wheat in different in the lowland (a), midland (b), and highland (c) agroecologies during 2030s, 2060s and 2080s under the three emission scenarios. The changes were computed considering all grid cells with SI $\geq$ 0.6.